DURBAN UNIVERSITY OF TECHNOLOGY
INYUVESI YASETHEKWINI YEZOBUCHWEPHESHE
CREATIVE. DISTINCTIVE. IMPACTFUL.

Synthesis, assessment, and application of two-dimensional ferromagnetic nanocomposites for the removal of microplastics from drinking water and wastewater effluent

Submitted in Fulfilment of the requirements for the Degree of Doctor of Philosophy in Biotechnology in the Faculty of Applied Science at the Durban University of Technology

Riona Indhur

Student Number: 21436062

2024

Supervisor: Prof. Sheena Kumari

Co-Supervisor: Dr. Arvind Kumar

Co-Supervisor: Prof. Faizal Bux

APPROVAL

I hereby approve the final submission of the following thesis.

Prof Sheena Kumari
Supervisor
Ph.D: Biosciences
Mangalore University, India

Dr Arvind Kumar
Co-Supervisor
Ph.D: Chemical Engineering
Indian Institute of Technology (IIT) Roorkee, India

Prof Faizal Bux
Co-Supervisor
Doctoral Degree in Technology:
Biotechnology Durban Institute of Technology
(DIT)

DECLARATION

I, Riona Indhur, 21436062, Prof Sheena Kumari (supervisor), Dr Arvind Kumar and Prof Faizal Bux (co-supervisors), herby declare that the following thesis: Title: Synthesis, assessment, and application of two-dimensional ferromagnetic nanocomposites for the removal of microplastics from drinking water and wastewater effluent, submitted for Doctor of Philosophy in Biotechnology at the Durban University of Technology:

1. Is the original work of the author and has not been submitted for a degree at any other University.
2. All references as detailed in the thesis are complete in terms of all published works consulted.

01/04/2025

Signature of Student **Date:**

01/04/2025

Signature of Supervisor **Date:**

02/04/2025

Signature of Co-Supervisor **Date:**

02/04/2025

Signature of Co-Supervisor **Date:**

DEDICATION

I dedicate this thesis to my beloved nani ma (grandmother) in heaven, whose love and wisdom continues to inspire me every day. Your guidance and spirit have been with me throughout this journey, and I hope to honour your memory with this work.

ACKNOWLEDGEMENTS

The completion of my Ph.D. thesis in Applied Sciences, at the Institute of Water and Wastewater Technology, marks the culmination of a challenging yet deeply rewarding three-year journey. This accomplishment would not have been possible without the support, guidance, and encouragement of numerous individuals and institutions to whom I am profoundly grateful.

First and foremost, I would like to express my deep sense of gratitude to God and the spiritual journey that has been a guiding force throughout my academic pursuit. The divine blessings and the inner strength derived from my spiritual practices have played a pivotal role in helping me navigate the challenges and achieve my goals.

I would like to express my heartfelt gratitude to my esteemed professor, Prof. Sheena Kumari. You are a force to be reckoned with and an amazing role model for all women in science. Your constant supervision, insightful feedback, and eye for detail have been critical in refining my research and ensuring its quality. Your patience and understanding, especially during the challenging phases of my project, have been a source of great comfort and motivation. I am grateful for the countless hours you have invested in reviewing my work and for the intellectual freedom you have afforded me, allowing me to explore and innovate within my field.

I would like to extend my deepest thanks and eternal gratitude to my mentor and co-supervisor, Dr. Arvind Kumar. Your invaluable guidance, unwavering support, and profound knowledge have been instrumental in shaping my research and academic development. Your belief in my potential and your encouragement during moments of doubt have inspired me to push the boundaries of my capabilities. I am deeply indebted to you for your mentorship and for providing me with the opportunities to expand my knowledge and grow within the field. Your

patience and kindness have been a guiding light throughout this journey. From you I have learnt a great many things, that have not only enriched my academic experience but also taught me invaluable lessons that extend far beyond the confines of this thesis. I am deeply appreciative of your support and the time you dedicated to helping me achieve this milestone. This thesis would not have been possible without your wisdom, understanding, and commitment, and for that, I am profoundly thankful.

To all the faculty members and staff at the Institute of Water and Wastewater Technology, I am immensely thankful for your support and assistance throughout my Ph.D. journey. Your expertise, encouragement, and the collaborative environment you foster have significantly contributed to my academic growth. I would also like to acknowledge the administrative staff for their efficiency and for always being there to assist with any logistical needs. In particular, I extend my deepest appreciation to Sasha, whose exceptional efficiency, timeliness, and proactive approach ensured that everything ran as smooth as possible. Your unwavering dedication and meticulous attention to detail were instrumental in navigating the administrative complexities, allowing me to focus on my research. Your constant readiness to assist and your remarkable ability to stay on top of every task made a significant difference. I would also like to express my gratitude to Karen, who never turned me away and was always willing to help. Thank you for always taking the time to assist me regardless of how busy you were. I would also like to extend my heartfelt thanks to Kriveshin and Uwais for their technical support throughout this journey. Your expertise and willingness to assist have been crucial in navigating the complexities of my research. Your prompt and efficient help, whether it was troubleshooting issues or providing insightful solutions, made a difference in my ability to complete this thesis.

I would like to express my deepest gratitude to my family for their unwavering support throughout this journey. To my beautiful mother, who has been my pillar of strength; your prayers and constant encouragement have been the guiding light that saw me through to the completion of this degree. To my incredible sister, your ability to lift my spirits and make me laugh, even in the most challenging moments, has been nothing short of therapeutic. Your humour and positivity have provided me with the strength to persevere, and your encouragement has been a vital source of motivation. Thank you for always being there for me, for understanding my struggles, and for bringing joy into my life. Your support has been invaluable, and I am deeply grateful. Thank you to my father for your steadfast support and encouragement. I am inspired by your hard work and hope to make a difference, just as you did. I am profoundly grateful to my mom, sister, and father for their sacrifices, and their emotional and financial support, which made this achievement possible. Thank you, Mom, Dad, and my dear sister, for everything. This achievement is as much yours as it is mine.

To my best friend Sumaine, your friendship has been a source of strength and motivation. Your words of encouragement during challenging times, and your ability to make me laugh when I needed it most have been instrumental. Your patience, understanding, and the countless hours you spent listening to my concerns and offering advice have made a significant impact on my ability to persevere and complete this thesis. Thank you for being such an incredible friend and for standing by me every step of the way.

I would like to extend my gratitude to my friends and colleagues Aaliyah, Sueyanka, and Kerisha. Your insightful advice and willingness to lend a helping hand have made the toughest parts of this journey manageable. Your camaraderie and positivity have made campus life fun. Thank you all for your friendship, understanding, and support.

I would also like to extend my sincerest thanks to the following institutions: University of Cape Town, Stellenbosch University, University of Free State and the University of Kwa-Zulu Natal for the use of their equipment for characterisation.

I am also profoundly grateful to everyone who provided the necessary resources and provisions to make this journey possible. Your generosity and support have been instrumental in creating a conducive environment for my research and studies. In closing, this thesis stands as a testament to the collective effort of all those who have supported and guided me. I am forever grateful for the roles each of you has played in my journey. Thank you for making this achievement possible. This acknowledgment reflects the profound appreciation and gratitude I feel towards everyone who has been part of this remarkable journey. Your support and guidance have been invaluable, and I am deeply thankful to each and every one of you.

ABSTRACT

The increase in microplastics (MPs) concentration in water matrices continues to pose a serious threat to aquatic ecosystems, and subsequently human health as a result of bioaccumulation within these aquatic organisms. Significant number of MPs have been detected from different water matrices including surface water and wastewater treatment effluent, globally. Recent reports from South Africa have also indicated their presence in tap water in low concentrations. Water treatment plants globally, are not optimised or designed for the removal of MPs. Therefore, technological innovations are required to alleviate the limitations embedded in these treatment systems. Nanotechnology has emerged as a pivotal technology to address a wide range of environmental challenges through performance enhancement. Therefore, this study investigated the removal of MPs from aquatic environments using magnetic nanocomposites (MNCs). This is the first study to the best of our knowledge that explicitly evaluates the performance of MNCs g-C_3N_4@Fe_3O_4 and BNNS@Fe_3O_4 for the removal of MPs. Herein, the application of each MNC is assessed for their removal efficiency of individual and multitudinous combinations of polystyrene (PS) and polyethylene (PE) MPs, including different size ranges. Additionally, these MNCs are applied in drinking water and real domestic wastewater effluent to determine their effectiveness against a combination of PS and PE MPs. Furthermore, a phytotoxicity study was also conducted to assess the toxicity of g-C_3N_4@Fe_3O_4 and BNNS@Fe_3O_4 on various common agricultural crops (*Hordeum vulgare L.* (barley wheat), *Cicer arietinum* (black chickpea) and *Vigna radiatus L.* (moong)). The recyclability study was performed for five successive rounds of reuse and each of the MNCs magnetic stability was assessed via VSM. Finally, a cost assessment analysis for MPs removal with the best-performing MNC (g-C_3N_4@Fe_3O_4) was also conducted as well as the mechanistic insights of the interactions between PE/PS MPs and the MNC was postulated.

The MNCs (g-C_3N_4@Fe_3O_4, BNNS@Fe_3O_4) were synthesized by conventional co-precipitation. Synthesized MNCs were characterised by various analytical techniques such as, XRD, TGA, FTIR, BET, XPS, SEM-EDX, TEM, VSM, and Zeta potential. The optimization of various parameters (pH, time, MNC dose, MP dose) were done through gradient experiments. Optimised parameters were applied in batch experiments to investigate g-C_3N_4@Fe_3O_4 and BNNS@Fe_3O_4 for the removal of different types and sizes of MPs (PE (125 μM), PS (25-180 μM), PE+PS combo (PE=125 and 25-180 μM) and PS (180-500 μM) from Milli-Q water, wastewater effluent and drinking water.

The maximum removal of PE (96.16%, size 125 μM), PS (92.5% , size 25-180 μM), PE+PS combo (94.89%, size PE=125 and 25-180 μM) and PS (45.62%, size 180-500 μM) were noticed with MNC g-C_3N_4@Fe_3O_4 under optimum operating conditions ([pH]= 4; time= 5 h; [MNC]= 1.2 g/L; [MP]= 0.5 g/L) from Milli-Q water. The maximum removal efficiency of PE (94.44%, size 125 μM), PS (85.96%, size 25-180 μM), PE+PS combo (88.28%, size PE=125 and 25-180 μM) and PS (38.77%, size 180-500 μM) were observed with MNC BNNS@Fe_3O_4 under optimum operating conditions ([pH] = 3; time= 12 h; [MNC]= 0.9 g/L; [MP] = 0.5 g/L) from Milli-Q water. A direct correlation was observed between the removal rate and the size of the MPs. The investigation of MNC removal efficiency in different water matrices yielded 93.7 and 86.56% from drinking water via g-C_3N_4@Fe_3O_4 and BNNS@Fe_3O_4, respectively. A removal rate of 91.91 and 83.78% was observed from domestic wastewater effluent filtered with a 0.22 μM filter for g-C_3N_4@Fe_3O_4 and BNNS@Fe_3O_4, respectively, whilst a removal rate of 90.28 and 82.23% was observed from the same domestic wastewater effluent (unfiltered) for g-C_3N_4@Fe_3O_4 and BNNS@Fe_3O_4, respectively. The results for filtered and unfiltered wastewater effluent are similar indicating that filtering plays no significant role in improving the removal efficiency. The reusability study revealed that both

MNCs retained a removal efficiency of more than 50% after 5 cycles whilst g-C_3N_4@Fe_3O_4 retained a removal efficiency of almost 80% after 3 cycles. The VSM results exhibited that both MNCs possess superparamagnetic behaviour which indicates that both BNNS@Fe_3O_4 and g-C_3N_4@Fe_3O_4 have excellent magnetic properties, enabling their application in practical settings. This was further confirmed by the after-treatment results wherein both MNCs retained their superparamagnetic properties after adsorption of the MPs, allowing for effective magnetic separation.

MNCs' phytotoxicity on common agricultural crops was assessed to investigate any potential ecotoxic effects on the crops. The phytotoxicity of domestic raw wastewater influent, final treated effluent, g-C_3N_4@Fe_3O_4, BNNS@Fe_3O_4, g-C_3N_4@Fe_3O_4 filtrate and BNNS@Fe_3O_4 filtrate were assessed through seed germination indices (G.I.%). The MNC filtrate of g-C_3N_4@Fe_3O_4 and BNNS@Fe_3O_4 revealed mild toxicity (approaching non-toxic) and no toxicity, respectively. The operating cost of g-C_3N_4@Fe_3O_4 for MPs removal from domestic wastewater effluent was approximately 41.09\$/m^3. This makes it is a cost-effective treatment when compared to literature. The four main potential interactions postulated to occur between the PS/PE MPs and g-C_3N_4@Fe_3O_4 and BNNS@Fe_3O_4 MNCs are: electrostatic interaction, π-π interaction, Van Der Waals forces and hydrogen bonding.

In conclusion, this thesis demonstrates the promising potential of MNCs (g-C_3N_4@Fe_3O_4 and BNNS@Fe_3O_4) for the efficient removal of MPs from various water matrices, including drinking water and final treated wastewater effluent. The remarkable removal efficiency and superparamagnetic properties of these materials, coupled with their low environmental toxicity and cost-effectiveness, highlight their feasibility for practical applications. This thesis further confers the understanding of g-C_3N_4@Fe_3O_4 and BNNS@Fe_3O_4 MNCs recyclability, therein promoting a circular economy and a sustainable approach for wastewater treatment. These

findings contribute to advancing sustainable wastewater treatment solutions and address the global challenge of MP pollution.

TABLE OF CONTENTS

LIST OF TABLES

LIST OF FIGURES

LIST OF EQUATIONS

$$\frac{\eta a}{\eta m} = \frac{CP/P0}{\left(1-\frac{P}{P0}\right)(1+(C-1)P/P0} \quad (1)$$

$$U_e = \frac{2\epsilon\zeta f(\kappa a)}{3\eta} \quad (2)$$

$$\eta = \frac{W0-Wf}{W0} \text{ x } 100\ \% \quad (3)$$

$$G.I.(\%) = \frac{Gs}{Gc} \text{ x } \frac{Ls}{Lc} \text{ x } 100 \quad (4)$$

$$\text{Operating cost (R)} = \frac{\text{Rand}}{\text{kW/h}} \text{ x kW x h} \quad (5)$$

ABBREVIATIONS

BET	Brunauer–Emmett–Teller analyzer
BJH	Barrett-Joyner-Halenda
CNT	Carbon Nano Tubes
d_{AVG}	Average diameter size
DM	Dynamic Membrane Technology
EDX	Energy-Dispersive X-ray Spectroscopy
FE-SEM	Field Emission Scanning Electron Microscopy
FTIR	Fourier-Transform Infrared Spectroscopy
GO	Graphene Oxide
HDPE	High Density Polyethylene
HDTMS	Hexadecyltrimethoxysilane
LDPE	Low Density Polyethylene
MBR	Membrane bioreactor
MF	Melamine Foam
MOF	Metal Organic Framework
MPs	Microplastics
MS	Magnetization Saturation
MS_a	Magnetization Saturation After adsorption
MS_b	Magnetization Saturation Before adsorption
NMs	Nanomaterials
NPs	Nanoplastics
PA	Polyamide
PE	Polyethylene
PES	Polyester
PET	Polyethylene Terephthalate
pH_{PZC}	Point of Zero Charge
PMMA	Polymethyl Methacrylate
POP	Persistent Organic Pollutant
PP	Polypropylene
PS	Polystyrene
PU	Polyurethane
PVC	Polyvinyl Chloride

PVDF	Polyvinylidene Fluoride
RO	Reverse Osmosis
TEM	Transmission Electron Microscopy
TDS	Total Dissolved Solids
TGA	Thermogravimetric Analysis
UF	Ultrafilration
UPW	Ultrapure water (Milli-Q water)
VSM	Vibrating Sample Magnetometer
WWTP	Wastewater Treatment Plant
XRD	X-ray Powder Diffraction
XPS	X-ray Photoelectron Spectroscopy

OUTPUTS (PUBLICATIONS)

1. Nanomaterials for microplastic removal from wastewater: Current state of the art nanomaterials and future prospects,

   Riona Indhur [a], Isaac Amoah [b], Faizal Bux [a], Sheena Kumari [a,*] (**Published**) ES & T Water

2. A Novel Approach for Microplastic Removal from Aqueous solution via Fe_3O_4 functionalized g-C_3N_4 and BNNS: Recyclability and Toxicity Assessment

   Riona Indhur, Arvind Kumar, Faizal Bux and Sheena Kumari Kuttan Pillai* (**submitted and under review**) Journal of Environmental Chemical Engineering

3. Recent advances in predicting and modelling of pharmaceutical removal by AOPs based on artificial intelligence and machine learning algorithms: current status, challenges and future direction

   Arvind Kumar, Abdul Gaffar Sheik, **Riona Indhur**, Faizal Bux and Sheena Kumari*

   Journal of Environmental Chemical Engineering

4. Recent advances in mechanistic insights into antibiotics degradation strategies via emerging advanced oxidation processes: legislation, challenges and future direction

   Arvind Kumar, **Riona Indhur**, Faizal Bux and Sheena Kumari *

   Journal of Hazardous Materials

5. Biochar-functionalised nanomaterial for the removal of emerging pollutants: Microplastics and Potentially Toxic Elements – A critical review

Tina Kenneth, **Riona Indhur**, Arvind Kumar, Faizal Bux, Sheena Kumari *

Springer Nature Biochar Journal

6. Mechanistic Insights for the Valorisation of plastic waste into value added products: Sustainable strategies, Current Challenges and Future Outlook

   Arvind Kumar, Lohith Kumar, **Riona Indhur**, Faizal Bux, Sheena Kumari*

   Science of the Total Environment

Additional co-authored publications related to the research/study area

7. Microplastic in Ecosystems: Abundance, Transportation, and Biodegradation

   Muneer Ahmad Malla, **Riona Indhur**, Nomalihle Malambule, Kelebogile Mosagale, Tyrone Moodley, Faizal Bux, and Sheena Kumari* (**Published**) ACS Bioremediation

8. Bridging Cost-Effectiveness and Efficiency: Advanced and Low Cost Adsorbents for Potential Toxic Elements Removal - Current status, Challenges and Future outlook,

   Arvind Kumar, **Riona Indhur**, Abdul Gaffar Sheik, Suresh Babu Naidu Krishna, Sheena Kumari, Faizal Bux (**Published**) Journal of Environmental Technology Reviews

9. A recent trend of microplastic removal based advanced oxidation processes: A critical review on microplastic degradation by sulfate radical based advanced oxidation processes

   Arvind Kumar[a,b]*, **Riona Indhur**, Sheena Kumari[a], Faizal Bux (**submitted and under review**) Science of the Total Environment

10. Book Chapter 16: Iron Irradiation Degradation of Polymer Nanocomposites

    Arvind Kumar, **Riona Indhur**, Faizal Bux and Sheena Kumari * (**submitted and under review**) Elsevier

CHAPTER ONE: Introduction

1.1.Background/Introduction

Over the past 70 years, global plastic production has surged dramatically, rising from just two million tonnes in 1950 to over 450 million tonnes today (Ritchie and Roser 2018). Initially developed to enhance human living conditions, plastic has now become one of the most prevalent materials in the world, but its environmental impact has escalated into a significant global concern (Ziani *et al.* 2023). This is because the majority of plastic products are non-biodegradable whereby their degradation persists for approximately over 100 years which is extremely disproportionate with the present plastic disposal rates (Gkatzioura *et al.* 2021). Presently, plastic pollution pervades all environmental compartments—air, water, and soil. The generation of plastic wastes threatens the wellbeing of a plethora of living organisms and environmental matrices, with marine life at the forefront. Tiny plastic particles called microplastics (MPs) have surfaced as a significant threat and they pose serious environmental hazards (Chellasamy *et al.* 2022).

Small synthetic polymer particles that are < 5 mm in diameter are characterised as MPs (Bamigboye *et al.* 2024). They are categorized into primary and synthetic based on their origin. A primary MP is made intentionally smaller to suit industrial use, whereas a secondary MP is produced from the breakdown of a larger plastic. The ubiquitous expulsion of MPs has enabled them to root themselves in a host of different environments such as seashores, oceans, reservoirs, rivers, lakes, fresh waters and the soil perpetuating negative effects (Chellasamy *et al.* 2022). There is a great threat to aquatic life due to the accumulation of plastic wastes in these habitats at significantly higher concentrations. The magnitude of the impact can be enhanced depending upon the toxicity of the adsorbed pollutants on MPs such as pesticides, metals or persistent organic pollutants (POPs) and the prospect of leaching of toxic chemicals

from the plastic additives (Bui *et al.* 2020). Additionally, MPs serve as reservoirs for pathogen transmission, which poses a threat to aquatic life and humans. Several mechanisms are employed by MPs to induce toxic effects in marine life. Toxicity could be directly triggered via the polymer materials utilised for plastic product manufacturing such as polystyrene (PS). For example, it is evidenced that PS harbours the ability to translocate in blood circulation and trigger reproductive disruption for marine filter feeders (Chen *et al.* 2006; Sussarellu *et al.* 2016). MPs can trigger inflammation and mutilate organisms owing to their sharp edges and minute size, with evidence illustrating that MP ingestion also triggers reproductive alterations and malnutrition in specific organisms (Besseling *et al.* 2017). These MPs have also been scrutinised for the repercussions they endow on human health. PS and polyethylene (PE) exposure causes necrosis, apoptosis and genotoxicity resulting in carcinogenesis, fibrosis and tissue damage (Singh *et al.* 2021d). PS, which is associated with the styrene particles/chemicals has also emerged as an endocrine disrupting chemical (Singh *et al.* 2021d). PE particles have been reported in the spleen, liver and lymph nodes of humans causing cytokines production and immune activation of macrophages (Singh *et al.* 2021d). The aforementioned implications do not encompass the full spectrum of the detrimental effect that MPs have on human health.

It has recently been brought to the fore that wastewater treatment plants (WWTPs) are a substantial source of MPs dissemination into the environment (Sun *et al.* 2019; Goh *et al.* 2022). Wastewater treatment plants (WWTP) have proven relatively efficient in removing MPs in that they showcase the capability to remove a great majority of MPs (Karapanagioti and Kalavrouziotis 2018). Albeit the highly efficient removal rates accomplished by WWTPs when processing hefty effluent volumes, even a modest amount of MPs released per effluent litre could result in significant concentrations of MPs infiltrating the receiving environment (Karapanagioti and Kalavrouziotis 2018). WWTPs are currently not optimised or designed for the removal of MPs (Iyare *et al.* 2020) which demonstrates a gap in industry to be explored

academically. Due to the limitations of current practices, there is a growing need for innovative and efficient technologies to augment MPs removal during wastewater treatment. The exploration of advanced technologies is imperative to address this critical gap in conventional water treatment methodologies.

In recent years, nanomaterials (NMs) characterized by dimensions ranging from 1 to 100 nanometres, have emerged as promising candidates for enhanced MP removal (Punia *et al.* 2021; Indhur *et al.* 2023). The unique properties of NMs, including their high surface area, mechanical strength, and tuneable reactivity, position them as viable tools for targeted and efficient MP capture (Singh 2016). NMs with high surface area-to-volume ratio, permits efficient utilization of resources and materials, ultimately leading to cost savings in various applications, from water treatment to catalysis (Yaqoob *et al.* 2020). Moreover, the ability to reuse NMs in multiple cycles without significant loss in their efficacy enhances their overall economic feasibility (Kumar *et al.* 2021b; Kumar *et al.* 2023a). The versatility of NMs in maintaining their structural and functional integrity over repeated applications underscores their sustainability and long-term cost-effectiveness (Kumar *et al.* 2021b; Kumar *et al.* 2023a). This therein makes them attractive options for environmentally conscious and economically viable solutions. In the previous years, various researchers have shown the remarkable sorption capacity of NMs for MPs removal from aqueous media (Sarcletti *et al.* 2021; Palliyarayil *et al.* 2023; Sacco *et al.* 2023).

However, the utilization of NMs in various applications, including environmental remediation such as MP removal from wastewater, has raised valid concerns regarding their potential toxicity. The unique physicochemical properties that make NMs effective for specific applications may also contribute to their interactions with biological systems and the environment (Fadeel and Garcia-Bennett 2010). Therefore, toxicity studies are imperative to comprehensively understand the potential adverse effects and ensure the safe deployment of

NMs. Therefore, rigorous investigation into the biological, ecological, and environmental impacts of NMs is essential for responsible and sustainable technological development.

To date, no studies have been reported on the removal of MPs by graphitic carbon nitride functionalised to magnetite (g-C_3N_4@Fe_3O_4) and boron nitride nanosheets functionalised to magnetite (BNNS@Fe_3O_4) and their potential toxicity. To the best of our knowledge, this is the first study to focus on the removal of MPs (PE and PS) by g-C_3N_4@Fe_3O_4 and BNNS@Fe_3O_4 from domestic final treated wastewater effluent and drinking water.

1.2.Scope:

Global plastic incidence has increased by 300 million metric tons in 2021. Since 1950, 8.5 billion tons of plastic has been produced worldwide with 367 million tons of plastic being produced in 2021 alone (Kain *et al.* 2022). South Africa has the 11th highest mass of mismanaged plastic waste annually with an estimated 630,000 tons being mismanaged within 50 km of the coastline annually (Kain *et al.* 2022). This mass accounts for 2% of the world's total mismanaged plastic waste and is greater than that contributed by countries housing larger populations within 50 km of the coast. This data demonstrates the imminent systemic threat that non-biodegradable plastics pose to the world's seas, freshwater sources, species, air, food supply and soil. Despite this, plastic production is predicted to increase exponentially over the next 20 years, with far more plastic being added to the already existing 6.5 billion tons of disposable plastic currently amassed throughout the globe (Kain *et al.* 2022).

Among the concerning detriments of this plastic pollution is the emergence of micro and nano plastics as contaminants in water bodies (Abuwatfa *et al.* 2021). This presents a major challenge to the provision of clean and safe water for the world population (Rosa *et al.* 2021) since they remain in the environment (Abuwatfa *et al.* 2021). The most prevalent MPs on aquatic surfaces are PS, PE and polypropylene (PP) (Abuwatfa *et al.* 2021). Growing concerns

associated with these MPs stems from their bioaccumulation (Goh *et al.* 2022), adverse side effects and potential toxicity to various ecological systems (Abuwatfa *et al.* 2021). Their dissemination affects not only the environment (Rosa *et al.* 2021), but also marine life (Abuwatfa *et al.* 2021) and human health (Rosa *et al.* 2021). Additionally, pollution of freshwater bodies contributes to the scarcity of freshwater as it adds additional pressure to the available resources.

Several conventional WWTPs have been rendered ineffective in circumventing the advent of these MPs and this greatly jeopardises satisfying increasingly stringent water quality standards (Rosa *et al.* 2021). There are increased reports of MPs from treated effluent globally (Gies *et al.* 2018; Kazour *et al.* 2019; Naji *et al.* 2021; Yang *et al.* 2021). Recent reports from South Africa have also indicated their presence in tap water in low concentrations (Wei *et al.* 2019). Therefore, technological innovations are required to alleviate the limitations embedded in these treatment systems (Hairom *et al.* 2021). Nanotechnology has materialized as a transformative technology, playing a crucial role in addressing various environmental challenges by significantly enhancing performance across multiple applications (Goh *et al.* 2022).

Albeit the recently emerging studies encompassing the use of NMs in wastewater treatment, the field of nanoremediation in WWTPs is still in its infancy. This illustrates a large gap and unexplored niche for the use of NMs for the removal of MPs. This project seeks to remedy the dire plastics situation by exploring and reducing this gap through the synthesis of magnetic NMs for MPs removal. The incorporation of the MNC into a functional wastewater treatment process should increase the removal efficiency of MPs in comparison to the conventional wastewater treatment system. In applying these functionalised MNCs independently, it is inevitable that the number of MPs that get released into the environment and drinking water

will be significantly reduced thereby bringing us a step closer to the UN's sustainable development goals 3 (Good health and well-being), 6 (Clean water and sanitation) and 11 (Sustainable cities and communities). The impact of this would be significant since it would promote fewer MPs being discharged into the ocean, therefore reducing the imminent threat on aquatic ecosystems and the environment. In removing MPs from drinking water, the impact would be equally as significant since it would promote cleaner, safer drinking water reducing the serious effects of MPs on human health. The use of MNCs also allows for recyclability since the MNC will be regenerated after use, allowing it to be used for many cycles before being rendered ineffective, as opposed to being employed once-off and then discarded. This promotes a circular economy. Furthermore, due to its recyclability, it promotes a cost-efficient factor and reduces overall wasting of resources as well as waste production (that would otherwise be generated from single-use MNCs). This also makes it a sustainable solution.

Hence, the primary objective of the present investigation is to evaluate the performance of g-C_3N_4@Fe_3O_4 and BNNS@Fe_3O_4 MNCs for the removal of MPs from water matrices. This investigation includes eight main aspects: (i) fabrication of g-C_3N_4@Fe_3O_4 and BNNS@Fe_3O_4 MNCs via co-precipitation method and subsequent analysis using various techniques, such as TGA, FTIR, BET, XRD, TEM, XPS, SEM with EDX, and Zeta potential; (ii) influence of operational parameters (i.e., MNC dose, MPs dose, solution pH and reaction time on the MPs removal; (iii) application of the optimized operating parameters on the removal of different types and sizes of MPs from Milli-Q water; and on the removal of MPs from domestic wastewater effluent and drinking water; (iv) MNC recyclability study; (v) MNC magnetic stability assessment; (vi) mechanistic insights between PS/PE MPs and MNCs; (vii) phytotoxicity study of MNCs on three different crops; (viii) a detailed assessment of treatment cost of the adsorption process for MPs removal.

1.3.Research Aim

Synthesis and assessment of two-dimensional ferromagnetic nanocomposites for the removal of MPs from treated water and wastewater and their recyclability and phytotoxicity assessment.

1.4.Objectives

1: Synthesis and characterisation of 2D g-C_3N_4@Fe_3O_4 and BNNS@Fe_3O_4 MNCs.

2: Optimization of key parameters i.e., MNC concentration, pH, time and MP dose for the removal of MPs.

3: Evaluation of the efficacy of each MNC for the removal of different size and types of MPs (PE, PS, PP) from drinking water and treated wastewater samples.

4: Determination of the MNCs regeneration and recyclability studies, and the assessment of magnetic stability of the MNCs using VSM.

5: Evaluating the phytotoxicity of MNCs on common agricultural crops to explore their potential ecotoxicity impact

6: Postulating interaction mechanistic insights between PS/PE MPs and the MNCs.

7: Economic assessment of the treatment process for MPs (PS/PE) removal using synthesised MNC.

1.5.Thesis framework:

The framework for this thesis is presented in the graphical schematic below.

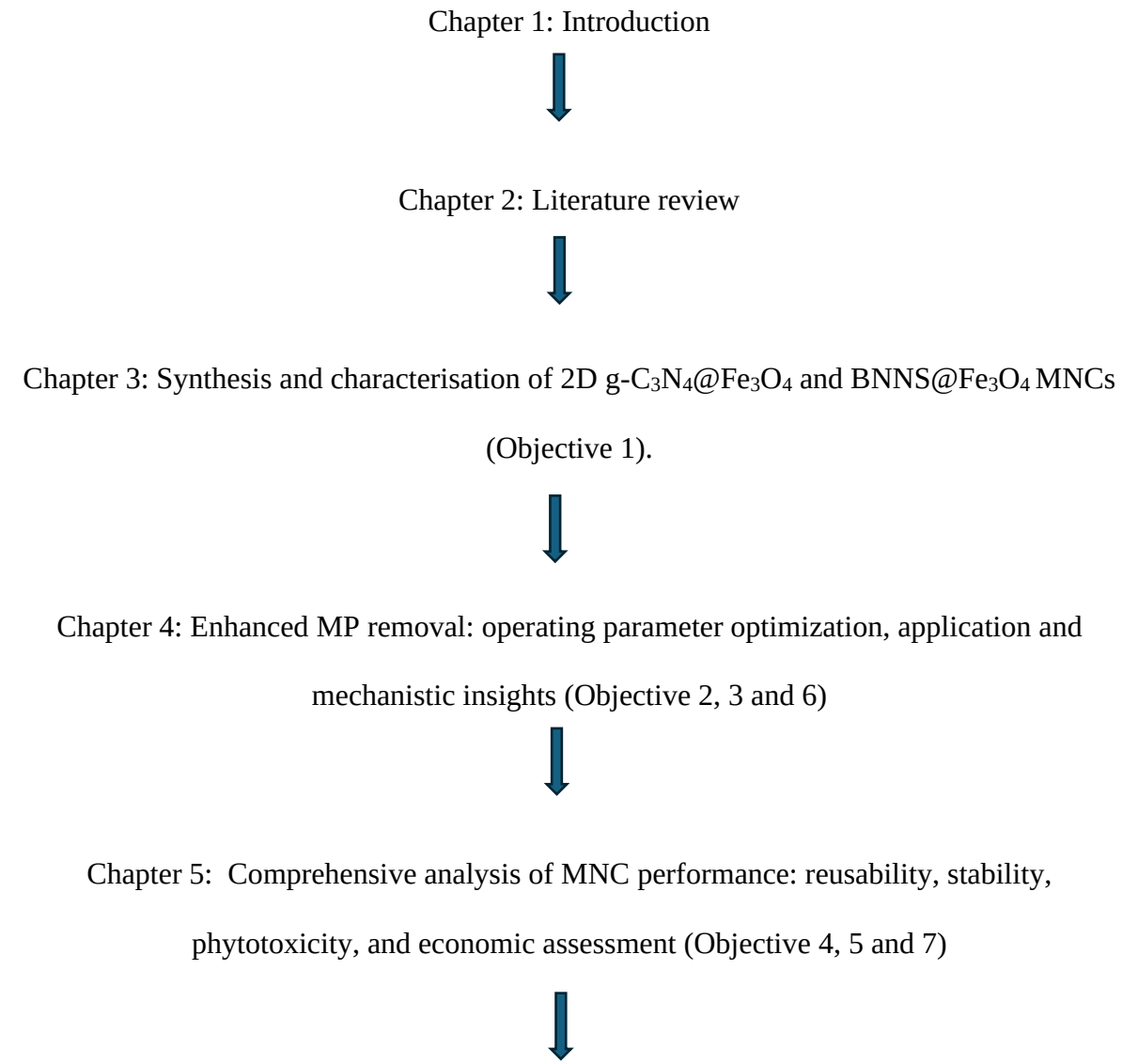

Figure 1: Framework for thesis

CHAPTER TWO: Literature Review

The following sections in this chapter have already been published in ACS ES&T Water Journal: *Indhur, R., Amoah, I., Bux, F. and Kumari, S., 2023. Nanomaterials for microplastic removal from wastewater: current state of the art nanomaterials and future prospects. ACS ES&T Water, 3(12), pp.3741-3754* (Front page, Appendix 1), with the exception of section 2.2. to 2.6.5.

2.1. Introduction

Over the past few decades the global plastic pollution challenge has increased (Gkatzioura *et al.* 2021) and continues to exhibit an exponential projected trajectory. Consequently, it is projected that by 2030, 53 million metric tons of unregulated plastic trash will be discharged into the aquatic environment annually (Borrelle *et al.* 2020; ECONOMY 2024). According to estimates from experts, every minute, the equivalent of one garbage truck's worth of plastic ends up in the ocean (ECONOMY 2024). This has prompted a lot of concern from the scientific community, which has embarked on a quest to counter the catastrophic consequences of this situation (Gkatzioura *et al.* 2021). The majority of plastic products are non-degradable, meaning they persist for more than 100 years. This extended lifespan is highly disproportionate to the current rates of plastic disposal (Gkatzioura *et al.* 2021). Among the concerning detriments of this plastic pollution is the emergence of MPs and nanoplastics (NPs) as contaminants in water bodies (Abuwatfa *et al.* 2021) which presents a significant challenge for the provision of clean and safe water (Rosa *et al.* 2021). MPs are tiny plastic particles with a diameter of less than 5 mm whilst NPs are smaller plastic debris with a diameter of less than 1 µm (Ahmed *et al.* 2022). The most commonly abundant MPs and NPs are PS, PE and PP (Abuwatfa *et al.* 2021). MPs and NPs ubiquity has placed them in almost all ecosystems including the ocean, rivers, lakes, freshwaters, groundwater, seashores and soil. Growing concerns associated with these MPs and NPs stems from their bioaccumulation in the food

chain (Goh *et al.* 2022), adverse side effects and potential toxicity to different ecological systems (Abuwatfa *et al.* 2021). This is because these emerging contaminants pose an imminent threat to the environment (Rosa *et al.* 2021), marine life (Abuwatfa *et al.* 2021) and human health (Rosa *et al.* 2021). Additionally, pollution of freshwater bodies contributes to the scarcity of freshwater adding additional pressure to the available resources.

2.2. Types of MPs and physicochemical properties

The types, compositions, sizes, and shapes of MPs are diverse. The most common MPs and NPs include polyurethane (PUR), polyamide (PA), polyethylene terephthalate (PET), polyester (PES), polyvinyl chloride (PVC) (Andrady 2017; Ahmed *et al.* 2022) with PS, PP and PE being the most ubiquitous (Abuwatfa *et al.* 2021). The structural composition of MPs is defined by their atom types and configurations (Table 1). This is crucial to understand since MPs composition dictates their physicochemical properties, including surface chemistry, density, crystallinity and the presence of additives. Crystallinity is a key property of polymers that influences the density of MPs (Ahmed *et al.* 2022). For instance, PP and PE are semi-crystalline polymers with densities lower than that of water. However, the MPs crystallinity evolves with weathering and aging, subsequently affecting other physicochemical properties such as particle size, shape, pollutant sorption capacity and additive leaching. Environmental MPs exhibit various sizes and shapes including flakes, lines, ellipses, particles, foam, films, fragments, pellets and fibres as reported in the literature (Figure 2) (Lares *et al.* 2018; Hidayaturrahman and Lee 2019).

Table 1: The structural composition of MPs and their molecular formula

MP	Structure	Molecular formula
PE	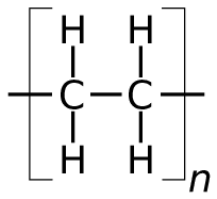	$(C_2H_4)_n$
PS	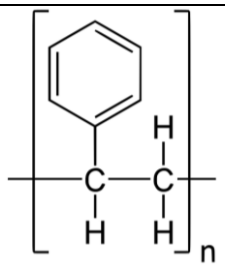	$(C_8H_8)_n$
PP	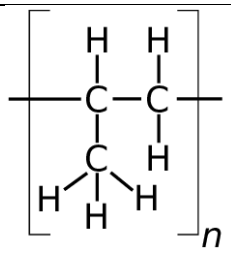	$(C_3H_6)_n$
PUR	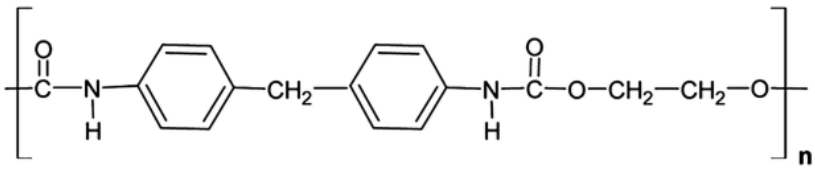	$C_{27}H_{36}N_2O_{10}$
PA	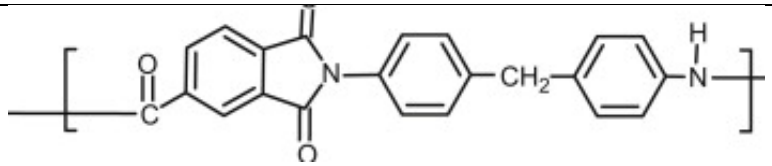	$(C_6H_{11}NO)_n$
PET	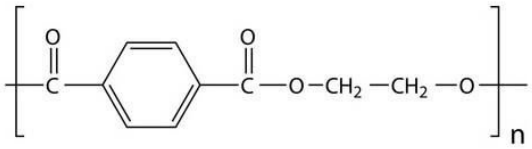	$(C_{10}H_8O_4)_n$

PES	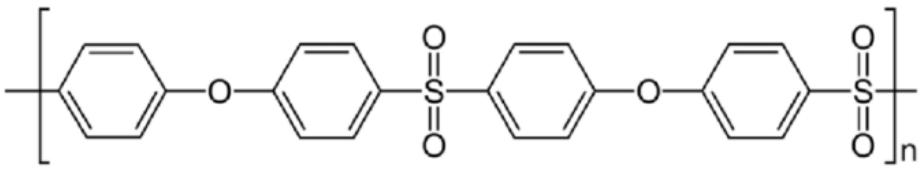	$(C_{12}H_8O_3S)_n$
PVC	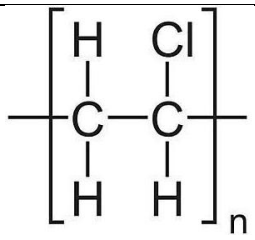	$C_2H_3Cl.$

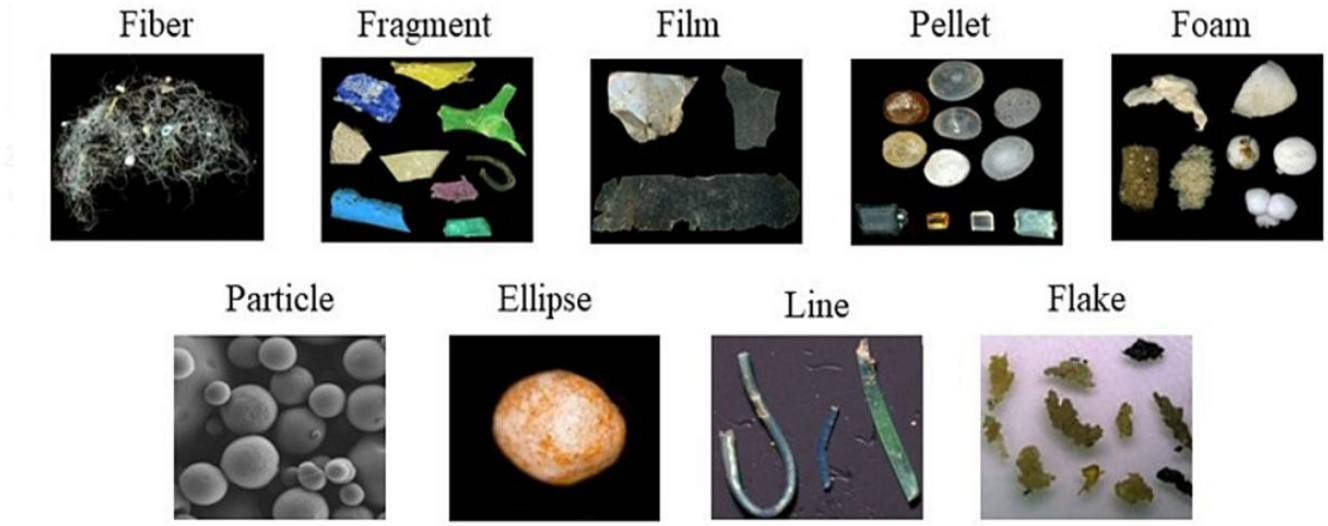

Figure 2: Categories of predominant MP forms (Veneral *et al.* 2023), Reproduced with permission from Elsevier

2.3. Source of microplastics

MPs are mainly produced in industrial settings and are released directly as small particles (Osman *et al.* 2023). Common consumer and industrial products such as cosmetics, hair care and skin care products, scrubbing agents in toiletries, deodorants, inks, and paints are significant sources of primary MPs as seen in Figure 3. Personal care items containing microbeads, such as toothpaste, shower gels, and facial cleansers, also contribute substantially

(An *et al.* 2020). These intentionally produced MPs are designed for specific uses, including personal care products and synthetic textiles.

Additionally, MPs can form from the breakdown of larger plastic materials through processes like fragmentation, aging, or weathering, resulting in secondary MPs (Sharma *et al.* 2021). These secondary MPs originate from the unintentional degradation of larger plastics due to chemical, physical, or biological stress, leading to their fragmentation (Figure 3). This process can introduce MPs into various aquatic and terrestrial ecosystems (Paul *et al.* 2020). The breakdown of polymers occurs through complex processes, often involving weathering and aging. Notable sources of secondary MPs include the fragmentation of plastic debris such as synthetic fibers, tires, and coatings (Paul *et al.* 2020). MPs such as PS, PE, and PP originate from primary plastic products like plastic bottles, clothing, and food packaging (Lares *et al.* 2018). Similarly, PES, PA, and PET MPs are derived from textiles in the fashion industry (Hernandez *et al.* 2017). Additionally, MPs can be unintentionally produced as secondary pollutants through human activities. For instance, Hartline et al. (2016) discovered that home washing machines release 1471–2121 microfibers per garment. Other significant sources include tire wear, vehicle transport, road markings, and brake wear, contributing approximately 0.81 kg per person annually (Hartline *et al.* 2016). Artificial turf is another source, emitting between 760 and 4500 tons of MPs each year (Kole *et al.* 2017). These produced MPs can enter water bodies, the terrestrial environment and atmosphere.

Figure 3: MPs derived from primary sources that are discharged directly and secondary sources that are created indirectly as a result of macroplastic debris disintegration (Borah *et al.* 2023), Reproduced with permission under a Creative Commons License, License CC BY 4.0 from (Borah *et al.* 2023)

2.4. Occurrence of microplastics in different environments

MPs ubiquity has placed them in various environmental systems, including the atmosphere, lithosphere and hydrosphere. Freshwater ecosystems, in particular, serve as significant sinks for MPs (Strungaru *et al.* 2019). A survey of Lake Huron in Canada revealed the presence of MPs along its shorelines (Zbyszewski and Corcoran 2011). Recent studies have reported diverse concentrations of MPs in river systems across Europe, Asia, North America and Australia (Ahmed *et al.* 2022). Littering on land significantly contributes to MP contamination in terrestrial environments (Hurley and Nizzetto 2018). This encompasses the illegal or improper disposal of industrial byproducts, activities related to recreation, runoff from wastewater treatment plants, waste from the plastic manufacturing industry, and street littering (Bowmer and Kershaw 2010). Additionally, plastics are found in various waste streams,

including industrial, agricultural, demolition, municipal, and construction wastes. In 2010, coastal countries generated 275 million tonnes of plastic waste (Jambeck *et al.* 2015). Terrestrial MP contamination also results from the application of sewage sludge as fertilizers (Corradini *et al.* 2019). Sewage sludge and organic composts can contain up to 15,385 MP particles per kilogram and 1200 milligrams per kilogram of MPs, respectively (Bläsing and Amelung 2018). Terrestrial environments also contain MPs from sources such as agricultural runoff, landfills, and other human activities, with an estimated 4–23 times higher MPs loading than marine systems (Horton *et al.* 2017a; Xu *et al.* 2020). Almost 80% of MPs originates on land (Lamichhane *et al*. 2023) and of this a great majority enter various water bodies. Additionally, MPs have been increasingly documented in the atmosphere (Allen *et al.* 2019). MPs are released into the atmosphere through various means, including transportation, industrial activities, and aerosol emissions. Wind can also disperse MPs from the ground into the air (Abbasi *et al.* 2019). Due to their low density and small size, MPs are easily transported through the air (Liu *et al.* 2019b). These particles often become mixed with water vapor or rain once they enter the atmosphere and subsequently fall onto land or into water bodies during precipitation (Klein and Fischer 2019). For instance, a study in Greater Paris found an average of 118 particles per square meter per day settling from the atmosphere (Dris *et al.* 2015). Additionally MPs have been found in living organisms such as fish, turtles, crabs and copepods (Rossatto *et al.* 2023). Table 2 summarizes recent reports on the occurrence and concentration of MPs in biota, sediment, soil and water.

Table 2: MPs global concentration in various countries

Country	Medium	Concentration [a]	Reference
Australia	Industrial soil	300–67,500 mg/kg	(Fuller and Gautam 2016)
Switzerland	Floodplain soil	<593 MPs/kg	(Scheurer and Bigalke 2018)
Germany	Farmland soil	0–1.25 MPs/ kg	(Piehl *et al.* 2018)
Chile	Soil	0.6–10.4 MPs/ g	(Corradini *et al.* 2019)
Pakistan	Soil	4483 ± 2315 MPs/kg	(Rafique *et al.* 2020)
Pakistan	Rawal lake water and sediments	Sediment = 104 MPs/kg; Water = 1.42 MPs/L	(Irfan *et al.* 2020b)
Pakistan	Urban surface water system	Sediment = 40,536 ± 202 MPs/m^2 ; Water 16,150 ± 80 MPs/m^3	(Irfan *et al.* 2020a)
India	Beach sediments	200–1150 MPs/kg	(Yaranal *et al.* 2021)
India	River	Indus river = 525–1752 MPs/kg; Brahmaputra river = 531–3485 MPs/kg	{Tsering, 2021 #983
North Carolina and Virginia, USA	Beach sediment	Dry sediment = 600–2200 MPs/kg	(Dodson *et al.* 2020)
Central Florida, USA	Birds of prey	1197 plastic pieces	(Carlin *et al.* 2020)
Mississippi Sound, USA	Surface water	12 to 381 MPs/L	(Scircle *et al.* 2020)
California, USA	Surface water	700,000 MPs/km^2	(Sutton *et al.* 2016)
California, USA	Jacksmelt	0.5 ± 1.4 MPs/ individual	(Rochman *et al.* 2015)
South America	Fish	18.5 ± 18.9 MPs/ individual	(Pazos *et al.* 2017)

China	Soil	7100–42,960 MPs/kg	(Zhang and Liu 2018)
East Cina Sea	Blue Mussel	2.5 g/L	(Kolandhasamy *et al.* 2018)
Austrailia	Fish and Shrimp	24 ± 31 MPs/g	(Nan *et al.* 2020)
China	Omnivorous and carnivorous fish	3 to 6.8 MPs/ individual	(Wang *et al.* 2021c)
China	Fish, crustacean, mollusks and sandworms	0.83 ± 0.99 to 3.87 ± 2.18 MPs/individual	(Wang *et al.* 2021a)
South Africa	Salt	1.33 ± 0.32 particles/ kg	(Fadare *et al.* 2021)
Vietnam	Surface water and sediment	0.35 to 2522 items/m^3	(Strady *et al.* 2021)

a-concentrations are in different units

2.4.1. Microplastics in aquatic environments

Primary sources of MPs in aquatic environments include residential sewage discharge of polymeric products such as packaging materials, plastic pots, personal care products, raw materials for manufacturing plastic goods, air blasting, and commercial discharges (Jiang 2018). Additionally, sources like plastic pellets, fishing gear, and building paints are estimated to release between 1,000 and 80,000 tons of MPs into surface water bodies annually (Vivekanand *et al.* 2021). MPs concentration in various aquatic systems such as lakes, rivers, and freshwater fish can reach up to 9,000 particles per cubic meter, with higher numbers reported in subtropical regions (Wang *et al.* 2017b). The primary reason for the high concentration of MPs in aquatic environments is due to improper solid waste management practices (Ahmed *et al.* 2022). For instance, in 2016, the European Union collected approximately 27.1 million tons of plastic waste, of which 41.6% was reused, 31.1% was recycled, and 27.3% was sent to landfill sites (Kumar *et al.* 2021c). This mismanagement

exacerbates the problem of plastic pollution in the environment. Approximately 80% of the plastic debris detected in marine environments comes from these terrestrial sources (Dris *et al.* 2015). There are indications that MPs particularly accumulate in rivers, lakes, and other small water bodies due to direct pollution. As water flows from rivers to coastal areas, the concentration of MPs decreases because they get diluted along the river's course. This suggests that rivers and inland water bodies are transporting MPs to offshore environments (Luo *et al.* 2019). Consequently, it is important to monitor water bodies as interconnected systems rather than in isolation. Additionally, various types of water bodies contain different kinds of MPs with varying morphologies, influenced by their distinct hydrological characteristics. For instance, MPs are often found in higher densities in river waters since the water flow tends to resuspend these particles rather than allowing them to settle (Nizzetto *et al.* 2016a).While most MPs originate from land-based sources, wastewater treatment plants (WWTPs) significantly contribute to MP pollution (Sun *et al.* 2019). It is estimated that 25% of primary MPs in the oceans are released from wastewater treatment systems (Boucher and Friot 2017), making these WWTPs a major contributing source of MPs

2.5. Hazardous effects of microplastics on aquatic life and human health

MPs have increasingly been recognized as a significant environmental threat, particularly impacting aquatic fauna and flora (Cole *et al.* 2011; Yadav *et al.* 2022; Shi *et al.* 2023). Research on freshwater microalgae has shown that exposure to MPs can alter gene expression and certain metabolic pathways, as well as cause various physical damages and oxidative stress to algae cells (Lagarde *et al.* 2016). MPs adhere to algae cell surfaces, leading to potential blockages in light absorption and gas exchange (Bhattacharya *et al.* 2010). This phenomenon was observed in *Chlorella* and *Scenedesmus* sp, where the accumulation of positively charged plastic nanoparticles on their surfaces reduced photosynthetic activity (Bhattacharya *et al.* 2010).

Marine organisms at different trophic levels can ingest MPs (Tanaka and Takada 2016). Most marine organisms acquire MPs from seawater or from lower trophic levels (Barboza *et al.* 2018). Various aquatic species, including bivalves, fish, zooplankton, benthic invertebrates, and large marine mammals, are reported to ingest MPs (Su *et al.* 2016). MP ingestion depends on the particle size and, to some extent, the physiological and behavioural characteristics of marine vertebrates and invertebrates (Horton *et al.* 2017b). Numerous ecotoxicological effects of MPs have been documented across various groups of aquatic organisms, as shown in Figure 4. In aquatic microorganisms, MPs can enter the circulatory system (Shi *et al.* 2020). Once ingested, MPs can penetrate cells and remain in tissues. For example, in the hemolymph of blue mussels (M. edulis), particles as small as 9.6 μm have been recorded (Peng *et al.* 2020). Recent studies have also reported adverse effects in *Girella* fish (*Girella laevifrons*), including circulatory disorders, inflammation, and alterations in intestinal tissues (Ahrendt *et al.* 2020). MP toxicity has also been linked to lipid accumulation in the liver and inflammation in zebrafish (Lu *et al.* 2016). A recent study on *Physalaemus cuvieri* tadpoles showed that exposure to PE MPs, combined with other pollutants, led to various biochemical and physiological responses (Bobori *et al.* 2022b, 2022a).

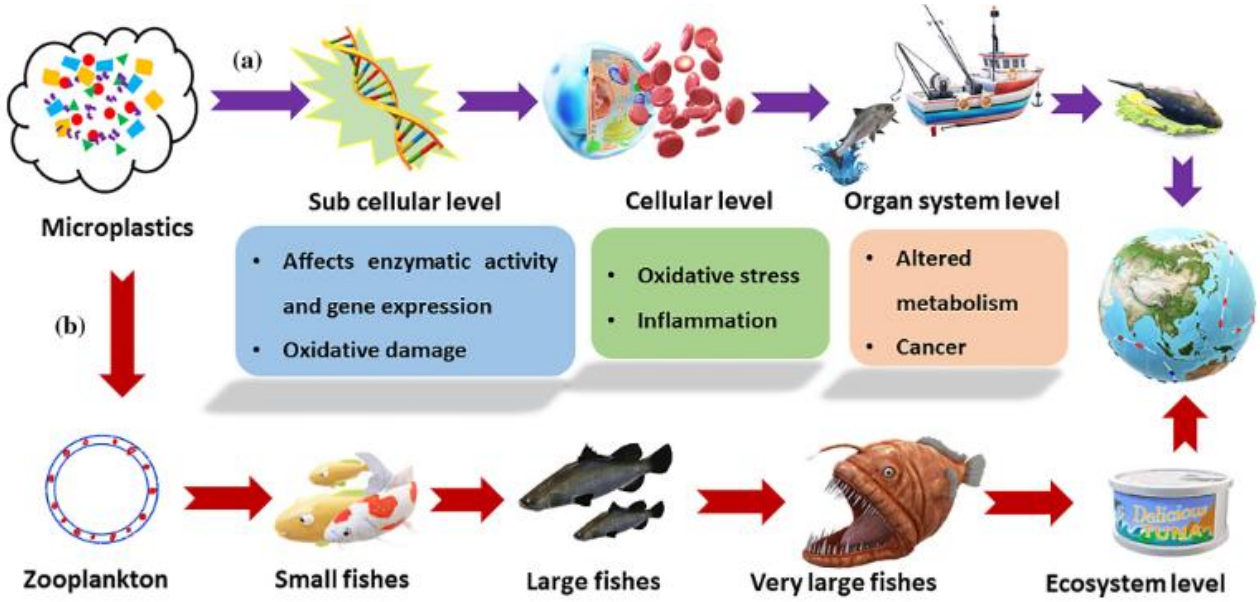

Figure 4: Diagram illustrating the movement of MPs: (a) transfer of MPs from the molecular to the ecosystem and (b) MPs ingestion from decreasing to increasing trophic levels (Borah *et al.* 2023), Reproduced with permission under a Creative Commons License, License CC BY 4.0 from (Borah *et al.* 2023)

MPs can accumulate in humans through various pathways. Seafood such as fish, marine animals, and microalgae are primary sources of MPs in the human diet (Li *et al.* 2020c; Walkinshaw *et al.* 2020). Additionally, different brands of salt, which provide essential nutrients and act as food preservatives, have been found to contain MPs. Between 2015 and 2018, a study found MPs in 128 brands of commercial salt, indicating the extent of MP contamination in the food chain (Peixoto *et al.* 2019; Pironti *et al.* 2021).. Herein, various human cell lines that represent tissues or cells were directly or indirectly exposed to PE MPs. Both sizes of PE-MPs increased nitric oxide levels in all cell lines and induced reactive oxygen species generation in THP-1, Jurkat, and U937 immune cell lines. A pro-inflammatory cytokine response was observed in HaCaT keratinocyte cells exposed to PE-MPs (Gautam *et al.* 2022). Additionally, once ingested, MPs can reach internal organs such as the kidneys and liver, causing adverse cellular effects. For example, a study examined toxicological impacts of 1 μM PS-MPs on human embryonic kidney (HEK 293) cells and human hepatocellular (Hep G2) liver cells (Goodman *et al.* 2022). Exposure to PS-MPs significantly reduced cellular proliferation. Over 70% of cells internalized 1 μM PS-MPs after 48 hours of exposure in both kidney and liver cells. Moreover, exposure to PS-MPs lead to cellular stress. These findings suggest that MP ingestion could lead to toxicological issues affecting cell metabolism and cell-cell interactions (Goodman *et al.* 2022).

2.6. Major routes of microplastic pollution in aquatic habitats

Aquatic microplastic pollution can be categorized into five major sources: fishing activities, hydro fluctuation belt, rainfall runoff and storm effect, sewage discharge and wastewater treatment plants (WWTPs) (Ashrafy *et al.* 2023).

2.6.1. Sewage discharge

MPs that are approximately 250 µm, are commonly found in various personal care products such as cosmetics, which may contain microbeads (0.5–5%) (Decker and Graber 2012; Chang 2015). Napper et al. (2015) revealed that a single use of an exfoliating wash can release between 4,500 and 94,500 microbeads (Napper *et al.* 2015), while approximately 4,000 microbeads are released from just one use of toothpaste (Carr *et al.* 2016). In addition to microbeads, synthetic fibers from textiles are found in most water bodies. Around 35% of these fibers are estimated to originate from synthetic fabrics (Boucher and Friot 2017). In Finland, it is estimated that washing machines release between 154,000 and 411,000 kg of microfibers annually, with fibers ranging from 10–20 µm in thickness and 100–1,000 µm in length (Sillanpää and Sainio 2017). Other products, including detergents, facial cleansers, jewellery, small buttons, glitter and other daily-use products (Gong and Xie 2020), also release MPs into wastewater systems. Furthermore, industrial wastewater is a significant source of MPs, which can originate from materials used for air blasting, styrofoam, pre-production plastic pellets, and synthetic textile production (Ashrafy *et al.* 2023). Sewage discharge contributes greatly to the introduction of MPs into marine ecosystems.

2.6.2. Rainfall runoff and storm events

Rainfall runoff is a key pathway for transporting tire and road wear particles into surface water (Kole *et al.* 2017). During storm events, untreated sewage containing MPs can overflow into aquatic systems (Yano *et al.* 2021). Researchers have recently explored how storms and floods

contribute to the movement of MPs into waterways and oceans (Gündoğdu *et al.* 2018). Common polymer types identified in stormwater runoff include PS, PVC, PP, PE and PET (Yano *et al.* 2021).

2.6.3. Hydro-fluctuation belt

The hydro-fluctuation belt (HFB), a strip of land along the edges of reservoirs, has been identified as a zone where MPs accumulate, particularly during periods of low water levels. The HFB serves as a potential conduit for the transport of MPs into nearby water systems, as MPs sink when water levels drop (Ashrafy *et al.* 2023).

2.6.4. Fishing activities

Fishing and other maritime activities are significant sources of MP pollution in aquatic environments (Zhao *et al.* 2015). Fishing debris, including ropes, fishing lines, floats, and buoys, often end up in marine ecosystems, where they eventually degrade into MPs. These materials pose serious threats to fish, mammals, and benthic environments (Prata *et al.* 2019).

2.6.5. Additional routes

Rather than coming from water-based sources, most plastics, or MPs, discovered in aquatic habitats come from land-based sources. The primary cause of MP pollution is human activity, which is heavily reliant on the everyday use of plastic products (Kershaw *et al.* 2019). Majority (98%) of primary MPs are said to come from land-based activities, and only 2% are said to come from ocean-based activities. MPs typically infiltrate aquatic habitats through inadequate waste management, unlawful dumping, and unavoidable discharges such those that occur during construction, recreation, farming, industrial activities and home consumption (Boucher and Friot 2017).

In both terrestrial and aquatic settings, agricultural practices such as the use of plastic film and organic fertilizers constitute a significant source of MP contamination (Nizzetto *et al.* 2016b;

Corradini *et al.* 2019). Globally, agricultural land has been covered with plastic mulching, which may be a source of MPs in both the terrestrial and aquatic environments (Piehl *et al.* 2018; Astner *et al.* 2019).

The concentration of MPs on popular beaches is mostly a result of the tourism sector. Travelers are a major source of the plastic bottles, food packets, plastic cups, and straws that end up in the waterways. Most people are ignorant of the detrimental consequences of MP contamination, and even those who are aware are seldom concerned about reducing it. MPs in drinking water is a significant issue that receives little attention. This is concerning since it is likely the route by which MPs are directly exposed to humans (Eerkes-Medrano *et al.* 2019).

2.6.6. MPs in wastewater treatment plants

Initially, WWTPs were not explicitly designed for the removal of MPs; however, each treatment stage in WWTPs can effectively remove a certain proportion of MPs. Sun et al. (2019) recently compiled data on MP removal efficiencies across different countries, outlining estimated removal rates for each treatment phase (Sun *et al.* 2019) (Figure 5).

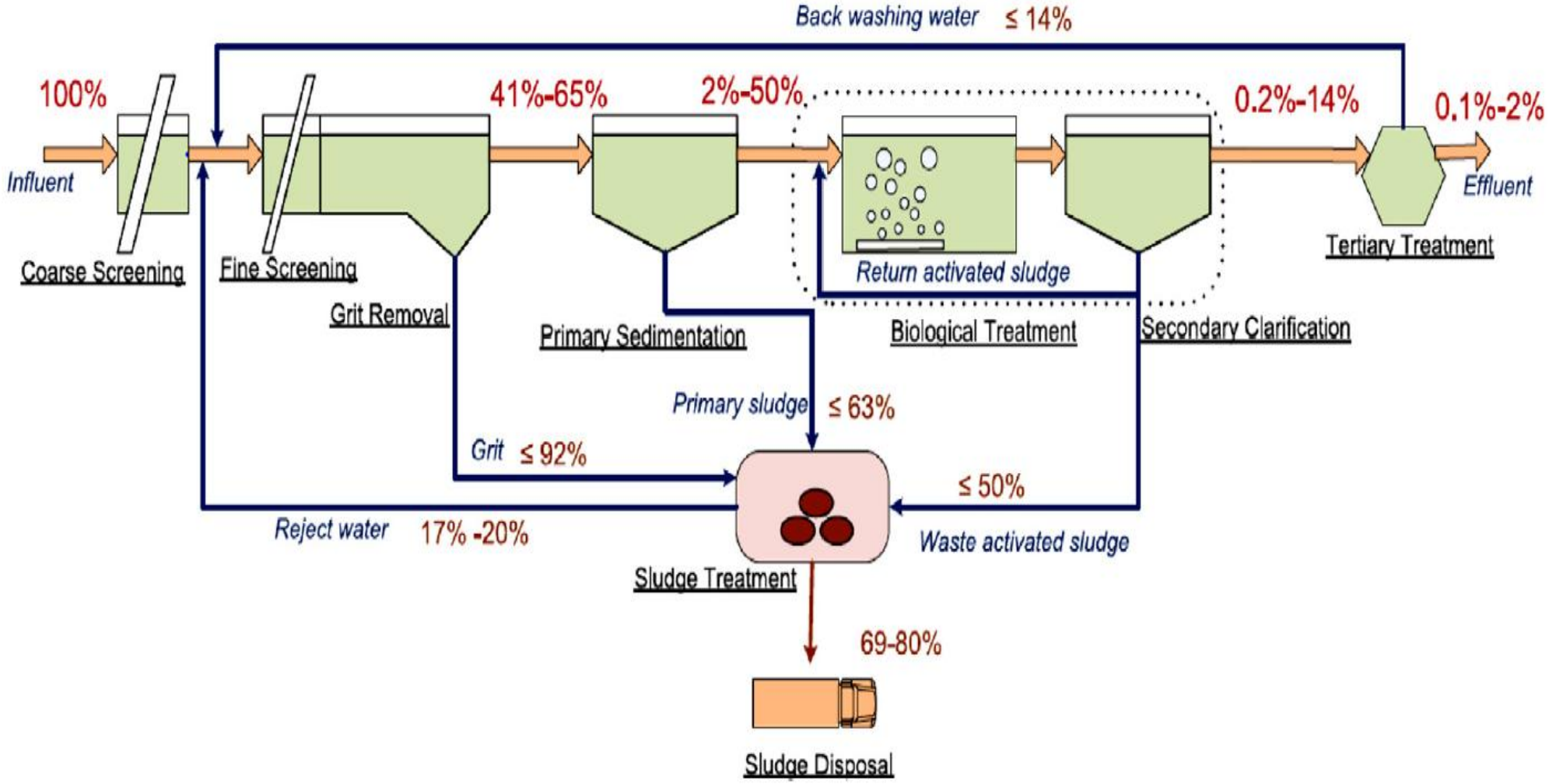

Figure 5: MPs journey through a WWTP displaying primary, secondary and tertiary treatment processes (Sun *et al.* 2019), Reproduced with permission from Elsevier

Conventional WWTP processes typically involve preliminary/primary, secondary, and tertiary treatments. In preliminary and primary treatments, approximately 35 to 59% and 50 to 98% of MPs are respectively removed (Sun *et al.* 2019). Air flotation aids in the removal of contaminants, particularly low-density MPs, by causing them to float to the surface for mechanical skimming. Subsequent sedimentation processes capture high-density MPs within solid flocs during grit removal and sedimentation for further sludge treatment (Ngo *et al.* 2019). The distribution of MPs between floating and sediment-bound forms is heavily influenced by their density; lower-density MPs like PA, PP, and PE tend to float, while higher-density MPs such as PET and PES are more likely to settle in sediment (Ngo *et al.* 2019). In the secondary treatment stage, MPs can be further reduced by 0.2 to 14% through biological treatment and sedimentation processes. Sludge flocs and bacterial extracellular polymers aid in accumulating and sinking MPs within the clarification tank, effectively removing larger MPs (Sun *et al.* 2019). Subsequently, tertiary treatment techniques further decrease MP presence to between 0.2 to 2%. Talvitie et al. (2017) compared the performance of various tertiary treatment methods such as disc filters, membrane bioreactors (MBR) dissolved air flotation and rapid sand filtration. Herein, it was concluded that MBR possesses the greatest removal efficiency (99.9%) (Talvitie *et al.* 2017). MBR also holds more promise as a technique in comparison to other membrane technologies such as reverse osmosis (RO), ultrafiltration (UF), dynamic membrane technology (DM), and (Poerio *et al.* 2019).

Concerns have been raised regarding the detrimental effects of MPs on biological treatment processes, impacting aerobic and anaerobic processes such as hydrolysis-acidification, methane and hydrogen production, and waste activated sludge digestion. Studies have shown that MPs like PET, PVC, PE, and PS introduce oxidative stress and various toxic substances such as heavy metals, persistent organic pollutants (POPs), additives and antibiotics which can inhibit enzymes and reduce cell viability (Wei *et al.* 2019; Wei *et al.* 2020; Hu *et al.* 2021).

Experiments demonstrated negligible impacts on nitrogen and phosphorus removal by ammonium-oxidizing bacteria (AOB), nitrite-oxidizing bacteria (NOB), denitrifiers, and polyphosphate-accumulating organisms (PAOs) despite the presence of MPs (Liu *et al.* 2019a), suggesting varying effects of MPs on different biological treatment processes even within the same type.

In tertiary treatments, researchers have investigated how MPs affect processes such as coagulation, MBR, UF, RO, and flocculation. For instance, the presence of PVC MPs hindered organic matter and ammonia removal in MBR systems due to membrane fouling (Li *et al.* 2020b). Similarly, irregular MPs can cause membrane wear in UF and RO processes (Zhang and Chen, 2020). Moreover, in the coagulation process, MPs can diminish the effectiveness of flocculants by interacting with salt flocculants due to their negative charge (Perren *et al.* 2018; Zhang and Chen 2020). Zhang and Chen (2020) conducted a comprehensive review on the effects of MPs on each segment of WWTPs.

During the WWTP process, MPs may be degraded into much smaller particles known as NPs, which are difficult to remove and detect. In addition, even a very modest amount of MPs released per litre of effluent can result in significant concentrations of MPs being released into the environment (Karapanagioti and Kalavrouziotis 2018). As a result, WWTPs are one of the most significant pathways for MPs entering aquatic environments. For example, Gies and teammates investigated the retention of MPs in a WWTP in Vancouver, Canada and revealed that a staggering ~1.76 trillion MPs per year enter the urban WWTP. In their investigation, it was revealed that 99% of the MPs that entered the WWTP were removed. However, due to the extremely large volumes, the 1% of MPs discharged into the environment equated to an astounding 30 billion MP particles per year being released into the sea (Gies *et al.* 2018). Therefore, there is an urgent need for rapid research and development in the area of MP removal from wastewater.

2.7. Application of nanomaterials for the removal of microplastics from water matrices

Presently, a plethora of treatment and removal technologies have been explored to ameliorate the removal of MPs/NPs. This includes thermal treatment, microbial degradation and physical methods such as filtration and adsorption (Goh *et al.* 2022). Recently, technological innovations in the form of NMs have risen as cutting-edge technology utilised at the forefront of various pollutant removal strategies (Chen *et al.* 2023; Hao *et al.* 2023; Wang *et al.* 2023; Wu *et al.* 2023). NMs have been developed and implemented as a mitigation strategy for the removal of MPs and NPs, among various other pollutants (Yeganeh *et al.* 2024). A NM is a material of which a single unit has a size of between 1 to 100 nm in at least one dimension (Buzea *et al.* 2007; Khalil *et al.* 2015). Thus, the use of NMs could strengthen the development of next-generation water supply systems. Remarkable features of nanoengineered materials generally include excellent mechanical properties, high surface area, recyclability, greater chemical reactivity, functionalisation, lower energy and cost requirements, and can be easily fabricated (Kokkinos *et al.* 2020). These attributes make NMs suitable for effective hydric remediation, removal and treatment of MPs/NPs (Kokkinos *et al.* 2020; Chellasamy *et al.* 2022). Thus far, a number of studies have been reported on the elimination of MPs/NPs via innovative combinations of NMs and bioremediation (Chellasamy *et al.* 2022). Consequently, the primary aim of this critical review is to enable the reader to gain sufficient knowledge to guide their selection of a suitable synthesis method for designing novel NMs for MPs/NPs removal from wastewater. In this review, we discuss the types of NMs that have the potential to remove MPs from water bodies, their mechanisms of action, and the properties of NMs and MPs/NPs that facilitate their interaction. In addition, the effects of water characteristics on MPs/NPs and NMs are explored, along with novel synthesis methods that will assist in removing MPs/NPs from wastewater.

2.7.1. Types of nanomaterials with microplastic removal potential from different water bodies

The removal of MPs and NPs by NMs has been documented in a limited number of studies in wastewater and drinking water treatment.(Li *et al.* 2018a). Table 3 summarize studies of different NMs and their reduction performance of specific MPs mainly at bench-scale with various water matrices. Studies involving the removal of MPs by NMs have primarily been conducted in seawater and synthetic water. This is useful for extrapolating the removal of MPs/NPs from wastewater, using synthetic and seawater as a starting point. As a consequence, this highlights the need for studies to be conducted using actual wastewater samples in order to provide a more realistic assessment of MPs/NPs removal from wastewater. For the seawater matrix, modified Fe-hexadecyltrimethoxysilane (Fe-HDTMS) nanoparticles and Fe_3O_4 nanoparticles are the most used. For Fe-HDTMS in seawater the MP removal efficiencies ranged from 59 to 100 % (Grbic *et al.* 2019). This reduction range can potentially be attributed to differences in size of the MPs as well as variation in the chemical composition of the MPs. Furthermore, the adsorption affinity to the hexadecyltrimethoxysilane NM between the specific MPs could vary depending on their surface chemistry. It can be hypothesised that the differences in the removal efficiencies might also be related to the fact that the sea water composition differed among the experiments because they were conducted in different geographical locations.

For the synthetic water matrix, Mn decorated N-doped Carbon nanotubes, 3D-reduced Graphene Oxide, UiO-66-OH Metal-Organic-Framework, and Graphene oxide functionalised OC_3N_4 nanoparticles were used for the removal of different types of MPs with low to varying removal efficiency (33-90.6%) (Kang *et al.* 2019; Chen *et al.* 2020; Sun *et al.* 2021). The water pH is critical since it determines the surface charge of the NM (Diao *et al.* 2022). This further

depends on both the exposed positive and negative molecules and the isoelectric points on both the MPs as well as the NM. The NM surface became positively charged in the experiments of Ray and team (Ray *et al.* 2020) since the e^- lone pairs behave as proton acceptors, and thus will repel the positively charged MPs, therefore, exhibiting decreased affinity to MP/NP adsorption and vice versa for a negatively charged MP/NP. However, no optimum range of pH is known to facilitate maximum MP removal.

Table 3: NMs and their removal efficiencies of specific MPs from different matrix's

MP type	Nanomaterial type	Matrix	Removal efficiency (%)	Level of the study	Reference
Cosmetic product-extracted MP	Mn decorated N-doped CNT	Synthetic water	50%	Laboratory scale batch experiments	(Kang *et al.* 2019)
PET, PE, PA	Magnetic CNTs	Kitchen waste treatment plant	PET, PE, PA: 100%	Laboratory scale batch experiments	(Tang *et al.* 2021)
PS, PE (size ranging from < 20 µM)	Fe-HDTMS	Seawater	PS: 88% PE: 96%	Laboratory scale batch experiments	(Grbic *et al.* 2019)
PET, HDPE, PS, PVC, PP (Size ranging from 1 mm to 8 mm)	Fe-HDTMS	Seawater	PP:96% PVC: 92% PU:105% PS: 96% HDPE: 96% PET: 74%	Laboratory scale batch experiments	(Grbic *et al.* 2019)
PE, PS, PVC, PP (Size ranging from 200 µM to 1 mm)	Fe-HDTMS	Seawater	PP: 89% PS: 100% PVC: 59% PE: 100%	Laboratory scale batch experiments	(Grbic *et al.* 2019)
PES, PE	Fe_3O_4	Seawater, Domestic sewage, Real river water	Seawater: 80.56% Domestic sewage: 82.28% Real river water: 81.333%	Laboratory scale batch experiments	(Shi *et al.* 2022b)
PS			99.9%		(Nabi *et al.* 2021)

	TiO_2 Nanoparticle film	Aqueous medium		Laboratory scale batch experiments	
PS	3D rGO	Synthetic water	72.63%	Laboratory scale batch experiments	(Yuan *et al.* 2020)
PMMA, PS, PVDF	UiO-66-OH MOF	Synthetic water	PS: Melamine/UiO-66-OH: 85.7% Melamine foam (MF): 46.7% PMMA: Melamine/UiO-66-OH: 88.2% MF: 44.1% PVDF: Melamine/UiO-66-OH: 90.1% MF: 33.0%	Laboratory scale batch experiments	(Chen *et al.* 2020)
PS	GO – OC_3N_4	Synthetic water	Chitin/GO: 89.6% Chitin/-OC_3N_4: 90.6% Chitin: 63.3%	Laboratory scale batch experiments	(Sun *et al.* 2021)

Abbreviations key: PS - Polystyrene; PE - Polyethylene; PES - Polyethersulfone; PA - Polyamide; PET -Polyethylene terephthalate; PVDF – Polyvinylidene fluoride; PMMA – Polymethyl methacrylate; PU – Polyurethane; PVC – Polyvinyl chloride; PP - Polypropylene; CNT - Carbon nanotube; HDTMS - Hexadecyltrimethoxysilane; 3D rGO – 3-Dimensional reduced graphene oxide; MOF – Metal organic framework

Nanoscale materials exhibit unique properties that can be exploited to overcome the limitations of their bulky counterparts composed of the same elements (Shandilya *et al.* 2016). One such unique feature is a large surface area displayed by NMs rendering it advantageous for photocatalysis and adsorption (Sarkar *et al.* 2023). Another characteristic of NMs is that the uptake capacity can be improved by increasing the NMs surface area, increasing the number of active sites present. This would enable an enhanced performance of full-scale treatment processes before the saturation point of the NMs is reached (Goh *et al.* 2022). Photocatalytic and adsorbent NMs have distinctive structural properties that permit the hierarchical design of nanohybrids to accomplish desirable synergistic outcomes. This enables the addition of new functional groups to the NM, hypothesised to improve MP/NP removal efficiency due to performance enhancement (Wang *et al.* 2022a). Furthermore, specific ligands may be introduced onto the NMs surface resulting in a novel selective binding of the target pollutant due to the newly reactive NM surface generated (Li *et al.* 2023). While there is a size difference between the NM adsorbents and MPs, the functionalized ligands can create chemical or electrostatic interactions that promote the adsorption process. These interactions, such as hydrogen bonding, Van Der Waals forces, or ionic interactions, can bridge the gap between the NMs and MPs, effectively facilitating their capture. Additionally, the high surface area of the nanomaterials ensures sufficient active sites are available for the adsorption process, compensating for the size disparity. This functionalization strategy is particularly beneficial in improving selectivity and efficiency in removing specific contaminants.

The studies referred to are mostly laboratory scale (small-scale) studies, so extrapolating reduction efficiencies to full-scale is difficult. High variability in MP removal between the different set-ups in the study of Chen and colleagues is evident (Chen *et al.* 2020). The diversified removal performances exhibited by the UiO-66-OH MOF vs MF in their study may be attributed to factors such as particle size (e.g., PS, ~183 nm; PMMA, ~325 nm and PVDF, ~260 nm) or zeta potentials (e.g., PMMA, -10.5 ± 2.7 mV; PS, -7.5 ± 1.2 mV and PVDF, -18.9 ± 2.3 mV) of MPs types. Another experiment was performed by Chen and team[20] using UiO-66-OH MOF to interrogate the effect of different MP particle sizes on the removal efficiency. UiO-66-OH MOF displayed almost the same removal efficiency for different particle sizes of PVDF which infers that zeta potentials may have a more critical role that particle size in MP removal efficiency. It is evident that the UiO-66-OH MOF removal efficiencies in comparison to the MF is significantly higher for each of the different MP types (PS: Melamine/UiO-66-OH: 85.7% MF: 46.7%; PMMA: Melamine/UiO-66-OH: 88.2% MF: 44.1%; PVDF: Melamine/UiO-66-OH: 90.1% MF: 33.0%). This is a clear indication of the superiority of nanohybrid materials (Chen *et al.* 2020).

Three different MP sizes were utilised in the study of Grbic and co-workers[19]. Of the large MP sizes to 8 mm), PET behaved differently from other MPs since the recoveries for PET fibres were significantly ($p < 0.05$) lower than all other MP types. It is hypothesised that this could be due to the difference in the PET fibres chemical composition and shape. The recovery rate of PU was greater than 100% as a result of the plastic fragmentation during handling and mixing. Fragmentation of the medium sized MPs was reported just as with the large MPs. It was reported that the fragmentation was most evident with PE microspheres, resulting in fragmented or deformed MP particles and exhibiting the highest recovery range of all MPs. This leads to the hypothesis that shape and chemical structure may impact recovery. The

medium MPs results are lower on average in comparison with the smaller and larger MPs. It is hypothesised that this is owing to the relatively lower surface-area to volume ratio of the medium size fraction (Grbic *et al.* 2019).

In a study by Shi and team, using artificial seawater, the removal rates of PP, PS and PE had a removal efficiency of small (~200) and large (~900) MPs that was higher than the medium (~500) MPs. A similar observation was made for the pure water system, where the removal rate of PE, PP, PS, and PET MPs was 79–94%, 80–90%, 81–93%, and 57–72%, respectively. However, the removal of PET was lower than the PS, PE and PP MPs of the same sizes. It is hypothesized that this is due to the chemical structure of the PET. Additionally, in pure water, removal efficiencies fluctuated among the different shapes of PE MPs [26]. The removal rate was 86.87 ± 6.92%, 93.09 ± 6.63%, 99.56 ± 0.68%, and 99.35 ± 1.13% to particles, fibres, films, and foams, respectively. Films exhibited a higher removal rate. This may be as a result of the large specific surface area that films display. This also shows that shape may have a role in the removal efficiency since alterations of the surface morphology can reflect the adsorption of Fe_3O_4. Different removal efficiencies of PE and PES fibres from different water bodies was received. The final removal rate of MPs in river water, domestic sewage, and seawater was 81.33%, 82.28%, and 80.56%, respectively (Shi *et al.* 2022b). There is a variation among the different matrixes. It is hypothesised that this is due to the intrinsic water characteristics differences of each water matrix.

A study by Sun and colleagues demonstrated that chitin could remove PS with an efficiency of 63.3%, and that the efficiency increased to 89.6% and 90.6% when functionalized to GO and O-C_3N_4, respectively (Sun *et al.* 2021). This increased adsorption was ascribed to the π-π interactions between the O-C_3N_4 or GO and the aromatic rings. This indicates that adding functional groups GO and O-C_3N_4 can significantly improve the chitins sponge adsorption

effect (Sun *et al.* 2021). Therefore, it is possible to conclude that adding the correct functional groups may improve the adsorptive properties and contribute to the development of a stronger nanoadsorbent.

All aforementioned NMs exhibit a clear affinity for MP/NP remediation. The removal efficiencies of NMs, therefore, demonstrate significant potential for enhancing their performance in removing different pollutants. Based on the current studies on NMs, further improvements can be achieved by modifying them to enhance the removal of MPs. This can be accomplished by synthesizing novel NMs with the objective of improving MP removal efficiency.

2.8. Interaction mechanisms between microplastics and nanomaterials

This chapters primary focus on the removal of MPs/NPs by NMs underscores the importance of comprehending the interaction mechanisms between NMs and MPs/NPs that facilitate their removal. Understanding these mechanisms is crucial to effectively harnessing NMs for efficient pollutant removal. However, studies that report on the interaction mechanism for the removal of MPs by NMs are limited. Therefore, only a few studies have been included since an interaction mechanism has been hypothesised or reported between a NM and MP in each study. The interactions between metal-based synthetic nanoparticles such as Cu-, TiO_2-, ZnO-, Ce- and Ag-nanoparticles and MPs have been assessed under laboratory scale conditions and will be elucidated in detail below (Li *et al.* 2020a; Li *et al.* 2020d; Li *et al.* 2020e; Ho and Leung 2021; Singh *et al.* 2021a; Singh *et al.* 2021c). Another interaction mechanism that has been reported is between 3D reduced graphene oxide (3D rGO) and MPs which will also be elucidated in detail below(Yuan *et al.* 2020).

The adsorption function of 3D rGO is due to the large specific surface area with several active sites which adsorbed the PS MPs tightly on both the surface and edge. 3D rGO's smooth

graphitic layer generates a π-π force, which will easily adsorb organic pollutants housing π-electrons which is displayed by PS. Hence, the adsorption mechanism revealed in their study was attributed to be the π-π interaction between the benzene ring of the PS and the carbon ring of the 3D rGO by electrostatic interaction which generated a stable complex (Figure 6). Furthermore, they were able to determine that the adsorption of these MPs was a spontaneous endothermic procedure through thermodynamic assessment. The studies were made in both lake water and tap water (Yuan *et al.* 2020) which highlight the potential that these 3D rGO NMs display to be utilised in different water body types for PS MP reduction.

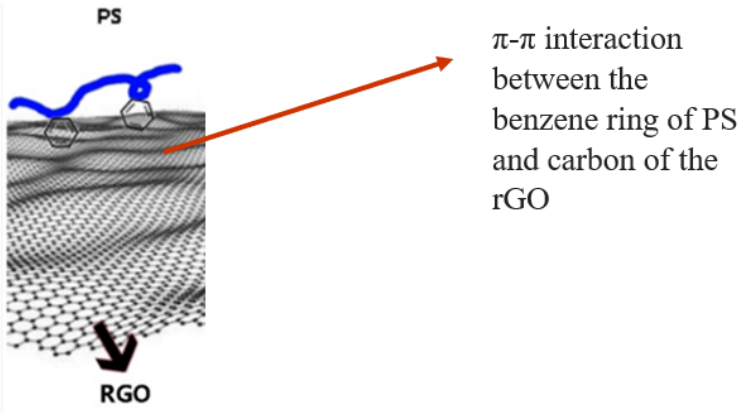

Figure 6: Schematic of π-π interaction between reduced Graphene Oxide and Polystyrene (Li *et al.* 2025). Amended with permission under a Creative Commons License, License CC BY 4.0 from (Li *et al.* 2025). Copyright 2018 MDPI

Further interaction mechanisms elucidated have all been between metal-based NMs and MPs/NPs. These studies (Li *et al.* 2020a; Li *et al.* 2020d; Li *et al.* 2020e; Ho and Leung 2021; Singh *et al.* 2021a; Singh *et al.* 2021c) reported a reduction in MPs and NPs large surface energy as a result of the physical interactions amongst them which lead to aggregation and additional interactions such as electrostatic interactions (Simmons *et al.* 2006). In particular, Li and colleagues investigated the interactions between citrate-coated silver nanoparticles (CC-AgNPs) with three different MPs (PS, PE and PP) in aquatic environments (ultra-pure water)

but did not find any significant interaction between the CC-AgNPs and the PE and PP MPs. However, they were able to uncover a mechanism of interaction between the CC-AgNPs and PS since the PS was able to interact with the CC-AgNPs in solution under laboratory conditions (Figure 7). Due to this interaction, the AgNPs were easily captured by the PS at lower mass ratios. The researchers also suggested that surface area and reticular formations, to some degree, influence the interactions between NMs and MPs. This is attributed to their report of PS displaying a larger surface area than that of PE or PP as well as PP and PE exhibiting smooth surfaces whilst PS showcased reticular formations. They postulated that as a result of increased aromaticity induced by the benzene ring, PS interacted with CC-AgNPs *via* π-π interactions. Additionally, the interaction was attributed to the presence of the phenyl group that endows available sites (π-π interactions) and occurrence of electrostatic interactions for the adsorption of CC-AgNPs on PS surface (Figure 7). This transpired due to a strong polar-polar interaction since the coated citrates are polar compounds and the PS polarity was increased by the phenyl group (Li *et al.* 2020d). The capture process is attributed to a monolayer adsorption and these findings demonstrate the complexities of the adsorption of AgNPs onto MPs.

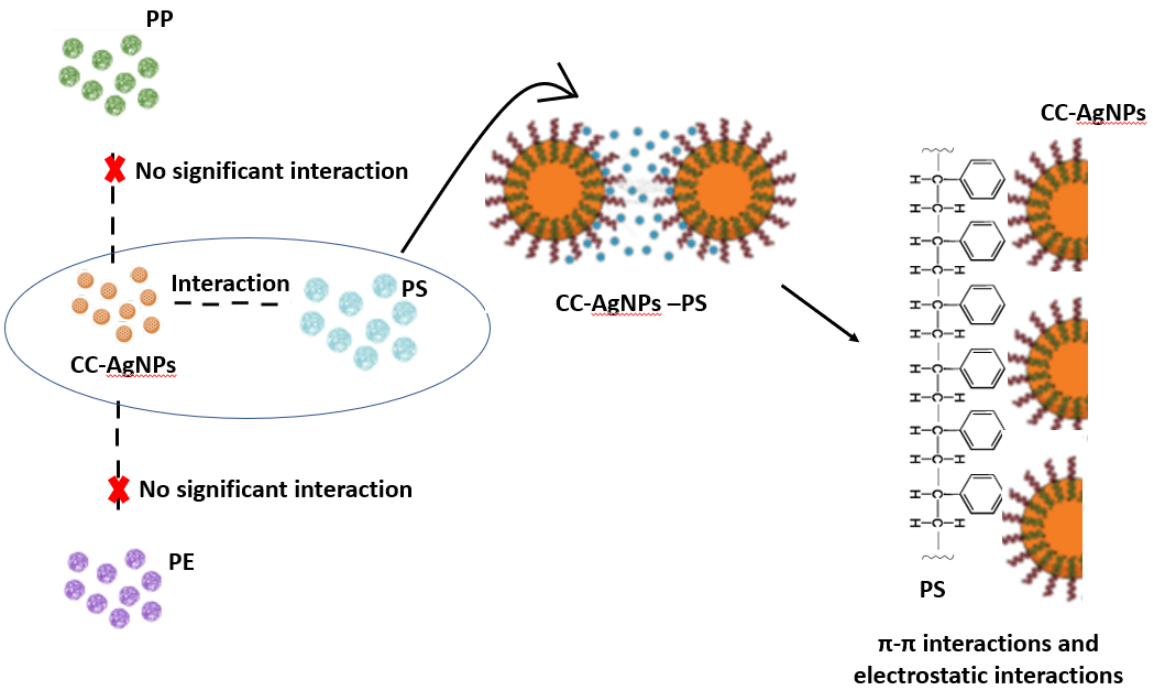

Figure 7: Schematic illustration of mechanism of action between CC-AgNPs and PS

Another study (Li *et al.* 2020e) investigated the heteroaggregation behaviour and mechanism of interaction between PS-NPs and cerium dioxide nanoparticles (CeO_2-NPs) in natural waters and synthetic medium. The study utilized PS-NPs with different surface properties (No surface properties, sulfonic, epoxy, amine and carboxyl) and CeO_2-NPs in an array of different surface water bodies such as ground, lake, rive and sea water. Herein it was hypothesised that there would be different heteroaggregation kinetics between PS and CeO_2-NPs due to the surface functionalisation of the PS and the surface waters complex physiochemical properties. The underlying interaction forces between CeO_2-NPs and the PS with differential functional groups were revealed through the evaluation of CeO_2-NPs influence on the aggregation kinetics of PS-NPs with different surface charges. It was also found that the PS-NPs critical coagulation concentrations depended on their surface coatings which exhibited a reduction in the presence of CeO_2-NPs. This was attributed to specific adsorption and/or electrostatics attraction (Li *et al.* 2020e). The basic mechanisms that transpire between NMs and MPs have been reported (Krystynik *et al.* 2021; Tang *et al.* 2021). Table 4 provides a summary on these basic mechanisms.

Table 4: Basic mechanism of action between a specific NM category and MPs/ NPs

Specific NM category based on their function	Example of NM type	Mechanism of action
Flocculant	Lysozyme amyloid fibrils (Shi *et al.* 2022a)	The interaction between NM and MPs/NPs is based on charge neutralisation wherein the MPs or NPs negative charge is neutralised by the flocculants positive charge. This results in the formation of flocs which can then be

		removed *via* filtration or sedimentation (Krystynik *et al.* 2021).
Photocatalyst	Au@Ni@TiO_2 micromotor (Bu *et al.* 2024)	Photocatalysis contains two types of reactions: photoreduction and photooxidation. Semiconductor NMs consist of an empty conduction band and a filled valence band. An electron is excited from the valence band to the conducting band which creates an electron vacancy in the valence band when a specific NM absorbs light that has energy equal to or higher than the semiconductors bandgap. The electron vacancy that is created corresponds to a positive charge which is known as a hole. The electron will then transfer to the adsorbed compound i.e. the MP which leads to a series of photoreduction and photooxidation processes that eventually degrade the MP.
Adsorbent	Magnetic carbon nanotubes (Tang *et al.* 2021) Fe_3O_4 nanoparticles (Shi *et al.* 2022b) Fe-HDTMS (Grbic *et al.* 2019)	The mechanism of action that occurs varies and is entirely dependent on the combination of nano-adsorbent and MP type. The mechanism of action could be π-π electron interaction, electrostatic interaction, hydrogen -bond interaction, hydrophobic interaction, π-π electron conjugation and complexation (Tang *et al.* 2021).
Filter membrane	Non-woven cellulose fabric impregnated with chitin nanocrystals (Yousefi *et al.* 2024) Non-woven cellulose fabric impregnated with cellulose nanocrystals (Yousefi *et al.* 2024)	Nano-filters that contain nano-sized sieves can be utilised effectively in the separation and removal of MPs and NPs from the effluent (Krystynik *et al.* 2021).

	Lignin-zeolite composite nanofiber membranes (Noman *et al.* 2024)

From the studies, it is important to note that the mechanism of action that occurs between a specific NM and MP is entirely dependent on the chemistry of the MP and the surface chemistry of the NM. Since majority of the studies elucidating a mechanism of interaction have been between metal-based NMs and MPs/NPs, there is much scope for the uncovering of interaction mechanisms between non-metal-based NMs and MPs/NPs.

2.9. The impact of water characteristics on nanomaterials interaction with microplastics

To elucidate the complex interactions between NMs and MPs/NPs, it is important to understand the factors that impact these interactions and how it relates to their surface characteristics and mode of action. There are several water characteristics that affect the mechanism of interactions listed in Table 4. For instance, Li and team have investigated concentrations of pH, ionic strength and humic acid (HA) and their influence on the interaction of the heteroaggregation kinetics between modified PS nanoplastics and CeO_2-NPs in four natural aquatic matrixes: groundwater, river water, lake water and seawater. The dominating factors of PS and CeO_2-NPs was shown to be ionic strength and natural organic matters (Li *et al.* 2020e). The negatively charged PS NPs were investigated separately with the CeO_2-NPs in each of the four different matrixes. Negligible aggregation was observed for groundwater, lake water and river water, whereas visible aggregation occurred in seawater. This was due to the higher ionic strength in the seawater, causing the particles to rapidly form aggregates. They also reported that the insufficient aggregation or aggregation hinderance that was observed in the other three samples (river water, ground water and lake water) can be attributed to the steric hinderance that was induced by the natural organic matters (NOM). This depicts how NOM water

characteristics impacted the third mechanism of interaction listed in table 4 (adsorption). Furthermore, it was reported that the incubation of CeO_2-NPs and PS nanoplastics under various pH concentrations (pH = 5, 7 and 9) caused significant differences in the colloidal stability and increase in diameter. Fast aggregation at pH 5 was reported. However, Li and colleagues noticed that as the pH increased, the attachment efficiency from the negatively charged PS NPs decreased significantly (Li *et al.* 2020e). This indicates that a high pH inhibits the heteroaggregation between CeO_2-NPs and negatively charged PS nanoplastics. In contrast, for positively charged PS-NH_2, an increased pH (pH = 7) led to a higher attachment efficiency between the PS-NH_2 and CeO_2-NPs. This confirms the significance and impact of electrostatic interactions in PS aggregation. Additionally, it reveals that there is no optimum range of pH that is known to facilitate maximum MP removal. Optimum pH conditions are dependent on the specific NM-MP/NP interaction. It was also highlighted that heteroaggregation of CeO_2-NPs and NH_2-coated PS was promoted by a relatively low HA concentration. This was attributed to the decrease in electrostatic hinderance as a result of the HA surface coating. Their findings demonstrate that nanoplastics behaviour in the environment could be influenced by the surrounding water characteristics including the concentration of organic and inorganic particles (Li *et al.* 2020e).

A study conducted by Singh and co-workers (Singh *et al.* 2021c) documented that organic matter, pH and salinity displays significant roles in the sorption and stability of PS surfaces and Ce-NPs. At low salinity level, the affinity between the Ce-NPs and MPs were low while, at a high salinity, higher binding between the Ce-NPs and MPs occurred. This was attributed to the competitive ions that were present at the binding site at low salt concentration. At a high ionic strength, the sorption quantity was assigned to the dominant self-aggregation phenomenon as a result of Ce-NPs charge screening which was followed by the attachment of these aggregated Ce-NPs to the MPs. MPs surface roughness also influenced the adsorption

process of Ce-NPs on the PS surface. Since the rough MPs surfaces were more exposed due to their rough nature, the competitive ions in the saline system found to cover the binding sites faster of the exposed surfaces since they are easily visible. Therefore, comparatively less sorption amount was observed for the pristine MPs. They also found that the pH played an important role in the Ce-NPs aggregation, their sorption and adhesion. The sorption quantity was greatly influenced by pH in that a decrease in sorption was observed with an increase in pH. At pH 4.5, a higher sorption was observed whilst at pH 6.5 the Ce-NPs were positively charged, and the MPs were negatively charged which resulted in an electrostatic interaction. CeO2-NPs aggregation was higher was greater at a higher pH of 10.5. They reported the sorption capacity decline to be attributed to the deprotonation of both the MPs and Ce-NPs which resulted in the repulsion between the surface of the Ce-NPs and the MPs since both surfaces are negatively charged (Singh *et al.* 2021c).

Studies have also reported the positive influence of heavy metals on adsorption kinetics of NMs and MPs/NPs. For example, a study conducted by Ho and Leung, discovered that in the presence of heavy metal cations, there was a higher sorption affinity for the Ce-NPs by the PS. This occurred due to complex formations between Me-PS (PS with co-existing metal ions) and NPs *via* electrostatic forces and Me-π-π-PS and Ce-NPs *via* bridge effects (Ho and Leung 2021). However, the complex formation on PS in the presence of the heavy metals was inhibited at higher ionic strength as a result of double-layer compression and competitive sorption (Ho and Leung 2021). Furthermore, the nature (e.g., electronegativity, ionic radius, valence state) of the heavy metal cations can substantially influence attachment and aggregation of PS and Ce-NPs. For example, a study (Singh *et al.* 2021a) documented that the PS and Ce-NPs mixture was less stable than the mixture with both PS and PAH (polycyclic aromatic hydrocarbons). This was attributed to the adsorption of the PAHs onto the MPs surface which stabilised the MPs (Singh *et al.* 2021a). The data obtained from these studies are

intriguing as they clearly illustrate the significant influence of water characteristics on MP/NP-NM interactions, offering valuable insights into this relationship. Recognizing the crucial role of these factors in shaping MP/NP-NM interactions provides a foundation for identifying key variables to manipulate in future experiments. By altering these variables, the interactions between MPs/NPs and NMs can be enhanced and optimized, leading to more effective pollutant removal strategies.

The studies thus far indicate that the interaction between the NMs and MPs/NPs are highly specific. Often, the impact of water characteristics on the interaction between the NMs and MPs/NPs is taken into consideration. Wastewater matrices are highly complex and contain significant concentrations of heavy metals, solids, microbes, dissolved and particulate matter, nutrients and micro-pollutants such as MPs/NPs (Farissi *et al.* 2023). It noteworthy that different compositions of different types of wastewaters constitute the wastewaters complexity. This creates a need to understand the impact of different water characteristics on the interaction between NM and MPs/NPs. Additionally, wastewater matrices are highly variable depending on the sample. Different wastewater effluents consist of various permutations of hydrocarbons, organic matter, nutrients (phosphorus and nitrogen), microbes, heavy metals and endocrine disruptors. This poses potential challenges since it may affect the removal of MPs/NPs. Furthermore, wastewater characteristics such as pH are unpredictable and may change during the treatment period. It is noteworthy that the presence of non-plastic products in high concentrations could influence MPs/NPs removal. A high concentration in microorganisms could result in biofilm formation. For example, a study by Dong and team, found that an increase in salinity inhibited microbial activity and affected the proliferation of bacteria. The salinity level is negatively correlated with the biofilm growth rate (Felisardo *et al.* 2024). This showcases the effect of how the water characteristic salinity impacted the third mechanism of action from table 4 (adsorption). This biofilm formation may encapsulate the MP/NP in

wastewater, altering the MPs/NPs surface chemistry. Thus, different wastewater complexities will present different challenges during bionanoremediation. Thus, it is imperative that these water characteristics be taken into consideration and NMs synthesized according to the application that it will be utilised for.

2.10. NM synthesis for potential wastewater applications

Physical, chemical, and biological methods have been used for synthesizing NMs for the removal of different contaminants (Figure 8). Yet only chemical synthesizing methods have been used with the application specifically for MP/NP removal from wastewater. It is noteworthy that all NMs listed in table 3 have been synthesised utilising chemical methods. NM synthesis methods used for the removal of MPs/NPs from wastewater are thus in its infancy. Physical and biological synthesis methods have yet to be explored for the removal of MPs/NPs from wastewater and their further potential are shortly discussed in section b and c.

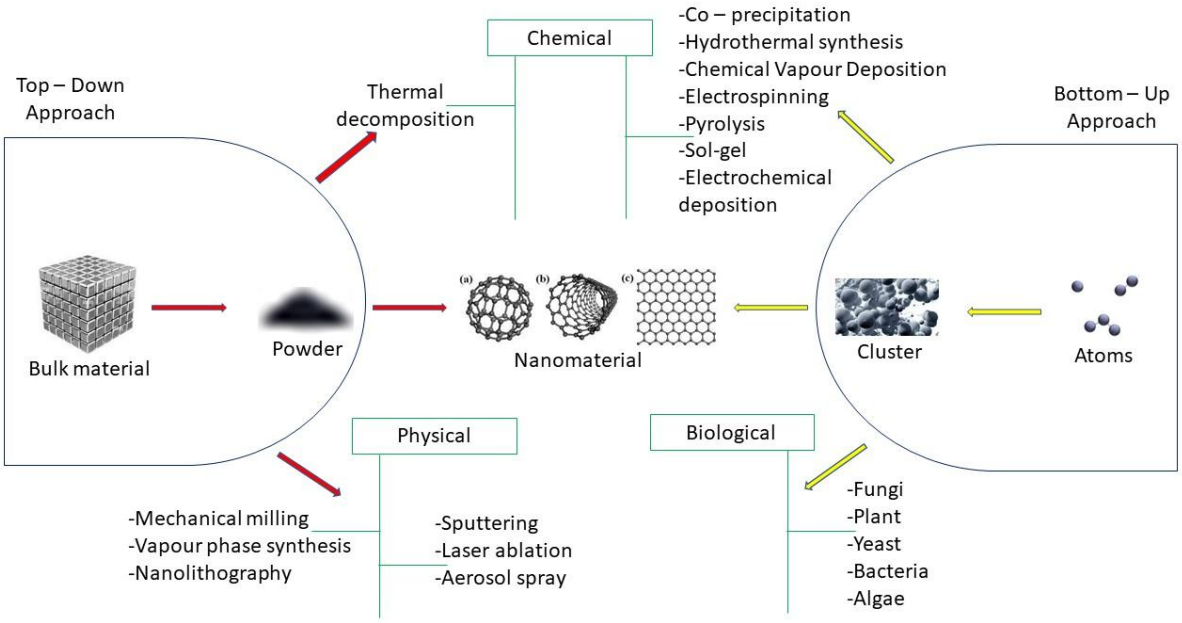

Figure 8: Schematic illustration of the top-down and bottom-up approach and the physical, chemical and biological methods they house (Liu *et al.* 2019b; Zhang *et al.* 2023). Adapted with permission under a Creative Commons License, License CC BY 4.0 from (Zhang *et al.*

2023). Copyright 2022 BUCURESTI and Creative Commons License, License CC BY 4.0 from (Liu *et al.* 2019b). Copyright 2021 MDPI

a. Chemical synthesis methods

Chemical methods are bottom-up approaches (Wang *et al.* 2022b) often understood as the assembly of molecular constituents or single atoms into larger nanostructures (Zeng *et al.* 2022). One of the most extensively exploited chemical techniques for the engineering of NMs is the hydrothermal method that has gained high attention due to the significant advantages over other methods (Adeleye *et al.* 2021). This is attributed to its high product purity, low-cost and mass efficiency (Shandilya *et al.* 2016). Moreover, synthesis of NMs can be done both at ambient temperatures and high temperatures. The NMs morphology can be well regulated utilising high- or low-pressure conditions. NMs may be synthesised with high vapour pressures with negligible material damage (Yamakov *et al.* 2004; Adeleye *et al.* 2021). Additional benefits exhibited include the easy control of reaction stoichiometry. It rarely requires calcination or pre-sintering steps (Adeleye *et al.* 2021). There is sufficient access to control the distribution, size, complex chemical composition and shape of the NM (Adeleye *et al.* 2021). This is advantageous for application in wastewater since the NMs synthesised would be better controlled to obtain specific surface chemistries and functionalities based on targeted reduction of specific MPs and pollutants in the wastewater. Furthermore, it is regarded as an environmentally friendly synthesis technology. Lastly, it is easy to scale-up to industrial demands (Adeleye *et al.* 2021). These benefits make it suitable for large scale industrial applications in the removal of MPs from wastewater (Adeleye *et al.* 2021). This synthesis method allows easy alterations to nanostructures and can produce a larger volume of product in comparison to other methods. For example, a study by Ye and colleagues presented self-propelling magnetically steerable iron oxides- MnO_2 core-shell micromotors with a large production capability in comparison with the previously developed micronanomotors by

template-assisted and physical vapor deposition methods (Ren *et al.* 2022). Furthermore, the study demonstrated the scalable synthesis of the two types of bubble-propelled iron oxides-MnO_2 core–shell micromotors (Fe_3O_4-MnO_2 and Fe_2O_3-MnO_2) for organic dye and MPs removal (Ren *et al.* 2022). Additionally, the Fe_2O_3-MnO_2 micrometer displayed efficient removal of suspended MPs and aqueous organics by the synergy of surface adsorption, catalytic degradation and adsorptive bubbles separation mechanisms.

The chemical sol-gel method has displayed superiority in the synthesis of silica nanoparticles over plasma synthesis, combustion synthesis, chemical vapor deposition, micro emulsion processing and hydrothermal methods (Vemury *et al.* 1997; Tani *et al.* 2003; Nagao *et al.* 2004). Thus, making it the most common method for silica nanoparticle synthesis due to the specific advantages it has over the aforementioned methods. NMs offer various advantages, such as their versatility, high purity, ease of production, homogeneity, and the ability to achieve modifications in their properties through parameter alteration. Furthermore, it offers synthesis at low temperatures and reaction kinetics may be controlled by varying the chemicals composition (Patidar and Srivastava 2021).

The sol-gel method is also referred to as the chemical solution deposition which is regarded as a pivotal method for the preparation of TiO_2 nanoparticles (Nabi *et al.* 2021). This is owing to the merits this method has to offer for TiO_2 nanoparticle synthesis. One primary benefit is that it is the simplest method wherein the nanoparticle morphology and size can be controlled via the reaction parameters being systematically monitored (Zhao *et al.* 2022). For example, a study by Li and team synthesised and modified the surface of TiO_2 nanoparticles using the sol-gel and emulsion polymerisation methods. Herein it was demonstrated that the photocatalyst polypyrrole-TiO_2 complex nanoparticles exhibited enhanced degradation of PE in comparison to that of TiO_2 or polypyrole as a photocatalyst (Liang *et al.* 2022). It is noteworthy that TiO_2 has poor affinity for organics/ pollutant treatment (MPs), especially in aquatic matrices.

However, modified TiO_2 properties are intrinsically different from pure TiO_2 properties with regard to contaminant adsorption, light adsorption, charge separation and ease of TiO_2 nanoparticle separation (Moma and Baloyi 2019; Nabi *et al.* 2021). Thus, modified TiO_2 will be able to improve performance and selectivity (Domínguez-Jaimes *et al.* 2021). Additional advantages include its low-cost making it economical for industrial applications in wastewater treatment. It is also an efficient method to produce high quality nanoparticles (Noroozi *et al.* 2022). For example, a study by Thomas and co-workers, investigated the photocatalytic degradation of PE using TiO_2 nanoparticles that were synthesised via the sol-gel method (Thomas *et al.* 2013). A comparative analysis was done between two different TiO_2 nanoparticles- the TiO_2-50 synthesised by Thomas and commercially available TiO_2-200. It was revealed that the TiO_2-50 displayed a higher percentage weight loss of PE compared to TiO_2-200. However, the shortcoming of this method is that the synthesis produces residual hydroxyl and or carbonyl groups. Organic solutions may be utilised which are toxic and harmful. It also requires a long processing time. Moreover, several reports are focused on TiO_2 modification especially for plastics degradation (Domínguez-Jaimes *et al.* 2021; Nabi *et al.* 2021). This makes it suitable for application in wastewater. Another benefit of this method is that it can produce a thin coating which ensures excellent adhesion between the top layer and the substrate making it suitable for wastewater treatment application when the target mechanism of interaction is adhesion between the nanoparticle and MPs/NPs present in the wastewater.

b. Physical synthesis method

Physical methods are a top-down approach which utilises initial macroscopic structures i.e., bulk material. These methods commences with large particles that are reduced to nanostructures (Wang *et al.* 2022b) through the breakdown of bulk materials (Zeng *et al.* 2022). Whilst there are no direct studies on the synthesis of NMs using physical methods for the

removal of MPs/NPs from wastewater, a linked approach is the generation of nanomembranes via the physical synthesis method electrospinning for the removal of MPs from water. A lignin-zeolite nanofiber membrane was fabricated by Bahi and colleagues with two important characteristics that make it suitable for application in wastewater treatment. Firstly, it has superior permeation rates and flux in comparison to commercially produced membranes (Dai *et al.* 2022) resulting in a larger volumetric mass flow of fluid passing through the membrane per unit area and time. Thus, large amounts of fluid containing MPs can be processed making it suitable for large-scale industrial wastewater applications. Secondly, the zeolite nanoparticles are uniformly dispersed which improves the mechanical properties of the NM (Dai *et al.* 2022). This characteristic enables the nanomembrane to support a large load of MPs which also facilitate for large-scale industrial applications in wastewater.

An additional physical synthesis method that could be exploited for the removal of MPs/NPs from wastewater are the laser ablation synthesis (LASiS), a commonly used method for obtaining colloidal solutions of nanoparticles in a variety of solvents but has yet to be utilised in the removal of MPs from wastewater. Different synthesis applications to produce a range of NMs with LASiS exist, such as nanowires, semiconductor quantum dots, core shell and carbon nanotube nanoparticles (Nozar *et al.* 2024). This synthesis method has the merits of simplicity in different suspensions making them tentatively effective for wastewater remediation. Additionally, the properties of the nanoparticles may be altered by selecting the nature of the liquid and laser parameter accordingly (Jamkhande *et al.* 2019). This enables the synthesis of NMs with specific surface chemistry based on the targeting of specific MPs/NPs to remediate in wastewater. The shortcoming of this method however is that prolong time laser ablation results in the generation of a large quantity of nanoparticles in the colloidal solution which result in blockage of the laser path. The laser energy also gets absorbed by the already formed nanoparticles instead of the target surface which results in the reduction of the ablation rate

(Zhang *et al.* 2024). Both shortcomings may be solved through a careful choice of fluidics. For example, the NMs prepared may be removed from the laser path by utilising a flow-through system (Feijoo *et al.* 2022). Additional drawbacks include high investment costs. The scalability of NMs synthesized by laser ablation is a subject of significant debate. For example, Sportelli and team curated the advantages and disadvantages of silver nanoparticle production using the laser ablation method. Herein, a drawback was argued in that the most diffused laser sources are incapable of silver nanoparticle production on an industrial scale. However, in contrast, a review by Fazio and co-workers presented laser synthesis of nanocolloids to be appealing for industrial manufacturing of functional NMs (Kumar *et al.* 2020a). This represents new information about nanoparticles scalability towards selected applications. Albeit wastewater remediation was not included in the areas of application. Similarly, a study by Zimbone and colleagues revealed that laser ablation was a versatile and scalable methodology in their synthesis of TiO_2 nanoparticles via the laser ablation method (Chen *et al.* 2022b). It is suggested that future work should be directed to this area to ensure an advancement in the applications including tentatively wastewater treatment.

Mechanical milling (high-energy ball milling), with similarities to the above method, has yet to be utilised in bionanoremediation to remove MPs from wastewater. However, it has been used to synthesise a NM with the ability to capture and remove MPs. In a study by Rius-Ayra and team, a superhydrophobic CuFeCo alloy powder was synthesised by combining liquid phase deposition and the high-energy ball milling synthesis method to remove high-density PE fibres from water (Xu *et al.* 2023). This study reveals the potential of this method for the synthesis of NMs that can be applied for the removal of MPs from wastewater. Additionally, the main advantage of this method is that it is useful for large scale production of nanoparticles with a high purity and superior physical properties in a cost-friendly manner. These benefits tentatively make it suitable for industrial applications in wastewater treatment (Ullah *et al.*

2014; Jamkhande *et al.* 2019). The pitfalls of this method is that it requires high energy, an extensive long period of milling time and the powder may get contaminated as a result of the steel balls (Ji *et al.* 2024).

c. Green synthesis method

Green synthesis approaches, often referred to as biosynthesis (Li *et al.* 2018b), has drawn a great amount of attention in NM formulation to overcome the limitations experienced by physical and chemical methods (Bouafia *et al.* 2020; Bouafia and Laouini 2021; Bouafia *et al.* 2021). The methodology for green synthesis is based on biological precursors such as bacteria, fungi, algae, yeast and plant extract (Figure 9). It is also dependent upon different reaction parameter conditions such as temperature, pH, pressure and solvent (solvents such as ionic liquids). Green synthesis has yet to be utilised for the synthesis of NMs with applications towards removal or degradation of MPs from wastewater. These methods use substances that stem from a biological origin such as reducing agents, ligands, capping agents and stabilisers (Terai and Kobayashi 2000). The reducing agents are utilised for metal ion reduction; however, the capping agents and stabilisers are used to control the size and shape of the NM as well as to prevent agglomeration. The ligands are employed to coat the NMs surface. These aforementioned biological reducing agents can be small molecules such as H_2, however, they are often larger molecules such as reducing polysaccharides, amides, flavonoids, aldehydes, polyphenols, ketones, alkaloids, various enzymes and carboxylic acid (Cao *et al.* 2024b) (Figure 9). Typical ligands include thiols, amines and phosphines whilst peptides, proteins and polysaccharides are found to be suitable stabilizers and capping agents (Li *et al.* 2024). These biological agents can be comprised of individual components or complex mixtures (polyphenols, saccharides, vitamins) derived from the biological materials, in both extracellular or intracellular settings (Ahmad *et al.* 2019b; Mohamed *et al.* 2019). It is essential that the plethora of compounds mentioned above be highlighted since complex mixtures

comprising of numerous different components will form, with each component acting as a reducing or capping agent and stabilizer selecting for a specific size and/or shape. This therefore results in a consortium of nanoparticles of different size and shape. In order to eliminate this issue, optimisation would have to be conducted in order to select for a single reducing or capping agent and stabiliser in order to obtain a uniform distribution of nanoparticles. This is challenging, time consuming and not cost effective. Therefore, it is imperative for the quality of research to be addressed in the context of biosynthesis techniques since there certainly appears to be areas that can be improved upon. This is because several studies exist where insufficient data regarding the production method is provided e.g., reaction conditions, specifications of reagent ratios etc. Most studies lack information concerning sample preparation for characterisation. Furthermore, it is worth noting that results from analyses are often quite poorly remarked on and are inadequately discussed in several present studies. Additionally, in studies regarding metal nanoparticle biosynthesis, concentration determination has been found to be a severe issue, with some studies utilising scientifically unsound shortcuts such as the concentration of nanoparticles being calculated directly from the initial precursor concentration, thereby adopting the assumption of 100% yield. An added issue that fails to be addressed often, is the applicability of novel research on nanoparticles green synthesis into their large-scale industrial manufacturing which can be helped by determining key variables that may be utilised (Terai and Kobayashi 2000) e.g., with modelling proposed by Cinelli and team (Su *et al.* 2016). Finally, it is important to also address the quality of research in NM synthesis in the context of the remaining top-down and bottom-up synthesis approaches (not just green methods). There also appears to be some studies on the synthesis process, but with inadequate information on the method used, since actual values utilised were not provided. The synthesis methodology is meant to be as detailed as possible to allow its reproducibility which is an area that needs improvement. Furthermore, it is critical that many

more polymer types beyond PE be studied for removal and biodegradation. Due to the numerous challenges involved, this area deserves significant attention and focus for future research and development.

Each of the starting materials utilised, have their own merits and pitfalls. Each of these advantages and disadvantages will be highlighted in terms of their applicability towards wastewater treatment. In bacterial NM synthesis the merit is that bacterial microorganisms are abundantly available making them relatively low-cost which makes them suitable for application in wastewater treatment. Bacteria also have the ability to adapt to extreme conditions making them versatile (Cao *et al.* 2024a). The drawback is that there is a safety risk when using bacterial microorganisms (Jamkhande *et al.* 2019). This is due to their potential pathogenicity. This therefore makes the selection criteria of the microorganism imperative to ensure the safety of the user. For NM synthesis using fungi, the benefit is that it is easy to scale-up which makes it appropriate for industrial applications in wastewater treatment. It offers economical flexibility and large surface area as a result of the mycelia. The productivity is greater when compared to bacteria since fungi secrete larger amounts of proteins, enzymes and metabolites due to the mycelia (AlZain *et al.* 2013; Jamkhande *et al.* 2019). The downside is that the nanoparticles that are produced using fungi are of variable size (Cao *et al.* 2024a). For the synthesis of NM using plant extract/products, the main advantage is that there is no potential pathogenicity. Additionally, the nanoparticles that are produced are fairly homogenous (Jamkhande *et al.* 2019). For example, Fe-ZnO nanoparticles were synthesised from a *hibiscus rosa-sinensis* leaf and applied for the degradation of low-density PE in a study by Lam and colleagues. The reducing agents present were mainly flavonoids and polyphenols (Singh and Chatterjee 2017). This enabled the synthesis to be fairly homogenous since there weren't several primary reducing agents producing different sizes and shapes of nanoparticles. The disadvantage is the production cost is high as a result of the heating temperatures that are

required (Cao *et al.* 2024a). Ultimately, the choice for the synthesis method depends on the specific application it will be utilised for and the desired properties of the nanoparticles.

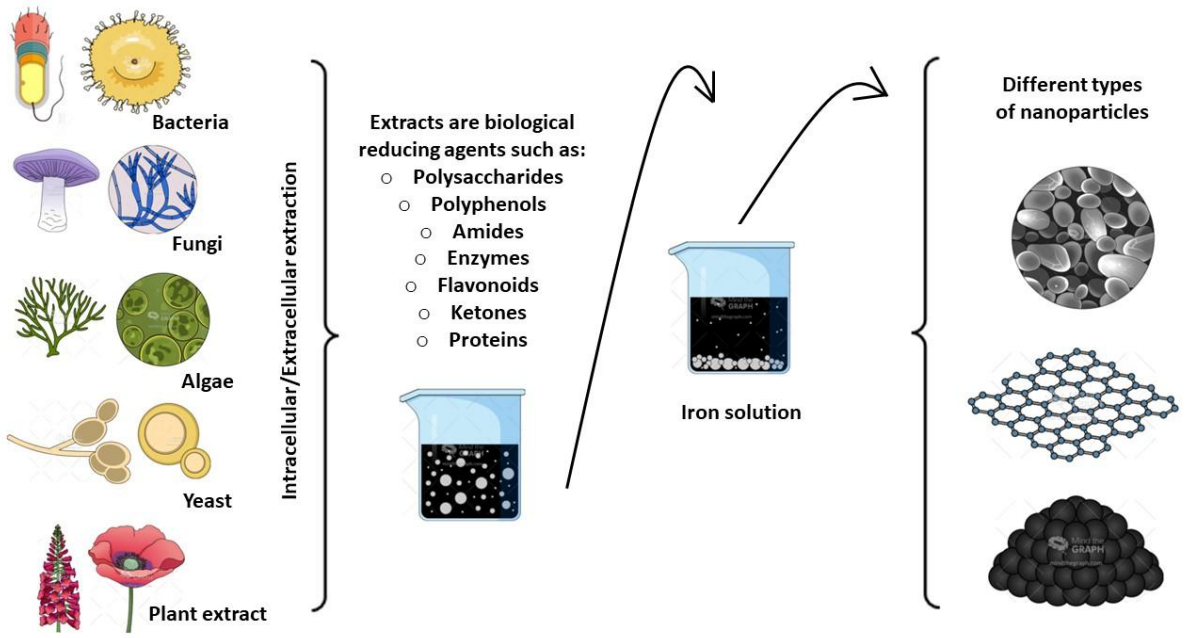

Figure 9: Schematic illustration of green synthesis of metal nanoparticles derived from biological precursors

From the available literature, it is clear that chemical synthesis has been at the forefront of NM development across all aspects. While the development of new NMs in this area is encouraging, it is important to explore physical and green synthesis methods in order to develop novel NMs that can reduce MPs and NPs in wastewater with a focus on environmental sustainability. It is necessary to conduct more research to understand how NMs affect the environment and how they can be minimized.

2.11. Strategies to consider regarding NMs toxicity

The rapid dissemination of nanotechnology into various industries such as soil remediation and water treatment has grown NM synthesis and production. Toxicity of NMs in aqueous solutions such as wastewater has gained a large amount of attention due to NMs bioavailability, and

ability to penetrate cells, tissues and organs (Ali *et al.* 2021). Nanoparticles leaching into aqueous and soil environments have raised concerns regarding their potential harm to humans, plants and the environment (Liu *et al.* 2018). This has created an uncertain atmosphere regarding the effects of these materials (Taghavi *et al.* 2013; Sonwani *et al.* 2021). A lack of technical information has created an appropriate context for advocates and rivals of NMs to present conflicting and ill-considered results. This has increased concerns regarding the use of NMs. Thus, sufficient studies that uncover the real, exact risks posed by NMs are critical. The data revealed by these studies can be valuable in minimizing the health and environmental risks potentially posed by NMs (Taghavi *et al.* 2013). Nanotoxicology has emerged to tackle the understanding between NMs and the environment (Touqeer *et al.* 2021). In contrast to typical contaminants, the analytical approach for nanotoxicology needs additional research and investigation (Hu *et al.* 2016). This is because the issues and concepts raised in this field are new and needs to be incorporated when selecting suitable analytical methods as well as incorporated into the experimental design (Tabrizchi and Kuchaki Rafsanjani 2020). One experimental design focused on a high-throughput assay integrated with omics was highlighted to globally investigate nanotoxicity (Hu *et al.* 2016). In the application of established toxicity tests, it is pivotal that extreme care be taken when interpreting the data to eliminate the reporting of false positive results (Tabrizchi and Kuchaki Rafsanjani 2020). Furthermore, it is recommended that the physiochemical properties of the NMs be assessed and analysed in relation to environmental safety and human health before its large-scale application.

To establish the suitable techniques for NM evaluation the Organisation for Economic Cooperation and Development (OECD), in 2006, developed a working party on manufactured NMs. According to the guide manual established, 26 physiochemical properties of the NM should be considered. Some of these properties are solubility, particle size and shape distribution, density, crystallinity, surface adsorbed species, purity and porosity/ surface area

(Grusho *et al.* 2017). Additionally, to mitigate the risks surrounding NMs, several government entities have implemented policies in the form of laws, guidelines, regulations, and legislation. However, there are no clear international laws, regulations, or legal standards for the handling, storing, labelling, screening for toxicity, or determining the environmental effects of NMs (Ali *et al.* 2021). There are several challenges associated with mitigating nanotoxicity, among which is their disposal techniques. Therefore, proper care should be taken when disposing of NMs to reduce leaching. Thus, it is crucial that correct strategies are implemented when synthesising NMs to ameliorate toxicity to the fullest extent.

CHAPTER THREE: Synthesis, surface area optimisation and characterisation of g-C_3N_4@Fe_3O_4 and BNNS@Fe_3O_4 MNCs

3.1. Introduction

NMs have been recognized for their significant potential in innovative water treatment technologies, enhancing water purification efficiency (Bottero *et al.* 2006; Qu *et al.* 2013a). Recent progress in this field presents opportunities to develop the next generation NMs for MP removal/degradation since this pollutant is a major challenge. Unlike current centralized systems, nanotechnology facilitates water treatment processes that are cost-effective, highly efficient, and less dependent on large infrastructure (Qu *et al.* 2013b). A key benefit of using NMs in water treatment is their applicability as point-of-use technologies, unlike most conventional methods which are designed for centralized treatment plants. Due to the high surface area, rapid dispersion, high reactivity, and excellent sorption capacity, NMs are excellent candidates for MPs removal. Additionally, they are not expected to produce harmful disinfection by-products, unlike traditional chemical disinfectants (Kunduru *et al.* 2017). Some NMs also exploit unique properties such as supermagnetism and paramagnetism (Qu *et al.* 2013a). Smaller NMs exhibit higher sorption capacities and greater magnetic properties in MNCs.

The ability to manipulate materials at the nanoscale opens up new possibilities for innovation and technological advancement. Historically, the development of NMs has been marked by breakthroughs in synthesis techniques and a deeper understanding of their structural and functional characteristics. The synthesis and characterization of NMs are critical steps in harnessing their potential. Understanding the intricate details of NM properties, such as magnetic behaviour, chemical stability, surface characteristics and interaction with other substances, is essential for optimizing their use in practical applications. Despite the progress

made, several challenges remain in achieving precise control over these properties during synthesis and in accurately characterizing the resulting synthesised NMs.

The chosen NMs for this study are boron nitride (BN) and graphitic carbon nitride (g-C_3N_4). The selection of these materials are based on 2 fundamental properties, (i) 2D NMs sub-nanometre and nanochannels pore structures are precisely controlled making them specifically attractive for NMs developed for use in water and wastewater treatment since these features aid in facilitating fluid transport and have highly selective molecular separation capability, (ii) these 2D NMs are more porous and have double-layer sheets, resulting in a high specific surface area and more active sites for improved adsorption (Goh *et al.* 2022). Additionally BN has excellent chemical and physical properties, making it a promising NM in several technological applications (Şen *et al.* 2018) including wastewater treatment. Several studies have reported the utilisation of these porous BN sheets for the organic molecules' removal from waste such as oils, pharmaceuticals and dyes (Zhang *et al.* 2012; Li *et al.* 2013a; Li *et al.* 2013b; Lei *et al.* 2015). One study in particular, by Bangari and colleagues (Bangari *et al.* 2019) used BNNS@Fe_3O_4 for the removal of Arsenic (V) from aqueous solution. Herein they compared the adsorption capacity of BNNS@Fe_3O_4 with 14 other adsorbents such as cupric oxide nanoparticles, Fe_3O_4, kaolinite, magnetite-reduced graphene oxide composites, IAC-Fe(III), Fe10MCM-41silica, iron oxide multiwalled carbon nanotube hybrid, nano-zero-valent iron on activated carbon, functionalised synthetic graphite, porous iron oxide on activated carbon, GO/ferric hydroxide composite, ZMA (Sonora), Fe-GO nanocomposite and Fe_3O_4-rGO nanocomposite (Bangari *et al.* 2019). The data revealed that the BNNS@Fe_3O_4 had the highest adsorption capacity among all aforementioned adsorbents, clearly indicating its superiority.

The graphitic carbon nitride is prominent for its structural stability, ease of synthesis, inexpensiveness and its proven efficacy for the environmental remediation of different

emerging contaminants through adsorption, oxidation and photocatalysis (Rosa *et al.* 2021). It is also the most stable allotrope of carbon nitride under ambient temperature (Ray *et al.* 2020). It exhibits significant electron-rich characteristics and maintains high chemical stability in a variety of solvents, such as water and alcohols, making it suitable for application in water and wastewater treatment. Moreover, g-C_3N_4@Fe_3O_4 possesses a porous structure and wide surface area with primary/secondary/tertiary and a fraction of sp^2π-conjugated amines which improves its chemiosorptive and physiosorptive affinity. This in turn improves its contaminant removal performance from contaminated water (Zhu *et al.* 2014; Oh *et al.* 2018). For example, Zhou et al., (2013) illustrated the use of the hydrothermal method to create g-C_3N_4@Fe_3O_4 nanospheres featuring a porous structure. Their experiments revealed that over 98% of methyl orange was eliminated, maintaining this high level of efficiency across five successive cycles. The NM could be rapidly retrieved using a magnet. This improved removal efficiency was credited to the formation of a heterojunction between g-C_3N_4 and Fe_3O_4 (Zhou *et al.* 2013). Furthermore, the inherent nitrogen functional groups, superior textural properties and porous structure make g-C_3N_4 an effective adsorbent in various applications. For example, Xiao et al., (2019) developed g-C_3N_4 nanosheets from guanidine hydrochloride, with a thickness of < 1.6 nm for removing both anionic and cationic heavy metals such as Cr(VI), Cd(II), and Pb(II). The reported remarkable adsorption capacities of g-C_3N_4 for Cr(VI), Cd(II), and Pb(II) were 684.5, 123.2, and 136.6 mg/g, respectively. The adsorption process was attributed to the tri-s-triazine units and nitrogen-containing groups in g-C_3N_4 (Xiao *et al.* 2019). This suggests that the properties of g-C_3N_4 make it an excellent choice for adsorption studies. Additionally, since tris-s-triazine has heterocyclic aromatic rings, it can bond with another compound that has aromatic rings, through π bonding. This makes it the perfect candidate for MPs removal since several MPs such as PUR, PA, PET, PES and PS MPs have an aromatic ring, therefore adsorption to these MPs will be favoured. Furthermore, functionalising Fe_3O_4 onto g-C_3N_4 to produce g-

C_3N_4@Fe_3O_4 enables low toxicity and enhances the MNCs durability whilst restricting g-C_3N_4 aggregation (Balakrishnan and Chinthala 2022).

The gap this study addresses lies in the limited research on the application of advanced nanocomposites, specifically g-C_3N_4@Fe_3O_4 and BNNS@Fe_3O_4, for the efficient removal of MPs from wastewater. While prior studies have explored the use of NMs for removing organic molecules, dyes, and heavy metals, their potential for MPs remediation remains underexplored. This study bridges that gap by synthesizing and characterizing these nanocomposites, leveraging their unique structural, chemical, and magnetic properties to improve adsorption efficiency and adaptability for wastewater treatment, particularly targeting MPs, a pressing environmental challenge. Therefore, this chapter focuses on the synthesis of BNNS@Fe_3O_4 and g-C_3N_4@Fe_3O_4 and their subsequent comprehensive characterisation (XRD, SEM-EDX, TEM, Zeta potential, TGA, XPS, FTIR and BET).

3.2. Materials and Chemicals

Ferric chloride hexahydrate (≥99.0% purity, CAS# 10025-77-1), iron(II) chloride tetrahydrate (≥99.0% purity, CAS # 13478-10-9), boric acid (≥99.5% purity, CAS# 10043-35-3), ammonium hydroxide solution (NH_4OH) (28% NH_3 in H_2O, ≥99.99% purity trace metals basis, CAS# 1336-21-6), urea (≥99.0 -100.5% purity, CAS# 57-13-6), sulfuric acid (H_2SO_4)(98% purity, CAS# 7664-93-9) and acetone EMPLURA® ((≥99.0 purity/assay, CAS# 67-64-1) were purchased from Merck. Melamine powder (99% purity, 100 mesh, CAS# 108-78-1) was obtained from DLD Scientific CC. All aforementioned chemicals were utilised as received unless otherwise stated. All solutions were prepared with ultrapure deionized Milli-Q water (18.2 MΩ cm), acquired from a Millipore water purification system in the laboratory.

3.3. Experimental procedure

3.3.1. Synthesis of MNCs

3.3.1.1. Synthesis of magnetically decorated graphitic carbon nitride (g-C_3N_4@Fe_3O_4) nanosheet:

i. Synthesis of g-C_3N_4

The synthesis process was achieved by the facile thermal polycondensation method via calcination, using equal amounts of melamine and urea in a 1:1 mass ratio. To achieve this, 30 grams of melamine and 30 grams of urea was combined and ground in a mortar and pestle, and thereafter moved to a covered crucible. Subsequently, the mixture was heated in a muffle furnace for a period of 4 hours. The heating temperatures were varied since this has an effect on the specific surface area of the MNC. Three different temperatures were utilised: 500, 550 and 600 °C to optimise the surface area. The crucibles were removed and placed into the desiccator to allow the mixture to cool to room temperature, resulting in the production of graphitic carbon nitride in the form of a yellow powder (Figure 35 (b), appendix 4), denoted as sample gCN500, gCN550 and gCN600 (Rosa *et al.* 2021). The calcination temperature producing the highest surface area was selected for up-scale.

ii. Synthesis of g-C_3N_4@Fe_3O_4 MNC

The magnetite-coated samples were acquired via the *in-situ* incorporation of Fe_3O_4 and g-C_3N_4. This was achieved through conventional co-precipitation using ammonium hydroxide solution. The methodology of Rosa and co-workers (Rosa *et al.* 2021) was followed with minor amendments. Briefly, 125 mg of each of the aforementioned sample gCN's were transferred to 18 mL of Milli-Q water, followed by ultrasonication at 55 °C in an ultrasound bath for 45 min. This was done to ensure homogenous dispersion of precursor gCN. Subsequently, 35 mg of $FeCl_2$•$4H_2O$ and 92 mg of $FeCl_3$•$6H_2O$ was solubilised in 1 mL Milli-Q water. Mixture gCN

was retained in the water bath whilst the temperature was increased to 80 °C under a high sonicating frequency. This was done to prevent aggregation of the precursor particles. The iron (II)-iron (III) solvent was added to the precursor mixture. The entire mixture then underwent sonication at 80 °C for 30 min. Afterward, the mixture was transferred to a magnetic stirrer plate (temperature 80 °C) with a burette system set up. 1 mL of NH_4OH was titrated in a dropwise manner, and the system was maintained at 80 °C for an additional 3.5 h with agitation. The mixture was then removed and left to cool at room temperature. The resultant dark brown/blackish powder settled to the bottom creating two phases. The solvent was pipetted out leaving the resulting powder to be separated magnetically. It washed first with ultra-pure water, then with acetone, and finally, dried at 80 °C until completely dry. This was followed by a second drying step at 105 °C for 24 h to ensure complete dehydration of the sample (Figure 35 (c), appendix 4). Figure 10 (a) is a schematic illustration of the process. The yield of the synthesised MNC ascertained was 28.6 g.

3.3.1.2. Optimisation of calcination temperature and synthesis of magnetically decorated boron nitride nanosheet (BNNS@Fe_3O_4)

i. Thermogravimetric analysis (TGA)

To determine calcination stability temperature of the precursor BNNS for BNNS@Fe_3O_4 synthesis, TGA was conducted. Thermogravimetric measurement of the mixed boric acid and urea, using a thermogravimetric analyzer (METTLER TOLEDO TGA-1) from 25 to 1000 °C, with a heating rate of 5 °C/min and a flow rate of 50 cc/min, under nitrogen atmosphere was performed. The thermograph generated was utilized to calculate the thermal degradation of the loadings of boric acid-urea mixture. The Broido technique was used to determine the activation-energy (Ea) of the degradation process as well as other kinetic parameters such as stability temperature.

ii. Synthesis of boron nitride nanosheet (BNNS)

Following the determination of the calcination temperature, boric acid and urea (precursors of BNNS synthesis) were combined at a fixed molar ratio of 1:48, 1:30, 1:15 and 1:5 boric acid : urea, after being ground using a mortar and pestle. This was done in the presence of methanol and without methanol (methanol was utilised as a quencher). Different fixed molar ratios were utilised since this affects the specific surface area of the MNC. Thereafter each of the mixtures were transferred to a crucible with a cover and heated up to the temperature ascertained from TGA for 8 h for calcination. Upon chemical reaction completion, the crucibles were transferred to the desiccator to cool to room temperature gradually yielding white (Figure 35 (f), appendix 4) BNNS48, BNNS30, BNNS15, BNNS5 and $BNNS48_M$, $BNNS30_M$, $BNNS15_M$ (with methanol). BNNS5 with methanol was not performed. This was done to optimise the surface area. The ratio with the highest surface area was selected for the scale-up.

iii. Synthesis of BNNS@Fe_3O_4 MNC

The methodology of Bangari et al. (2019) and Rosa et al. (2021) were used as a guide with several modifications in this dual-purpose step (synthesis and surface optimisation). Briefly, of each of the aforementioned BNNS samples, 600 mg was added separately in 86.4 mL of DI Milli-Q water. Thereafter the samples were subjected to ultrasonication at 55 °C in an ultrasound bath for 45 min. Consequently, 35 mg of $FeCl_2 \cdot 4H_2O$ and 92 mg of $FeCl_3 \cdot 6H_2O$ was solubilised in 1 mL Milli-Q water. The solution was retained in the water bath whilst the temperature was increased to 80 °C under a high sonicating frequency. Thereafter, the iron (II)-iron (III) solvent was added. The entire mixture then underwent sonication at 80 °C for 30 min. Afterward, the mixture was transferred to a magnetic stirrer plate (temperature 80 °C) with a burette system set up. NH_4OH (3mL) was titrated in a dropwise manner to reach pH 8 since this is critical for the synthesis of magnetic nanoparticles. The system was maintained at 80 °C for an additional 3.5 h with agitation. Upon reaction completion, the solution was transferred

to the muffle furnace in crucibles with lids. Thereafter, the furnace was heated to 175 °C for 12 h, after which it was transferred to the desiccator to reach room temperature gradually. The black powder was washed with Milli-Q water, then acetone and then dried at 65 °C. The dried powder underwent heating at 300 °C for 2 h in a muffle furnace (Figure 35 (g), appendix 4). This was done to enhance the binding of the Fe_3O_4 nanoparticles (Bangari *et al.* 2019). Figure 10 (b) is a schematic illustration of the process. The yield of the synthesised MNC ascertained was 34.8 g.

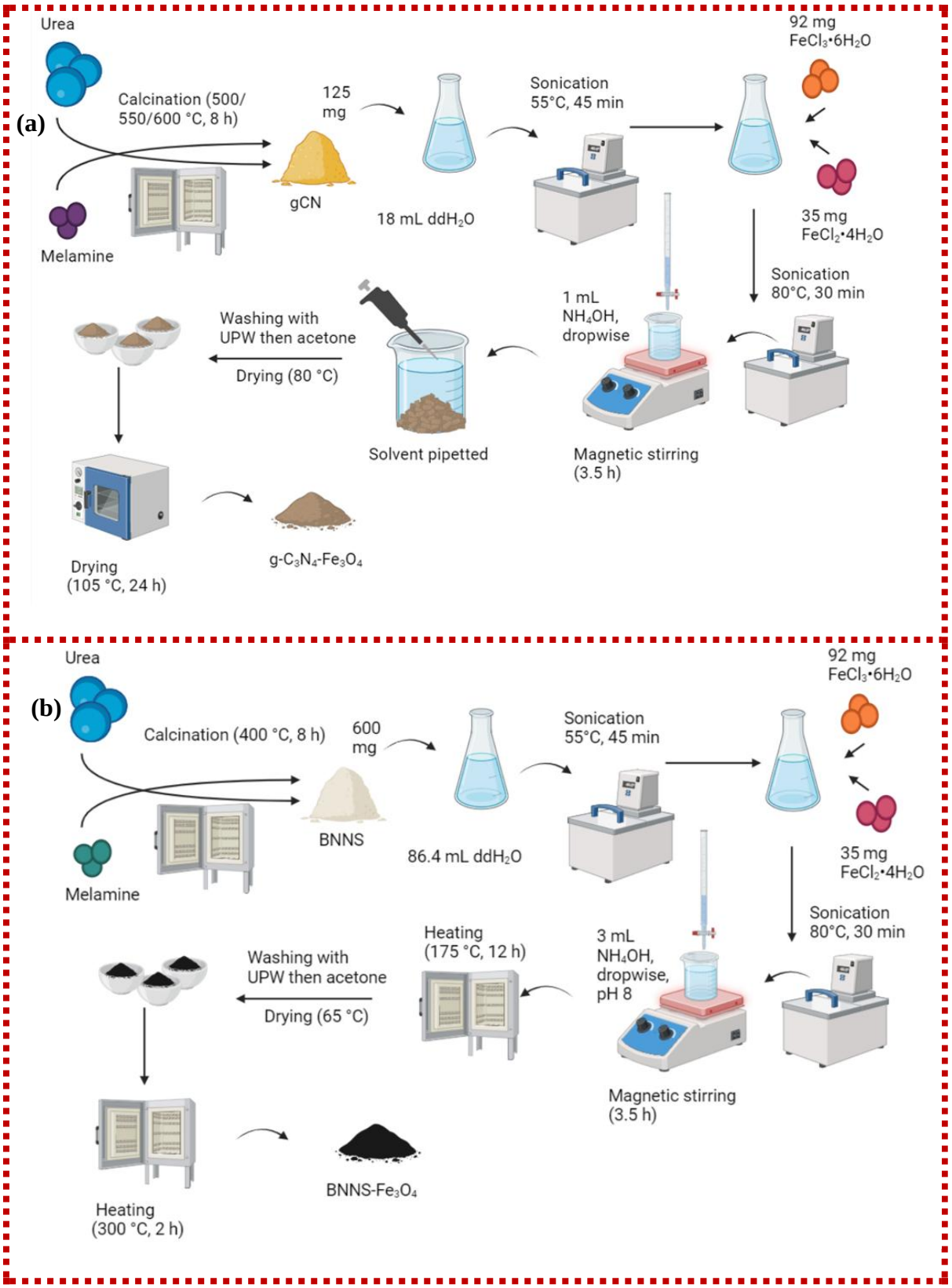

*UPW- Ultrapure water (Milli-Q water)

Figure 10: Illustration summation of the synthesis of (a) g-C_3N_4@Fe_3O_4 and (b) BNNS@Fe_3O_4

3.4. MNC physicochemical characterisation, instrumentation, and measurements

3.4.1. Brunauer-Emmett-Teller (BET)

The Brunauer-Emmett-Teller (BET) specific surface area (S_{BET}), total pore volume (V_{pore}) and average pore diameter (d_{pore}) of synthesised g-C_3N_4@Fe_3O_4 and BNNS@Fe_3O_4 were measured (Micromeritics' Tristar II 2030) by employing nitrogen adsorption/desorption technique at -196 °C. To eliminate moisture and atmospheric contaminants, the samples was degassed in a vacuum chamber for 12 h at 350 °C in preparation for BET analysis. The BET adsorption/desorption isotherm was represented graphically by plotting the BET sorption isotherm model. The plot consists of "amount adsorbed" vs "relative pressure" ($P/P0$). The model provides the quantity of adsorption at a constant temperature relative to the quantity in a single monolayer using equation 1:

$$\frac{\eta a}{\eta m} = \frac{CP/P0}{\left(1-\frac{P}{P0}\right)(1+(C-1)P/P0} \qquad (1)$$

where ηa is the amount adsorbed, ηm is the monolayer coverage, P is the pressure of the adsorbtive, $P0$ represents its saturated vapor pressure at the constant experimental temperature and C is a parameter that links the liquid adsorbate's enthalpy of vaporization to the initial layer's adsorption strength. Sample mass utilised was 1 g.

3.4.2. Fourier transform infrared spectroscopy (FTIR)

The functional groups in the MNCs were analysed utilising an FTIR spectrometer (Agilent Cary 630 FTIR Spectrometer with diamond ATR sampling module) over the spectral ranges of 4000–400 cm^{-1}. The OPUS software was utilised. Approximately 100 mg powder of each sample (g-C_3N_4@Fe_3O_4 and BNNS@Fe_3O_4) was employed.

3.4.3. X-ray diffraction (XRD)

The crystalline phases of the synthesised MNCs were evaluated via XRD system (Bruker D2 Phaser Diffractometer with Bragg−Brentano geometry, Germany) with Cu Kα radiation (λ = 1.5418 Å) at 30 kV and 10 mA. The intensity data was captured with a Lynxeye detector with 2θ scans performed in the range 4−90° with a 0.020° step size at 0.5 s per step. Samples were spun at 30 rpm. By using PANanalytical Xpert Pro high score software to compare the JCPDS-ICDD library database, the crystallographic structure and phase were detected. The average crystal size of synthesised g-C_3N_4@Fe_3O_4 and BNNS@Fe_3O_4 were determined by Debye–Scherrer equation ($D = k\lambda/\beta\cos\theta$), where k is the Scherrer constant (0.89), λ is the X-ray wavelength and ß is the full width at half maxima (FWHM) of the diffraction peak.

3.4.4. Zeta potential (ζ)

Zeta potential (ζ) was conducted using the Malvern Panalytical PN3702 Zetasizer Nano ZS to determine the point of zero charge (PZC)/ isoelectric point (IEP) for the optimisation of g-C_3N_4@Fe_3O_4/BNNS@Fe_3O_4 – MPs surface interaction. The electric field was applied across the sample, resulting in particle electrophoretic mobility. This movement was measured by observing the light scattering of the particles. The zeta potential, ζ, was then calculated utilising the Henry equation (equation 2):

$$U_e = \frac{2\epsilon\zeta f(\kappa a)}{3\eta} \qquad (2)$$

where U_e represents the electrophoretic mobility, ϵ is the dielectric constant, η is the absolute zero-shear viscosity of the medium, f (κa) is the Henry function, and κa is a parameter that measures the ratio of the particle radius to the Debye length (Clogston and Vermilya 2005). Samples were prepared in medium with low ionic strength (10 mM NaCl). Samples were prepared from pH 2 – 12, in increments of 2. Before sample preparation, the suspending medium was filtered through a membrane with a pore size of 0.2 µM. A luer-lock tipped

syringe was employed to load 750 µL into the zeta cells and all bubbles were dislodged. Both ports were capped, and the zeta cell was placed into the instrument in contact with the electrodes. Prior to beginning the measurements, a 2 min equilibration time was performed. Thereafter, the samples were processed.

3.4.5. Thermogravimetric analysis

The TGA was done as previously described in section 3.3.1.2. (i).

3.4.6. Field emission scanning electron microscopy (FE-SEM) with EDX

To ascertain the surface morphology and elemental composition of the MNCs, SEM-EDX analysis was performed using a Zeiss MERLIN field emission scanning electron microscope (Carl Zeiss Microscopy, Munchen, Germany). A Zeiss InLens Secondary Electron (SE), and Backscattered Electron (BSE) Detector and Zeiss Smart SEM software were used to generate images. The samples were chemically quantified by qualitative Energy Dispersive X-Ray Spectrometry (EDS) using an Oxford Instruments® X-Max 20 mm2 detector and Oxford Aztec software (Oxford Instruments, Oxfordshire OX13 5QX, United Kingdom). Images were captured at a very low pressure and 20 kV.

3.4.7. Transmission electron microscopy (TEM)

Using a TEM (FEI Tecnai G2 20 S-Twin), the interior morphology of synthesised g-C_3N_4@Fe_3O_4 and BNNS@Fe_3O_4 equipped with an EELS detector and EDAX were examined. A small quantity of the MNC material (~100 mg) was combined with ethanol and sonicated for 15 minutes prior to analysis. After the resultant solution dried, it was put onto the carbon-coated copper TEM grid (200 mesh) for analysis.

3.4.8. X-ray photoelectron spectroscopy (XPS)

Using a 100 μm diameter monochromatic Al-Ka (1486 eV) anode operating at 15 kV and 25 W as the X-ray source, X-ray photoelectron spectroscopy (PHI 5000 Scanning ESCA Microprobe) was used to evaluate the surface composition and electronic state of the components of g-C_3N_4@Fe_3O_4 and BNNS@Fe_3O_4 by analysing different binding energy peaks. With a pass energy set to 2.95 eV, the analyser achieves a resolution of ≤ 0.5 eV. Survey scan spectra characterisation parameters were 187 eV Pass energy, 1 eV/step, 100 ms/step, 3 cycles, UHV Base Pressure 7.2E-9 Torr with 1x1 mm raster sputter rate of approximately 12 nm/min. Using the multipack tool (Multiscience GmbH Software Ltd., Germany), the XPS spectral peaks were deconvoluted, identifying chemical compounds and their electronic states using Gaussian–Lorentz fits. To minimize surface charging, an argon ion gun with low energy monatomic argon ions (Ar^+) and a low energy neutralizer electron gun were employed. The binding energy calibration is conducted using the high energy peak of Cu 2p3 at 932.62 eV and the low energy peak of Au 4f7 at 83.96 eV, maintaining a constant difference of 848.66 eV. The analyser's work function is set to 3.7 eV to position the Ag3d5 peak at 368.27 ± 0.1 eV. The elimination of Kα3,4, Kα5,6, and Kβ X-ray lines, as well as the Al Bremsstrahlung radiation background, while narrowing the Al Kα1,2 line to approximately 0.26 eV FWHM was ensured. This narrow line width allows for high energy resolution in both core and valence band spectra, preventing overlaps caused by X-ray satellite-induced photoemission peaks.

3.5. Results and Discussion

3.5.1. Synthesis and surface area optimisation of g-C_3N_4@Fe_3O_4 and BNNS@Fe_3O_4

3.5.1.1. Thermogravimetric analysis

The first step was to determine the temperature at which calcination of BNNS@Fe_3O_4 would occur. Herein, TGA was utilised to evaluate the thermal stability of BNNS@Fe_3O_4 conferring a calcination temperature (Ebnesajjad 2011; Wang *et al.* 2015; El-Azazy *et al.* 2021). TGA was conducted on the dried BNNS precursor (boric acid and urea mixture) attained prior to calcination as exhibited in Figure 37 (e), (appendix 4). The sample underwent heating to 1000 °C at a rate of 5 °C/min. From the thermograph (Figure 11), it was observed that the initial weight loss phase transpired below 115 °C and is attributed to the removal of physically adsorbed moisture (Kumar and Prasad 2020). Subsequently, a second weight loss phase occurred between 115 and 315 °C, followed by a third weight loss phase between 315 and 490 °C. These latter phases likely correspond to the oxidation and combustion of $–NH_2$ groups present in the sample. Almost complete weight loss of the sample was achieved at approximately 400 °C. Consequently, a calcination temperature of 400 °C was selected for the precursor's transformations into their final configurations. Once the calcination temperature had been determined, the next step involves the synthesis and surface optimization of the nanosheets. This dual-purpose step (synthesis and optimisation) is critical as it ensures that the BNNS@Fe_3O_4 possess the desired surface characteristics, enhancing their functional properties for downstream applications.

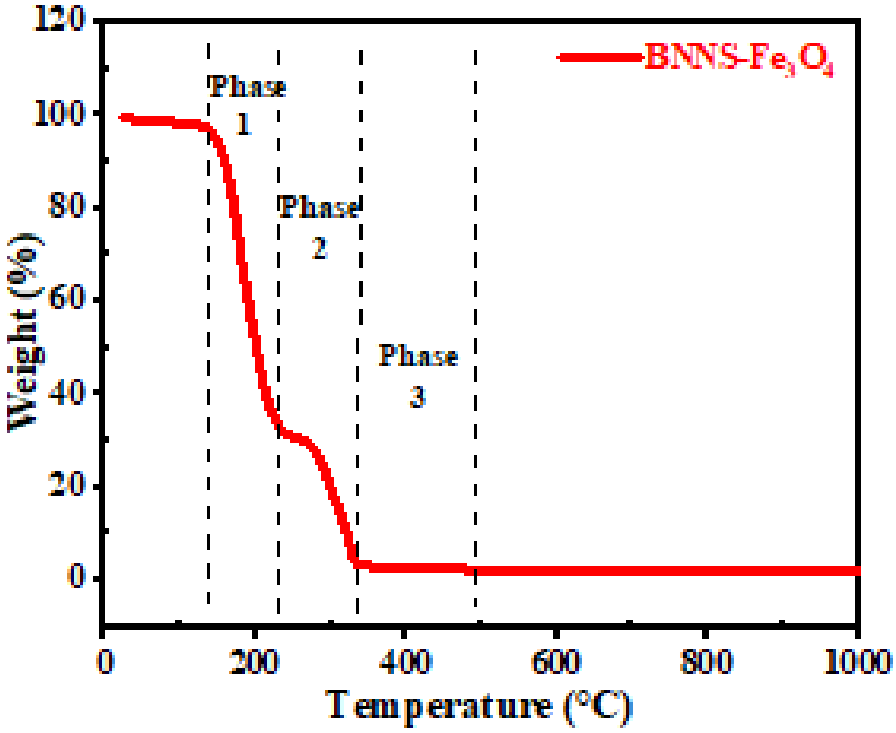

Figure 11: TGA thermograph of BNNS@Fe_3O_4

3.5.1.2. Surface area (S_{BET}) optimisation by varying calcination temperature for g-C_3N_4@Fe_3O_4 and calcination ratio for BNNS@Fe_3O_4

Several different temperature values and boric-acid : urea ratios were utilised to optimise the specific surface area (S_{BET}) of g-C_3N_4@Fe_3O_4 and BNNS@Fe_3O_4, respectively (Table 5 and 6, respectively). The parameters that produced the largest surface area were further selected for large scale synthesis of the respective MNCs for the experiments. For g-C_3N_4@Fe_3O_4, at 500, 550 and 600 °C, a specific surface area of 37.72, 38.42 and 66.88 m^2/g was ascertained (Table 5). Author Rosa et al. (2021) synthesised g-$C_3N_{4@}Fe_3O_4$ via two different methods: conventional coprecipitation and homogenous coprecipitation and reported a surface area of 52.7 m^2/g and 42.9 m^2/g, respectively. In this study, conventional coprecipitation was used and after optimization, a maximum surface area of 66.88 m^2/g was observed. This is in good agreement with literature since the surface area reported in this study is similar to the results reported by the previous study. Herein, the largest surface area was obtained at 600 °C,

therefore, this was selected as the optimum calcination temperature for g-C_3N_4@Fe_3O_4 synthesis. In the case of BNNS@Fe_3O_4, different boric-acid : urea ratios were investigated, with and without methanol (Table 6). The results showed that using methanol with ratios of 1:48, 1:30, and 1:15, the specific surface areas obtained were as follows: 43.04 m^2/g, 53.03 m^2/g and 79.08 m^2/g, respectively. In addition, without using methanol the specific surface areas observed were 48.03 m^2/g, 68.5 m^2/g, 87.04 m^2/g and 100.54 m^2/g, for ratios 1:48, 1:30, 1:15 and 1:5, respectively. Herein, it was observed that the inclusion of methanol during the synthesis of BNNS@Fe_3O_4 resulted in a decrease in specific surface area. This phenomenon can be attributed to methanol's role as a quenching agent, which can lead to rapid termination of particle growth during the formation of nanomaterials. Such abrupt cessation can cause premature aggregation of particles, thereby reducing the overall surface area. Additionally, methanol may influence the solubility and dispersion of precursors, further affecting the nucleation and growth processes, ultimately leading to denser structures with diminished porosity and surface area. Thus, methanol's quenching effect likely interfered with the formation of optimal porous structures in BNNS@Fe_3O_4, contributing to the observed decrease in surface area. Without methanol, the synthesis proceeded with fewer disruptions, allowing for higher specific surface area and better structural integrity which is consistent with the experimental results (Schreuders *et al.* 2005; Chen *et al.* 2015). Herein, the largest specific surface area was attained at ratio 1:5. Hence, this was chosen as the optimum calcination ratio for BNNS@Fe_3O_4 synthesis. The surface area of ratio 1:5 (methanol) was not investigated due to the data indicating that the larger surface areas were obtained without methanol. A study by Bangari et al. (2019) synthesised BNNS@Fe_3O_4, with similar methodology to the current study. Herein they reported a surface area of 119 m^2/g utilizing a single ratio of 1:48, whereas in the present study, various ratios were explored. In this study, after optimization, the

maximum surface area was noticed to be 100.54 m^2/g for ratio 1:5, as results shown in table 6, which is similar to the reported literature.

Table 5: Surface area optimisation for g-C_3N_4@Fe_3O_4 MNC

Temperature	g-C_3N_4@Fe_3O_4 (m^2/g)
500 °C	37.72
550 °C	38. 42
600 °C	**66.88**

Table 6: Surface area optimisation for BNNS@Fe_3O_4 MNCs

Boric acid : urea ratio	BNNS@Fe_3O_4 (m^2/g)
1:48 (methanol)	43.04
1:48	48.03
1:30 (methanol)	53.03
1:30	68.5
1:15 (methanol)	79.08
1:15	87.04
1:5	**100.54**

3.5.2. Characterisation of the synthesized MNCs

3.5.2.1. X-ray Diffraction (XRD)

The crystalline phases and structure of both fresh and used g-C_3N_4@Fe_3O_4 and BNNS@Fe_3O_4 MNCs were examined by recording XRD patterns in the range of 5°- 90°. The diffraction patterns positioned near 2θ values 41.51°, 74.23°, 35.12°, 50.53°, 35.29°, 74.49°, 67.41°, 67.26° and 21.26° index to plane (103), (224), (112), (004), (200), (400), (321), (231) and (011), respectively, exhibited common phase with orthorhombic crystalline structure of g-C_3N_4@Fe_3O_4 (Figure 12 (a)) and excellent accord with JCPDS PDF #01-075-1609, space

group – 74/Imma, from JCPDS database analysed by Xpert high score software. MNC BNNS@Fe_3O_4 (Figure 12 (b)) exhibited a similar diffraction pattern for Fe_3O_4 phase, crystalline structure and JCPDS PDF # as g-C_3N_4@Fe_3O_4 with only 2θ value peak intensity percentages being different. This similarity between g-C_3N_4@Fe_3O_4 and BNNS@Fe_3O_4 is attributed to the Fe_3O_4 nanoparticle formation, whilst the difference could be ascribed the supporting material. Similar results have been reported by previous researchers for g-C_3N_4@Fe_3O_4 and BNNS@Fe_3O_4 MNCs (Bangari *et al.* 2019; Rosa *et al.* 2021; Dawn *et al.* 2022). In addition, g-C_3N_4@Fe_3O_4 and BNNS@Fe_3O_4 crystalline structure are in strong agreement with the TEM crystallographic shape (orthorhombic) in Figure 16 (e-f) and in Figure 43-44, appendix 8. Moreover, the XRD patterns of the used MNCs closely resembled those of the fresh MNCs. No discernible structural alterations or additional peaks were noted in the patterns; however, an increase in pattern intensity was observed in the case of both MNCs. Hence, both MNCs showed excellent chemical stability and can be recycled for the purification of MPs in wastewater.

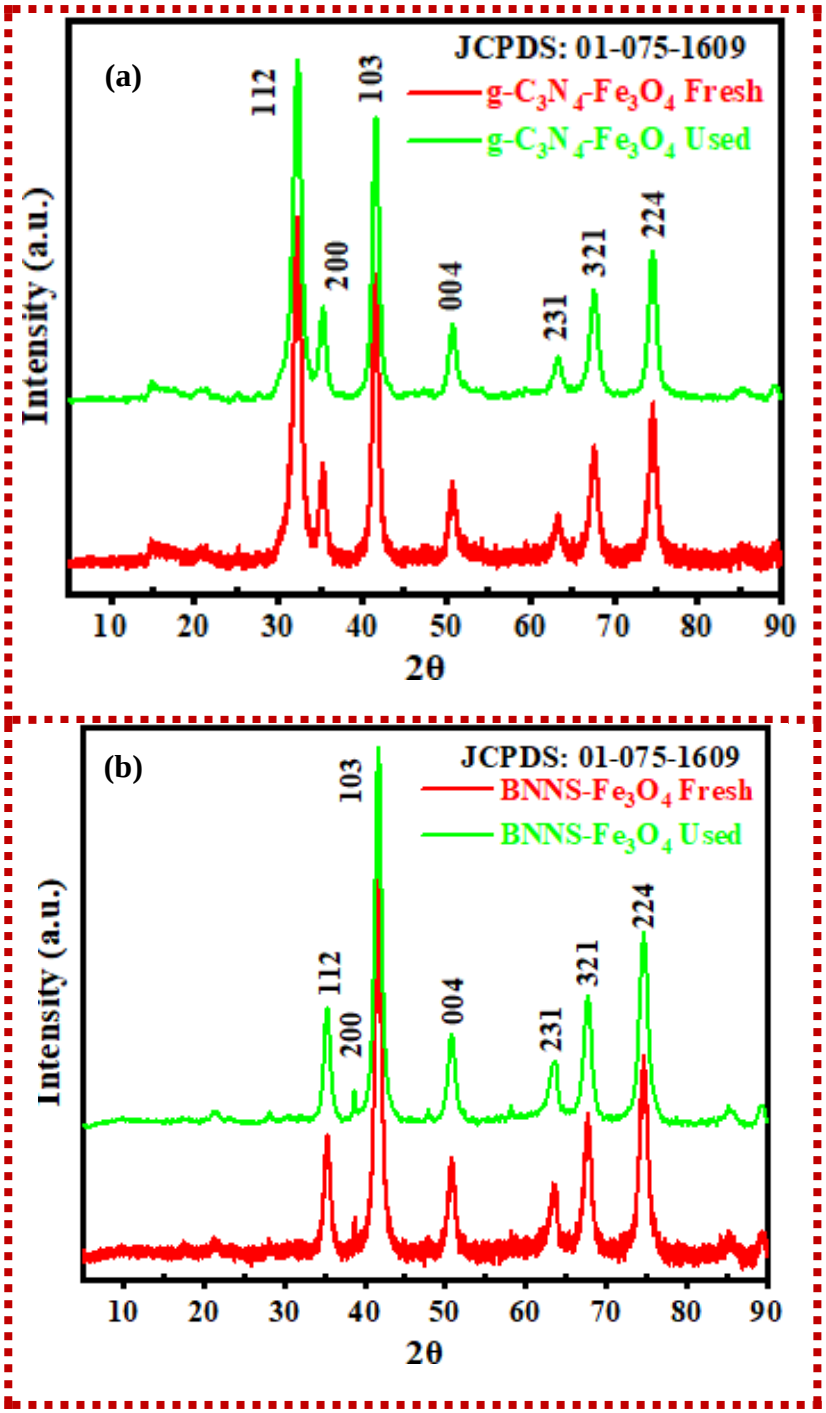

Figure 12: XRD spectra of (a) fresh and used g-C_3N_4@Fe_3O_4, (b) fresh and used BNNS@Fe_3O_4

3.5.2.2. Fourier-Transform Infrared (FTIR) Spectroscopy

FTIR spectroscopy was employed to capture the distinct vibrational patterns of the functional groups (Eid 2022) present on the fresh and used MNCs within the range of 4000-400 cm^{-1} as depicted in Figure 13 corresponding to g-C_3N_4@Fe_3O_4 and BNNS@Fe_3O_4. In Figure 13 (a), the spectra vibration modes assigned to the g-C_3N_4 and Fe_3O_4 phases are identified. The spectral band at 576 cm^{-1} is ascribed to the Fe-O group in the tetrahedral and octahedral sites (Wang *et al.* 2018) whilst the band at 807 cm^{-1} is associated with the Fe-O-Fe group. This suggests that the iron oxide nanoparticles were integrated into the carbon nitride structure. The band at 890 cm^{-1} corresponds to tris-s-triazine (Praus *et al.* 2017) heptazine ring and displays out-of-plane bending vibration, which demonstrates that the graphitic carbon nitride is a nanosheet 2D material (Chouhan *et al.* 2023). The spectral band at 1250 cm^{-1} represents -CH_3 group whilst the high intensity bands from 1280 cm^{-1} to 1700 cm^{-1} depicts CN heterocycles vibration in graphitic carbon nitride (Lin *et al.* 2017). The C=C stretching vibration is designated to the spectral band 1586 cm^{-1}. Band 3082 cm^{-1} and 3243 cm^{-1} represents residual N-H stretching vibration that is attributed to primary and secondary amines (Tian *et al.* 2020). The moisture band of 3433 cm^{-1} exhibits stretching of hydroxyl (OH) group which indicates that strong hydrogen bonds are present (Kumari *et al.* 2015). The bands maintained high intensity in the fresh and used sample, indicating that the structural configuration of the g-C_3N_4@Fe_3O_4 remained unchanged. Similar results have been reported by Rosa et al. (2021). In Figure 13 (b), the Fe profile (Fe-O, Fe-OH, Fe-O-Fe) of BNNS@Fe_3O_4 was identified. The vibration band at around 440 cm^{-1} (Fekri Aval *et al.* 2016) and between 583-636 cm^{-1} illustrates symmetrical stretching vibration of Fe-O (Xia *et al.* 2009). The spectral band at 857 cm^{-1} indicates stretching vibration of Fe-O-Fe (Du *et al.* 2013) whilst the structural vibration of Fe-OH corresponds to band 1030 cm^{-1} (Lunge *et al.* 2014). The spectral band at 1400 cm^{-1} is attributed to the in-plane vibration of sp^2-bonded B-N bonds (Kumari *et al.* 2015), whilst the

band at 782 cm^{-1} is designated to the out-of-plane vibration of the B-N-B bond (Bangari *et al.* 2019). The degree and intensity of out-of-plane vibration in B–N–B bonds are correlated with the arrangement of BNNSs layers i.e., its stacking order (Bangari *et al.* 2020). Herein, the stacking order is similar to BNNS@Fe_3O_4 synthesized by Bangari and team indicating a 2D MNC (Bangari *et al.* 2020). The band at 1638 cm^{-1} indicates bending vibration of water vapour (H-O-H) adsorbed on the MNCs surface (Kumari *et al.* 2015). The low-intensity bands at 2857 cm^{-1} and 2923 cm^{-1} are ascribed to the -BNH_2 group which forms at the edges (Liu *et al.* 2015). Lastly, the broad band at 3429 cm^{-1} represents the stretching of hydroxyl (B-OH) which represents the moisture, and the broadness of the spectral band indicates the presence of strong hydrogen bonding (Kumar *et al.* 2023a). The bands maintained high intensity in the fresh and used sample, indicating that the structural configuration of the BNNS@Fe_3O_4 remained unchanged. Similar results have been reported by Bangari et al. (2019).

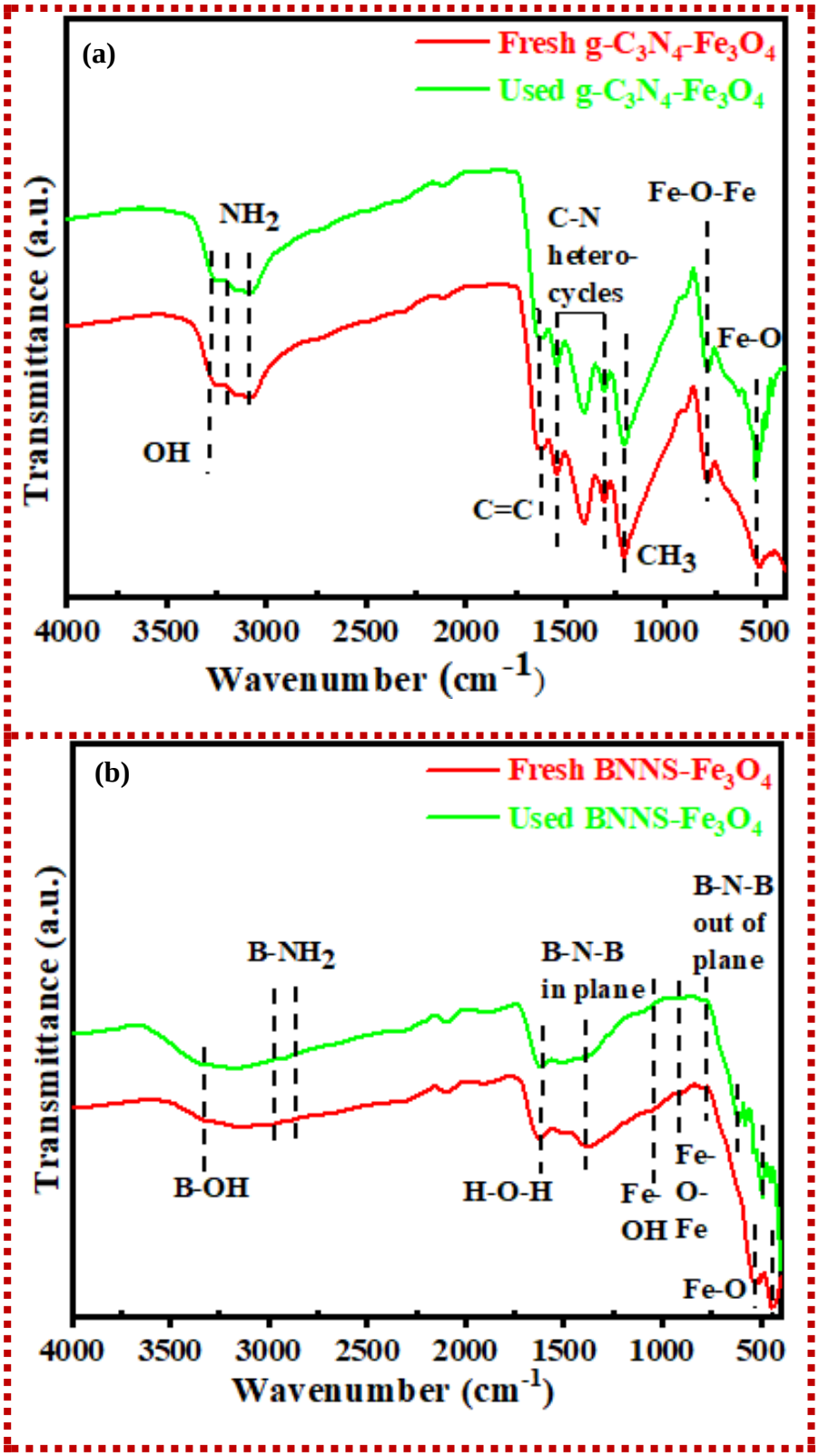

Figure 13: FTIR spectra of (a) fresh and used g-C_3N_4@Fe_3O_4, (b) fresh and used BNNS@Fe_3O_4

3.5.2.3. Zeta (ζ) potential

Zeta potential was utilised to measure the reactivity of the surface (Ferraris *et al.* 2018) of g-C_3N_4@Fe_3O_4 and BNNS@Fe_3O_4 and ascertain the point of zero charge (pH_{pzc})/ isoelectric point as shown in Figure 14. For g-C_3N_4@Fe_3O_4, the zeta potential is almost zero in acidic conditions (pH ~3) and progressively decreased with an increasing in pH (-36.3 mV at pH ~11). This was attributed to the substitution of ≡C–NH_2 groups on the g-C_3N_4 surface with ≡C–OH groups, leading to its heightened deprotonation (≡C–O^-) in aqueous solutions at elevated pH levels (Zhu *et al.* 2015). For BNNS@Fe_3O_4, the zeta potential followed a similar pattern to g-C_3N_4@Fe_3O_4, wherein the zeta potential progressively decreased with an increase in pH (-44.1 mV at pH ~11). Similarly, this is designated to the protonation of the hydroxyl functional group on the BNNS@Fe_3O_4 particle surface (Wang *et al.* 2021b). Herein, the pH_{pzc} was established to be 4.3. The heightened negativity of the zeta potential above pH 7 and pH 8 for g-C_3N_4@Fe_3O_4 and BNNS@Fe_3O_4, respectively, can be attributed to the incorporation of Fe_3O_4 on the supporting material g-C_3N_4 and BNNS surface (Rosa *et al.* 2021). These magnetic nanoparticles act as a diprotic acid, resulting in deprotonation with the formation of three distinct surface sites, primarily ≡$Fe(OH_2)^+$, ≡FeOH and ≡$Fe(O)^-$ in strongly acidic, neutral and alkaline conditions, respectively, for both for g-C_3N_4@Fe_3O_4 and BNNS@Fe_3O_4 (Campos *et al.* 2017; Wang *et al.* 2021b).

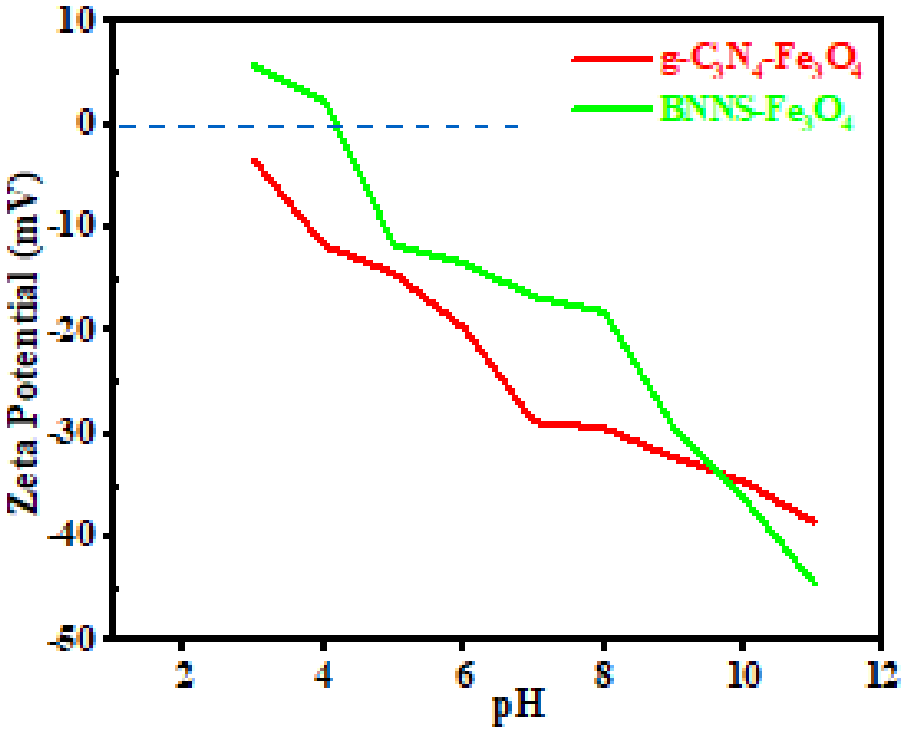

Figure 14: Zeta potential of g-C_3N_4@Fe_3O_4 and BNNS@Fe_3O_4

3.5.2.4. Surface morphology of fresh and used g-C_3N_4@Fe_3O_4 and BNNS@Fe_3O_4 MNCs

The surface morphology of fresh and used g-C_3N_4@Fe_3O_4 and BNNS@Fe_3O_4 MNCs were analysed by FESEM as shown in Figure 15 (a-d), and their elemental composition was analysed by EDX, as shown in Figure 16 (a-d). The FESEM micrograph (Figure 15 (a-b)) of fresh g-C_3N_4@Fe_3O_4 and BNNS@Fe_3O_4 exhibited a granular-like porous structure with interconnected agglomerated particles. Additionally, they exhibited a more compact sheet-like structure. The similar morphology of g-C_3N_4@Fe_3O_4 and BNNS@Fe_3O_4 MNCs have been reported by various researchers (Bangari *et al.* 2019; Bangari *et al.* 2020; Sahoo *et al.* 2020). After treatment, a small change in morphology of used g-C_3N_4@Fe_3O_4 and BNNS@Fe_3O_4, were noticed such as irregular and roughing of the surface and a decrease in the porosity as shown in Figure 15 (c-d). This might be caused by intermediate compounds formed during the reaction accumulating inside the pore as well as reduction of the active sites due to leaching

(Kumar *et al.* 2021a), Additionally, the MPs can block or cover the surface pores thereby altering the smoothness of the surface, creating a more irregular or uneven surface. The decrease in porosity may potentially be attributed to the aggregation of MNCs resulting in the formation of larger clusters which leads to changes in the overall particle size and surface structure. The originally dispersed MNC may now appear as aggregated masses with reduced surface area and porosity (Kumar *et al.* 2021b). Furthermore, both NMs displayed closely packed spherical-like nonuniform particles with smooth surface as shown in Figure 15 (a-b). After treatment, large, lumped particles in the size of few micrometres were observed as depicted in Figure 15 (c-d). This is similar observation to previously reported work for g-C_3N_4@Fe_3O_4 and BNNS@Fe_3O_4 (Bangari *et al.* 2020; Rosa *et al.* 2021). In addition, the elemental mapping of fresh g-C_3N_4@Fe_3O_4 and BNNS@Fe_3O_4 MNCs were done to ascertain the elemental content and its distribution on the surface. Based on the elemental mapping, the metal ions and oxygen are homogeneously distributed on the adsorbent surface for both MNCs as shown in Figure 16 (a-b). Furthermore, EDX spectra of fresh g-C_3N_4@Fe_3O_4 and BNNS@Fe_3O_4 adsorbent showed an intense signal of elements Fe and O indicating that these are the major components on the MNCs. The elemental composition (wt.%) was almost close to stoichiometric composition in MNC sample as inserted table in EDX micrographs in Figure 16 (c-d).

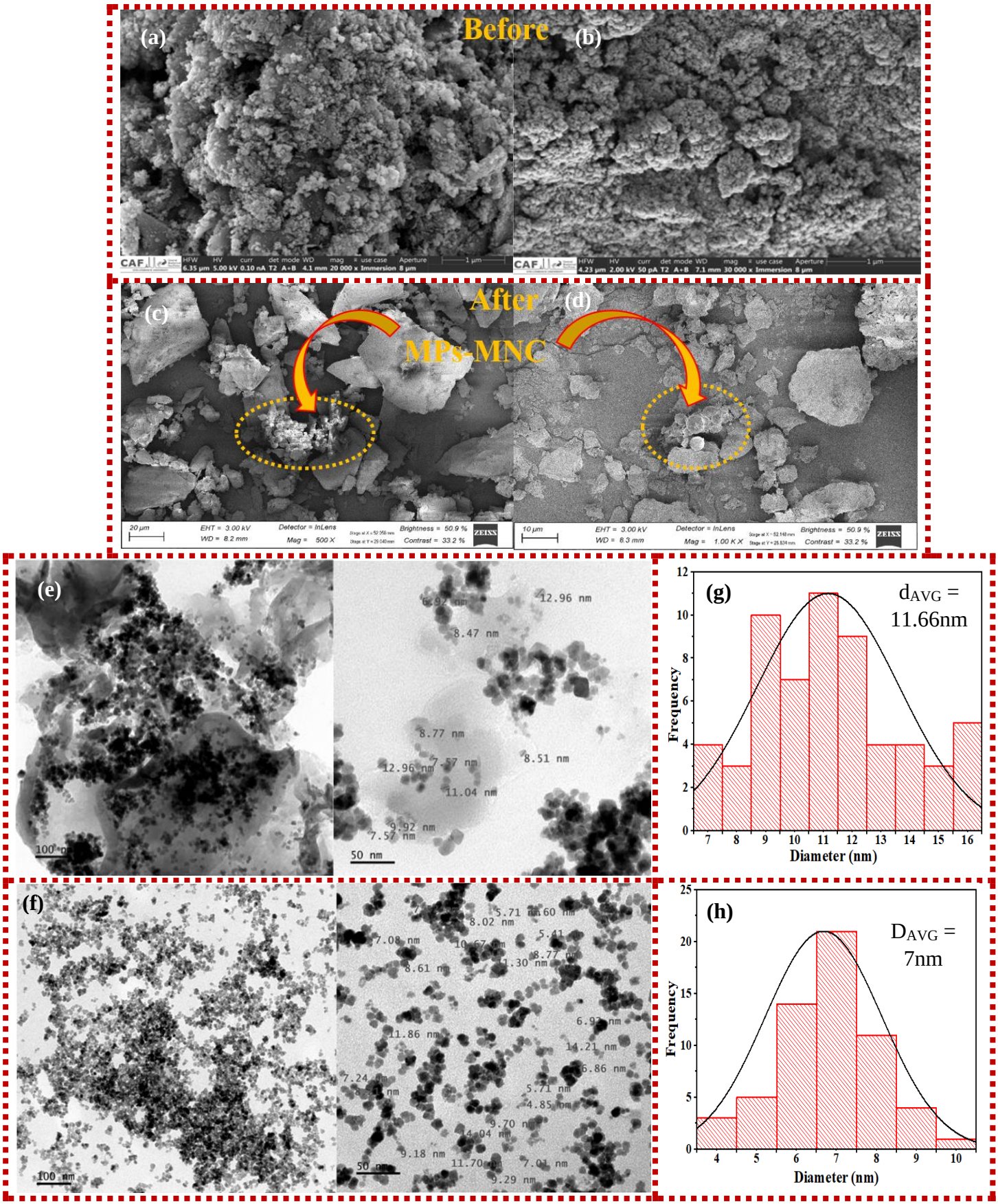

Figure 15: SEM micrograph of fresh (a) g-C_3N_4@Fe_3O_4, (b) BNNS@Fe_3O_4, used (c) g-C_3N_4@Fe_3O_4, (d) BNNS@Fe_3O_4, TEM micrograph of (e) g-C_3N_4@Fe_3O_4, (f) BNNS@Fe_3O_4 and Histogram plot of (g) g-C_3N_4@Fe_3O_4 and (h) BNNS@Fe_3O_4

The internal morphology and crystalline characteristics of the g-C_3N_4@Fe_3O_4 and BNNS@Fe_3O_4 MNCs were investigated using TEM micrographs, as depicted in Fig. 2. The micrographs, captured at scales of 50 and 100 nm as displayed in Fig. 2(e-g) for g-C_3N_4@Fe_3O_4 and BNNS@Fe_3O_4, respectively, revealed spherical o-sized particles arranged in agglomerated and interconnected configurations, forming a complex network structure with irregular dimensions and uniformly dispersed particles. These particles were in orthorhombic shape (Fig. S2 (e-f)), consistent with JCPDS PDF #01–075-1609, space group – Imma/74, aligning well with the XRD findings and confirming the Fe_3O_4 phase functionalized with g-C_3N_4@Fe_3O_4 and BNNS@Fe_3O_4. Notably, Fig. 2(e) clearly illustrates the presence of granular g-C_3N_4 sheets with iron oxide evenly distributed across them, while in Fig. 2(g), BNNS is observed with iron oxide uniformly dispersed. Furthermore, the mean average particle sizes, as depicted in histogram plot Fig. 2(f-h), were determined using image processing software (Image J Software). As depicted in the histogram plots shown in Fig. 2(f) and (h), the d_{AVG} values were 11.66 and 7 nm for g-C_3N_4@Fe_3O_4 and BNNS@Fe_3O_4, respectively. This is consistent with the BET data since the surface area and particle size are inversely related (Singh and Nalwa 2007). Therefore, the smaller the nanoparticle, the larger the surface area. The BET results confer that BNNS@Fe_3O_4 has the larger surface area which is in good agreement with it having the smaller nanoparticle size of 7 nm as indicated by the histogram plot.

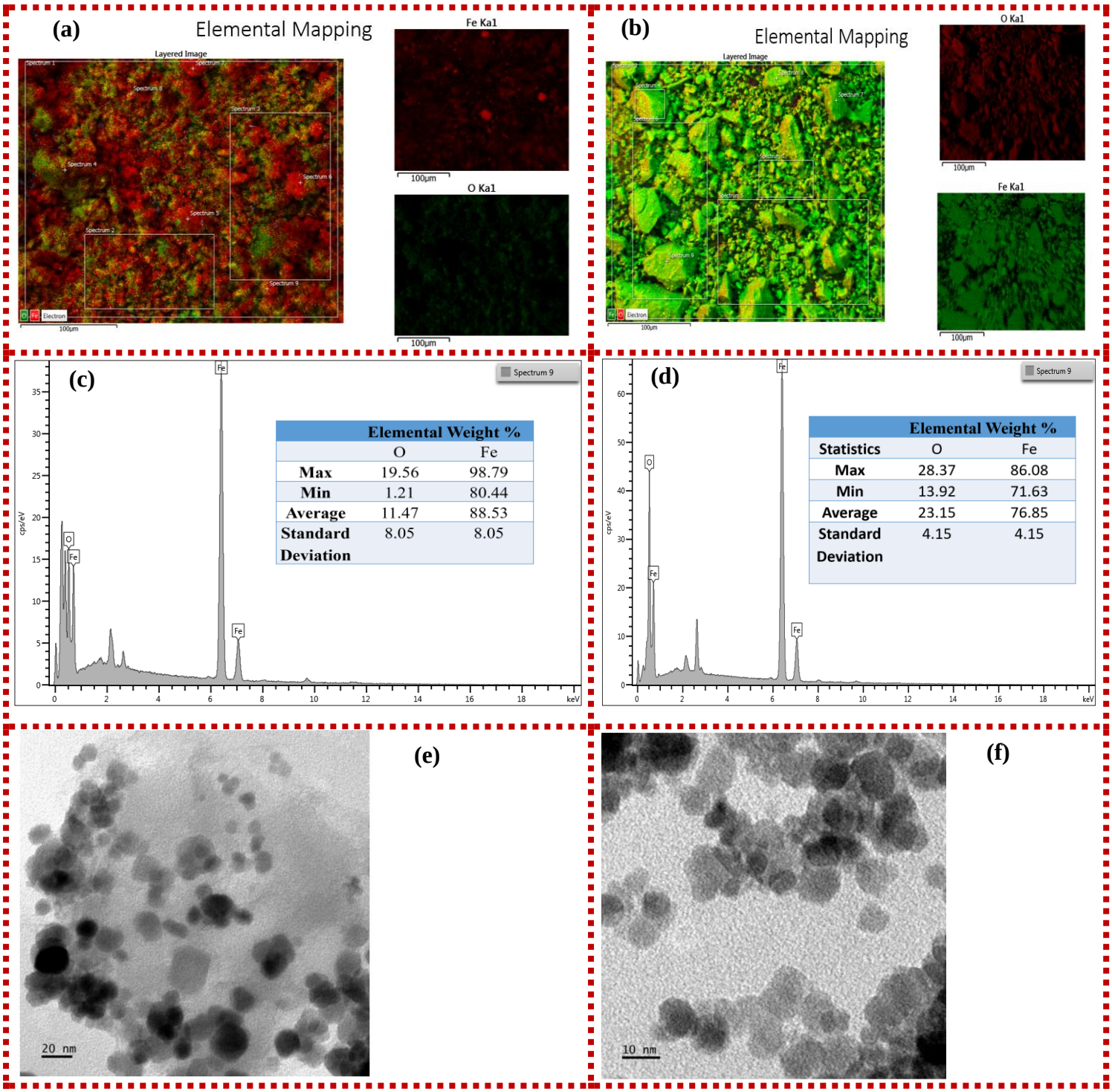

Figure 16: EDX micrographs of (a) g-C_3N_4@Fe_3O_4, (b) BNNS@Fe_3O_4, Elemental weight percentage composition of (c) g-C_3N_4@Fe_3O_4, (d) BNNS@Fe_3O_4 and TEM micrographs of (e) g-C_3N_4@Fe_3O_4, (f) BNNS@Fe_3O_4

3.5.2.5. Textural properties analysis: Brunauer-Emmett-Teller (BET)

The textural characteristics, such as porosity and specific surface area of g-C_3N_4@Fe_3O_4 and BNNS@Fe_3O_4 were assessed via N_2 physical adsorption–desorption method. Both samples revealed type IV hysteresis loop isotherms as shown in Figure 37, appendix 6, which indicate that the structures are mesoporous with a high adsorption capacity in the higher relative pressure region ($P/P_0 > 0.8$) (Tian *et al.* 2020; Rosa *et al.* 2021; Goel *et al.* 2022). The calculated BET surface areas (S_{BET}) were determined by computing the area under the adsorption branch of the isotherm within the linear region (P/P_0: 0.06–0.2 for g-C_3N_4@Fe_3O_4; P/P_0: 0.05-0.18 for BNNS@Fe_3O_4).

The texture properties of fresh g-C_3N_4@Fe_3O_4 were observed S_{BET} (54 m^2/g), V_{pore} (0.21 cm^3/g), and d_{pore} (170 Å); and for BNNS@Fe_3O_4 were observed S_{BET} (96 m^2/g), V_{pore} (0.19 cm^3/g), and d_{pore} (106 Å), respectively, as presented in Table 7. Several other studies have been reported similar ranges of S_{BET} and V_{pore} for g-C_3N_4@Fe_3O_4 and BNNS@Fe_3O_4 (Bangari *et al.* 2019; Bangari *et al.* 2020; Rosa *et al.* 2021). The inclusion of finer particles is believed to induce the exfoliation of g-C_3N_4 and BNNS sheets, resulting in increased S_{BET} and V_{pore}, as suggested by Yang and team (Yang *et al.* 2016). It's crucial to note that larger surface areas can offer more active sites for sorption, thereby enhancing performance and facilitating the adsorption, desorption, and diffusion of reactants and products (Wang and Yang 2017; Dee *et al.* 2023). Therefore, besides being manipulable through magnetic field application, the integration of magnetic nanoparticles can also contribute to improved efficiency in pollutant removal. Remarkably, following the adsorption of MPs, there was a notable reduction in the surface area and cavity characteristics (V_{pore}, and d_{pore}) of g-C_3N_4@Fe_3O_4 and BNNS@Fe_3O_4. The S_{BET}, V_{pore}, and d_{pore} of g-C_3N_4@Fe_3O_4 decreased to 32.28 m^2/g, 0.14 cm^3/g, and 155 Å, respectively, whilst BNNS@Fe_3O_4 properties decreased to 71.97 m^2/g, 0.18 cm^3/g, and 76 Å for S_{BET}, V_{pore}, and $d_{pore,}$ respectively. Several factors may lead to the decrease in the S_{BET},

V_{pore}, and d_{pore} of the used MNCs after treatment. These factors encompass: (a) the deposition of carbon impurity within the MNC pores, appearing as intermediate compounds produced during the reaction, and (b) the collapse of the MNC pores (Parvas *et al.* 2019; Kumar *et al.* 2023a).

Table 7: Textural properties analysis of fresh and used g-C_3N_4@Fe_3O_4 and BNNS@Fe_3O_4

MNC	S_{BET} (m^2/g)	V_{pore} (cm^3/g),	d_{pore} (Å)
Fresh g-C_3N_4-Fe_3O_4	54	0.21	170
Used g-C_3N_4-Fe_3O_4	32.28	0.14	155
Fresh BNNS-Fe_3O_4	96	0.19	106
Used BNNS-Fe_3O_4	71.97	0.18	76

3.5.2.6. X-ray Photoelectron Spectroscopy (XPS)

The surface composition, valance state, and oxygen vacancies of MNCs were investigated using XPS analysis (Kumar *et al.* 2020b). The survey scan spectrum before and after treatment (physiosorption), as displayed in Figure 17 (a-b) exhibited intense signals of Fe2p, B1s, O1s, C1s, N1s, in BNNS@Fe_3O_4 and Fe2p, O1s, C1s, N1s in g-C_3N_4@Fe_3O_4, which confirms the presence of elements in the respective samples. The Fe2p core-level XPS spectra of BNNS@Fe_3O_4, exhibited in Figure 18 (a) was deconvoluted into four characteristic bands of Fe species located near binding energies ~724.3 eV, ~711.1 eV, ~721.2 eV and ~708 eV. The bands at ~721.2 eV and ~724.3 eV correspond to $Fe2p_{1/2}$ Fe^{3+} and Fe^{2+} oxidation states. The bands at ~711.1 and ~708 eV correspond to $Fe2p_{3/2}$ Fe^{2+} and Fe^{3+} oxidation states (An *et al.* 2014; Nene *et al.* 2016). After treatment, there is no significant change noticed at bands located at $Fe2p_{3/2}$ corresponding to binding energy ~711.1 and ~708 eV (Fe^{2+} and Fe^{3+} oxidation states). For $Fe2p_{1/2}$, spectral band located at ~724.3 eV exhibited no change in binding energy,

however, a decrease in peak intensity was observed whilst spectral band located at ~721.2 eV shifted towards the higher binding energy of ~721.8 eV. This might be due to an alteration in the relative composition of Fe^{3+} and Fe^{2+} phase on the MNC surface. Similarly, in the case of NM g-C_3N_4@Fe_3O_4, the Fe2p core-level XPS spectra (Figure 18 (b)) deconvoluted into four characteristic bands. Two characteristic spectral bands positioned at ~720.9 eV and ~724.1 eV can be attributed to $Fe2p_{1/2}$ Fe^{3+} and Fe^{2+} oxidation states whilst the bands at ~707.7 eV and ~711.2 eV can be attributed to $Fe2p_{3/2}$ Fe^{3+} and Fe^{2+} oxidation states, respectively. After treatment, no significant changes were observed in the spectral peak intensity and there was no observable shift in the binding energy of both $Fe2p_{1/2}$ and $Fe2p_{3/2}$. The bands in the $Fe2p_{1/2}$ and $Fe2p_{3/2}$ states indicate the presence of Fe^{3+} and Fe^{2+} ions thereby confirming the existence of Fe_3O_4 particles (Zhao *et al.* 2017). Numerous studies have reported similar results for both MNCs (BNNS@Fe_3O_4 and g-C_3N_4@Fe_3O_4) (Ai *et al.* 2019; Zhong *et al.* 2020; Li *et al.* 2022). The C1s spectra of BNNS@Fe_3O_4 and g-C_3N_4@Fe_3O_4 were each deconvoluted into three characteristic peaks as displayed in Figure 19 (a-b), respectively. For BNNS@Fe_3O_4, the bulk of the carbon atoms in the MNC maintained their hexagonal crystalline structure (2D), as evidenced by the primary component band, which is located at ~284.1 eV and correlated to the graphitic C–C bonds (Matsoso *et al.* 2017). The creation of boron carbide bonds, either as BC_3 or B_4C, is attributed to the component band at lower binding energy (~282.8 eV) (Uddin *et al.* 2005). Moreover, the last band, which is positioned at a higher binding energy of ~287 eV, is ascribed to oxygenated C atoms (C=O and N–C=O/O–C=O) near the domain boundaries and/or defect sites (Lin *et al.* 2012). After treatment, there is a decrease in peak intensity of C–C bonds with a shift towards a higher binding energy of ~284.8 eV, whilst a minute shift towards higher binding energy of ~287.1 eV is observed for oxygenated C atoms (C=O and N–C=O/O–C=O), with a decrease in peak intensity. The band correlating to BC_3 or B_4C (sp^2 hybridised C) was enhanced with the band shifting slightly towards a higher binding energy of ~283 eV. This may

be attributed to the formation of some intermediates during the reaction due to the cleavage of the MP polymer chain that is adsorbed on the surface. In Figure 19 (b), in the case of g-C_3N_4@Fe_3O_4, the intense spectral bands located near binding energy of ~283.4 eV and ~284.8 eV and ~287.1 eV can be attributed to sp^2 C–C bonding, C–N– group bonding configurations, and sp^3 hybridised carbon atoms (C−NH_x), respectively (Lin *et al.* 2012). The sp^2 C–C bonding matches the sp^2 hybridized carbon of triazine ring (N=C−N) (Xing *et al.* 2022). After treatment, band corresponding to C–N– group bonding configurations was enhanced with a shift towards the higher binding energy of ~285.1 eV whilst no change in the binding energy of the sp^2 C–C bonding was observed, with a decrease in band intensity, indicating no deformation in the structure of the g-C_3N_4@Fe_3O_4 NM. A decrease in band intensity was also noticed for C−NH_x which could be attributed to the adsorption of MPs on the surface of NM. Furthermore, deconvoluted O1s spectrum produced three spectral bands for BNNS@Fe_3O_4 and g-C_3N_4@Fe_3O_4 as shown in Figure 20 (a-b), respectively. For BNNS@Fe_3O_4, corresponding to the bonds O=C/O-C (lattice oxygen), Fe-O (surface adsorbed oxygen) bonding configuration and O-H/O–B (carbonated oxygen) bonds is spectral band ~529.2 eV, ~531.1 eV and ~532.3 eV, respectively (Matsoso *et al.* 2017; Rosa *et al.* 2021). After treatment, the surface adsorbed oxygen and carbonated oxygen displayed no significant changes in the binding energy, however peak intensity for carbonated oxygen decreased. The areas of fitted peaks represents the oxygen species composition (Kumar *et al.* 2021a). Therefore the decrease in the composition of carbonated oxygen indicates the consumption of oxidative oxygen species (Kumar *et al.* 2021a). The lattice oxygen peak intensity increased and shifted towards a higher binding energy of ~529.5 from ~529.2 eV. This may be due to potential structural alteration as a result of the physiosorption of the MPs in the lattice spacing. It's interesting to note that O-N bonds could also be responsible for the component band at ~529.2 eV (Matsoso *et al.* 2017). Regarding the O1s XPS core spectra for g-C_3N_4@Fe_3O_4, the Fe-O (surface adsorbed oxygen)

bonds correspond to spectral band located at ~531.2 eV, whereas the O-H (carbonated oxygen) group corresponds to the spectral band positioned at ~532 eV (Tang *et al.* 2016; Zhao *et al.* 2019). The final spectral band at ~527.5 eV can be attributed to lattice oxygen (Figure 20 (b)). After treatment, no change in binding energy was noticed for carbonated oxygen, however the peak intensity decreased. The surface adsorbed oxygens peak intensity decreased in the chemisorption reaction and the binding energy was shifted toward a lower binding energy whilst the lattice oxygen peak intensity was increased and shifted towards a higher binding energy corresponding to ~528.1 eV. This could potentially be attributed to structural alteration due to the physiosorption of MPs. It is important to note that in the O1s spectra of both g-C_3N_4@Fe_3O_4 and BNNS@Fe_3O_4, the highest bands present correspond to Fe-O bonding configuration. This indicates that majority of the O atoms are bonded to Fe atoms. Two component bands that corresponded to sp^2-N–B (~398.0 eV) and N–C (~399.2 eV) were generated by deconvolution of the N1s signal for BNNS@Fe_3O_4 exhibited in Figure 21 (a). This MNC has sections of pyrrolic domains, as shown by the presence of N–C bonding topologies. Furthermore, the comparatively high and pronounced sp^2-N-B peaks demonstrated the great affinity of nitrogen for boron atoms, strongly suggesting the existence of h-BN domains (Matsoso *et al.* 2017), indicating the existence of sheets. There were no significant changes noticed in the band intensity and binding energy of the deconvoluted bands in the N1s spectra after treatment. Similarly, N1s spectrum of g-C_3N_4@Fe_3O_4 was deconvoluted in to two characteristic bands as depicted in Figure 21 (b). Spectral bands ~398.2 eV and ~399.1 eV corresponds to sp^2 hybridisation N (C–N=C) and tertiary nitrogen bonding to carbon atoms in the arrangement of (N–$(C)_3$) (Li *et al.* 2022). After treatment, there were no significant changes observed in the binding energy of the deconvoluted bands in the N1s spectra. However, a decrease in (N–$(C)_3$) band intensity was noticed whilst an enhancement of band correlating to sp^2 hybridisation N (C–N=C) was noticed. Therefore, only a change in composition was

observed. In addition, the B1s spectra of BNNS@Fe_3O_4 (Figure 22) was deconvoluted into three bands where atomic bonding of sp^2–B–N, B–O and B–Fe bonding configuration corresponds to binding energy ~189.4 eV, ~194.2 eV and ~196 eV, respectively. The intense spectral band located at ~196 eV indicates that B atoms are strongly bonded with Fe. After treatment, bands corresponding to sp^2–B–N and B–Fe bonding configuration displayed a minute shift towards a higher binding energy from ~189.4 eV to ~189.5 eV and ~196 eV to ~196.2 eV, respectively, with both bands exhibiting a decrease in intensity. Band corresponding to B–O revealed no significant alteration in band intensity and binding energy. Similar results have been reported for all XPS spectrum signals for BNNS@Fe_3O_4 (Matsoso *et al.* 2017; Dee *et al.* 2023) and for g-C_3N_4@Fe_3O_4 (Rosa *et al.* 2021; Li *et al.* 2022), respectively.

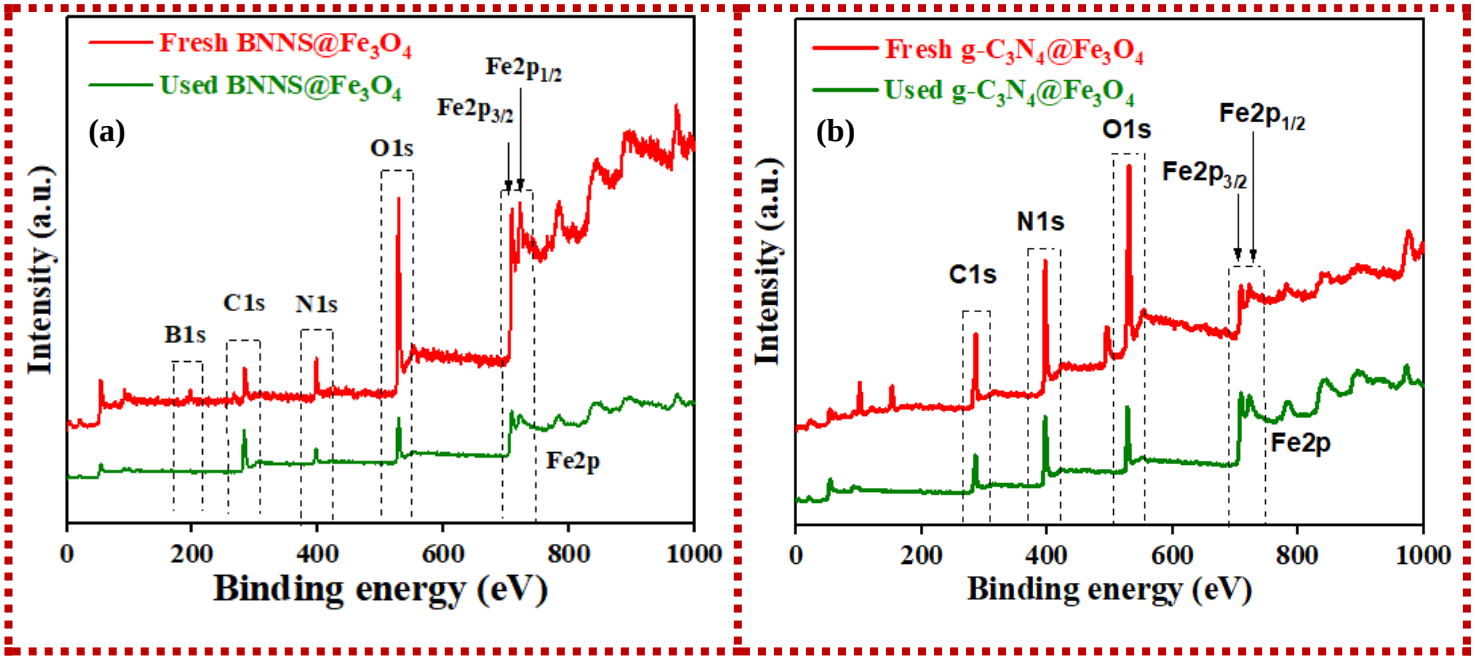

Figure 17: XPS spectra of BNNS@Fe_3O_4 and g-C_3N_4@Fe_3O_4: survey scan spectra of (a) fresh and used BNNS@Fe_3O_4, (b) fresh and used g-C_3N_4@Fe_3O_4

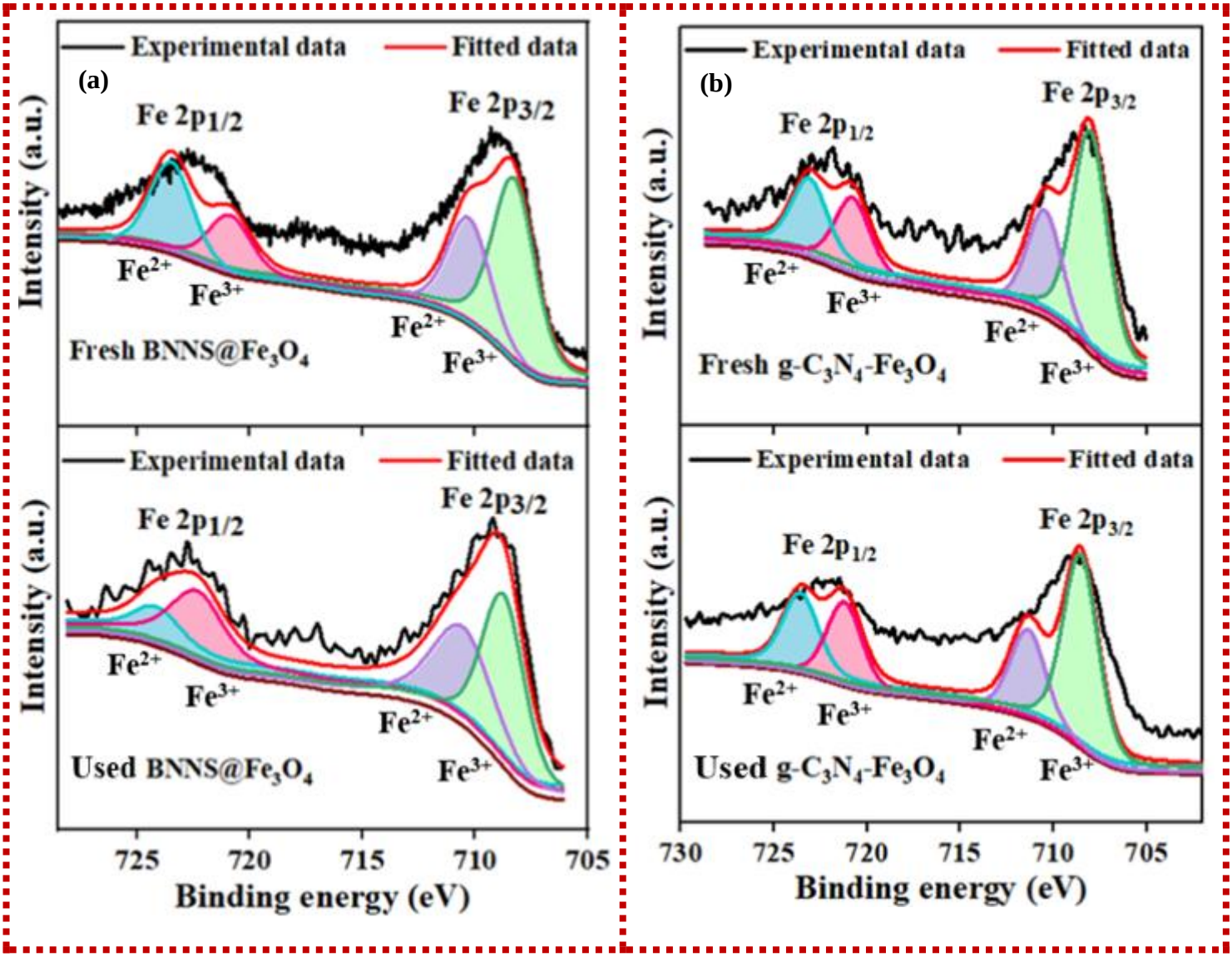

Figure 18: XPS spectra of BNNS@Fe_3O_4 and g-C_3N_4@Fe_3O_4: Fe2p spectra of (a) fresh and used BNNS@Fe_3O_4, (b) fresh and used g-C_3N_4@Fe_3O_4

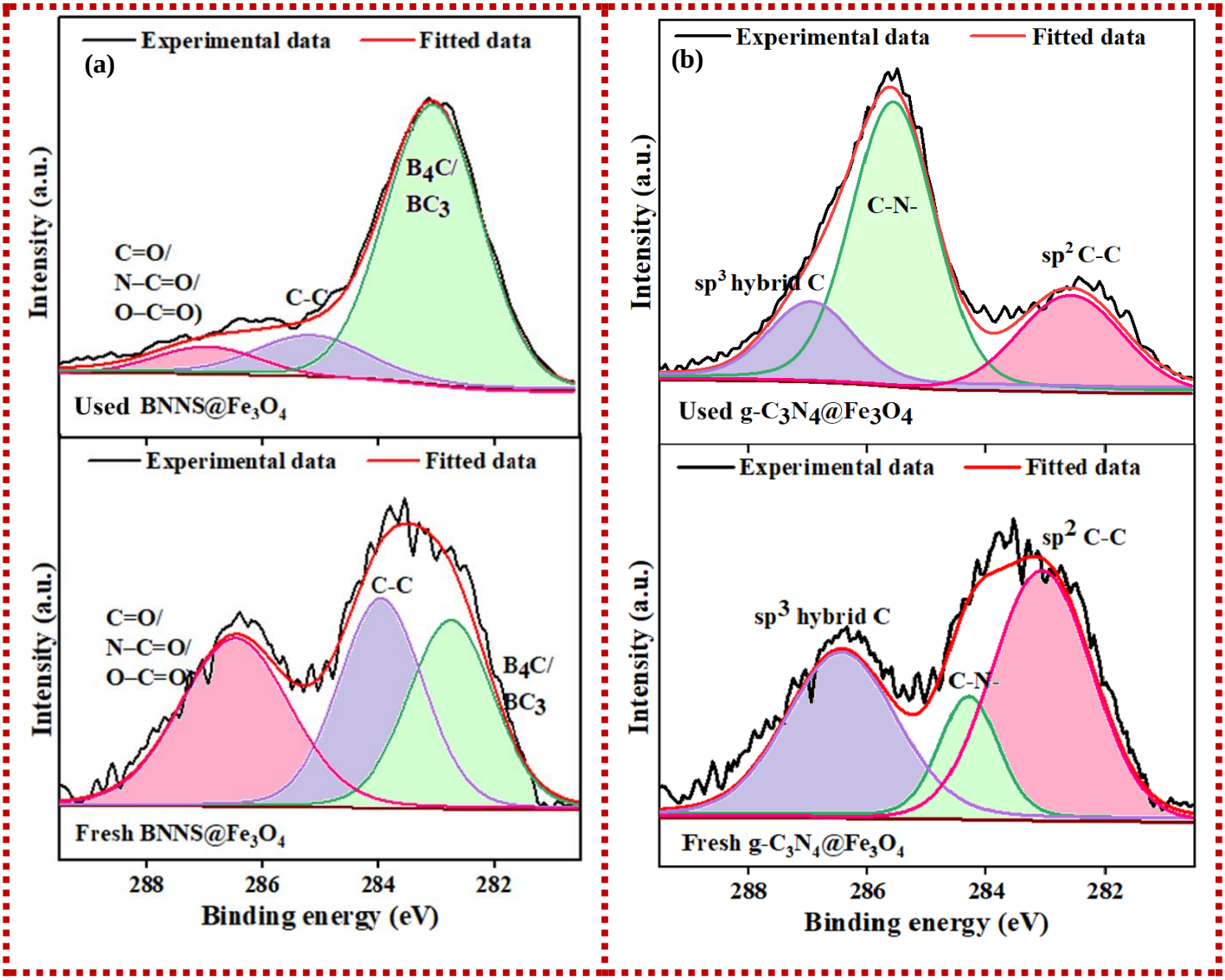

Figure 19: XPS spectra of BNNS@Fe_3O_4 and g-C_3N_4@Fe_3O_4: C1s spectra of (a) used and fresh BNNS@Fe_3O_4, (b) used and fresh g-C_3N_4@Fe_3O_4

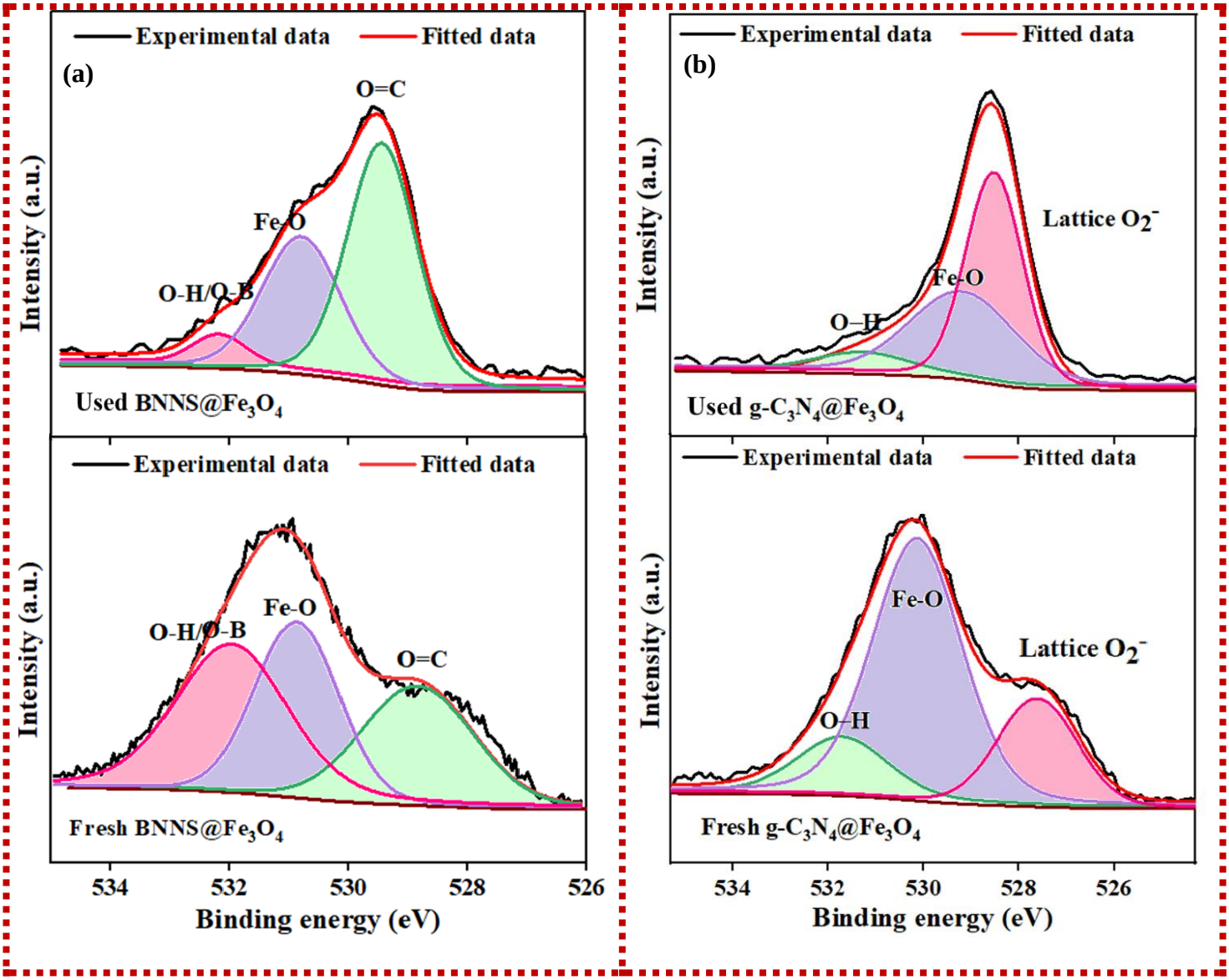

Figure 20: XPS spectra of BNNS@Fe_3O_4 and g-C_3N_4@Fe_3O_4: O1s spectra of (a) used and fresh BNNS@Fe_3O_4, (b) used and fresh g-C_3N_4@Fe_3O_4

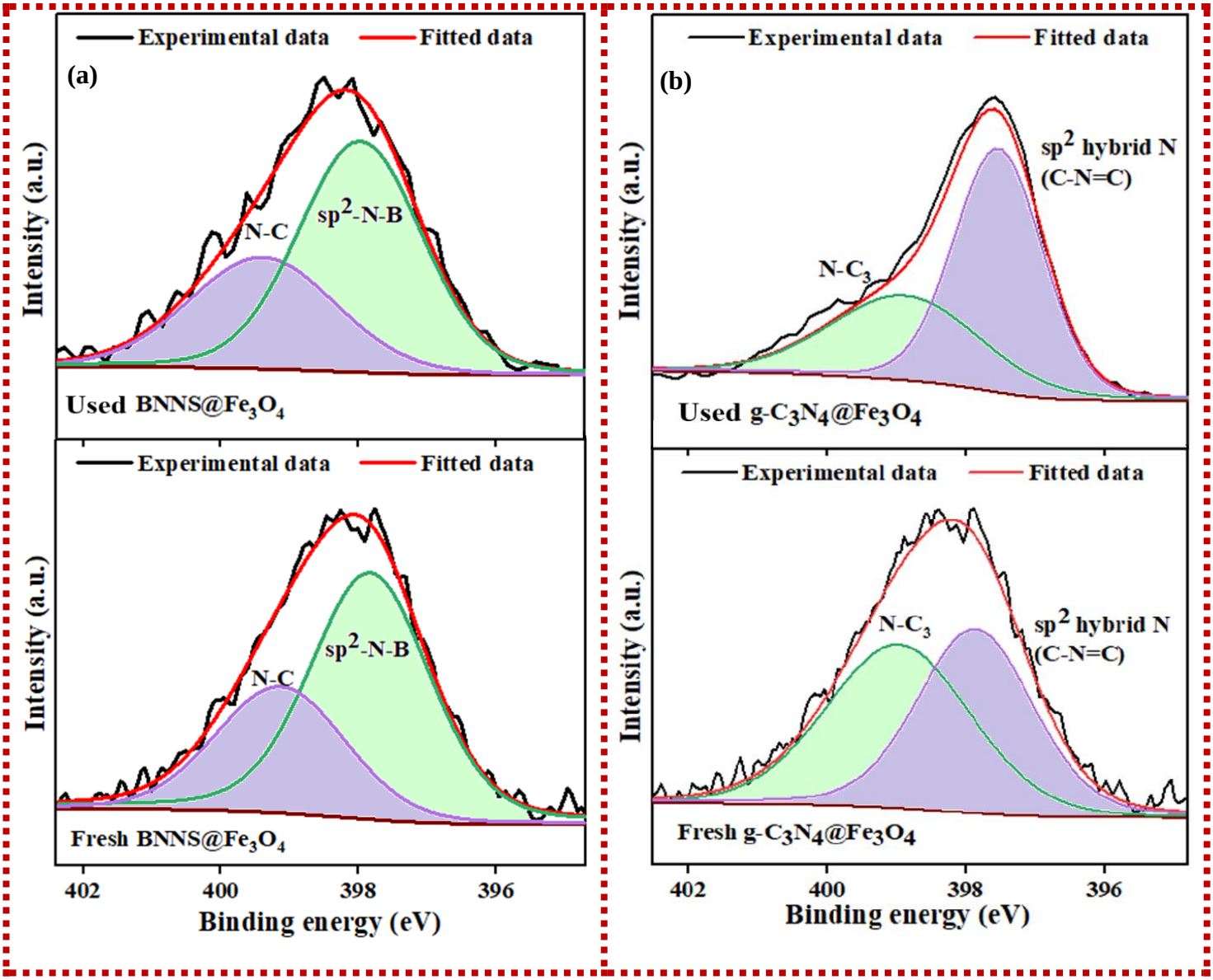

Figure 21: XPS spectra of BNNS@Fe_3O_4 and g-C_3N_4@Fe_3O_4: N1s spectra of (a) used and fresh BNNS@Fe_3O_4, (b) used and fresh g-C_3N_4@Fe_3O_4

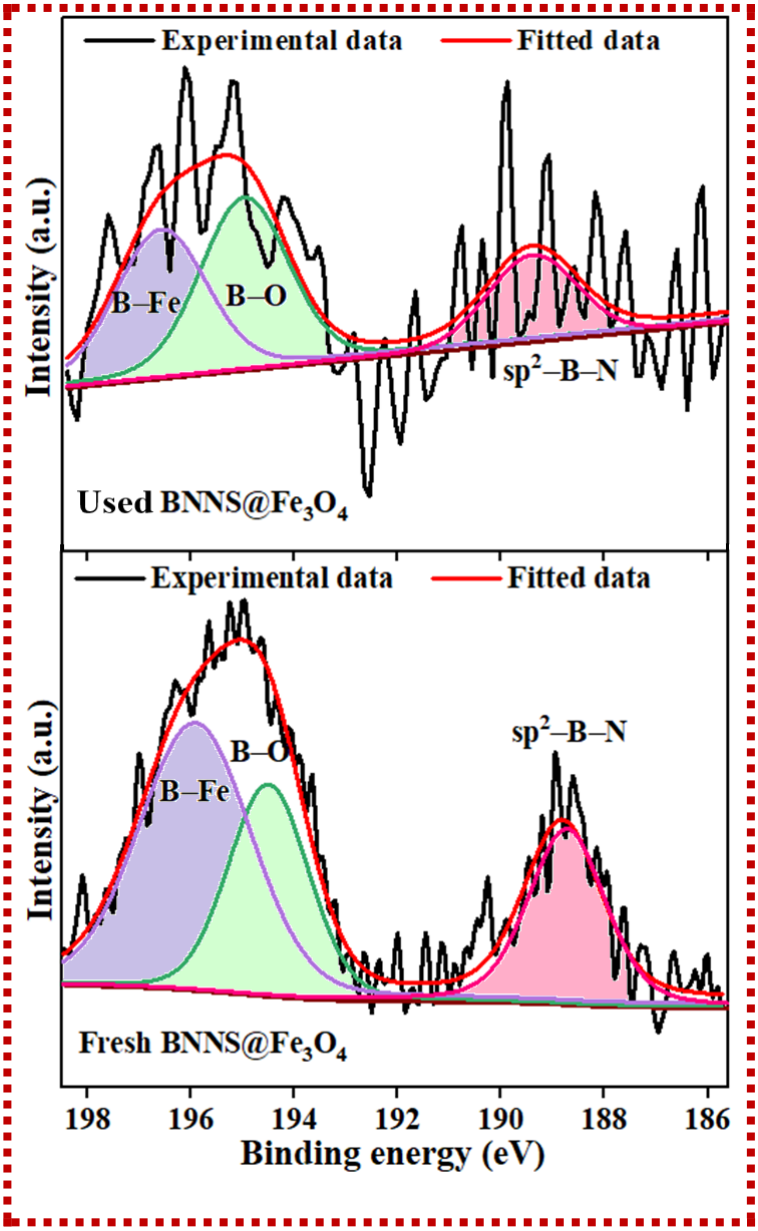

Figure 22: XPS spectra of $BNNS@Fe_3O_4$ and g-$C_3N_4@Fe_3O_4$: B1s spectra of used and fresh $BNNS@Fe_3O_4$

3.6. Conclusions

In conclusion, the comprehensive characterization of the synthesized g-C_3N_4@Fe_3O_4 and BNNS@Fe_3O_4 MNCs through various analytical techniques, including XRD, FTIR, zeta potential, FESEM, TEM, BET, TGA, and XPS, revealed detailed insights into their structural, morphological, and textural properties. The highest specific surface area was attained at ratio 1:5 (boric acid : urea) for BNNS@Fe_3O_4, while the largest surface area was obtained at 600 °C for g-C_3N_4@Fe_3O_4. The surface area for g-C_3N_4@Fe_3O_4 and BNNS@Fe_3O_4 was 54 and 96 m^2/g, respectively. The XRD patterns confirmed the orthorhombic crystalline structure of both MNCs, with excellent chemical stability observed in used samples. FTIR spectra identified key functional groups, indicating robust integration of iron oxide nanoparticles into the g-C_3N_4 and BNNS matrices. Zeta potential measurements highlighted the surface reactivity and point of zero charge/ isoelectric point, while FESEM and TEM analyses elucidated the granular, porous morphology and homogeneous distribution of Fe_3O_4 on the surface. In addition, BET analysis determined the specific surface area and pore-cavity characteristics of the MNCs, revealing that g-C_3N_4@Fe_3O_4 had larger pore-cavity characteristics, leading to more active sites being present which enhances their adsorption capabilities. Moreover, XPS provided detailed information of surface composition and oxidation states. The MNCs were confirmed to be 2D structures making them most suitable for application in water matrices. Overall, the MNCs demonstrated a porous morphology, excellent structural integrity and chemical stability, making them strong candidates for sustainable drinking water and wastewater treatment for MP removal.

CHAPTER FOUR: Optimization of operational parameters magnetic nanocomposite dose, pH, time and MP dose for microplastic removal

4.1. Introduction

The presence of hazardous MPs in aquatic environments poses significant health risks to biota, motivating researchers to develop effective methods for removing these pollutants from drinking water and wastewater. To achieve maximum removal efficiencies and sorption capacities of contaminants on sorbent materials, it is essential to optimize the purification technology by fine-tuning the independent process variables to their optimal values (Bayuo *et al.* 2022). Several treatment methods have been investigated to remove contaminants from both synthetic and real wastewaters, such as filtration, ion exchange, chemical precipitation, electrocoagulation, bioremediation, and adsorption (Mahmoud *et al.* 2021). However, except for the adsorption process, these methods often have significant drawbacks, including high costs, the generation of large volumes of waste, and failure to meet international standards (Egirani *et al.* 2021).

The effectiveness of the adsorption process (sorption capacities of potential adsorbents) is influenced by various factors (Nazari *et al.* 2021). Research has shown that the physicochemical properties of the solutions—such as presence of interfering ions, temperature, pH, agitation/shaking speed and time, initial contaminant concentration (dose), and particle size—significantly affect the performance of any adsorbent. To examine the interactions among these independent factors, a significant amount of sorption studies have been conducted (Bayuo *et al.* 2022). With regards to determining interactive behaviour between the independent variables during the adsorption process, the conventional experimental techniques typically dictate that by varying one variable at a time, the influence of operating factors on the adsorption of pollutants (MPs) onto NMs can be assessed (Bayuo *et al.* 2022).

Numerous studies on NMs have been conducted to date in an effort to develop applications for pollutant abatement in water treatments, and they exhibit remarkable promise as an indispensable means of adsorbing pollutants from wastewater due to optimising various operating parameters (Hanafiah *et al.* 2018). For example, PS MPs were eliminated using ZIF-67, wherein investigations were conducted into the effects of multiple factors, including ZIF-67 dose, MPs concentration, sample pH, temperature, and contact time. Under optimised operating parameters, ZIF-67 eliminated roughly 92.1% of PS MPs (Wan *et al.* 2022), displaying noteworthy removal. In a different study, PS-NPs were extracted from water using a bimetallic carbon composite (CuNi@C). There were variations in the operating parameters pH, time, and CuNi@C dose. Maximum PS-NP elimination was determined to be 99.18% at optimised parameters of CuNi@C dose: 0.3 g/L, pH:4 and reaction time: 11 h (Zhou *et al.* 2022). In a study by Zheng et al. (2022), the very effective polydopamine enhanced magnetic chitosan (PDA-MCS) aerogels were created to adsorb PET MPs. Herein, pH, time, PDA-MCS dose, and temperature were the variable operational parameters for the MP removal experiments. A remarkable removal efficiency of 91.6% was reported (Zheng *et al.* 2022).

In the case of chemically modified NMs, the greater surface area also offers more reactive surfaces. Therefore, it is beneficial to apply chemically modified/ functionalised NMs for pollutant removal from water matrices. It is still unknown what interaction mechanisms allow contaminants such as MPs to be removed from aqueous solutions (Mathur *et al.* 2022). Sorption is one of the forefront techniques for extracting pollutants from tainted water because of the chemical interactions that occur between NMs and pollutant (MPs) (Xiong *et al.* 2015). NMs with large adsorptive surfaces, entraps pollutants via functional groups that include physical and chemical interactions in the adsorption mechanism. The interaction mechanisms between pollutants (MPs) and NMs are highly specific, influenced by the unique properties of both the NM used and the target pollutant (Menéndez-Pedriza and Jaumot 2020). Factors such as

surface charge, specific functional groups, and size of the NM may influence the nature of the interactions. Additionally, the MPs chemical structure, size, available surface area, and crystallinity significantly affect how it binds or interacts with the NM to remove the pollutant from wastewater (Menéndez-Pedriza and Jaumot 2020). NM-based adsorption in wastewater treatment may be divided into three fundamental categories (Saleh and Gupta 2014) based on the kind of NM used: nano-adsorbents, nanomembranes, and nano-catalysts (Palani *et al.* 2021). Herein, this chapter focuses on the optimisation of nano-adsorbents g-C_3N_4@Fe_3O_4 and BNNS@Fe_3O_4 for the removal of MPs from drinking water and wastewater. Once optimized, the MNCs are evaluated for their efficacy in the application removal of different size and types of MPs from Milli-Q water as well as MPs removal from wastewater and drinking water. Lastly, this chapter investigates the mechanistic interactions between the MPs and MNCs based on quantum chemistry calculations in literature as well as the XPS results.

4.2. Materials

PE powder (avg. particle size 125 µM CAS # 9002-88-4), PP (3 mm SKU# GF28090122), high density PE (HDPE, 5 mm, SKU# GF21422900), low density PE (LDPE, 5mm, SKU# GF93085308), acetone EMPLURA® ((≥99.0 purity/assay, CAS# 67-64-1) and sodium hydroxide pellets EMSURE® (≥99% purity/assay CAS# 1310-73-2) were purchased from Merck. Steel mesh sieves (25, 180 and 500 µM) were designed by and purchased from Yaksha Scientific. Liquid nitrogen was purchased from Afrox (Linde Company). Neodymium fishing magnet with stainless steel hook (75mm diameter, pulling force 250kg) was obtained from Lichro Chemical and Laboratory Supplies C. All aforementioned chemicals were utilised as received unless otherwise stated. All solutions were prepared with ultrapure deionized Milli-Q water (18.2 MΩ cm), acquired from a Millipore water purification system in the laboratory.

4.2.1. Preparation of PS-MPs

In this study, plastic cups were used a source of PS MPs. The plastic cups were broken into equal pieces and transferred to a coffee grinder (200W, 240V). Thereafter, approximately 160 mL of liquid nitrogen was added to the coffee grinder and ground for ~1 min 30 sec with a break of 20 sec (to prevent overheating). This was done for several rounds until the PS exhibited a fine powder consistency. The PS powder was then passed through different size sieves (500 µM, 180 µM and 25 µM) to obtain MPs particles with similar size range for the following experiments. This resulted in the collection of 2 sets of PS-MPs viz., PS (180-500 µM) and PS (25-180 µM).

4.3. Experimental procedure

4.3.1. Adsorption experiments for optimisation of parameters

4.3.1.1. Determination of optimum adsorbent dose

A combination of two different MP types, PS and PE (PE=125 µM, PS = 25-180 µM) were spiked into separate flasks containing 250 mL Milli-Q water, each at a MP concentration of 0.5 g/L (Shi *et al.* 2022b). For the appropriate dosage of MNC needed, a concentration gradient experiment was conducted. Five different groups of MNC were set at 0.3, 0.6, 0.9, 1.2 and 1.5 g/L, respectively. Three parallel experiments were performed for each of the concentration groups to ensure that the experiment is conducted in triplicate. After the addition of the MNC, the flasks were agitated using a shaking incubator at 25 °C at 150 rpm (Shi *et al.* 2022b) for five hours. Thereafter the MPs-MNC complex was removed via the application of a magnet with magnetic force: ~250 Kg. Subsequently, the MPs-MNC complex was separated from the magnetic surface and collected in a beaker using ultra-pure water. This was then subjected to filtering utilising a vacuum filter apparatus with a 0.22 µM filter paper. Subsequently, the samples were dried at 50 °C for 10 min. The MPs-MNC complex underwent MNC regeneration

wherein the MPs and MNC was separated from each other according to section 4.3.3. The MPs were then weighed. Following this, the removal efficiency was calculated using Eq. (3) (section 4.3.4.) (Shi *et al.* 2022b). It is important to note that these experiments were performed separately for BNNS@Fe_3O_4 and g-C_3N_4@Fe_3O_4 MNC to assess their individual efficiency.

4.3.1.2. Determination of optimal pH

A series of experiments were conducted, wherein six different pH groups (2, 3, 4, 5, 7 and 9) were set up to determine the optimal pH for both BNNS@Fe_3O_4 and g-C_3N_4@Fe_3O_4 MNCs separately, for the removal of PS and PE MPs (PE=125 µM, PS = 25-180 µM). Three parallel experiments were performed for each of the groups to ensure that the experiment was conducted in triplicate and the average was taken. To each pH group, the same concentration of MNC was added (optimum adsorbent dose). The treatment duration was conducted at a fixed time. After treatment, the MPs-MNC complex underwent MNC regeneration (section 4.3.3.) to ensure their complete separation and the estimation of MPs removal efficacy, according to section 4.3.4., was calculated to establish an optimal pH (Shi *et al.* 2022b).

4.3.1.3. Determination of optimal treatment time

The experiments were conducted for 2, 3, 4, 5, 6, 8 and 10 hours for g-C_3N_4@Fe_3O_4 whilst treatment hours 2, 3, 4, 5, 6, 8, 10, 12, 14 were employed for BNNS@Fe_3O_4. All the experiments were done in triplicate. To each set of triplicate experiments, the same concentration of MNC was added (optimum adsorbent dose) whilst the pH was adjusted to the optimum values, respectively. After treatment, the MPs-MNC complex underwent MNC regeneration (section 4.3.3.) to ensure their complete separation and the estimation of MPs removal efficacy according to section 4.3.4. (Shi *et al.* 2022b).

4.3.1.4. Determination of optimal MPs dose

All aforementioned studies were conducted utilising a standard of 0.5 g. L^{-1} (Shi *et al.* 2022b). A gradient experiment was conducted wherein four different MP groups (0.25, 0.5, 0.75 and 1 g/L) were set to determine the optimum MPs (PE=125 µM, PS = 25-180 µM) dose for both BNNS@Fe_3O_4 and g-C_3N_4@Fe_3O_4 MNC separately. The MPs were added in a 1:1 ratio of PE:PS (0.25 g/L: 0.25 g/L). All experiments were conducted in triplicate. The optimum adsorbent dose, optimum treatment time and optimum pH parameters were used. After treatment analysis was the same as above (Shi *et al.* 2022b). Figure 23 is a schematic depiction of the optimisation of the operational parameters for the removal of MPs.

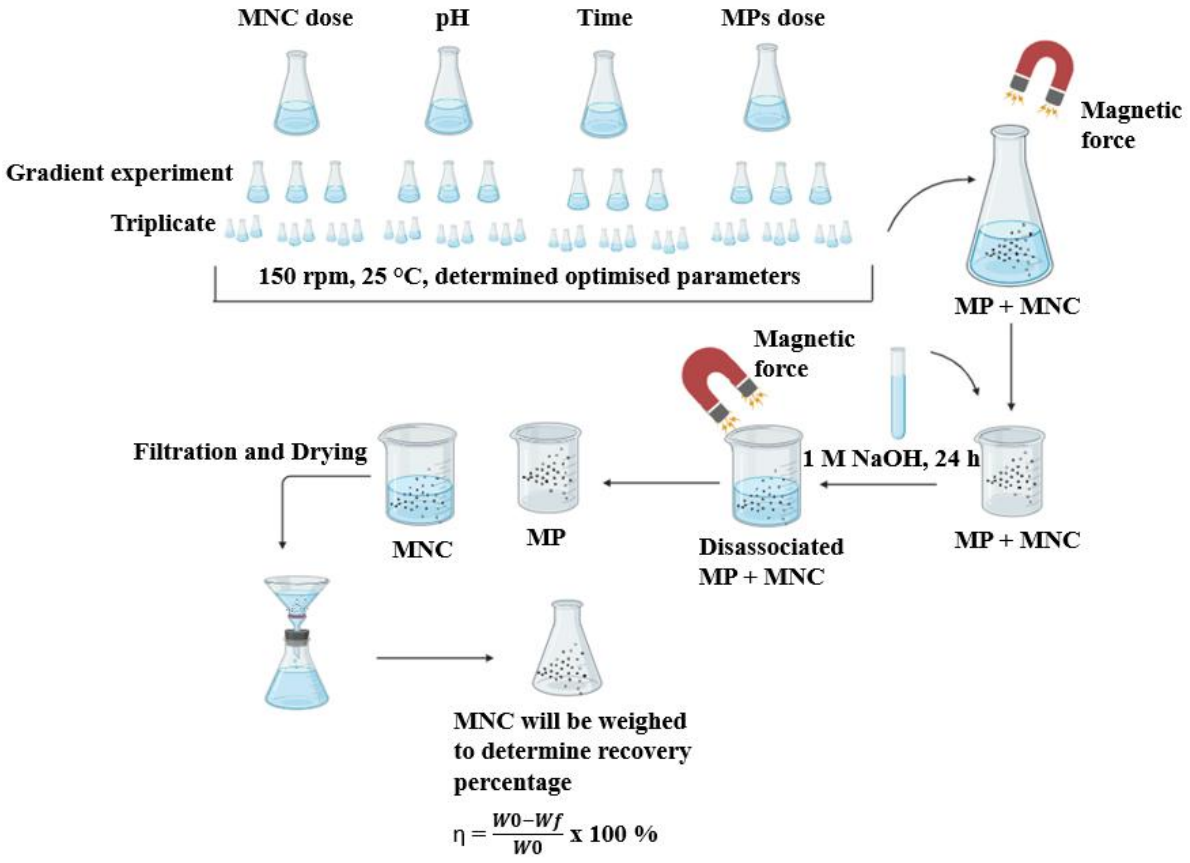

Figure 23: Schematic depiction of the optimisation of operational parameters for the removal of MPs

4.3.2. Application of optimised parameters for MP removal from wastewater and drinking water

4.3.2.1. Removal of different size and types of MPs using the optimal conditions

The efficiency of the MNCs on different types and sizes of MPs was assessed via the use of a range of MPs (PE (125 µM), PS (25-180 µM), PE+PS combo (PE=125 µM, PS = 25-180 µM), PS (180-500 µM), PP (3 mm), LDPE (5 mm) and HDPE (5 mm)) in Milli-Q water. Milli-Q water flasks were spiked with different sets of MPs, followed by dosing of the MNCs separately. The optimum operating parameters were employed, and all experiments were performed as described above (section 4.3.1.1., 4.3.3. and 4.3.4.) and in triplicate to ensure validity of the data. The residual MNC in Milli-Q water was recovered employing a strong magnet with magnetic force: ~250 Kg post-removal treatment. This was done to eliminate potential secondary treatment (Shi *et al.* 2022b).

4.3.2.2. Removal of MPs from drinking water and treated wastewater

A combination of two different types of MPs (PE=125 µM, PS = 25-180 µM) were spiked into different water matrices (final treated effluent and drinking water). All wastewater was ascertained from a domestic WWTP whilst the drinking water was sourced from the tap. A combination of MPs was utilised to simulate the confines/parameters of wastewater and drinking water. The optimum operating parameters were utilised. Since the optimum MP dose was 0.5 g/L, PE (125 µM) and PS (25-180 µM) were each added in a 1:1 ratio (0.25 g/L: 0.25 g/L) and the experiment was performed in triplicate. Oscillation treatment was conducted at 180 rpm at 25 °C (Shi *et al.* 2022b). After treatment, the MPs-MNC complex was subjected to the same process mentioned in section 4.3.3 and 4.3.4. The filtrate from the drinking water experiments were collected and stored for subsequent experiments.

4.3.3. Regeneration of the MNCs

The adsorption capacity of BNNS@Fe_3O_4 decreases with an increase in pH (Bangari *et al.* 2019). Therefore, in order to regenerate the MNC and dislodge the MPs from it, the used adsorbent (BNNS@Fe_3O_4) was added into 1.0 M NaOH for 24 h at an oscillation treatment of 180 rpm (Bangari *et al.* 2019). The same was performed for the g-C_3N_4@Fe_3O_4 MNC.

4.3.4. MPs Removal calculation

After MNC regeneration, the MNCs and the removed MPs were separated into 2 beakers using a magnet. These MPs were then weighed and denoted as MP final. The removal efficiency of MPs was calculated according to MPs mass via simulative experiments. Each component in the subsequent formula can be understood as follows:

$$\eta = \frac{W0-Wf}{W0} \text{ x } 100\ \% \qquad (3)$$

where, η is defined as the MPs removal (%); W_0 is the initial mass of the MPs (g); W_f is the final mass of the MPs (g). All experiments were performed separately for BNNS@Fe_3O_4 and g-C_3N_4@Fe_3O_4 MNC to assess their individual efficiency (Shi *et al.* 2022b).

4.4. Results and Discussion

4.4.1. Reaction parameter influence on MPs removal

4.4.1.1. MNC dose

MNC dosage is a critical factor and serves as a primary source of active sites for initiating MPs removal. A high MNC dose could increase the expenses associated with the treatment process and potentially generate secondary pollution by producing a significant volume of leachate containing heavy metal (Fe) ions (Singh and Lo 2017; Kumar *et al.* 2021a). Therefore, it is essential to optimize the MNC dose for MPs removal. The g-C_3N_4@Fe_3O_4 and BNNS@Fe_3O_4 MNC dose was optimized for the removal of MPs by varying dosage of MNC within the range

0.3-1.5 g/L as shown in Figure 24. The MPs removal gradually increased from 22.76 to 67.91% and 33.69 to 65.15% for g-C_3N_4@Fe_3O_4 and BNNS@Fe_3O_4, respectively, with an increase in adsorbent dose from 0.3 to 1.2 g/L and 0.3 to 0.9 g/L for g-C_3N_4@Fe_3O_4 and BNNS@Fe_3O_4 respectively at the reaction conditions (i.e., MPs dose: 0.5 g/L; natural pH: 7.3; reaction temperature: 25 °C and reaction time: 5 h (for g-C_3N_4@Fe_3O_4), and 10 h (for BNNS@Fe_3O_4)). The removal efficiencies of MPs significantly improved with an increase in MNC dose up to 1.2 g/L (g-C_3N_4@Fe_3O_4) and 0.9 g/L (BNNS@Fe_3O_4), mainly due to the greater availability of surface area and adsorption sites (Rosa *et al.* 2021). However, further increasing the MNC dosage beyond 1.2 g/L (g-C_3N_4@Fe_3O_4) and 0.9 g/L (BNNS@Fe_3O_4), resulted in a decrease in MPs removal. Hence, 1.2 g/L (g-C_3N_4@Fe_3O_4) and 0.9 g/L (BNNS@ Fe_3O_4) were chosen the optimal MNC dose and used in subsequent experiments. This decrease could be attributed to MNC overdose. An elevated dosage of adsorbent creates additional active sites for binding, typically resulting in an increase in the adsorption efficiency. However, when the adsorbent dosage becomes excessively high, it can lead to the formation of aggregates, consequently resulting in a decreased number of available active sites and thereby, a reduction in adsorption (Padmavathy *et al.* 2016; Pfeifer and Skerget 2020). A similar trend wherein a decrease is observed after the optimum adsorbent dose has been reported by Bangari and team (Bangari *et al.* 2019).

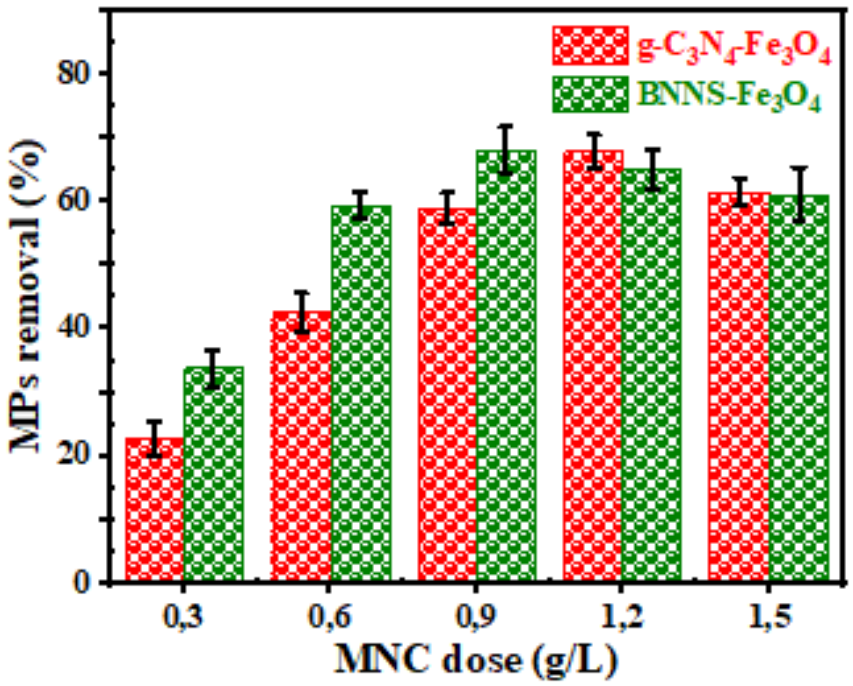

Figure 24: Optimisation of MNC dose (g/L) for g-C_3N_4@Fe_3O_4 and BNNS@Fe_3O_4

4.4.1.2. Influence of initial pH

Previous studies have documented that the surface charge of the adsorbent is altered in response to the initial pH of the solution and has a strong effect on surface binding sites (Ates and Oymak 2020; Adegoke *et al.* 2023; Mohrazi and Ghasemi-Fasaei 2023; Tatarchuk *et al.* 2023). The effects of pH on MPs removal were explored with a wide pH range (2-9) for g-C_3N_4@Fe_3O_4 and BNNS@Fe_3O_4. As illustrated in Figure 25, the removal efficiency of MPs increased from pH 2 (41.80%) to pH 4 (96.06%) for g-C_3N_4@Fe_3O_4. This can be correlated to the pH and zeta potential. As the pH increases from 2 to 4, the zeta potential continuously decreases, causing the surface charge of the MNC to shift from negative at pH 2 to positive at pH 4.This results in the g-C_3N_4@Fe_3O_4becoming positively charged at pH 4, facilitating strong interaction of negatively charged MPs with active sites as a result of electrostatic interaction and Van Der Waals forces (Subbaramaiah *et al.* 2013; Singh and Lo 2017; Kumar *et al.* 2020b). MPs often possess negative charges due to functional groups such as carboxyl (-COOH), hydroxyl (-OH)

and Carbonyl (-C=O) groups present on their surface, which confer a negative surface charge. Additionally, in wastewaters or experimental solutions, negatively charged ions (e.g., Cl^-, SO_4^{2-}, NO_3^-) can adsorb onto the MP surfaces, imparting a negative charge. These groups dissociate in aqueous environments, imparting a negative charge to the MPs. Ultimately, allowing them to adsorb to the positively charged MNC. Thereafter, removal efficiency begins to decrease continuously from pH 5 (82%) to 9 (15.10%) at reaction conditions (i.e., g-C_3N_4@Fe_3O_4 dose 1.2 g/L, MPs dose 0.5 g/L, temperature 25 °C and time 5 h). This can be attributed to the increasingly negative values of zeta potential in alkaline medium, which reduces the electrostatic interactions between the negatively charged MPs and the negatively charged sites of the MNC, resulting in decreased adsorption of MPs (Rosa *et al.* 2021). The steady reduction in removal efficiency is ascribed to the gradual decline in protonation in strong acidic medium. In the case of BNNS@Fe_3O_4, as can be deduced from Figure 25, MPs removal efficiency improved as pH increased from pH 2 (36.07%) to pH 3 (82.58%). The removal efficiency diminished as pH increases, with pH 5 having the lowest MPs removal efficiency (18.79%), whilst pH 7 and 9 exhibited no removal. Therefore, the electrostatic repulsion is enhanced with a stepwise increase in pH, resulting in decreased adsorption until there is no adsorption. This can be correlated to the pH_{pzc}. At pH values below the pH_{pzc}, the surface active sites of the BNNS@Fe_3O_4 become positively charged as a result of H^+ ion reactions. This leads to significant electrostatic attraction and Van Der Waals forces between the BNNS@Fe_3O_4 and negatively charged MPs species, facilitating high adsorption. Conversely, when the pH exceeds the pH_{pzc}, the surface charge of the MNC becomes negative due to the adsorption of OH^- ions. This results in the repulsion of negatively charged MPs species (Bangari *et al.* 2019). Herein the pH_{pzc} for BNNS@Fe_3O_4 is pH 4.3, whilst the optimum pH was observed to be pH 3 owing to the aforementioned described interaction. A large decrease is observed in removal efficiency between pH 3 (82.58%) and pH 4 (31.92%) (approaching deprotonation). Since pH 4.3 exhibits

a surface charge of 0, surface active sites on BNNS@Fe_3O_4 at pH 4 are still positively charged allowing MPs removal, however it is a weaker acid than pH 3 and is weakly protonated due to fewer H^+ ions, hence the lower removal efficiency. At pH 5, the removal efficiency is 18.79% due to the scarce H^+ ions which impart a weak positive charge to the active sites of BNNS@Fe_3O_4, permitting limited removal. At pH 7 and 9, 0% removal of MPs is facilitated as a result of the strongly negatively charged BNNS@Fe_3O_4 surface active sites due to the abundance of OH^- ions present in the strong alkaline medium which displays strong electrostatic repulsion to negatively charged MPs.

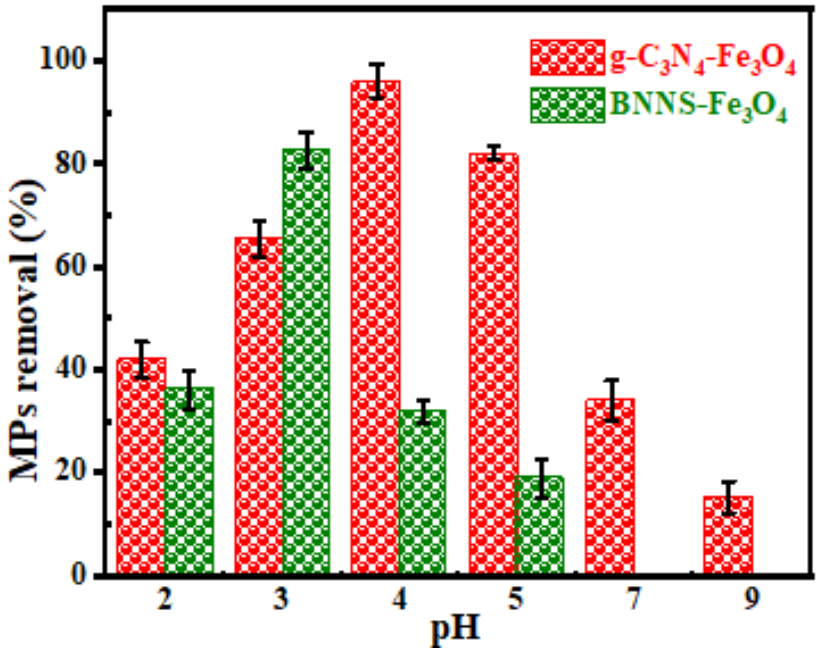

Figure 25: Optimisation of pH for g-C_3N_4@Fe_3O_4 and BNNS@Fe_3O_4

4.4.1.3. Influence of sorption time

The sorption time of MPs removal with g-C_3N_4@Fe_3O_4 and BNNS@Fe_3O_4 MNC were optimized within the range of 2- 14 h, as shown in Figure 26. Initially, both experiments were conducted with identical durations; however, it was observed that the removal efficiency continued to increase for BNNS@Fe_3O_4. Consequently, the experiment was extended until a plateau was reached to fully capture the removal efficiency dynamics of BNNS@Fe_3O_4. The

MPs removal efficiency gradually increased with time from 2 h (59.87%) to 5 h (94.89%) for g-C_3N_4@Fe_3O_4 and from 2 h (9.78%) to 12 h (88.28%) for BNNS@Fe_3O_4, respectively at reaction conditions (i.e., g-C_3N_4@Fe_3O_4 dose 1.2 g/L, MPs dose 0.5 g/L, pH_0 4, and temperature 25 °C; and BNNS@Fe_3O_4 dose 0.9 g/L, MPs dose 0.5 g/L, pH_0 3, and temperature 25 °C). This increase is due to the availability of more surface binding sites on the MNCs surface (Sahoo *et al.* 2020), allowing electrostatic interaction and Van Der Waals forces to form (Ray *et al.* 2020). In the case of BNNS@Fe_3O_4 there was a decrease from 12 h (88.28%) to 14 h (82.14%). This is due to insufficient surface binding sites on the MNC (Sahoo *et al.* 2020). This phenomenon may be caused by the formation of nanoparticle aggregates or possibly flocs which may have blocked the active sites of the MNC resulting in a reduced number of available active sites (Tu *et al.* 2006; Yadav and Srivastava 2017; Kumar *et al.* 2020b). In the case of g-C_3N_4@Fe_3O_4, a decrease was observed from 5 h (94.89%) to 8 h (87.4%), followed by a slight increase at 10 h (88.81%). This decrease can also be attributed to the formation of MNC aggregates (Tu *et al.* 2006; Yadav and Srivastava 2017; Kumar *et al.* 2020b). However, the slight increase may be ascribed to the nanoparticle floc formation breaking during the prolonged oscillation treatment, resulting in a slight increase in the availability of available active sites. A similar trend wherein a decrease is observed after the optimum time has been reported (Bangari *et al.* 2019). According to the S_{BET}, BNNS@Fe_3O_4 should be the better-performer since it has a larger surface area. Yet, the results clearly showcase g-C_3N_4@Fe_3O_4 as the better-performing MNC. This is due to the larger V_{pore}, d_{pore}, and σ_{pore} of g-C_3N_4@Fe_3O_4. Typically, a larger surface area equates to more available active sites that can interact with the reactant molecule (Worstell 2014). However, this usually means that the V_{pore}, d_{pore}, and σ_{pore} has increased accordingly. The higher pore volume, pore diameter and pore width indicate larger pore-volume cavities present in the g-C_3N_4@Fe_3O_4, leading to more active sites being present (Goel *et al.* 2022), (V_{pore} is significantly greater, whilst d_{pore} is

more than 2x greater and σ_{pore} is almost 2x greater than BNNS@Fe_3O_4), thereby facilitating a higher removal efficiency. Moreover, the textural properties also suggest that g-C_3N_4@Fe_3O_4 is a more porous MNC, due to the presence of more pore-volume cavities (Goel *et al.* 2022).

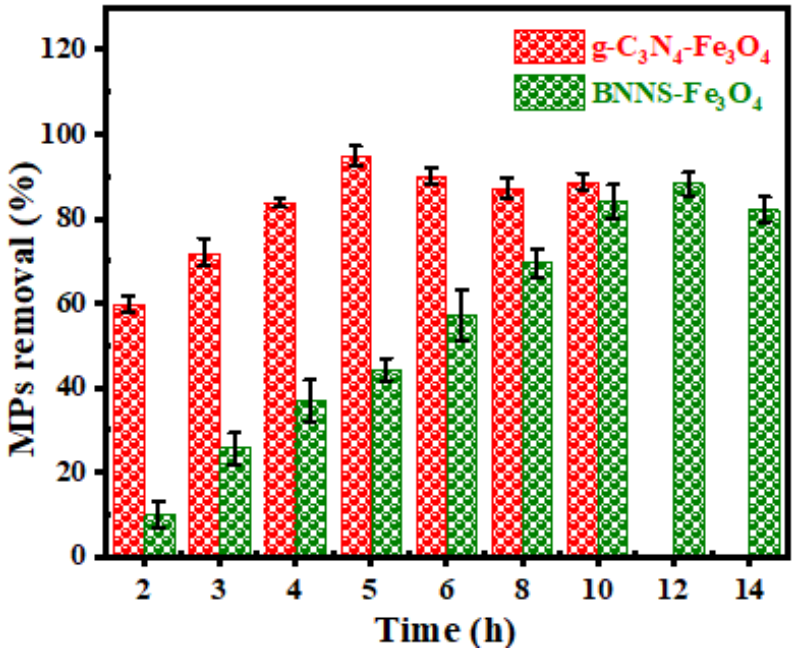

Figure 26: Optimisation of time for g-C_3N_4@Fe_3O_4 and BNNS@Fe_3O_4

4.4.1.4. Influence of initial dose of MPs

The contaminant dose (MPs) is essential since it provides the MPs removal limit/capacity per adsorbent dose. The MPs utilised for all optimization experiments are a combination of PE+PS MPs (PE=125 µM, PS = 25-180 µM). Using a combination of two types of MPs for optimization provides a more comprehensive assessment of the removal process by accounting for variations in size and composition, and better simulates real-world conditions where multiple MP types are present. This approach enhances the generalizability and effectiveness of the removal method, ensuring it performs robustly across diverse scenarios. The effects of different doses of MPs were evaluated within the ranges 0.25-1 g/L, as displayed in Figure 27. The removal efficiency gradually decreased from 95.56% (0.25 g/L) to 41.17% (1.0 g/L) for g-C_3N_4@Fe_3O_4 and 89.05% (0.25 g/L) to 36.4% (1.0 g/L) for BNNS@Fe_3O_4, at the reaction

conditions (g-C_3N_4@Fe_3O_4 dose 1.2 g/L, pH_0 4, temperature 25 °C, time 5 h; BNNS@Fe_3O_4 dose 0.9 g/L, pH_0 3, temperature 25 °C, time 12 h). Interestingly, as the MPs dose concentration increased, the removal efficiency significantly decreased. This could be ascribed to an increase of the MPs resulting in insufficient availability of active sites, causing the remainder of MPs to remain behind in solution. A slight reduction in the removal efficiency were noticed from MPs dose 0.25 g/L (95.56%) to 0.5 g/L (94.89%) for g-C_3N_4@Fe_3O_4, and 0.25 g/L (89.05%) to 0.5 g/L (87.14%) for BNNS@Fe_3O_4, respectively. This minimal reduction indicates the abundance of active sites present on both adsorbents surface, i.e. the saturation limit was not reached at 0.25 g/L. Hence, 0.5 g/L was chosen as the optimum MPs dose. However, a significant reduction MPs were noticed while further increasing the initial dose of MPs from 0.5 g/L (94.89% and 87.14%) to 0.75 g/L (72.2% and 66.39%) for g-C_3N_4@Fe_3O_4 and BNNS@Fe_3O_4, respectively, revealing that beyond 0.5 g/L, the saturation capacity was reached, with any MPs dose beyond this being unfavourable. Similar trend have been observed by Shi and team for MPs removal (Shi *et al.* 2022b).

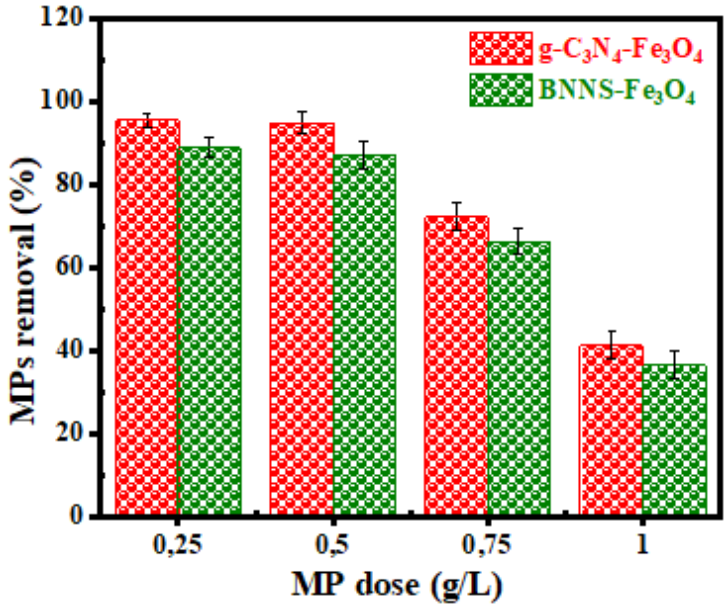

Figure 27: Optimisation of MP dose (g/L) (PE+PS (PE=125 µM, PS = 25-180 µM)) for g-C_3N_4@Fe_3O_4 and BNNS@Fe_3O_4

4.4.2. Application of optimized key parameters for MPs removal

4.4.2.1. Removal of different size and types of MPs from Milli-Q water

In this study, different size and types of MPs were utilised to assess the efficacy of g-C_3N_4@Fe_3O_4 and BNNS@Fe_3O_4 as displayed in Figure 36, appendix 5. The maximum removal of PE (96.16%, size 125 µM), PS[1] (92.5% , size 25-180 µM), PE+PS combo (94.89%, size PE=125 µM and 25-180 µM), PS[2] (45.62%, size 180-500 µM), PP (0%, size 3 mm), LDPE (0%, size 5 mm) and HDPE (0%, size 5 mm) were noticed with MNC g-C_3N_4@Fe_3O_4 under optimum operating conditions (g-C_3N_4@Fe_3O_4 dose 1.2 g/L, pH_0 4, MPs dose 0.5 g/L, temperature 25 °C, time 5 h) from Milli-Q water. Similarly, the maximum removal efficiency of PE (94.44%, size 125 µM), PS (85.96%, size 25-180 µM), PE+PS combo (88.28% , size PE=125 µM and 25-180 µM), PS (38.77%, size 180-500 µM), PP (0%, size 3 mm), LDPE (0%, size 5 mm) and HDPE (0%, size 5 mm) were observed with MNC BNNS@Fe_3O_4 under optimum operating conditions (BNNS@Fe_3O_4 dose 0.9 g/L, MPs dose 0.5 g/L, pH_0 3, and temperature 25 °C) from Milli-Q water (Figure 28). Similar results have been reported for PS and PE MPs in a study by Shi et al. (2022), wherein they examined the removal of PS, PE and PP MPs from pure water (Milli-Q water) by NM Fe_3O_4. There were three size-different groupings for each type of MP: approximately 900, 500, and 200 µM. The removal efficiency of PE, PP and PS MPs was 79–94%, 80–90% and 81–93%, respectively (Shi *et al.* 2022b). Evidenced by literature, size of MPs strongly influences their removal efficacy, which is consistent with the results from the present study. A decrease in removal efficiency as MPs size increases was observed. This indicates that the MNCs, at optimised operating conditions, are ineffective at removing large MPs, potentially due to weak hydrogen bonding and Van Der Waals forces. As a result of the large MPs size (PP, LDPE and HDPE), the magnet (magnetic force: ~250 kg) was unable to remove the MPs from solution. This could be due to the lack of intermolecular Van Der Waals force and weak H-bonding between the MPs and MNCs

(Szalewicz *et al.* 2003; Horiuchi *et al.* 2022). The results clearly dictate that size plays a crucial role in MPs removal efficiency. This is consistent with the literature. For example a study investigated the removal of different MPs (PS, PP and PE) and found that small MPs (~200 µM) and large MPs (~900 µM) was always greater than medium MPs (~500 µM) (Shi *et al.* 2022b). Both MNC g-C_3N_4@Fe_3O_4 and BNNS@Fe_3O_4, exhibited the highest removal efficiency of PE due to its smaller size (125 µM), enabling maximum interaction between active sites and MPs. However, the PS (25-180 µM) removal displayed a lower removal efficiency than the PE+PS combo (size PE=125 µM and 25-180 µM) for both MNCs, albeit consisting of MPs with size > 25 µM. This can be ascribed to the PS range containing more MPs of the size >125 µM, resulting in a slightly reduced removal efficiency than the PE (125 µM). This is due to the reduced interaction between the surface available active sites and the slightly larger MPs. Based on the aforementioned, it is plausible to postulate that smaller sized MPs (MPs < 125 µM) and NPs will exhibit a higher removal efficiency. Furthermore, both g-C_3N_4@Fe_3O_4 and BNNS@Fe_3O_4 MNCs have proven to be efficient for the removal of different polymer types.

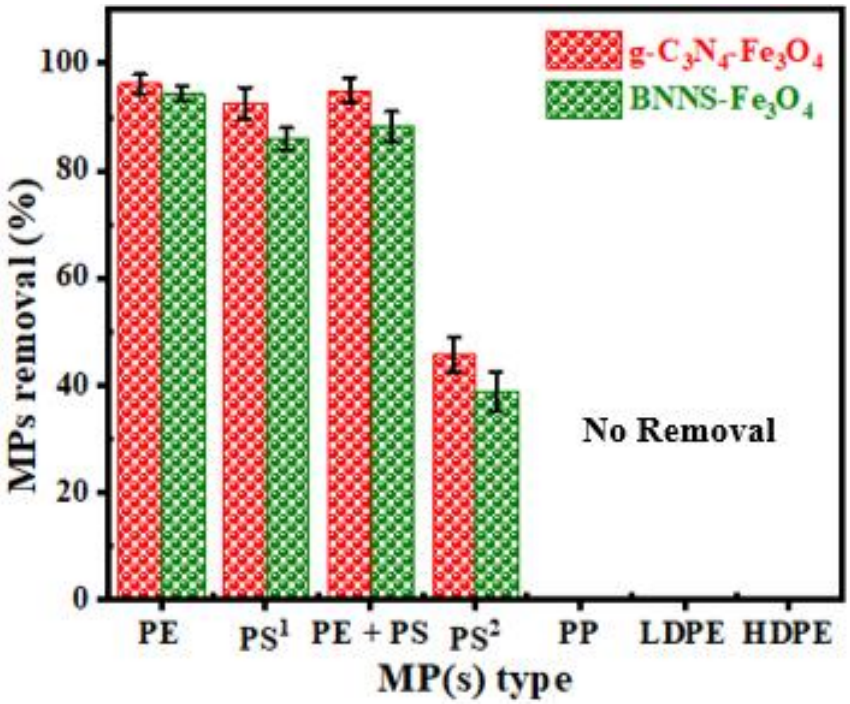

Figure 28: Application of optimised parameters for g-C_3N_4@Fe_3O_4 and BNNS@Fe_3O_4: Removal of different size and types of MPs (PS^1- 25-180; PS^2- 180-500 µM)

4.4.2.2. Removal of MPs from drinking water and treated domestic wastewater

It is imperative that the MNCs be evaluated for their removal efficiencies in real wastewater effluent. Herein, samples of domestic final treated wastewater effluent were collected from a wastewater treatment plant, located in Durban, South Africa. The investigation of MPs removal efficiency in different water matrices yielded 93.7 and 86.56% from drinking water via g-C_3N_4@Fe_3O_4 and BNNS@Fe_3O_4, respectively. The removal efficiency of MPs from Milli-Q water to drinking water is similar, there is only a slight decrease. The slight reduction could be due to the presence of an extremely low concentration of total dissolved solids (Shah *et al.* 2023) which could physically block the active sites on the MNCs surface preventing access of those active sites to the MPs. Furthermore, it may be attributed to the low concentration of ionic impurities such as cadmium, chlorine, fluoride, nitrate and nitrite which is commonly present in drinking water (Shah *et al.* 2023), which bond to the active sites further impeding the MPs removal efficiency. Similar results have been reported by Elmaci, 2020 where MNC

C@Fe_3O_4 was utilised as an adsorbent for the removal of PS beads (3 µM) from drinking water. This study was done as a proof of concept to determine the viability of applying magnetic NMs for MPs removal from drinking water. Using an external magnet, the MPs were successfully extracted from the drinking water after adhering to the composite surface (Elmacı 2020). The domestic wastewater effluent was subjected to filtering with a 0.22 µM filter. This was done to remove any bacteria present since the surface of the bacterial outer membrane is net negatively charged, due to the carboxyl groups and ionized phosphate that are concentrated on the bacterial surface, with rare exceptions (Wilhelm *et al.* 2021). Due to its bacterial surface, electrostatic interactions allow metal NMs to bind to bacterial cells (Makabenta *et al.* 2021; Jiang *et al.* 2024). Therefore, eliminating the presence of negatively charged bacteria eliminates its competition with the negatively charged MPs to occupy active sites on the MNCs surface. A removal efficiency of 91.91 and 83.78% was observed from domestic wastewater effluent filtered with a 0.22 µM filter for g-C_3N_4@Fe_3O_4 and BNNS@Fe_3O_4, respectively, whilst a removal efficiency of 90.28 and 82.23% was observed from the same domestic wastewater effluent (unfiltered) for g-C_3N_4@Fe_3O_4 and BNNS@Fe_3O_4, respectively (Figure 29). Authors Grbic et al. (2019) have reported the similar results wherein they developed a technique that uses the hydrophobic surface of plastics to magnetize and extract them magnetically. They produced plastic-binding, hydrophobic Fe nanoparticles that enable magnetic recovery. A recovery of 92% of 10−20 µM PE and PS beads and 93% of >1 mm MPs (PE, PET, PS, PU, PVC, PP) from saltwater was observed. Additionally, 84% of MPs (PE, PS, PU, PVC, PP) from freshwater, with sizes ranging from 200 µM to 1 mm (Grbic *et al.* 2019). The results for filtered and unfiltered domestic wastewater effluent were almost similar with the filtered sample exhibiting a slightly higher removal efficiency. Moreover, filtering reduces the TDS which reduces the ionic effect in the filtered sample. Therefore, filtering may aid in improving MP removal efficiencies in complex substrates such as wastewater. The decrease in removal

efficiency between the drinking water and the domestic wastewater effluent was expected and could be attributed to various ions present in the wastewater effluent. A few of the anionic species (SO_4^{2-}, HCO_3^-, Cl^- and NO_3^-ions) that are frequently found in wastewater significantly affects the performance of the adsorption process by multitudinous ways such as altering the pH levels and competing for available active sites on the MNC surface area (Kumar *et al.* 2023b). Both MNCs, g-C_3N_4@Fe_3O_4 and BNNS@Fe_3O_4, exhibited acidic properties, performing optimally in acidic media due to protonation of their surface-active sites, which facilitated strong electrostatic interactions with negatively charged MPs.

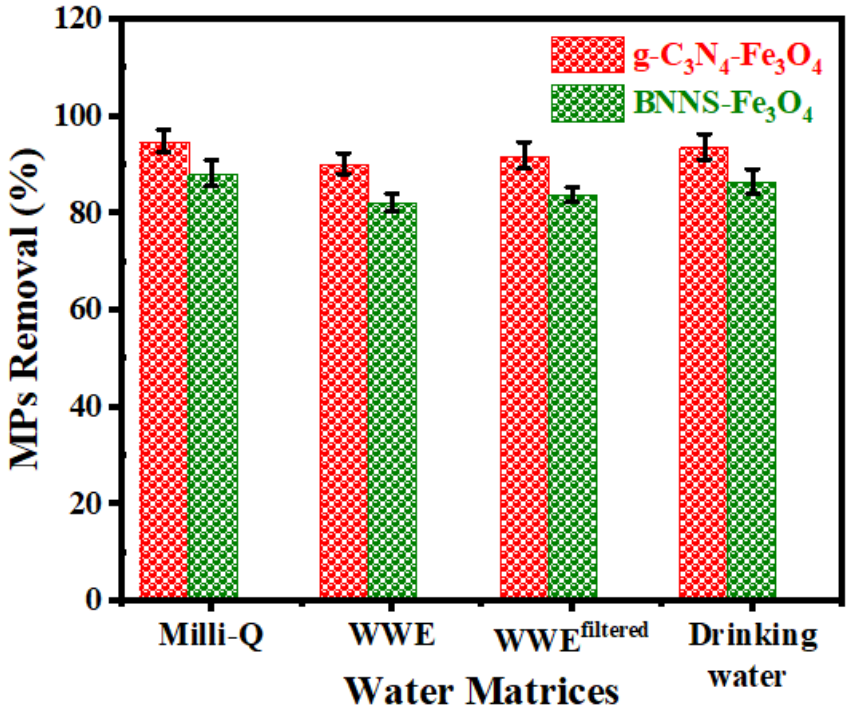

Figure 29: Application of optimised parameters for g-C_3N_4@Fe_3O_4 and BNNS@Fe_3O_4: Removal of MPs from different water matrices (Milli-Q water, WWE: Final treated wastewater effluent, $WWE^{filtered}$: Final treated wastewater effluent filtered with 0.22 µM)

4.4.3. Plausible mechanism of action/Mechanistic insights

Understanding the surface chemistry of the PS/PE MPs interacting with g-C_3N_4@Fe_3O_4 and BNNS@Fe_3O_4, would assist in postulating the adsorbent-adsorbate mechanism of action as

displayed in Figure 30. To the best of our knowledge, the removal of MPs by g-C_3N_4@Fe_3O_4 (Figure 30 (a)) and BNNS@Fe_3O_4 (Figure 30 (b)) has not yet been reported. Therefore, this section discusses the potential removal mechanism of MPs via these MNCs. During the adsorption process, the adsorbate molecules may adhere to the surface of adsorbents through various interactions, which are contingent upon the properties of both the adsorbent material and the adsorbate species. These interactions may include hydrophobic, Van Der Waals forces, hydrogen bonding, π-π electron interactions and electrostatic forces, among others (Islam *et al.* 2018; Sahoo *et al.* 2020). Calculations using quantum chemistry have demonstrated that π-electrons are present on the surface of h-BN (Liu *et al.* 2022); π electrons have also been confirmed on the surface of g-C_3N_4 (Sahoo *et al.* 2020). The PS-MPs are aromatic molecules that have π electrons. Therefore, π-π electron interactions mostly favours the adsorption of PS-MPs onto g-C_3N_4@Fe_3O_4 and BNNS@Fe_3O_4 MNCs.

Hydrogen dipole-dipole bonding occurs between hydrogen on –$(C_8H_8)_n$–/ –$(C_2H_4)_n$–(PS/PE MPs) and an electronegative atom with a lone pair of electrons on the MNCs. Moreover, weak hydrogen bonds involve less polar X-H groups acting as proton donors, such as C-H bonds (Trefil 2001; Szalewicz *et al.* 2003; Hage 2013; Horiuchi *et al.* 2022). For BNNS@Fe_3O_4, H-bonding could occur with O or N atoms from C=O, N–C=O/O–C=O, O–C, Fe–O, O–B, O–H, sp^2–B–N whereas for g-C_3N_4@Fe_3O_4, H-bonding could transpire with O or N atoms from tertiary nitrogen bonding to carbon atoms in the arrangement of (N–$(C)_3$), C–N–, Fe–O, O–H. These specific elemental compositions, along with the chemical and electronic states of the atoms within the MNCs have been ascertained from the XPS spectra (Figure 18-22). Moreover, both MNCs possess a porous structure and wide surface area with primary/secondary/tertiary and a fraction of sp^2π-conjugated amines which improves its chemiosorptive and physiosorptive adsorbent-adsorbate affinity (Oh *et al.* 2018). Herein, the N atom in the sp^2π-conjugated amines has an electron lone pair thus facilitating additional H-bonding with PS/PE

MPs. Lastly, H-bonding can occur where X-H attaches to a π bond. Thus, H-bonding may involve the interaction of electronegative atoms on MNCs (e.g., O or N) with H atoms on functional groups of PS/PE MPs, but direct H-bonding with the aromatic protons of PS MPs may be unlikely due to their limited polarization. Therefore, while these protons are indeed weakly polar, hydrogen bonding in this context is less likely to occur directly with aromatic protons. Instead, the hydrogen bonding interactions described in the discussion are more plausibly associated with functional groups present on the MNCs and MPs, such as N–(C)3 and C=O groups on the MNCs and –CH2– or oxygen-containing groups (e.g., –C=O) on the MPs. These interactions are supported by the lone pair electrons on nitrogen or oxygen atoms within the MNCs, which act as hydrogen bond acceptors (Trefil 2001; Szalewicz *et al.* 2003; Hage 2013; Horiuchi *et al.* 2022).

Further interactions may occur between the MNCs and PS/PE MPs. PS/PE MPs are anionic polymers. From the pH adsorption experiments of PS/PE MPs, maximum adsorption transpired at pH_0 4 and pH_0 3 for g-C_3N_4@Fe_3O_4 and BNNS@Fe_3O_4 MNCs, respectively. At a lower pH, the MNC surfaces become protonated due to H^+ ions binding to functional groups, leading to a net positive charge. This facilitates the attraction of negatively charged PS/PE MPs through strong electrostatic interactions, in addition to weak Van Der Waals forces (Ray *et al.* 2020). This occurs through the protonation of the surface (the H^+ ions contributing a positive charge to the MNCs) since the e^- lone pairs behave as proton acceptors. However, at a higher pH, the $OH^–$ ions in the alkaline solution compete with the negatively charged PS/PE MPs to adsorb onto the MNCs surface. This surface then becomes negatively charged and thus repels the negatively charged PS/PE MPs through electrostatic repulsion therefore exhibiting decreased affinity to PS/PE MPs adsorption (Ray *et al.* 2020). In the case of g-C_3N_4@Fe_3O_4, this was ascribed to the replacement of ≡C–NH_2 groups on the surface of g-C_3N_4 with ≡C–OH groups, resulting in increased deprotonation (≡C–O–) when exposed to aqueous solutions with higher

pH levels (Zhu *et al.* 2015). Furthermore, the Fe_3O_4 that is functionalised onto each of the supporting materials (g-C_3N_4 and BNNS) dissociates into Fe^{2+} and Fe^{3+} ions which are abundantly and homogeneously distributed on the supporting materials surface, therein, increasing the surfaces' positive charge, enabling a stronger electrostatic interaction between MNCs and PS/PE MPs.

Based on the preceding explanation, the adsorption of PS/PE MPs onto g-C_3N_4@Fe_3O_4 and BNNS@Fe_3O_4 MNCS could be attributed to four potential interactions: electrostatic interaction, π-π interaction, Van Der Waals forces and hydrogen bonding as illustrated in Fig. 7(a-b). It is important to note that in Figure 30, Fe_3O_4 is functionalized onto the supporting materials (g-C_3N_4 and BNNS) and is not chemically part of the aromatic structure. This functionalization enhances the magnetic properties and positive charge on the MNC surfaces, facilitating interactions such as electrostatic forces. The schematic is intended to highlight the potential mechanisms rather than represent exact molecular configurations.

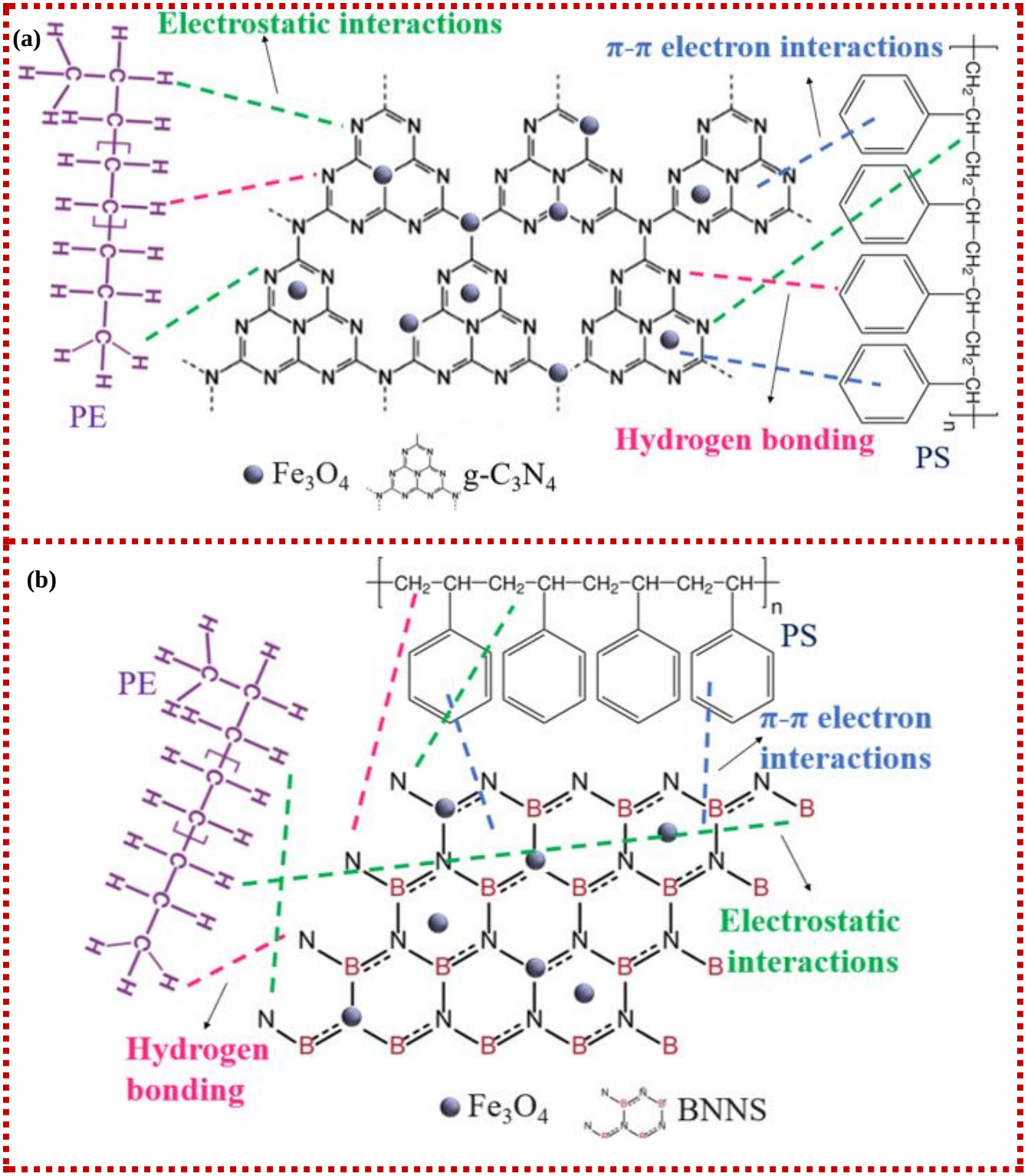

Figure 30: Interaction mechanistic insights between PS/PE MPs and (a) g-C_3N_4@Fe_3O_4, (b) BNNS@Fe_3O_4 MNCs

4.5. Conclusions

In conclusion, the optimization of MNC dosage is crucial for effective MPs removal, with g-C_3N_4@Fe_3O_4 and BNNS@Fe_3O_4 demonstrating optimal performance at 1.2 g/L and 0.9 g/L, respectively. pH also found to significantly influence MPs removal, with the best performance observed at acidic conditions (pH 4 for g-C_3N_4@Fe_3O_4 and pH 3 for BNNS@Fe_3O_4). The sorption time required for maximum MPs removal was identified as 5 hours for g-C_3N_4@Fe_3O_4 and 12 hours for BNNS@Fe_3O_4, with further increases leading to decreased efficiency due to nanoparticle aggregation, obstructing active sites. The initial dose of MPs also played a crucial role, with optimal removal efficiencies observed at an MPs dose of 0.5 g/L. Application of the optimized parameters to real water matrices demonstrated the efficacy of g-C_3N_4@Fe_3O_4 and BNNS@Fe_3O_4 in removing different sizes and types of MPs from Milli-Q water, drinking water, and treated domestic wastewater. g-C_3N_4@Fe_3O_4 consistently outperformed BNNS@Fe_3O_4, likely due to its superior textural properties, including higher pore volume, diameter, and width, which facilitated greater active site availability. Optimal conditions for g-C_3N_4@Fe_3O_4 achieved remarkable removal efficiency of up to 96.16% removal of PE (125 µm), while BNNS@Fe_3O_4 reached 94.44%. The removal of different combinations of MPs (size and types) followed the same pattern, with smaller MPs demonstrating significantly higher removal efficiencies due to enhanced interaction with the active sites on the MNC surfaces. Thus, both g-C_3N_4@Fe_3O_4 and BNNS@Fe_3O_4 MNCs have proven to be efficient for the removal of different polymer types as well as various polymer sizes. Larger MPs (PP, LDPE, HDPE, size 3 mm, 5 mm and 5 mm, respectively) showed no removal, likely due to weak intermolecular forces and hydrogen bonding. Additionally, the study found comparable removal efficiencies for drinking water and domestic wastewater. In practical applications, both MNCs showed high removal efficiencies in various water matrices, with minor decreases

in efficiency in more complex water compositions, underscoring the robustness and practical applicability of these MNCs for MPs removal.

CHAPTER FIVE: Comprehensive analysis of magnetic nanocomposite performance: reusability, magnetic stability (VSM), phytotoxicity, and cost evaluation

5.1. Introduction

Performance analysis of MNCs is critical since it directly influences their removal efficiency, reliability, and applicability in diverse fields such as wastewater treatment. This is particularly relevant in adsorption-based methods, where high-performance MNCs can significantly enhance efficacy. While the adsorption method is not yet commercially available, it has the potential to eliminate most pollutants in a reversible and economical way (Rasheed 2022). Coalescing adsorption approaches with additional features such as magnetism leads to a more efficient and commercially feasible purification technology (Mironyuk *et al.* 2019). Numerous studies have demonstrated the feasibility of MNCs for removing a wide range of water contaminants, including heavy metals, pharmaceuticals, emerging organic pollutants, chemical wastes, dyes, radionuclides, and pathogens (Wang *et al.* 2021e). This demonstrates their versatility in pollutant removal, making them promising candidates for the removal of MPs from water and wastewater. Additionally, the extensive benefits of MNCs include large-scale production capability, customizable properties, facile functionalization, recyclability, biocompatibility, targetability, easy separation, high adsorption rate, and low toxicity. These properties make MNCs highly valuable for environmental applications (Du *et al.* 2020). As a result, MNCs have become a significant focus of recent research (Wang *et al.* 2021e), particularly in the removal of emerging contaminants such as MPs (Baresel *et al.* 2019). For example, core-shell superparamagnetic artificial nano-melanin NMs can magnetically remove PS spheres (950 nm) through hydrophobic, electrostatic, and Van Der Waals interactions with an average removal efficiency of 89.3% (Chen *et al.* 2022a). Numerous additional MNCs have been examined for MP removal such as Mg/Zn modified magnetic biochars (Singh *et al.*

2021b; Wang *et al.* 2021d), magnetic polyoxometalate-supported ionic liquid phases (magPOM-SILPs) (Misra *et al.* 2020), and magnetic CNTs (Tang *et al.* 2021).

However, the potential toxicity of MNCs have not been thoroughly investigated (Rasheed 2022). Typically, MNCs have varying impacts on plants, ranging from neutral to hazardous, contingent on their environmental circumstances, exposure methods, application durations, doses, sizes, types and targeted plant species (Kah *et al.* 2018; Kolbert *et al.* 2022). MNCs are able to penetrate cells via cell membranes with ease due to their active surfaces and nano size. Once within the cell, they can cause toxicity by interacting with different intracellular proteins. In addition to potentially affecting nutrient absorption, MNCs that accumulate in plants can also adversely control cellular activities through interactions with different cellular structures (Muzammil *et al.* 2023). This interaction may lead to phytotoxicity linked with MNCs (Lee *et al.* 2008; El-Temsah and Joner 2012; Li *et al.* 2015; Muzammil *et al.* 2023). Hence, it is critical that more studies be performed to assess the phytotoxicity of different NMs since each NM will confer different phytotoxic effects.

Additionally, NMs have been extensively researched as adsorbents to develop a process-based, frugal and straightforward separation method. The reduction of capital expenses is due to the aforementioned recyclability and regeneration properties of NMs (Rasheed 2022). Furthermore, the need for on-site remediation development, pilot-scale operation, and economic feasibility necessitates an economic assessment of the method (Rasheed 2022). Therefore, this chapter focuses on a rough economic assessment of the MNCs synthesis and adsorption treatment process using the best-performing MNC. Additionally, it includes recyclability studies on the MNCs. This chapter also assesses the magnetic stability of the MNCs. Finally, it covers phytotoxicity studies related to the MNCs

5.2. Materials

This investigation utilised the same materials that were employed in Section 4.2. of Chapter 4, ensuring the reliability and validity of the experimental results.

5.3. Experimental procedure

5.3.1. MNC recyclability/reusability study

5.3.1.1. Regeneration of the MNCs

The experiments outlined in this reusability study were meticulously conducted in strict accordance with the detailed methodology described in Section 4.3.3 of Chapter 4.

5.3.1.2. MPs Removal calculation and reusability assessment

The experiments detailed in this study were carried out with precision, strictly following the comprehensive procedure outlined in Section 4.3.4 of Chapter 4. Once the removal efficiency was calculated, the recovered MNCs then underwent the experiment again in the second cycle. This was done for 5 cycles. Figure 31 is a diagram illustrating g-C_3N_4@Fe_3O_4 and BNNS@Fe_3O_4 MNCs recyclability. It is important to note that these experiments were performed separately for BNNS@Fe_3O_4 and g-C_3N_4@Fe_3O_4 MNC to assess their individual efficiency (Shi *et al.* 2022b).

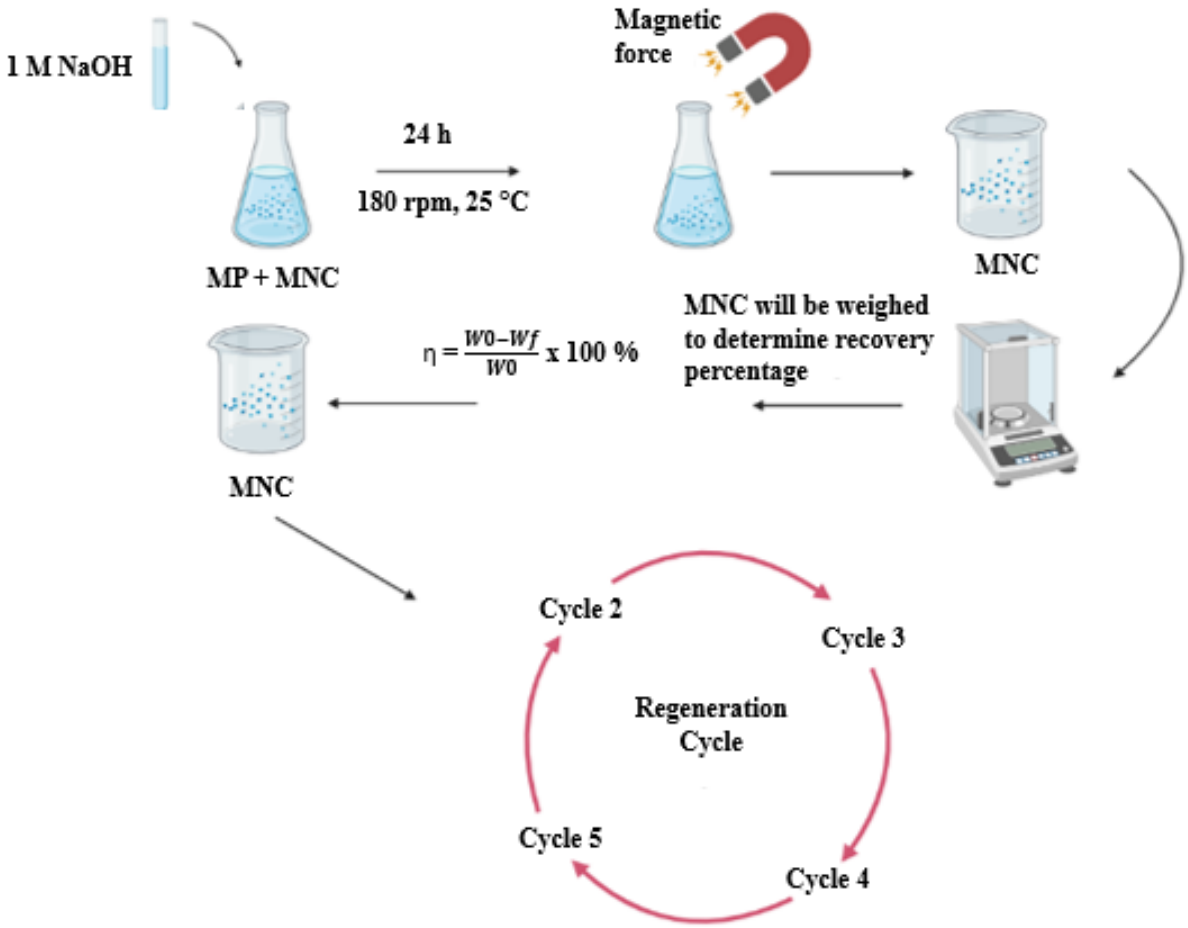

Figure 31: Schematic illustration of recovery and recyclability of g-C_3N_4@Fe_3O_4 and BNNS@Fe_3O_4 MNCs

5.3.2. Magnetic stability assessment via vibrating magnetometer sample (VSM)

Each MNC underwent VSM characterisation of fresh and used MNC. Utilizing a commercial Vibrating Sample Magnetometer from Cryogenic Limited (9T-2T-2T VECTOR SYSTEM WITH VIBRATING SAMPLE MAGNETOMETER), temperature-dependent and field-dependent magnetic characterizations were performed at 300 K, with samples in isolated static gas chamber. Vibration amplitude and frequency were set at 2 mm and 20 Hz, respectively. The noise base was set at 1 x 10^{-6} emu and 10 sec integration time while the noise level was at 2 x 10^{-6}. A 20-bit superconducting magnetic power supply was utilised. The dynamic range

utilised was standard (108). The central field homogeneity for VSM was 0.01% over 3cm x Ø 1 cm cylinder at field centre.

5.3.3. Phytotoxicity study

Phytotoxicity studies were performed to assess the toxicity of MPs-containing wastewater and the MNCs on three different plant species: *Vigna radiatus L.* (moong), *Cicer arietinum* (chickpea) and *Hordeum vulgare L.* (barley), respectively. Seven different experiments were conducted per crop: tap water (control), untreated wastewater (raw wastewater influent), treated (chlorinated) wastewater (final treated effluent), BNNS@Fe_3O_4, g-C_3N_4@Fe_3O_4, BNNS@Fe_3O_4 filtrate and g-C_3N_4@Fe_3O_4 filtrate, to evaluate the seed germination indices (G.I.). The filtrate are the samples collected during the drinking water filtration. Prior to phytotoxicity assessment, 10 seeds of each species underwent sterilisation by soaking for 2 min in 3% H_2O_2 solution. This was followed by 5 rounds of washing with Milli-Q water (Ravindran *et al.* 2016). All experiments were performed in triplicate with the mean average data reported. The germination index G.I. (%) was calculated after 10 days of seed germination via the equation 4:

$$G.I.(\%) = \frac{Gs}{Gc} \text{ x } \frac{Ls}{Lc} \text{ x } 100 \qquad (4)$$

Where Ls and Lc represent the value of root elongation (radical length) in the sample water and control sample, respectively, whilst Gs and Gc are given as the number of seeds that germinated in the sample water and control sample (tap water) (Kumar *et al.* 2023a).

5.3.4. Cost Assessment

The implementation of any research project at the full scale requires careful consideration of treatment cost estimation. Typically, the total cost of any treatment is the product of the investment, operating, and capital costs. An approximate economic evaluation of the running

expenses for treating wastewater containing MPs by best-performing NM was conducted. The cost of chemical reagents for NM synthesis, the cost of reagents for the physiosorption process, and the cost of energy were all included in the operation cost (in $\$/m^3$ wastewater) that was computed. It is important to remember that this study is only a rough tool and that the values were only found through experimentation. The formula utilised is as follows (equation 5):

$$\text{Operating cost (R)} = \text{Unit price x Machine power x time}$$

$$\text{Operating cost (R)} = \frac{\text{Rand}}{\text{kW/h}} \text{ x kW x h} \qquad (5)$$

The price per 1 unit electricity was R1.84 kWh and the reagents used for synthesis were melamine, urea ferric chloride hexahydrate, ammonium hydroxide, iron(II) chloride tetrahydrate. The MNC cost was calculated for the optimum dose whilst total operating cost was calculated per L of treated MP-NMs solution.

5.4. Results and Discussion

5.4.1. Recyclability of MNCs

Recyclability and economic feasibility of the MNCs stand as a pivotal element for the practical implementation in industrial settings. The recyclability assessment was performed for five consecutive cycles under optimum operating conditions (g-C_3N_4@Fe_3O_4 dose1.2 g/L, pH_0 4, MPs dose 0.5 g/L, temperature 25 °C and time 5 h; BNNS@Fe_3O_4 dose 0.9 g/L, pH_0 3, MPs dose 0.5 g/L, temperature 25 °C and time 12 h), as illustrated in Figure 32. In the first cycle, MPs removal was observed to be 94.89% and 88.28% for g-C_3N_4@Fe_3O_4 and BNNS@Fe_3O_4, respectively. Following each experimental cycle, the used catalyst was recovered by magnetic separation, followed by multiple rinses with Milli-Q water, and subsequently dried at 120 °C for 12 h. To ensure all MPs were removed from the MNC surface, the MNC underwent catalyst regeneration as described in Section 4.3.3 of Chapter 4. To gather a sufficient quantity of MNC for the subsequent cycle, numerous parallel runs were conducted. The regenerated MNCs were

then reused under the same optimal operating conditions, resulting in slight losses of MPs removal efficiency in each cycle. The MPs removal efficiency gradually decreased from 94.89% (1st), to 91.85%, 79.74%, 67.14%, and 56.38% in 2nd, 3rd, 4th and 5th cycle, respectively for g-C_3N_4@Fe_3O_4. For BNNS@Fe_3O_4 removal of MPs, a reduction of 88.28% (1st) to 77.53%, 69.18%, 58.5% and 51.22% for the 2nd, 3rd, 4th and 5th cycle, respectively was observed. In our study a loss of 16% and 19% efficiency was observed for g-C_3N_4@Fe_3O_4 and BNNS@Fe_3O_4, respectively, after 3 cycles. Similar results were reported by Rosa and team wherein they exhibited a loss of 18% activity after 3 successive runs for g-C_3N_4@Fe_3O_4 (Rosa *et al.* 2021). This may be ascribed to possible leaching of iron ions resulting in suppressed active sites (Fe^{2+}/Fe^{3+}) on the MNCs surface (Hammouda *et al.* 2017; Qin *et al.* 2018; Kumar *et al.* 2021a).

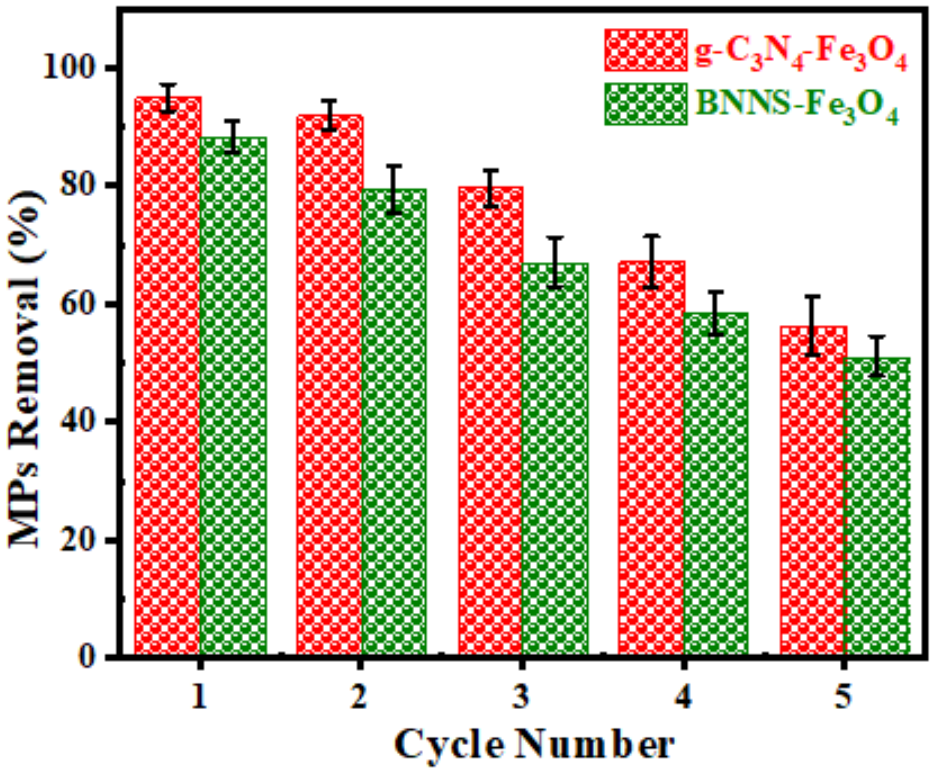

Figure 32: g-C_3N_4@Fe_3O_4 and BNNS@Fe_3O_4 MNCs recyclability over 5 cycles of MPs removal

5.4.2. Magnetic stability assessment via VSM

The vibrating sample magnetometer is the most often used technique to measure magnetic characteristics of MNCs in relation to temperature, time, and magnetic field (Yadav *et al.* 2020). Furthermore, the VSM analysis provides an indication of whether the magnetization is parallel or perpendicular to the substrate-defined plane (Shirsath and Shirivastava 2015). In the current finding, magnetization saturation (MS) was detected at a pressure range of 0–30 000 gauss (0–3 Tesla) for BNNS@Fe_3O_4 and g-C_3N_4@Fe_3O_4 before adsorption (MS_b) and after (MS_a) adsorption. The MS_b and MS_a for BNNS@Fe_3O_4 was determined to be 61.94 and 51.83 emu/g, respectively (Figure 33 (a)), while for g-C_3N_4@Fe_3O_4 (Figure 33 (b)) the MS_b was 16.52 and MS_a was 13.44 emu/g. These results indicate that MNC magnetization increases as the strength of the applied magnetic field increases, until the saturation point is reached. Before and after treatment curves for BNNS@Fe_3O_4 display superparamagnetic behaviour since no hysteresis, remanence (M_r) and coercivity (H_c) were found (Ahmad *et al.* 2019a). A similar result is reported for g-C_3N_4@Fe_3O_4 since the curves also exhibit superparamagnetic behaviour. Herein, the MS_b for both MNCs are high in comparison to a study by Prasad et al. (2017), which revealed the MS_b for Fe_3O_4@rGO and Fe_3O_4 to be 12.6 and 15.3 emu/g, respectively (Prasad *et al.* 2017). The MS_b for both MNCs are higher than the MS_b for Fe_3O_4 which is excellent since generally, the addition of the supporting material decreases the MS considerably. Additionally, a study by Wang et al. (2017), investigated the VSM of BNNS@Fe_3O_4 wherein the MS_b was found to be 6 emu/g (Wang *et al.* 2017a). In contrast, in this study, the observed VSM value was 61.94 emu/g, indicating an enhanced magnetic moment and thus superior magnetic properties of the synthesised BNNS@Fe_3O_4 MNC over the reported MNC in literature. This improvement in the magnetic characteristics makes the current synthesised BNNS@Fe_3O_4 a more desirable MNC. Furthermore, Wang et al. (2017) reported that the BNNS@Fe_3O_4 MNCs exhibit a negligible hysteresis curve, suggesting that

they function as superparamagnets. This behaviour is in line with the observation that each Fe_3O_4 nanoparticle scattered on BN nanospheres has an average diameter of approximately 10 nm and is single-domain, meaning that it comprises a single magnetic domain (Wang *et al.* 2017a). This is similar and consistent with the results obtained from the present investigation for BNNS@Fe_3O_4. Several studies have reported the VSM for g-C_3N_4@Fe_3O_4 functionalised to an additional supporting material/nanoparticles (Mousavi and Habibi-Yangjeh 2016, 2018a, 2018b). Mousavi and Habibi-Yangjeh, 2016 investigated the VSM of g-C_3N_4@Fe_3O_4-BiOI. In their study, the MS_b was 8.7 emu/g (Mousavi and Habibi-Yangjeh 2016). Similarly, a study conducted by Mousavi and Habibi-Yangjeh utilized VSM to determine the MS_b of g-C_3N_4@Fe_3O_4-$CoWO_4$. In this study, they reported a MS_b of 7.04 emu/g, (Mousavi and Habibi-Yangjeh 2018a) while in another study, they reported a MS_b of 6 emu/g for g-C_3N_4@Fe_3O_4-$NiWO_4$ (Mousavi and Habibi-Yangjeh 2018b). All those studies revealed the S-shape curve with no hysteresis indicating that these MNCs are superparamagnetic (Mousavi and Habibi-Yangjeh 2016, 2018a, 2018b). This is also consistent and similar to the results ascertained in the present study. In addition, the MS_b obtained in the present study is more than double that reported in previous studies. This is indicative of a higher magnetic moment, and therefore a superior magnetic MNC, offering great potential in a variety of applications. The size of the particles has a significant impact on their magnetic characteristics. A mean diameter of less than 20 nm is required for nanoparticles to be considered superparamagnetic (Namanga *et al.* 2013). Therefore, the VSM results for both MNCs are in good agreement with the TEM results since BNNS@Fe_3O_4 average particle size is 7 nm and g-C_3N_4@Fe_3O_4 average particle size is 11.66 nm. Additionally, both MNCs have a single magnetic domain. This is advantageous since all their magnetic moments are aligned in the same direction, thus the application of an external magnetic field results in the largest possible magnetization for that specific MNC (March 2014). This indicates that both MNCs have excellent magnetic properties enabling them to be

applied in practical applications (Shirsath and Shirivastava 2015). The results after treatment for both BNNS@Fe_3O_4 and g-C_3N_4@Fe_3O_4 MNCs exhibit a decrease in MS. This can be attributed to the adsorption of MPs to the MNCs. The adsorbed MPs cause a decrease in magnetization due to their weight contribution (Ahmad *et al.* 2019a). However, the superparamagnetic properties of the MNCs are still retained since they were sufficient enough to perform effective magnetic separation via external field application (Ahmad *et al.* 2019a). After shaking for a minute, the MNCs were found to evenly distributed throughout the aqueous solution when the applied magnetic field was withdrawn. This demonstrates the high levels of magnetic stability and redispersibility, making them effective adsorbents for real-world uses in low-magnetization environments (Santhosh *et al.* 2017).

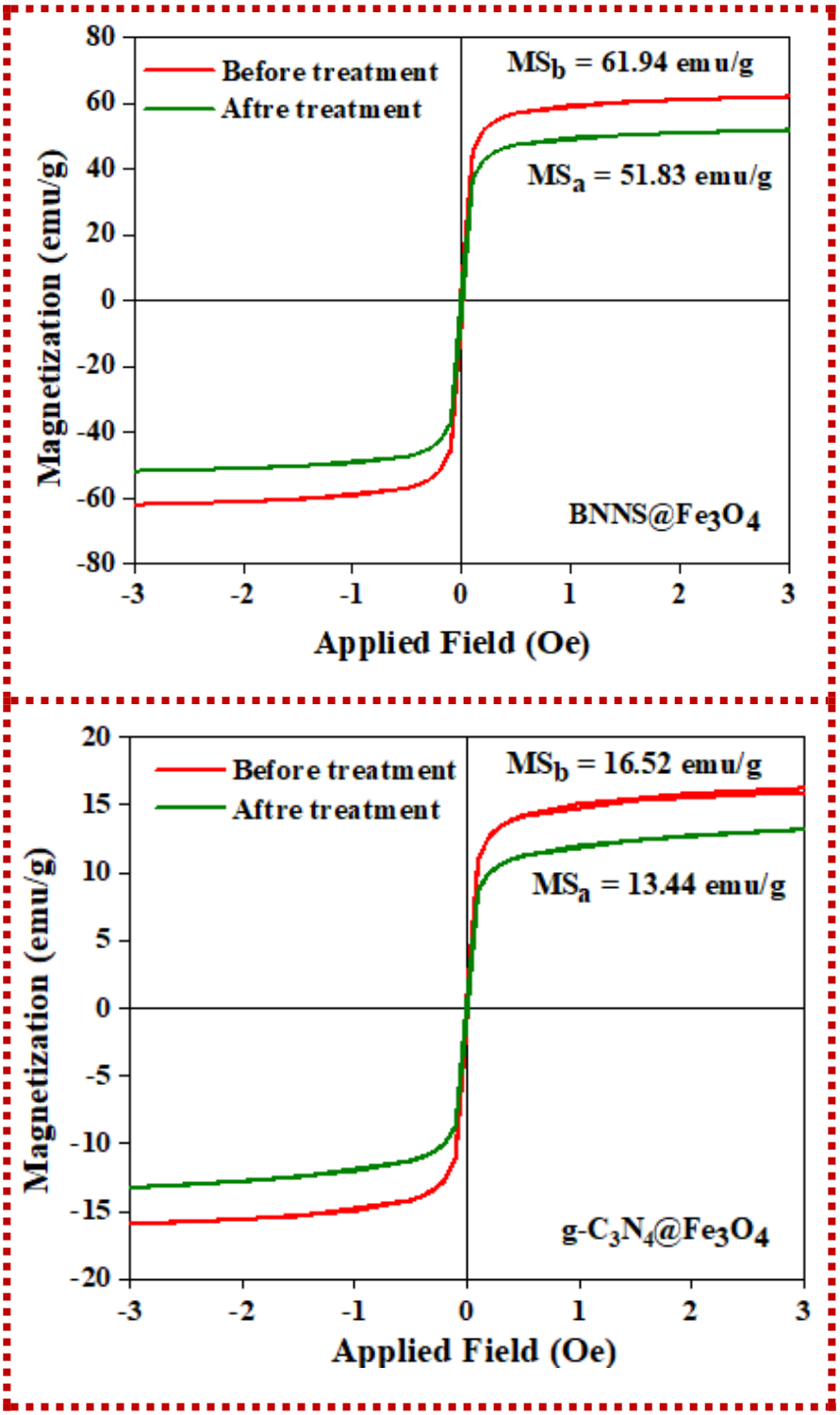

Figure 33: Magnetization curves before (fresh) and after (used) adsorption of MPs by (a) BNNS@Fe_3O_4 and (b) g-C_3N_4@Fe_3O_4 by VSM

5.4.3. Phytotoxicity study

Understanding the effects of MNCs on plants, is crucial in the field of biotechnology when assessing the safety of MNCs in agricultural and environmental applications. Beyond direct plant effects, understanding phytotoxicity helps in assessing ecotoxicity and broader ecological impacts. Several studies revealed that industrial and domestic wastewater effluent contain high concentrations of MPs (Gies *et al.* 2018; Kazour *et al.* 2019; Naji *et al.* 2021; Van Do *et al.* 2022) which are toxic and pose a threat to common agricultural crops' growth either by delaying seed germination or impeding crop growth through nutrient absorption inhibition (Mészáros *et al.* 2023). Additionally, there have been reports of adverse effects of MNCs on plant growth, such as interference in plant roots, decreased photosynthesis, and suppression of seed germination (Gao *et al.* 2023). Similarly, numerous researchers have reported the toxicity of wastewater on a range of agricultural crops, including black chickpea (Kumar *et al.* 2021a), mustard (Mazhar *et al.* 2019), wheat, moong (Singh *et al.* 2013; Kumar *et al.* 2021a; Kumar *et al.* 2023a), and some vegetable crops (such as tomato, chili, onion, and cucumber)(Ramana *et al.* 2002). There is however a lack of technical data (insufficient studies) available on MNCs toxicity on agricultural crops (Indhur *et al.* 2023). Therefore, in this study the phytotoxicity effects of the domestic raw wastewater influent and final treated effluent, and the effects of g-C_3N_4@Fe_3O_4 and BNNS@Fe_3O_4 MNCs were assessed to determine their effect on 3 different common plant species, i.e., *Hordeum vulgare L.* (barley wheat), *Cicer arietinum* (black chickpea) and *Vigna radiatus L.* (moong) in conjunction with seed germination indices as depicted in Figure 34 (a). These crops were chosen since they exhibit a range of sensitivities to environmental stressors, making them effective indicators of phytotoxic effects. Additionally, since they are common cultivated crops, they have significant agronomic value. Thus, studying these crops helps in assessing the potential impact of pollutants on important food sources and agricultural systems. Lastly, these three crops exhibit diverse growth conditions, therefore

testing multiple species provides a broader understanding of how pollutants affect these crops. From the results, the toxicity indicator based on the G.I.%. The G.I.% for barley was observed to be 63.15% (raw wastewater influent), 84.24% (final treated effluent), 24.6% (g-C_3N_4@Fe_3O_4), 71.06% (g-C_3N_4@Fe_3O_4 filtrate), 30.1% (BNNS@Fe_3O_4) and 82.32% (BNNS@Fe_3O_4 filtrate) (Figure 34 (b). For moong, the G.I.% was determined to be 38.48% (raw wastewater influent), 69.81% (final treated effluent), 22.8% (g-C_3N_4@Fe_3O_4), 67.19% (g-C_3N_4@Fe_3O_4 filtrate), 39.85% (BNNS@Fe_3O_4) and 81.73% (BNNS@Fe_3O_4 filtrate). For black chickpea, the G.I.% was calculated to be 34.99% (raw wastewater influent), 67.02% (final treated effluent), 28.6% (g-C_3N_4@Fe_3O_4), 77.3% (g-C_3N_4@Fe_3O_4 filtrate), 37% (BNNS@Fe_3O_4) and 84% (BNNS@Fe_3O_4 filtrate) (Figure 34 (b)). A G.I. (%) value less than 50% indicates a high level of phytotoxicity, a value between 50-80% indicates a moderate level of phytotoxicity, and a value greater than 80% indicates that the substance is not naturally poisonous to plant species. It is observed that the impact of domestic raw wastewater influent showed mild toxicity and final treated effluent showed non-toxicity on barley, whilst domestic raw wastewater influent is toxic and final treated effluent is mildly-toxic for the moong and black chickpea species. This is probably due to the abiotic stress tolerance genes in barley, enabling the plant to flourish in a variety of environmental circumstances (Abdelghany *et al.* 2024). The effects of the g-C_3N_4@Fe_3O_4 and BNNS@Fe_3O_4 MNC powder was also examined and used as a control for the filtrate samples. The results indicated that these MNCs have a toxic effect on all 3 crops based on their low G.I.% values (Figure 34 (b)). This may be attributed to the accumulation of nanoparticles around the crop root, interfering with nutrient assimilation and root growth (Thiruvengadam *et al.* 2024). It is important to note that during the experimental procedure all MNCs powder and residual MNCs powder are recovered during the filtering step, ensuring complete retrieval of MNCs powder. Therefore, there is no circumstance in which MNCs powder will be discharged; it was simply utilised as a control for

the filtrate samples. It is critical to remove MNCs after treatment to prevent their subsequent discharge into the environment and mitigate potential ecological and health hazards. A study by Lee et al. (2010), scrutinised the effects of Fe_3O_4 (~50 nm) nanoparticles at 3 different concentrations (4000, 2000 and 400 mg/L) on *Arabidopsis thaliana* (Mouse-ear cress). They reported no significant effect of Fe_3O_4 nanoparticles on seed germination (Lee *et al.* 2010), whereas in contrast, the present study utilised 500 mg/L and reports significant inhibition on seed germination for both g-C_3N_4@Fe_3O_4 and BNNS@Fe_3O_4 MNCs. Due to the selective permeability of seed coat pores, interactions between solid or particulate matter and the crop are restricted until the radicles appear and make direct contact with the growth medium (Wierzbicka and Obidzińska 1998). However, intracellular spaces within the seed coat parenchyma, which are less than ~10 µm in size, can be filled with aqueous media, allowing for the passage of tiny particles and soluble nutrients to the developing embryo (Van Dongen *et al.* 2003). This mechanism may explain the significant inhibition caused by the smaller, monodisperse g-C_3N_4@Fe_3O_4 (average particle size = ~11 nm) and BNNS@Fe_3O_4 (average particle size = 7 nm) MNCs. A study by Konate et al. (2018) examined the effects of bulk and nano-Fe_3O_4 on cucumbers (2000, 500 and 50 mg/L). Herein, it was observed that the high bulk-Fe_3O_4 concentration (500 and 2000 mg/L) caused phytotoxicity regarding enzyme activity and biomass. For nano-Fe_3O_4, the phytotoxicity depended on the particle properties (primarily aggregation and size), since significant biomass inhibition was observed at 50 mg/L while for bulk-Fe_3O_4, it was dependent on the concentration (Konate *et al.* 2018). When assessing the exposure of MNCs and their harmful consequences in the environment, it is necessary to take into account the particle size as a significant component that can affect the bioavailability of MNCs. It is important to note that there is limited reports on the phytotoxicity of iron MNCs (Konate *et al.* 2018). According to Zhu et al.'s (2008) investigation into the uptake and accumulation of engineered iron nanoparticles by pumpkin plants, Fe_3O_4 nanoparticles were

found to be transported and stored in plant tissues (Zhu *et al.* 2008). However, Wang et al. (2011) demonstrated that ryegrass and pumpkin plants did not accumulate magnetic nanoparticles (Wang *et al.* 2011). Noteworthy is the suggestion made by Zhu et al. (2008) that varying plant species react differently to the effects of nanoparticles. According to Bystrzejewska-Piotrowska et al. (2012), *Lepidium sativum* and *Pisum sativum L*. may accumulate Fe_3O_4. Bystrzejewska-Piotrowska et al. (2012) proposed that the growth solution and other media exhibited dose-dependent accumulation of magnetite nanoparticles (Bystrzejewska-Piotrowska *et al.* 2012). According to some earlier research, Fe_3O_4 nanoparticles, may have favorable, negative, or no effects on plant development, root elongation, and seed germination (Konate *et al.* 2018) and is dependent on the synthesised Fe_3O_4 size as well as crop species. Therefore, the results presented in this study is consistent with literature. Additionally, the g-C_3N_4@Fe_3O_4 filtrate and BNNS@Fe_3O_4 filtrate exhibited mild toxicity (almost non-toxic) and non-toxicity, respectively. This suggests that use and recovery of the MNCs render it safe for application. It is also possible that g-C_3N_4@Fe_3O_4 is mildly toxic (almost non-toxic) because it has a greater number of ferric ions (Fe^{2+}/Fe^{3+}) that can leach out, enabling a slightly higher degree of leaching than in BNNS@Fe_3O_4. Ultimately, this indicates that the proper use of MNCs via filtering of the MNC solution not only ensures recovery but greatly diminishes the environmental impact of these MNCs, rendering them appropriate for usage.

(a)

(b)	*Hordeum vulgare L.*	*Vigna radiatus L.*	*Cicer arietinum*
TW			
UWW			
TWW			
g-C_3N_4@Fe_3O_4			
g-C_3N_4@Fe_3O_4 Filtrate			
BNNS@Fe_3O_4			
BNNS@Fe_3O_4 Filtrate			

Figure 34: Phytotoxicity asssessment of (a) *Hordeum vulgare L*, *Vigna radiatus L.* and *Cicer arietinum* (TW: Tap water (control), UWW: untreated wastewater, TWW: treated wastewater, GCN: g-C_3N_4@Fe_3O_4, GCNF: g-C_3N_4@Fe_3O_4 filtrate BNNS: BNNS@Fe_3O_4, BNNSF:

BNNS@Fe_3O_4 filtrate) and (b) Toxicity indicator: red (toxic), blue (mild toxicity), green (non-toxicity)

5.4.4. Economic assessment

A crucial component of carrying out research at the plant size is estimating the treatment process's running costs. Therefore, the operating cost of implementing optimal g-C_3N_4@Fe_3O_4 MNC for MPs removal in domestic wastewater effluent was estimated. The overall MPs removal cost comprises of the chemical reagent cost and energy cost as assessed by previous literature (Kumar *et al.* 2021b; GadelHak *et al.* 2023; Kumar *et al.* 2023a). Thus, an approximate economic study of the running expenses of the adsorption process was conducted as shown in table 8, wherein the treatment process's total running costs were calculated to be 41.09$/$m^3$ of domestic wastewater in lab scale. Thus far, there are currently no economic assessment studies available for comparison for MP removal using different NMs in the adsorption process. This treatment cost (41.09$/$m^3$) however can be significantly decreased when treating domestic wastewater at a large scale, in addition to the adsorbent being utilised for multiple cycles. In a previous study by Kumar and team, wherein they utilised NM $LaCu_xFe_{1-x}O_3$ series perovskite-like catalyst for ABS resin wastewater treatment, a cost of 75.60$/$m^3$ was reported (Kumar *et al.* 2021a). The treatment cost of catalytic wet peroxidation process for the degradation of pyridine with catalysts GAC and nFe/GAC were reported to be 248$/$m^3$ (Subbaramaiah *et al.* 2013) and 99.62$/$m^3$ (Gosu *et al.* 2018), respectively. Similarly, another study evaluated the removal of dye from wastewater via Fe/ZnO catalyst via the same process. Herein they reported a total operating cost of 332$/$m^3$ (Priyanka and Srivastava 2013). Moreover, two different studies were performed utilising a Fenton-like oxidation process ($UV/O_3/H_2O_2/Fe^{+2}$) for the degradation of atrazine and 2-propanol. The reported estimated cost was 248$/$m^3$ (González *et al.* 2020) and 94$/$m^3$ (Canizares *et al.* 2009), respectively. Furthermore, additional cost estimations have been reported by various authors for the remediation of industrial wastewater. Cosmetic industry wastewater, sugar industry wastewater

and highly acidic wastewater, all revealed a cost estimation of 217.36$/m^3 (Patidar and Srivastava 2022), 248$/m^3 (Sahu *et al.* 2015) and 436$/m^3 (Goyal and Srivastava 2017), respectively, for their treatment. Therefore, the above results indicate that the overall operating cost of g-C_3N_4@Fe_3O_4 adsorption of MPs from domestic wastewater is a cost-effective process in comparison with the reported literature.

Table 8: Operating cost of best-performing MNC g-C_3N_4@Fe_3O_4 for MPs removal from wastewater effluent

Reagent	**Reagent and running cost for g-C_3N_4@Fe_3O_4 synthesis**		
	Cost per unit	**Price per g/unit**	
Ferric chloride hexahydrate	R 102/kg	0.102	
Iron(II) chloride tetrahydrate	R 119/kg	0.119	
Ammonium hydroxide	R 106/L	0.106	
Urea	R 32/kg	0.032	
Melamine	R 124/kg	0.124	
Catalyst cost per g		R 0.483	
*MNC cost per optimum dose		R 0.579	
	Running cost of adsorption process		
	Cost per unit	Price for a single run	Price per L
Power consumption	R 1.84/kWh	0.276	R0.184
Total operating cost per L solution			R0.763
Total operating cost per m^3 solution			R763 (41.09$)

Note: 1$ = 18.56 South African Rand in May 2024. *MNC cost at optimum dose of 1.2 g/L.

5.5. Conclusions

This study investigated the sustainability of g-C_3N_4@Fe_3O_4 and BNNS@Fe_3O_4 through recyclability, magnetic stability, phytotoxicity and economic feasibility for the removal of MPs. The recyclability tests revealed a gradual decline in MPs removal efficiency over five consecutive cycles. For g-C_3N_4@Fe_3O_4, the efficiency decreased from 94.89% in the first cycle

to 56.38% in the fifth cycle, while for BNNS@Fe_3O_4, it dropped from 88.28 to 51.22%. The VSM data displayed that both MNCs possess superparamagnetic behaviour and are in accordance with the TEM data. It further demonstrated that both MNCs retained their superparamagnetic properties after adsorption to MPs, enabling effective magnetic separation. This indicates that they have the potential to be applied in industrial applications. Phytotoxicity assessments indicated that the positive controls in which the MNCs were exposed directly to the crops, were toxic to barley, black chickpea, and moong, whereas their filtrates exhibited reduced toxicity and no toxicity. These findings underscore the importance of proper use and recovery (filtering) of the MNCs to mitigate their environmental impact, making them safer for agricultural applications. Economically, the operating cost of MPs removal using g-C_3N_4@Fe_3O_4 was estimated at \$41.09/m^3 of domestic wastewater effluent at a lab scale, which is significantly lower compared to other reported methods, such as catalytic wet peroxidation and Fenton-like oxidation processes. This cost-effectiveness, combined with the ability to reuse MNCs, highlights the practical viability of g-C_3N_4@Fe_3O_4 for large-scale wastewater treatment applications. Further research is recommended to enhance the stability and recyclability of these MNCs and to explore their long-term environmental impacts.

CHAPTER SIX: Overall Conclusions and Recommendations

This study aimed to investigate 2D g-C_3N_4@Fe_3O_4 and BNNS@Fe_3O_4 MNCs for the removal of MPs from drinking water and treated wastewater.

6.1. Major conclusions/ Significant findings based on the objectives of the study

- This study offered a novel, cutting-edge approach for eliminating PE/PS MPs by g-C_3N_4@Fe_3O_4 and BNNS@Fe_3O_4 from drinking water and domestic wastewater effluent, which has application potential to reduce the amount of MP pollution.
- The comprehensive characterization of g-C_3N_4@Fe_3O_4 and BNNS@Fe_3O_4 MNCs revealed their chemical and structural properties. Analytical techniques such as XRD, FTIR, zeta potential, FESEM-EDX, TEM and XPS confirmed the MNCs crystalline structure, size and morphology, surface composition, valance state, oxygen vacancies and robust integration of iron oxide nanoparticles. TGA confirmed the thermal stability and BET confirmed the surface area for optimization and textural properties. The MNCs were confirmed to be 2D structures making them most suitable for application of MP removal in water matrices. Additionally, the MNCs demonstrated a porous morphology, excellent structural integrity and chemical stability, making them strong candidates for sustainable drinking water and wastewater treatment for MP removal.
- In this study, both g-C_3N_4@Fe_3O_4 and BNNS@Fe_3O_4 MNCs have shown to be remarkably efficient for the removal of different polymer types as well as various polymer sizes from Milli-Q water. The maximum removal of PE (96.16%, size 125 µM), PS (92.5% , size 25-180 µM), PE+PS combo (94.89%, size PE=125 µM and 25-180 µM), PS (45.62%, size 5180-500 µM), PP (0%, size 3 mm), LDPE (0%, size 5 mm) and HDPE (0%, size 5 mm) were noticed with catalyst g-C_3N_4@Fe_3O_4 under optimum operating conditions ([pH]= 4; time= 5 h; [MNC]= 1.2 g/L; [MP]= 0.5 g/L) from Milli-

Q water. The maximum removal efficiency of PE (94.44%, size 125 μM), PS (85.96%, size 25-180 μM), PE+PS combo (88.28% , size PE=125 μM and 25-180 μM), PS (38.77%, size 180-500 μM), PP (0%, size 3 mm), LDPE (0%, size 5 mm) and HDPE (0%, size 5 mm) were observed with catalyst BNNS@Fe_3O_4 under optimum operating conditions ([pH] = 3; time= 12 h; [MNC]= 0.9 g/L; [MP] = 0.5 g/L) from Milli-Q water.

- Both MNCs, g-C_3N_4@Fe_3O_4 and BNNS@Fe_3O_4 were successfully utilised in the removal of MPs from drinking water and domestic wastewater effluent. The performance of MNCs in different water matrices yielded varying results. A removal efficiency of 93.7 and 86.56% from drinking water via g-C_3N_4@Fe_3O_4 and BNNS@Fe_3O_4, respectively, was achieved. A removal efficiency of 91.91 and 83.78% was observed from domestic wastewater effluent filtered with a 0.22 μM filter for g-C_3N_4@Fe_3O_4 and BNNS@Fe_3O_4, respectively, whilst a removal efficiency of 90.28 and 82.23% was observed from the same domestic wastewater effluent (unfiltered) for g-C_3N_4@Fe_3O_4 and BNNS@Fe_3O_4, respectively.
- The reusability study revealed that both MNCs retained a removal efficiency of more than 50% after 5 cycles whilst g-C_3N_4@Fe_3O_4 retained a removal efficiency of almost 80% after 3 cycles. This suggests that both MNCs can be utilized for multiple cycles before disposal. Their sustained performance underscores their cost-effectiveness and potential to support a circular economy, offering significant financial benefits for industrial applications. The reusability study further shows that both MNCs exhibit high stability and retain satisfactory performance even after the fifth cycle.
- In this study, MS was observed for BNNS@Fe_3O_4 and g-C_3N_4@Fe_3O_4 within a pressure range of 0–30,000 gauss. The results showed that both MNCs exhibited superparamagnetic behaviour, with no hysteresis, remanence, or coercivity. The findings further aligned with TEM results, indicating that both BNNS@Fe_3O_4 and g-

C_3N_4@Fe_3O_4 have excellent magnetic properties, enabling their application in practical settings. Despite a decrease in MS after treatment due to the adsorption of non-magnetic MPs, the materials retained their superparamagnetic properties, allowing for effective magnetic separation.

- The study assessed the phytotoxicity of raw wastewater influent, final treated wastewater effluent, g-C_3N_4@Fe_3O_4, BNNS@Fe_3O_4, on barley, black chickpea and moong crops. While final treated wastewater effluent showed mild to no toxicity, the raw influent had toxic effects, particularly on moong and black chickpea. The MNCs in powder form exhibited significant toxicity across all crops, but their filtrates were much less harmful, with BNNS@Fe_3O_4 filtrate showing no toxicity. This suggests that while MNCs pose environmental risks if not properly filtered, their appropriate recovery significantly mitigates their impact, making them feasible for use in wastewater treatment.
- Interaction mechanistic insights between PS/PE MPs and MNCs were proposed based on the chemical structure of the PS/PE MPs, surface composition, valance state, oxygen vacancies analysed by XPS analysis, as well as quantum chemistry literature. The physio-sorption of PS/PE MPs onto g-C_3N_4@Fe_3O_4 and BNNS@Fe_3O_4 MNCS were attributed to four potential interactions: electrostatic interaction, π-π interaction, Van Der Waals forces and hydrogen bonding.
- A rough economic assessment of the process revealed that the total operating cost for the adsorption process is approximately 41.09\$/m^3 of domestic wastewater effluent at the lab scale. This cost is expected to decrease when treating larger volumes of domestic wastewater, along with the recycling of the MNC for multiple cycles. Consequently, the overall operating cost for g-C_3N_4@Fe_3O_4 adsorption removal of MPs from domestic wastewater can be considered as cost-effective compared to reported literature

confirming its viability as an economical solution for domestic wastewater treatment, making it a promising candidate for commercial use.

6.2. Limitations of the study

The study, while providing valuable insights into the removal of MPs using MNCs, is not without certain limitations. These limitations highlight areas where further research and exploration are necessary to improve the applicability and generalizability of the findings.

- This study focused on a specific subset of MP types (PE, PS, PP) and sizes, which does not represent the full spectrum of MPs found in water environments. Smaller particle sizes were not included, thereby reducing the generalizability of the findings. Furthermore, the sizes of the PP, LDPE, and HDPE MPs used in this study were significantly larger (in the mm range) compared to the PS and PE MPs (in the μM range). This discrepancy was due to the commercial unavailability of smaller LDPE, HDPE, and PP MPs, which also poses a limitation in the assessment of MNC performance. The reduced variation in LDPE, HDPE and PP MP sizes presents a notable limitation of this study, as the removal efficiency may differ significantly for smaller-sized MPs.

6.3. Recommendations and Future research

Based on the findings of the current study, several areas have been identified as deserving further investigation to strengthen the development of the technology for industrial-scale implementation. The following recommendations are proposed for future research:

- The MNCs g-C_3N_4@Fe_3O_4 and BNNS@Fe_3O_4 demonstrated remarkable efficiencies for MPs removal, displaying a discernible relationship between the removal efficiency and the size of the MPs (the smaller the MPs, the higher the removal efficiency).

Therefore, there is a prospect for enhanced efficacy by targeting nanoplastics for removal.

- Multiple types of wastewaters from various geographical locations should be investigated for comprehensive analysis.
- MNCs g-C_3N_4@Fe_3O_4 and BNNS@Fe_3O_4 could be activated by various advanced oxidation processes for MPs degradation. Additionally, the intermediate products of MPs can be identified, and based on that, degradation pathways can be proposed.
- The method used for synthesizing catalysts significantly impacts their physicochemical properties. Therefore, it would be beneficial to investigate alternative synthesis methods, such as metal impregnation, the hydrothermal method or surface templating method, to maintain high activity and stability for the removal of MPs from wastewater.
- Future studies should be done to verify leaching of iron, employing analysis such as inductively coupled plasma mass spectrometry (ICP-MS) or atomic absorption spectroscopy (AAS) can be employed to quantify the amount of iron in the solution after the adsorption cycles.
- While this study has provided valuable insights into the effects of MNCs on plants, including their potential toxicity and impact on plant growth, a comprehensive assessment of the environmental fate of these MNCs is necessary to fully address their long-term ecological risks. Future studies should focus on developing bioremediation strategies to completely remove or neutralize any residual MNCs from agricultural environments. This could involve the use of specific plants or microorganisms capable of degrading, accumulating, or transforming MNCs into less harmful by-products, thereby mitigating the risk of ecological and health hazards.
- Future studies should incorporate extrapolating from lab scale to pilot scale since the developed system is efficient and can be scaled up.

REFERENCES

Abbasi, S., Keshavarzi, B., Moore, F., Turner, A., Kelly, F. J., Dominguez, A. O. and Jaafarzadeh, N. 2019. Distribution and potential health impacts of microplastics and microrubbers in air and street dusts from Asaluyeh County, Iran. *Environmental pollution*, 244: 153-164.

Abdelghany, A. M., Lamlom, S. F. and Naser, M. 2024. Dissecting the resilience of barley genotypes under multiple adverse environmental conditions. *BMC Plant Biology*, 24: 16.

Abuwatfa, W. H., Al-Muqbel, D., Al-Othman, A., Halalsheh, N. and Tawalbeh, M. 2021. Insights into the removal of microplastics from water using biochar in the era of COVID-19: A mini review. *Case Studies in Chemical and Environmental Engineering*, 4: 100151.

Adegoke, K., Akinnawo, S., Adebusuyi, T., Ajala, O., Adegoke, R., Maxakato, N. and Bello, O. 2023. Modified biomass adsorbents for removal of organic pollutants: a review of batch and optimization studies. *International Journal of Environmental Science and Technology*, 20: 11615-11644.

Adeleye, A. T., John, K. I., Adeleye, P. G., Akande, A. A. and Banjoko, O. O. 2021. One-dimensional titanate nanotube materials: Heterogeneous solid catalysts for sustainable synthesis of biofuel precursors/value-added chemicals—a review. *Journal of materials science*, Article ID: 1-26.

Ahmad, I., Siddiqui, W. A. and Ahmad, T. 2019a. Synthesis and characterization of molecularly imprinted magnetite nanomaterials as a novel adsorbent for the removal of heavy metals from aqueous solution. *Journal of Materials Research and Technology*, 8: 4239-4252.

Ahmad, S., Munir, S., Zeb, N., Ullah, A., Khan, B., Ali, J., Bilal, M., Omer, M., Alamzeb, M. and Salman, S. M. 2019b. Green nanotechnology: A review on green synthesis of silver nanoparticles—An ecofriendly approach. *International journal of nanomedicine*, Article ID: 5087-5107.

Ahmed, R., Hamid, A. K., Krebsbach, S. A., He, J. and Wang, D. 2022. Critical review of microplastics removal from the environment. *Chemosphere*, 293: 133557.

Ahrendt, C., Perez-Venegas, D. J., Urbina, M., Gonzalez, C., Echeveste, P., Aldana, M., Pulgar, J. and Galbán-Malagón, C. 2020. Microplastic ingestion cause intestinal lesions in the intertidal fish Girella laevifrons. *Marine Pollution Bulletin*, 151: 110795.

Ai, Q., Yuan, Z., Huang, R., Yang, C., Jiang, G., Xiong, J., Huang, Z. and Yuan, S. 2019. One-pot co-precipitation synthesis of Fe3O4 nanoparticles embedded in 3D carbonaceous matrix as anode for lithium ion batteries. *Journal of materials science*, 54: 4212-4224.

Ali, S. S., Al-Tohamy, R., Koutra, E., Moawad, M. S., Kornaros, M., Mustafa, A. M., Mahmoud, Y. A.-G., Badr, A., Osman, M. E. and Elsamahy, T. 2021. Nanobiotechnological advancements in agriculture and food industry: Applications, nanotoxicity, and future perspectives. *Science of the Total Environment*, 792: 148359.

Allen, S., Allen, D., Phoenix, V. R., Le Roux, G., Durántez Jiménez, P., Simonneau, A., Binet, S. and Galop, D. 2019. Atmospheric transport and deposition of microplastics in a remote mountain catchment. *Nature Geoscience*, 12: 339-344.

AlZain, M. A., Soh, B. and Pardede, E. 2013. A Survey on Data Security Issues in Cloud Computing: From Single to Multi-Clouds. *J. Softw.*, 8: 1068-1078.

An, L., Liu, Q., Deng, Y., Wu, W., Gao, Y. and Ling, W. 2020. Sources of microplastic in the environment. *Microplastics in terrestrial environments: Emerging contaminants and major challenges*, Article ID: 143-159.

An, Q., Lv, F., Liu, Q., Han, C., Zhao, K., Sheng, J., Wei, Q., Yan, M. and Mai, L. 2014. Amorphous vanadium oxide matrixes supporting hierarchical porous Fe3O4/graphene nanowires as a high-rate lithium storage anode. *Nano letters*, 14: 6250-6256.

Andrady, A. L. 2017. The plastic in microplastics: A review. *Marine pollution bulletin*, 119: 12-22.

Ashrafy, A., Liza, A. A., Islam, M. N., Billah, M. M., Arafat, S. T., Rahman, M. M. and Rahman, S. M. 2023. Microplastics pollution: a brief review of its source and abundance in different aquatic ecosystems. *Journal of Hazardous Materials Advances*, 9: 100215.

Astner, A., Hayes, D., O'Neill, H., Evans, B., Pingali, S., Urban, V. and Young, T. 2019. Mechanical formation of micro-and nano-plastic materials for environmental studies in agricultural ecosystems. *Science of the Total Environment*, 685: 1097-1106.

Ates, A. and Oymak, T. 2020. Characterization of persimmon fruit peel and its biochar for removal of methylene blue from aqueous solutions: thermodynamic, kinetic and isotherm studies. *International Journal of Phytoremediation*, 22: 607-616.

Balakrishnan, A. and Chinthala, M. 2022. Comprehensive review on advanced reusability of g-C3N4 based photocatalysts for the removal of organic pollutants. *Chemosphere*, 297: 134190.

Bamigboye, O., Alfred, M. O., Bayode, A. A., Unuabonah, E. I. and Omorogie, M. O. 2024. The growing threats and mitigation of environmental microplastics. *Environmental Chemistry and Ecotoxicology*, Article ID.

Bangari, R. S., Singh, A. K., Namsani, S., Singh, J. K., Sinha, N. J. A. a. m. and interfaces. 2019. Magnetite-coated boron nitride nanosheets for the removal of arsenic (V) from water. 11: 19017-19028.

Bangari, R. S., Yadav, V. K., Singh, J. K. and Sinha, N. 2020. Fe3O4-Functionalized boron nitride nanosheets as novel adsorbents for removal of arsenic (III) from contaminated water. *ACS omega*, 5: 10301-10314.

Barboza, L. G. A., Vethaak, A. D., Lavorante, B. R., Lundebye, A.-K. and Guilhermino, L. 2018. Marine microplastic debris: An emerging issue for food security, food safety and human health. *Marine pollution bulletin*, 133: 336-348.

Baresel, C., Schaller, V., Jonasson, C., Johansson, C., Bordes, R., Chauhan, V., Sugunan, A., Sommertune, J. and Welling, S. 2019. Functionalized magnetic particles for water treatment. *Heliyon*, 5.

Bayuo, J., Rwiza, M. and Mtei, K. 2022. Response surface optimization and modeling in heavy metal removal from wastewater—a critical review. *Environmental Monitoring and Assessment*, 194: 351.

Besseling, E., Quik, J. T., Sun, M. and Koelmans, A. A. 2017. Fate of nano-and microplastic in freshwater systems: A modeling study. *Environmental pollution*, 220: 540-548.

Bhattacharya, P., Lin, S., Turner, J. P. and Ke, P. C. 2010. Physical adsorption of charged plastic nanoparticles affects algal photosynthesis. *The journal of physical chemistry C*, 114: 16556-16561.

Bläsing, M. and Amelung, W. 2018. Plastics in soil: Analytical methods and possible sources. *Science of the total environment*, 612: 422-435.

Bobori, D. C., Dimitriadi, A., Feidantsis, K., Samiotaki, A., Fafouti, D., Sampsonidis, I., Kalogiannis, S., Kastrinaki, G., Lambropoulou, D. A. and Kyzas, G. Z. 2022a. Differentiation in the expression of toxic effects of polyethylene-microplastics on two freshwater fish species: Size matters. *Science of the Total Environment*, 830: 154603.

Bobori, D. C., Dimitriadi, A., Feidantsis, K., Samiotaki, A., Fafouti, D., Sampsonidis, I., Kalogiannis, S., Kastrinaki, G., Lambropoulou, D. A. and Kyzas, G. Z. 2022b. Toxic effects of polyethylene-microplastics on freshwater fish species: implications for human health. *Public Health Toxicology*, 2.

Borah, S. J., Gupta, A. K., Gupta, A., Bhawna, Kumar, S., Sharma, R., Kumar, R., Kumar, P., Dubey, K. K. and Kaushik, S. 2023. Grasping the supremacy of microplastic in the environment to understand its implications and eradication: a review. *Journal of Materials Science*, 58: 12899-12928.

Borrelle, S. B., Ringma, J., Law, K. L., Monnahan, C. C., Lebreton, L., McGivern, A., Murphy, E., Jambeck, J., Leonard, G. H. and Hilleary, M. A. 2020. Predicted growth in plastic waste exceeds efforts to mitigate plastic pollution. *Science*, 369: 1515-1518.

Bottero, J. Y., Rose, J. and Wiesner, M. R. 2006. Nanotechnologies: tools for sustainability in a new wave of water treatment processes. *Integrated Environmental Assessment and Management: an International Journal*, 2: 391-395.

Bouafia, A. and Laouini, S. E. 2021. Plant-mediated synthesis of iron oxide nanoparticles and evaluation of the antimicrobial activity: a review. *Mini-Reviews in Organic Chemistry*, 18: 725-734.

Bouafia, A., Laouini, S. E., Khelef, A., Tedjani, M. L. and Guemari, F. 2021. Effect of ferric chloride concentration on the type of magnetite (Fe3O4) nanoparticles biosynthesized by aqueous leaves extract of artemisia and assessment of their antioxidant activities. *Journal of Cluster Science*, 32: 1033-1041.

Bouafia, A., Laouini, S. E. and Ouahrani, M. R. 2020. A review on green synthesis of CuO nanoparticles using plant extract and evaluation of antimicrobial activity. *Asian Journal of Research in Chemistry*, 13: 65-70.

Boucher, J. and Friot, D. 2017. *Primary microplastics in the oceans: a global evaluation of sources*. Iucn Gland, Switzerland.

Bowmer, T. and Kershaw, P. 2010. *Proceedings of the GESAMP International Workshop on Microplastic Particles as a Vector in Transporting Persistent, Bio-accumulating and Toxic Substances in the Ocean, 28-30th June 2010, UNESCO-IOC, Paris*. GESAMP.

Bu, X., Li, J., Wang, J., Li, Y. and Zhang, G. 2024. Boosting charge transfer promotes photocatalytic peroxymonosulfate activation of S-doped CuBi2O4 nanorods for ciprofloxacin degradation: Key role of Ov–Cu–S and mechanism insight. *Chemical Engineering Journal*, Article ID: 153075.

Bui, X.-T., Nguyen, P.-T., Nguyen, V.-T., Dao, T.-S. and Nguyen, P.-D. 2020. Microplastics pollution in wastewater: Characteristics, occurrence and removal technologies. *Environmental Technology & Innovation*, 19: 101013.

Buzea, C., Pacheco, I. I. and Robbie, K. 2007. Nanomaterials and nanoparticles: sources and toxicity. *Biointerphases*, 2: MR17-MR71.

Bystrzejewska-Piotrowska, G., Asztemborska, M., Stęborowski, R., Polkowska-Motrenko, H., Danko, B. and Ryniewicz, J. 2012. Application of neutron activation for investigation of Fe3O4 nanoparticles accumulation by plants. *Nukleonika*, 57: 427-430.

Campos, A. F. C., Medeiros, W. C. d., Aquino, R. and Depeyrot, J. 2017. Surface charge density determination in water based magnetic colloids: a comparative study. *Materials Research*, 20: 1729-1734.

Canizares, P., Paz, R., Sáez, C. and Rodrigo, M. A. 2009. Costs of the electrochemical oxidation of wastewaters: a comparison with ozonation and Fenton oxidation processes. *Journal of Environmental Management*, 90: 410-420.

Cao, X.-q., Shang, M.-y., Shang, Y.-n., Wu, D., Xia, C., Zhang, Y.-z., Zhang, Y. and Kan, Y.-j. 2024a. Electrocatalytic degradation of ofloxacin by self-doped copper/carbon cathode materials derived from waste printed circuit boards. *Journal of Water Process Engineering*, 64: 105668.

Cao, Z., Meng, Y., Liu, Y. and Shang, S. 2024b. Green degradation of ofloxacin in electric Fenton based on Fe3+/Fe2+ internal cycling within Fe3O4 under neutral condition. *Journal of Environmental Chemical Engineering*, Article ID: 113280.

Carlin, J., Craig, C., Little, S., Donnelly, M., Fox, D., Zhai, L. and Walters, L. 2020. Microplastic accumulation in the gastrointestinal tracts in birds of prey in central Florida, USA. *Environmental Pollution*, 264: 114633.

Carr, S. A., Liu, J. and Tesoro, A. G. 2016. Transport and fate of microplastic particles in wastewater treatment plants. *Water research*, 91: 174-182.

Chang, M. 2015. Reducing microplastics from facial exfoliating cleansers in wastewater through treatment versus consumer product decisions. *Marine pollution bulletin*, 101: 330-333.

Chellasamy, G., Kiriyanthan, R. M., Maharajan, T., Radha, A. and Yun, K. 2022. Remediation of microplastics using bionanomaterials: A review. *Environmental Research*, Article ID: 112724.

Chen, J., Tan, M., Nemmar, A., Song, W., Dong, M., Zhang, G. and Li, Y. 2006. Quantification of extrapulmonary translocation of intratracheal-instilled particles in vivo in rats: effect of lipopolysaccharide. *Toxicology*, 222: 195-201.

Chen, S., Yang, Q., Wang, H., Zhang, S., Li, J., Wang, Y., Chu, W., Ye, Q. and Song, L. 2015. Initial reaction mechanism of platinum nanoparticle in methanol–water system and the anomalous catalytic effect of water. *Nano letters*, 15: 5961-5968.

Chen, Y.-J., Chen, Y., Miao, C., Wang, Y.-R., Gao, G.-K., Yang, R.-X., Zhu, H.-J., Wang, J.-H., Li, S.-L. and Lan, Y.-Q. 2020. Metal–organic framework-based foams for efficient microplastics removal. *Journal of Materials Chemistry A*, 8: 14644-14652.

Chen, Y., Ouyang, L., Liu, N., Li, F., Li, P., Sun, M., Qin, H., Li, Y., Xiang, X. and Wu, L. 2022a. pH-responsive magnetic artificial melanin with tunable aggregation-induced stronger magnetism for rapid remediation of plastic fragments. *Journal of Hazardous Materials*, 435: 128962.

Chen, Z., Li, Y., Cai, Y., Wang, S., Hu, B., Li, B., Ding, X., Zhuang, L. and Wang, X. 2023. Application of covalent organic frameworks and metal–organic frameworks nanomaterials in organic/inorganic pollutants removal from solutions through sorption-catalysis strategies. *Carbon Research*, 2: 8.

Chen, Z., Yang, L., Luo, X., Xie, D., Zhao, C., Qiu, R. and Huang, Z. 2022b. Electrochemical degradation of doxycycline in a three-dimensional vermiculite/peroxymonosulfate electrode system: Mechanism, kinetics, and degradation pathway. *Separation and Purification Technology*, 296: 121402.

Chouhan, R. S., Gačnik, J., Živković, I., Nair, S. V., Van de Velde, N., Vesel, A., Šket, P., Gandhi, S., Jerman, I. and Horvat, M. 2023. Green synthesis of a magnetite/graphitic carbon nitride 2D nanocomposite for efficient Hg 2+ remediation. *Environmental Science: Nano*, 10: 2658-2671.

Clogston, J. D. and Vermilya, A. 2005. Measuring Zeta Potential of Nanoparticles: Version 1.2. *National Cancer Institute's Nanotechnology Characterization Laboratory Assay Cascade Protocols [Internet]*, Article ID.

Cole, M., Lindeque, P., Halsband, C. and Galloway, T. S. 2011. Microplastics as contaminants in the marine environment: a review. *Marine pollution bulletin*, 62: 2588-2597.

Corradini, F., Meza, P., Eguiluz, R., Casado, F., Huerta-Lwanga, E. and Geissen, V. 2019. Evidence of microplastic accumulation in agricultural soils from sewage sludge disposal. *Science of the total environment*, 671: 411-420.

Dai, J., Feng, H., Shi, K., Ma, X., Yan, Y., Ye, L. and Xia, Y. 2022. Electrochemical degradation of antibiotic enoxacin using a novel PbO2 electrode with a graphene nanoplatelets inter-layer: characteristics, efficiency and mechanism. *Chemosphere*, 307: 135833.

Dawn, R., Zzaman, M., Faizal, F., Kiran, C., Kumari, A., Shahid, R., Panatarani, C., Joni, I., Verma, V. and Sahoo, S. 2022. Origin of magnetization in silica-coated Fe3O4 nanoparticles revealed by soft X-ray magnetic circular dichroism. *Brazilian Journal of Physics*, 52: 99.

Decker, A. and Graber, E. M. 2012. Over-the-counter acne treatments: a review. *The Journal of clinical and aesthetic dermatology*, 5: 32.

Dee, G., O'Donoghue, O., Rafferty, A., Gannon, L., McGuinness, C. and Gun'ko, Y. K. 2023. Boron Nitride Nanosheets Functionalized with Fe3O4 and CoFe2O4 Magnetic Nanoparticles for Nanofiltration Applications. *ACS Applied Nano Materials*, 6: 12526-12536.

Diao, Z.-H., Huang, S.-T., Chen, X., Zou, M.-Y., Liu, H., Guo, P.-R., Kong, L.-J. and Chu, W. 2022. Peroxymonosulfate-assisted photocatalytic degradation of antibiotic norfloxacin by a calcium-based Ag3PO4 composite in water: Reactivity, products and mechanism. *Journal of Cleaner Production*, 330: 129806.

Dodson, G. Z., Shotorban, A. K., Hatcher, P. G., Waggoner, D. C., Ghosal, S. and Noffke, N. 2020. Microplastic fragment and fiber contamination of beach sediments from selected sites in Virginia and North Carolina, USA. *Marine Pollution Bulletin*, 151: 110869.

Domínguez-Jaimes, L. P., Cedillo-González, E. I., Luévano-Hipólito, E., Acuña-Bedoya, J. D. and Hernández-López, J. M. 2021. Degradation of primary nanoplastics by photocatalysis using different anodized TiO2 structures. *Journal of Hazardous Materials*, 413: 125452.

Dris, R., Gasperi, J., Rocher, V., Saad, M., Renault, N. and Tassin, B. 2015. Microplastic contamination in an urban area: a case study in Greater Paris. *Environmental Chemistry*, 12: 592-599.

Du, Y., Fan, H., Wang, L., Wang, J., Wu, J. and Dai, H. 2013. α-Fe 2 O 3 nanowires deposited diatomite: highly efficient absorbents for the removal of arsenic. *Journal of materials chemistry A*, 1: 7729-7737.

Du, Z.-D., Cui, Y.-Y., Yang, C.-X. and Yan, X.-P. 2020. Synthesis of magnetic amino-functionalized microporous organic network composites for magnetic solid phase extraction of endocrine disrupting chemicals from water, beverage bottle and juice samples. *Talanta*, 206: 120179.

Ebnesajjad, S. 2011. Surface and material characterization techniques. In: *Handbook of adhesives and surface preparation*. Elsevier, 31-48.

ECONOMY, A. C. 2024. MOBILIZING FEDERAL ACTION ON PLASTIC POLLUTION: PROGRESS, PRINCIPLES, AND PRIORITIES. Article ID.

Eerkes-Medrano, D., Leslie, H. A. and Quinn, B. 2019. Microplastics in drinking water: A review and assessment. *Current Opinion in Environmental Science & Health*, 7: 69-75.

Egirani, D., Latif, M. T., Wessey, N., Poyi, N. R. and Shehata, N. 2021. Preparation and characterization of powdered and granular activated carbon from Palmae biomass for mercury removal. *Applied Water Science*, 11: 1-11.

Eid, M. M. 2022. Characterization of Nanoparticles by FTIR and FTIR-Microscopy. In: *Handbook of Consumer Nanoproducts*. Springer, 1-30.

El-Azazy, M., Nabil, I., Hassan, S. S. and El-Shafie, A. S. 2021. Adsorption characteristics of pristine and magnetic olive stones biochar with respect to clofazimine. *Nanomaterials*, 11: 963.

El-Temsah, Y. S. and Joner, E. J. 2012. Impact of Fe and Ag nanoparticles on seed germination and differences in bioavailability during exposure in aqueous suspension and soil. *Environmental toxicology*, 27: 42-49.

Elmacı, G. 2020. Microwave-assisted rapid synthesis of C@ Fe3O4 composite for removal of microplastics from drinking water. *Adıyaman University Journal of Science*, 10: 207-217.

Fadare, O. O., Okoffo, E. D. and Olasehinde, E. F. 2021. Microparticles and microplastics contamination in African table salts. *Marine pollution bulletin*, 164: 112006.

Fadeel, B. and Garcia-Bennett, A. E. 2010. Better safe than sorry: Understanding the toxicological properties of inorganic nanoparticles manufactured for biomedical applications. *Advanced drug delivery reviews*, 62: 362-374.

Farissi, S., Zakkariya, S., Akhilghosh, K. A., Prasanthi, T., Muthukumar, A. and Muthuchamy, M. 2023. Electrooxidation of amoxicillin in aqueous solution with graphite electrodes: Optimization of degradation and deciphering of byproducts using HRMS. *Chemosphere*, 345: 140415.

Feijoo, S., Kamali, M., Pham, Q.-K., Assoumani, A., Lestremau, F., Cabooter, D. and Dewil, R. 2022. Electrochemical Advanced Oxidation of Carbamazepine: Mechanism and optimal operating conditions. *Chemical Engineering Journal*, 446: 137114.

Fekri Aval, S., Akbarzadeh, A., Yamchi, M. R., Zarghami, F., Nejati-Koshki, K. and Zarghami, N. 2016. Gene silencing effect of SiRNA-magnetic modified with biodegradable copolymer nanoparticles on hTERT gene expression in lung cancer cell line. *Artificial cells, nanomedicine, and biotechnology*, 44: 188-193.

Felisardo, R. J. A., Brillas, E., Cavalcanti, E. B. and Garcia-Segura, S. 2024. Revealing degradation of organic constituents of urine during the electrochemical oxidation of ciprofloxacin via boron-doped diamond anode. *Separation and Purification Technology*, 331: 125655.

Ferraris, S., Cazzola, M., Peretti, V., Stella, B. and Spriano, S. 2018. Zeta potential measurements on solid surfaces for in vitro biomaterials testing: surface charge, reactivity upon contact with fluids and protein absorption. *Frontiers in bioengineering and biotechnology*, 6: 60.

Fuller, S. and Gautam, A. 2016. A procedure for measuring microplastics using pressurized fluid extraction. *Environmental science & technology*, 50: 5774-5780.

GadelHak, Y., El-Azazy, M., Shibl, M. F. and Mahmoud, R. K. 2023. Cost estimation of synthesis and utilization of nano-adsorbents on the laboratory and industrial scales: A detailed review. *Science of The Total Environment*, 875: 162629.

Gao, M., Chang, J., Wang, Z., Zhang, H. and Wang, T. 2023. Advances in transport and toxicity of nanoparticles in plants. *Journal of Nanobiotechnology*, 21: 75.

Gautam, R., Jo, J., Acharya, M., Maharjan, A., Lee, D., Kc, P. B., Kim, C., Kim, K., Kim, H. and Heo, Y. 2022. Evaluation of potential toxicity of polyethylene microplastics on human derived cell lines. *Science of the Total Environment*, 838: 156089.

Gies, E. A., LeNoble, J. L., Noël, M., Etemadifar, A., Bishay, F., Hall, E. R. and Ross, P. S. 2018. Retention of microplastics in a major secondary wastewater treatment plant in Vancouver, Canada. *Marine Pollution Bulletin*, 133: 553-561.

Gkatzioura, A., Zafirakou, A. and Zorpas, A. A. 2021. Wastewater treatment plants' contribution in microplastics' contamination of surface water. Effluent concentration and detection techniques review. *DESALINATION AND WATER TREATMENT*, 227: 26-33.

Goel, H., Saini, K., Razdan, K., Khurana, R. K., Elkordy, A. A. and Singh, K. K. 2022. In vitro physicochemical characterization of nanocarriers: a road to optimization. In: *Nanoparticle Therapeutics*. Elsevier, 133-179.

Goh, P., Kang, H., Ismail, A., Khor, W., Quen, L. and Higgins, D. 2022. Nanomaterials for microplastic remediation from aquatic environment: Why nano matters? *Chemosphere*, Article ID: 134418.

Gong, J. and Xie, P. 2020. Research progress in sources, analytical methods, eco-environmental effects, and control measures of microplastics. *Chemosphere*, 254: 126790.

González, T., Dominguez, J., Cuerda-Correa, E., Correia, S. and Donoso, G. 2020. Selecting and improving activated homogeneous catalytic processes for pollutant removal. Kinetics, mineralization and optimization. *Journal of environmental management*, 256: 109972.

Goodman, K. E., Hua, T. and Sang, Q.-X. A. 2022. Effects of polystyrene microplastics on human kidney and liver cell morphology, cellular proliferation, and metabolism. *ACS omega*, 7: 34136-34153.

Gosu, V., Sikarwar, P. and Subbaramaiah, V. 2018. Mineralization of pyridine by CWPO process using nFe0/GAC catalyst. *Journal of Environmental Chemical Engineering*, 6: 1000-1007.

Goyal, A. and Srivastava, V. C. 2017. Treatment of highly acidic wastewater containing high energetic compounds using dimensionally stable anode. *Chemical Engineering Journal*, 325: 289-299.

Grbic, J., Nguyen, B., Guo, E., You, J. B., Sinton, D. and Rochman, C. M. 2019. Magnetic extraction of microplastics from environmental samples. *Environmental Science & Technology Letters*, 6: 68-72.

Grusho, A., Zabezhailo, M., Zatsarinnyi, A. and Piskovskii, V. 2017. On some artificial intelligence methods and technologies for cloud-computing protection. *Automatic Documentation and Mathematical Linguistics*, 51: 62-74.

Gündoğdu, S., Çevik, C., Güzel, E. and Kilercioğlu, S. 2018. Microplastics in municipal wastewater treatment plants in Turkey: a comparison of the influent and secondary effluent concentrations. *Environmental Monitoring and Assessment*, 190: 1-10.

Hage, D. S. 2013. Reference module in chemistry, molecular sciences and chemical engineering. In: Proceedings of *Elsevier Inc.*

Hairom, N. H. H., Soon, C. F., Mohamed, R. M. S. R., Morsin, M., Zainal, N., Nayan, N., Zulkifli, C. Z. and Harun, N. H. 2021. A review of nanotechnological applications to detect and control surface water pollution. *Environmental Technology & Innovation*, 24: 102032.

Hammouda, S. B., Zhao, F., Safaei, Z., Srivastava, V., Ramasamy, D. L., Iftekhar, S. and Sillanpää, M. 2017. Degradation and mineralization of phenol in aqueous medium by heterogeneous monopersulfate activation on nanostructured cobalt based-perovskite catalysts ACoO3 (A= La, Ba, Sr and Ce): characterization, kinetics and mechanism study. *Applied Catalysis B: Environmental*, 215: 60-73.

Hanafiah, M. M., Hashim, N. A., Ahmed, S. and Muhammad, A. A. 2018. Removal of chromium from aqueous solutions using a palm kernel shell adsorbent. *Desalination and Water Treatment*, 118: 172-180.

Hao, M., Liu, Y., Wu, W., Wang, S., Yang, X., Chen, Z., Tang, Z., Huang, Q., Wang, S. and Yang, H. 2023. Advanced porous adsorbents for radionuclides elimination. *EnergyChem*, Article ID: 100101.

Hartline, N. L., Bruce, N. J., Karba, S. N., Ruff, E. O., Sonar, S. U. and Holden, P. A. 2016. Microfiber masses recovered from conventional machine washing of new or aged garments. *Environmental science & technology*, 50: 11532-11538.

Hernandez, E., Nowack, B. and Mitrano, D. M. 2017. Polyester textiles as a source of microplastics from households: a mechanistic study to understand microfiber release during washing. *Environmental science & technology*, 51: 7036-7046.

Hidayaturrahman, H. and Lee, T.-G. 2019. A study on characteristics of microplastic in wastewater of South Korea: Identification, quantification, and fate of microplastics during treatment process. *Marine pollution bulletin*, 146: 696-702.

Ho, W.-K. and Leung, K. S.-Y. 2021. The crucial role of heavy metals on the interaction of engineered nanoparticles with polystyrene microplastics. *Water Research*, 201: 117317.

Horiuchi, S., Ishibashi, S. and Tokura, Y. 2022. Hydrogen-bonded organic molecular ferroelectrics/antiferroelectrics. In: *Organic Ferroelectric Materials and Applications*. Elsevier, 47-84.

Horton, A. A., Svendsen, C., Williams, R. J., Spurgeon, D. J. and Lahive, E. 2017a. Large microplastic particles in sediments of tributaries of the River Thames, UK–Abundance, sources and methods for effective quantification. *Marine pollution bulletin*, 114: 218-226.

Horton, A. A., Walton, A., Spurgeon, D. J., Lahive, E. and Svendsen, C. 2017b. Microplastics in freshwater and terrestrial environments: Evaluating the current understanding to identify the knowledge gaps and future research priorities. *Science of the total environment*, 586: 127-141.

Hu, K., Tian, W., Yang, Y., Nie, G., Zhou, P., Wang, Y., Duan, X. and Wang, S. 2021. Microplastics remediation in aqueous systems: Strategies and technologies. *Water Research*, 198: 117144.

Hu, X., Li, D., Gao, Y., Mu, L. and Zhou, Q. 2016. Knowledge gaps between nanotoxicological research and nanomaterial safety. *Environment International*, 94: 8-23.

Hurley, R. R. and Nizzetto, L. 2018. Fate and occurrence of micro (nano) plastics in soils: Knowledge gaps and possible risks. *Current Opinion in Environmental Science & Health*, 1: 6-11.

Indhur, R., Amoah, I., Bux, F. and Kumari, S. 2023. Nanomaterials for Microplastic Removal from Wastewater: Current State of the Art Nanomaterials and Future Prospects. *ACS ES&T Water*, Article ID.

Irfan, M., Qadir, A., Mumtaz, M. and Ahmad, S. R. 2020a. An unintended challenge of microplastic pollution in the urban surface water system of Lahore, Pakistan. *Environmental science and pollution research*, 27: 16718-16730.

Irfan, T., Khalid, S., Taneez, M. and Hashmi, M. Z. 2020b. Plastic driven pollution in Pakistan: the first evidence of environmental exposure to microplastic in sediments and water of Rawal Lake. *Environmental Science and Pollution Research*, 27: 15083-15092.

Islam, M. T., Saenz-Arana, R., Hernandez, C., Guinto, T., Ahsan, M. A., Kim, H., Lin, Y., Alvarado-Tenorio, B. and Noveron, J. C. 2018. Adsorption of methylene blue and tetracycline onto biomass-based material prepared by sulfuric acid reflux. *RSC advances*, 8: 32545-32557.

Iyare, P. U., Ouki, S. K. and Bond, T. 2020. Microplastics removal in wastewater treatment plants: a critical review. *Environmental Science: Water Research & Technology*, 6: 2664-2675.

Jambeck, J. R., Geyer, R., Wilcox, C., Siegler, T. R., Perryman, M., Andrady, A., Narayan, R. and Law, K. L. 2015. Plastic waste inputs from land into the ocean. *Science*, 347: 768-771.

Jamkhande, P. G., Ghule, N. W., Bamer, A. H. and Kalaskar, M. G. 2019. Metal nanoparticles synthesis: An overview on methods of preparation, advantages and disadvantages, and applications. *Journal of drug delivery science and technology*, 53: 101174.

Ji, Y., Zhang, L., He, Y., Gu, J., Zhou, Y., Wei, G., Li, B. and Wei, L. 2024. Efficient degradation of ciprofloxacin by peroxymonosulfate activated using red mud-based ZIF-67 composite as a heterogeneous catalyst. *Separation and Purification Technology*, 337: 126407.

Jiang, H., Li, L., Li, Z. and Chu, X. 2024. Metal-based nanoparticles in antibacterial application in biomedical field: Current development and potential mechanisms. *Biomedical Microdevices*, 26: 12.

Jiang, J.-Q. 2018. Occurrence of microplastics and its pollution in the environment: A review. *Sustainable production and consumption*, 13: 16-23.

Kah, M., Kookana, R. S., Gogos, A. and Bucheli, T. D. 2018. A critical evaluation of nanopesticides and nanofertilizers against their conventional analogues. *Nature nanotechnology*, 13: 677-684.

Kain, G., Doucette, C. and Bossie, R. 2022. Let's Get Serious About It: Plastic-Free Campus Initiative. Article ID.

Kang, J., Zhou, L., Duan, X., Sun, H., Ao, Z. and Wang, S. 2019. Degradation of cosmetic microplastics via functionalized carbon nanosprings. *Matter*, 1: 745-758.

Karapanagioti, H. and Kalavrouziotis, I. 2018. Microplastics in Wastewater Treatment Plants—A totally preventable source. In: Proceedings of *Sixth International Marine Debris Conference (6IMDC) Book of Abstracts. 6IMDC, co-hosted by the National Oceanic and Atmospheric Administration (NOAA) and the United Nations Environment (UN Environment) in San Diego, California*. 12-16.

Kazour, M., Terki, S., Rabhi, K., Jemaa, S., Khalaf, G. and Amara, R. 2019. Sources of microplastics pollution in the marine environment: Importance of wastewater treatment plant and coastal landfill. *Marine Pollution Bulletin*, 146: 608-618.

Kershaw, P., Turra, A. and Galgani, F. 2019. Guidelines for the monitoring and assessment of plastic litter and microplastics in the ocean. Article ID.

Khalil, H. A., Dungani, R., Hossain, M., Suraya, N., Aprilia, S., Astimar, A., Hayawin, Z. N. and Davoudpour, Y. 2015. Mechanical properties of oil palm biocomposites enhanced with micro to nanobiofillers. In: *Biocomposites*. Elsevier, 401-435.

Klein, M. and Fischer, E. K. 2019. Microplastic abundance in atmospheric deposition within the Metropolitan area of Hamburg, Germany. *Science of the Total Environment*, 685: 96-103.

Kokkinos, P., Mantzavinos, D. and Venieri, D. 2020. Current trends in the application of nanomaterials for the removal of emerging micropollutants and pathogens from water. *Molecules*, 25: 2016.

Kolandhasamy, P., Su, L., Li, J., Qu, X., Jabeen, K. and Shi, H. 2018. Adherence of microplastics to soft tissue of mussels: a novel way to uptake microplastics beyond ingestion. *Science of the total environment*, 610: 635-640.

Kolbert, Z., Szőllősi, R., Rónavári, A. and Molnár, Á. 2022. Nanoforms of essential metals: from hormetic phytoeffects to agricultural potential. *Journal of experimental botany*, 73: 1825-1840.

Kole, P. J., Löhr, A. J., Van Belleghem, F. G. and Ragas, A. M. 2017. Wear and tear of tyres: a stealthy source of microplastics in the environment. *International journal of environmental research and public health*, 14: 1265.

Konate, A., Wang, Y., He, X., Adeel, M., Zhang, P., Ma, Y., Ding, Y., Zhang, J., Yang, J. and Kizito, S. 2018. Comparative effects of nano and bulk-Fe3O4 on the growth of cucumber (Cucumis sativus). *Ecotoxicology and environmental safety*, 165: 547-554.

Krystynik, P., Strunakova, K., Syc, M. and Kluson, P. 2021. Notes on Common Misconceptions in Microplastics Removal from Water. *Applied Sciences*, 11: 5833.

Kumar, A., Omar, R. A. and Verma, N. 2020a. Efficient electro-oxidation of diclofenac persistent organic pollutant in wastewater using carbon film-supported Cu-rGO electrode. *Chemosphere*, 248: 126030.

Kumar, A. and Prasad, B. 2020. Catalytic peroxidation of acrylonitrile aqueous solution by Ni-doped CeO2 catalysts: characterization, kinetics and thermodynamics. *International journal of environmental science and technology*, 17: 1809-1824.

Kumar, A., Prasad, B. and Garg, K. K. 2020b. Catalytic peroxidation of acrylic acid from aqueous solution incorporated with highly active La 0.5 Sr 0.5 BO 3 (B= Cu, Fe and Ni) perovskite-like catalysts. *Journal of Environmental Health Science and Engineering*, 18: 897-913.

Kumar, A., Prasad, B. and Garg, K. K. 2021a. Enhanced catalytic activity of series LaCuxFe1-xO3 (x= 0.2, 0.4, 0.6, 0.8) perovskite-like catalyst for the treatment of highly toxic ABS resin wastewater: Phytotoxicity study, parameter optimization and reaction pathways. *Process Safety and Environmental Protection*, 147: 162-180.

Kumar, A., Prasad, B., Kumari, S. and Bux, F. 2023a. Mechanistic insight into SO4•−/• OH radical for enhancing stability and activity of LaMO3 perovskite toward detoxification of bulk pharmaceutical wastewater: Stoichiometric efficiency and controlled leaching study. *Separation and Purification Technology*, 319: 123967.

Kumar, A., Prasad, B., Sandhwar, V. K. and Garg, K. K. 2021b. Mechanistic insight into heterogeneous Fenton-like catalysis with M-Al2O3/SiO2 (M= Fe, Co and Ni) for acrylonitrile mineralization from real ABS resin wastewater: Optimization and toxicity assessment. *Journal of Environmental Chemical Engineering*, 9: 105177.

Kumar, A., Sheik, A. G., Prasad, B., Kumari, S. and Bux, F. 2023b. Ultrasound-induced PMS activation for acrylonitrile degradation with series LTZ perovskite-like catalysts: Synergistic and mechanistic insight. *Journal of Environmental Chemical Engineering*, 11: 111246.

Kumar, M., Chen, H., Sarsaiya, S., Qin, S., Liu, H., Awasthi, M. K., Kumar, S., Singh, L., Zhang, Z. and Bolan, N. S. 2021c. Current research trends on micro-and nano-plastics as an emerging threat to global environment: a review. *Journal of Hazardous Materials*, 409: 124967.

Kumari, M., Pittman Jr, C. U. and Mohan, D. 2015. Heavy metals [chromium (VI) and lead (II)] removal from water using mesoporous magnetite (Fe3O4) nanospheres. *Journal of colloid and interface science*, 442: 120-132.

Kunduru, K. R., Nazarkovsky, M., Farah, S., Pawar, R. P., Basu, A. and Domb, A. J. 2017. Nanotechnology for water purification: applications of nanotechnology methods in wastewater treatment. *Water purification*, Article ID: 33-74.

Lagarde, F., Olivier, O., Zanella, M., Daniel, P., Hiard, S. and Caruso, A. 2016. Microplastic interactions with freshwater microalgae: hetero-aggregation and changes in plastic density appear strongly dependent on polymer type. *Environmental pollution*, 215: 331-339.

Lamichhane, G., Acharya, A., Marahatha, R., Modi, B., Paudel, R., Adhikari, A., Raut, B., Aryal, S. and Parajuli, N. 2023. Microplastics in environment: global concern, challenges, and controlling measures. *International Journal of Environmental Science and Technology*, 20: 4673-4694.

Lares, M., Ncibi, M. C., Sillanpää, M. and Sillanpää, M. 2018. Occurrence, identification and removal of microplastic particles and fibers in conventional activated sludge process and advanced MBR technology. *Water research*, 133: 236-246.

Lee, C. W., Mahendra, S., Zodrow, K., Li, D., Tsai, Y. C., Braam, J. and Alvarez, P. J. 2010. Developmental phytotoxicity of metal oxide nanoparticles to Arabidopsis thaliana. *Environmental Toxicology and Chemistry: An International Journal*, 29: 669-675.

Lee, S., Cha, E. J., Park, K., Lee, S. Y., Hong, J. K., Sun, I. C., Kim, S. Y., Choi, K., Kwon, I. C. and Kim, K. 2008. A near-infrared-fluorescence-quenched gold-nanoparticle imaging probe for in vivo drug screening and protease activity determination. *Angewandte Chemie International Edition*, 47: 2804-2807.

Lei, W., Liu, D. and Chen, Y. 2015. Highly crumpled boron nitride nanosheets as adsorbents: scalable solvent-less production. *Advanced Materials Interfaces*, 2: 1400529.

Li, D., Ji, J., Yuan, Y. and Wang, D. 2020a. Toxicity comparison of nanopolystyrene with three metal oxide nanoparticles in nematode Caenorhabditis elegans. *Chemosphere*, 245: 125625.

Li, H., Li, N., Xu, C., Huang, J., Du, J., Li, F., Lyu, S. and Xu, S. 2025. Highly efficient activation of peroxymonosulfate by MOF derived CoS2@ C for degradation of ciprofloxacin. *Separation and Purification Technology*, 352: 128275.

Li, J., Jiang, X., Guan, H., Liu, Z., Li, J., Lin, Z., Li, F. and Xu, W. 2023. Visible-light-driven peroxymonosulfate activation by robust TiO2-base nanoparticles for efficient removal of sulfamethoxazole. *Environmental Pollution*, 334: 122150.

Li, J., Lin, J., Xu, X., Zhang, X., Xue, Y., Mi, J., Mo, Z., Fan, Y., Hu, L. and Yang, X. J. N. 2013a. Porous boron nitride with a high surface area: hydrogen storage and water treatment. 24: 155603.

Li, J., Xiao, X., Xu, X., Lin, J., Huang, Y., Xue, Y., Jin, P., Zou, J. and Tang, C. 2013b. Activated boron nitride as an effective adsorbent for metal ions and organic pollutants. *Scientific reports*, 3: 1-7.

Li, J., Zuo, K., Wu, W., Xu, Z., Yi, Y., Jing, Y., Dai, H. and Fang, G. 2018a. Shape memory aerogels from nanocellulose and polyethyleneimine as a novel adsorbent for removal of Cu (II) and Pb (II). *Carbohydrate Polymers*, 196: 376-384.

Li, L., Liu, D., Song, K. and Zhou, Y. 2020b. Performance evaluation of MBR in treating microplastics polyvinylchloride contaminated polluted surface water. *Marine pollution bulletin*, 150: 110724.

Li, L., Wang, Z., Gu, Y., Zhao, Y., Sun, P., Meng, F. and Lyu, G. 2024. Uniformly deposition of iron phosphide quantum dots on the microscopic spongy B-C3N4 and its efficient degradation of ciprofloxacin by photo-self-Fenton process. *Colloids and Surfaces A: Physicochemical and Engineering Aspects*, 699: 134627.

Li, N., Wu, X., Zhuang, W., Xia, L., Chen, Y., Wu, C., Rao, Z., Du, L., Zhao, R. and Yi, M. 2020c. Fish consumption and multiple health outcomes: Umbrella review. *Trends in Food Science & Technology*, 99: 273-283.

Li, P., Zou, X., Wang, X., Su, M., Chen, C., Sun, X. and Zhang, H. 2020d. A preliminary study of the interactions between microplastics and citrate-coated silver nanoparticles in aquatic environments. *Journal of hazardous materials*, 385: 121601.

Li, X., He, E., Xia, B., Van Gestel, C. A., Peijnenburg, W. J., Cao, X. and Qiu, H. 2020e. Impact of CeO2 nanoparticles on the aggregation kinetics and stability of polystyrene nanoplastics: Importance of surface functionalization and solution chemistry. *Water Research*, 186: 116324.

Li, X., Schirmer, K., Bernard, L., Sigg, L., Pillai, S. and Behra, R. 2015. Silver nanoparticle toxicity and association with the alga Euglena gracilis. *Environmental Science: Nano*, 2: 594-602.

Li, X., Zhang, D., Sheng, F. and Qing, H. 2018b. Adsorption characteristics of Copper (II), Zinc (II) and Mercury (II) by four kinds of immobilized fungi residues. *Ecotoxicology and environmental safety*, 147: 357-366.

Li, Z., Cheng, X., Liu, Y., Liu, H., Jiang, Y. and Wang, N. 2022. Intumescent flame retardancy and smoke suppression of Eucommia ulmoides gum/natural rubber blends based on synergistic gC 3 N 4@ Fe 3 O 4 nanocomposites. *RSC advances*, 12: 21704-21712.

Liang, J., Chen, K., Duan, X., Zhao, L., Qiu, H., Xu, X. and Cao, X. 2022. pH-dependent generation of radical and nonradical species for sulfamethoxazole degradation in different carbon/persulfate systems. *Water Research*, 224: 119113.

Lin, H., Liu, Y., Deng, J., Xie, S., Zhao, X., Yang, J., Zhang, K., Han, Z. and Dai, H. 2017. Graphitic carbon nitride-supported iron oxides: High-performance photocatalysts for the visible-light-driven degradation of 4-nitrophenol. *Journal of Photochemistry and Photobiology A: Chemistry*, 336: 105-114.

Lin, T. W., Su, C. Y., Zhang, X. Q., Zhang, W., Lee, Y. H., Chu, C. W., Lin, H. Y., Chang, M. T., Chen, F. R. and Li, L. J. 2012. Converting graphene oxide monolayers into boron carbonitride nanosheets by substitutional doping. *Small*, 8: 1384-1391.

Liu, F., Yu, J., Ji, X. and Qian, M. 2015. Nanosheet-structured boron nitride spheres with a versatile adsorption capacity for water cleaning. *ACS Applied Materials & Interfaces*, 7: 1824-1832.

Liu, H., Yin, J., Zhang, J., Ran, H., Lv, N., Jiang, W., Li, H., Zhu, W. and Li, H. 2022. Ag atom anchored on defective hexagonal boron nitride nanosheets as single atom adsorbents for enhanced adsorptive desulfurization via S-Ag bonds. *Nanomaterials*, 12: 2046.

Liu, H., Zhou, X., Ding, W., Zhang, Z., Nghiem, L. D., Sun, J. and Wang, Q. 2019a. Do microplastics affect biological wastewater treatment performance? Implications from bacterial activity experiments. *ACS Sustainable Chemistry & Engineering*, 7: 20097-20101.

Liu, K., Wang, X., Fang, T., Xu, P., Zhu, L. and Li, D. 2019b. Source and potential risk assessment of suspended atmospheric microplastics in Shanghai. *Science of the total environment*, 675: 462-471.

Liu, Q., Li, P., Zhao, W., Cai, W., Yu, S. and Leung, V. C. 2018. A survey on security threats and defensive techniques of machine learning: A data driven view. *IEEE access*, 6: 12103-12117.

Lu, Y., Zhang, Y., Deng, Y., Jiang, W., Zhao, Y., Geng, J., Ding, L. and Ren, H. 2016. Uptake and accumulation of polystyrene microplastics in zebrafish (Danio rerio) and toxic effects in liver. *Environmental science & technology*, 50: 4054-4060.

Lunge, S., Singh, S. and Sinha, A. 2014. Magnetic iron oxide (Fe3O4) nanoparticles from tea waste for arsenic removal. *Journal of Magnetism and Magnetic Materials*, 356: 21-31.

Luo, W., Su, L., Craig, N. J., Du, F., Wu, C. and Shi, H. 2019. Comparison of microplastic pollution in different water bodies from urban creeks to coastal waters. *Environmental pollution*, 246: 174-182.

Mahmoud, A. S., Mohamed, N. Y., Mostafa, M. K. and Mahmoud, M. S. 2021. Effective chromium adsorption from aqueous solutions and tannery wastewater using bimetallic Fe/Cu nanoparticles: response surface methodology and artificial neural network. *Air, Soil and Water Research*, 14: 11786221211028162.

Makabenta, J. M. V., Nabawy, A., Li, C.-H., Schmidt-Malan, S., Patel, R. and Rotello, V. M. 2021. Nanomaterial-based therapeutics for antibiotic-resistant bacterial infections. *Nature Reviews Microbiology*, 19: 23-36.

March, S. R. 2014. Superparamagnetic nanoparticles and the separation problem. Article ID.

Mathur, J., Goswami, P., Gupta, A., Srivastava, S., Minkina, T., Shan, S. and D. Rajput, V. 2022. Nanomaterials for water remediation: an efficient strategy for prevention of metal (loid) hazard. *Water*, 14: 3998.

Matsoso, B. J., Ranganathan, K., Mutuma, B. K., Lerotholi, T., Jones, G. and Coville, N. J. 2017. Synthesis and characterization of boron carbon oxynitride films with tunable composition using methane, boric acid and ammonia. *New Journal of Chemistry*, 41: 9497-9504.

Mazhar, S., Ditta, A., Bulgariu, L., Ahmad, I., Ahmed, M. and Nadiri, A. A. 2019. Sequential treatment of paper and pulp industrial wastewater: Prediction of water quality parameters by Mamdani Fuzzy Logic model and phytotoxicity assessment. *Chemosphere*, 227: 256-268.

Menéndez-Pedriza, A. and Jaumot, J. 2020. Interaction of environmental pollutants with microplastics: a critical review of sorption factors, bioaccumulation and ecotoxicological effects. *Toxics*, 8: 40.

Mészáros, E., Bodor, A., Kovács, E., Papp, S., Kovács, K., Perei, K. and Feigl, G. 2023. Impacts of plastics on plant development: recent advances and future research directions. *Plants*, 12: 3282.

Mironyuk, I., Tatarchuk, T., Naushad, M., Vasylyeva, H. and Mykytyn, I. 2019. Highly efficient adsorption of strontium ions by carbonated mesoporous TiO2. *Journal of Molecular Liquids*, 285: 742-753.

Misra, A., Zambrzycki, C., Kloker, G., Kotyrba, A., Anjass, M. H., Franco Castillo, I., Mitchell, S. G., Güttel, R. and Streb, C. 2020. Water purification and microplastics removal using magnetic polyoxometalate-supported ionic liquid phases (magPOM-SILPs). *Angewandte Chemie International Edition*, 59: 1601-1605.

Mohamed, A. A., Fouda, A., Abdel-Rahman, M. A., Hassan, S. E.-D., El-Gamal, M. S., Salem, S. S. and Shaheen, T. I. 2019. Fungal strain impacts the shape, bioactivity and multifunctional properties of green synthesized zinc oxide nanoparticles. *Biocatalysis and Agricultural Biotechnology*, 19: 101103.

Mohrazi, A. and Ghasemi-Fasaei, R. 2023. Removal of methylene blue dye from aqueous solution using an efficient chitosan-pectin bio-adsorbent: Kinetics and isotherm studies. *Environmental monitoring and assessment*, 195: 339.

Moma, J. and Baloyi, J. 2019. Modified titanium dioxide for photocatalytic applications. *Photocatalysts-Applications and Attributes*, 18: 10-5772.

Mousavi, M. and Habibi-Yangjeh, A. 2016. Magnetically separable ternary g-C3N4/Fe3O4/BiOI nanocomposites: novel visible-light-driven photocatalysts based on graphitic carbon nitride. *Journal of colloid and interface science*, 465: 83-92.

Mousavi, M. and Habibi-Yangjeh, A. 2018a. Decoration of Fe3O4 and CoWO4 nanoparticles over graphitic carbon nitride: novel visible-light-responsive photocatalysts with exceptional photocatalytic performances. *Materials Research Bulletin*, 105: 159-171.

Mousavi, M. and Habibi-Yangjeh, A. 2018b. Integration of NiWO4 and Fe3O4 with graphitic carbon nitride to fabricate novel magnetically recoverable visible-light-driven photocatalysts. *Journal of materials science*, 53: 9046-9063.

Muzammil, S., Ashraf, A., Siddique, M. H., Aslam, B., Rasul, I., Abbas, R., Afzal, M., Faisal, M. and Hayat, S. 2023. A review on toxicity of nanomaterials in agriculture: Current scenario and future prospects. *Science Progress*, 106: 00368504231221672.

Nabi, I., Ahmad, F. and Zhang, L. 2021. Application of titanium dioxide for the photocatalytic degradation of macro-and micro-plastics: A review. *Journal of Environmental Chemical Engineering*, 9: 105964.

Nagao, D., Osuzu, H., Yamada, A., Mine, E., Kobayashi, Y. and Konno, M. 2004. Particle formation in the hydrolysis of tetraethyl orthosilicate in pH buffer solution. *Journal of colloid and interface science*, 279: 143-149.

Naji, A., Azadkhah, S., Farahani, H., Uddin, S. and Khan, F. R. J. C. 2021. Microplastics in wastewater outlets of Bandar Abbas city (Iran): A potential point source of microplastics into the Persian Gulf. 262: 128039.

Namanga, J., Foba, J., Ndinteh, D. T., Yufanyi, D. M. and Krause, R. W. M. 2013. Synthesis and Magnetic Properties of a Superparamagnetic Nanocomposite "Pectin-Magnetite Nanocomposite". *Journal of Nanomaterials*, 2013: 137275.

Nan, B., Su, L., Kellar, C., Craig, N. J., Keough, M. J. and Pettigrove, V. 2020. Identification of microplastics in surface water and Australian freshwater shrimp Paratya australiensis in Victoria, Australia. *Environmental Pollution*, 259: 113865.

Napper, I. E., Bakir, A., Rowland, S. J. and Thompson, R. C. 2015. Characterisation, quantity and sorptive properties of microplastics extracted from cosmetics. *Marine pollution bulletin*, 99: 178-185.

Nazari, A., Nakhaei, M. and Yari, A. R. 2021. Arsenic adsorption by TiO 2 nanoparticles under conditions similar to groundwater: batch and column studies. *International Journal of Environmental Research*, 15: 79-91.

Nene, A. G., Takahashi, M. and Somani, P. R. 2016. Fe3O4 and Fe nanoparticles by chemical reduction of Fe (acac) 3 by ascorbic acid: role of water. *World Journal of Nano Science and Engineering*, 6: 20-28.

Ngo, P. L., Pramanik, B. K., Shah, K. and Roychand, R. 2019. Pathway, classification and removal efficiency of microplastics in wastewater treatment plants. *Environmental Pollution*, 255: 113326.

Nizzetto, L., Bussi, G., Futter, M. N., Butterfield, D. and Whitehead, P. G. 2016a. A theoretical assessment of microplastic transport in river catchments and their retention by soils and river sediments. *Environmental Science: Processes & Impacts*, 18: 1050-1059.

Nizzetto, L., Futter, M. and Langaas, S. 2016b. *Are agricultural soils dumps for microplastics of urban origin?* : ACS Publications.

Noman, M., Yu, G., Awugichew, D. T. and Li, X. 2024. Synthesis of surficial-modified green biochar catalyst generated by biogas residue biochar and potential application for catalytic ozonation degradation of ciprofloxacin. *Environmental Research*, Article ID: 119314.

Noroozi, R., Gholami, M., Farzadkia, M. and Jonidi Jafari, A. 2022. Degradation of ciprofloxacin by CuFe2O4/GO activated PMS process in aqueous solution: performance, mechanism and degradation pathway. *International Journal of Environmental Analytical Chemistry*, 102: 174-195.

Nozar, S., Hosseini, S. M. P., Chaibakhsh, N. and Amini, M. 2024. Light-assisted catalytic ozonation for efficient degradation of ciprofloxacin using NiO/MoS2 nanocomposite. *Journal of Photochemistry and Photobiology A: Chemistry*, 448: 115343.

Oh, J., Shim, Y., Lee, S., Park, S., Jang, D., Shin, Y., Ohn, S., Kim, J. and Park, S. 2018. Structural insights into photocatalytic performance of carbon nitrides for degradation of organic pollutants. *Journal of Solid State Chemistry*, 258: 559-565.

Osman, A. I., Hosny, M., Eltaweil, A. S., Omar, S., Elgarahy, A. M., Farghali, M., Yap, P.-S., Wu, Y.-S., Nagandran, S. and Batumalaie, K. 2023. Microplastic sources, formation, toxicity and remediation: a review. *Environmental Chemistry Letters*, 21: 2129-2169.

Padmavathy, K., Madhu, G. and Haseena, P. 2016. A study on effects of pH, adsorbent dosage, time, initial concentration and adsorption isotherm study for the removal of hexavalent chromium (Cr (VI)) from wastewater by magnetite nanoparticles. *Procedia Technology*, 24: 585-594.

Palani, G., Arputhalatha, A., Kannan, K., Lakkaboyana, S. K., Hanafiah, M. M., Kumar, V. and Marella, R. K. 2021. Current trends in the application of nanomaterials for the removal of pollutants from industrial wastewater treatment—a review. *Molecules*, 26: 2799.

Palliyarayil, A., Kumar Borah, R. and Vernekar, A. A. 2023. Magnetic Peroxidase Nanozyme Gears Up for Microplastic Removal and Deconstruction. *Chemistry-Methods*, 3: e202300012.

Parvas, M., Haghighi, M. and Allahyari, S. 2019. Catalytic wet air oxidation of phenol over ultrasound-assisted synthesized Ni/CeO2–ZrO2 nanocatalyst used in wastewater treatment. *Arabian Journal of Chemistry*, 12: 1298-1307.

Patidar, R. and Srivastava, V. C. 2021. Mechanistic and kinetic insights of synergistic mineralization of ofloxacin using a sono-photo hybrid process. *Chemical Engineering Journal*, 403: 125736.

Patidar, R. and Srivastava, V. C. 2022. Ultrasound enhanced electro-fenton mineralization of benzophenone: kinetics and mechanistic analysis. *ACS ES&T Water*, 3: 1595-1609.

Paul, M. B., Stock, V., Cara-Carmona, J., Lisicki, E., Shopova, S., Fessard, V., Braeuning, A., Sieg, H. and Böhmert, L. 2020. Micro-and nanoplastics–current state of knowledge with the focus on oral uptake and toxicity. *Nanoscale Advances*, 2: 4350-4367.

Pazos, R. S., Maiztegui, T., Colautti, D. C., Paracampo, A. H. and Gómez, N. 2017. Microplastics in gut contents of coastal freshwater fish from Río de la Plata estuary. *Marine pollution bulletin*, 122: 85-90.

Peixoto, D., Pinheiro, C., Amorim, J., Oliva-Teles, L., Guilhermino, L. and Vieira, M. N. 2019. Microplastic pollution in commercial salt for human consumption: A review. *Estuarine, Coastal and Shelf Science*, 219: 161-168.

Peng, L., Fu, D., Qi, H., Lan, C. Q., Yu, H. and Ge, C. 2020. Micro-and nano-plastics in marine environment: Source, distribution and threats—A review. *Science of the total environment*, 698: 134254.

Perren, W., Wojtasik, A. and Cai, Q. 2018. Removal of microbeads from wastewater using electrocoagulation. *ACS omega*, 3: 3357-3364.

Pfeifer, A. and Skerget, M. 2020. A review: a comparison of different adsorbents for removal of Cr (VI), Cd (II) and Ni (II). *Turkish Journal of Chemistry*, 44: 859-883.

Piehl, S., Leibner, A., Löder, M. G., Dris, R., Bogner, C. and Laforsch, C. 2018. Identification and quantification of macro-and microplastics on an agricultural farmland. *Scientific reports*, 8: 17950.

Pironti, C., Ricciardi, M., Motta, O., Miele, Y., Proto, A. and Montano, L. 2021. Microplastics in the environment: intake through the food web, human exposure and toxicological effects. *Toxics*, 9: 224.

Poerio, T., Piacentini, E. and Mazzei, R. 2019. Membrane processes for microplastic removal. *Molecules*, 24: 4148.

Prasad, C., Murthy, P. K., Krishna, R. H., Rao, R. S., Suneetha, V. and Venkateswarlu, P. 2017. Bio-inspired green synthesis of RGO/Fe3O4 magnetic nanoparticles using Murrayakoenigii leaves extract and its application for removal of Pb (II) from aqueous solution. *Journal of environmental chemical engineering*, 5: 4374-4380.

Prata, J. C., da Costa, J. P., Lopes, I., Duarte, A. C. and Rocha-Santos, T. 2019. Effects of microplastics on microalgae populations: a critical review. *Science of The Total Environment*, 665: 400-405.

Praus, P., Svoboda, L., Ritz, M., Troppová, I., Šihor, M. and Kočí, K. 2017. Graphitic carbon nitride: Synthesis, characterization and photocatalytic decomposition of nitrous oxide. *Materials Chemistry and Physics*, 193: 438-446.

Priyanka and Srivastava, V. C. 2013. Photocatalytic oxidation of dye bearing wastewater by iron doped zinc oxide. *Industrial & Engineering Chemistry Research*, 52: 17790-17799.

Punia, P., Bharti, M. K., Chalia, S., Dhar, R., Ravelo, B., Thakur, P. and Thakur, A. 2021. Recent advances in synthesis, characterization, and applications of nanoparticles for contaminated water treatment-A review. *Ceramics International*, 47: 1526-1550.

Qin, H., Xiao, R. and Chen, J. 2018. Catalytic wet peroxide oxidation of benzoic acid over Fe/AC catalysts: effect of nitrogen and sulfur co-doped activated carbon. *Science of the total environment*, 626: 1414-1420.

Qu, X., Alvarez, P. J. and Li, Q. 2013a. Applications of nanotechnology in water and wastewater treatment. *Water research*, 47: 3931-3946.

Qu, X., Brame, J., Li, Q. and Alvarez, P. J. 2013b. Nanotechnology for a safe and sustainable water supply: enabling integrated water treatment and reuse. *Accounts of chemical research*, 46: 834-843.

Rafique, A., Irfan, M., Mumtaz, M. and Qadir, A. 2020. Spatial distribution of microplastics in soil with context to human activities: a case study from the urban center. *Environmental Monitoring and Assessment*, 192: 1-13.

Ramana, S., Biswas, A., Kundu, S., Saha, J. and Yadava, R. 2002. Effect of distillery effluent on seed germination in some vegetable crops. *Bioresource technology*, 82: 273-275.

Rasheed, T. 2022. Magnetic nanomaterials: Greener and sustainable alternatives for the adsorption of hazardous environmental contaminants. *Journal of Cleaner Production*, 362: 132338.

Ravindran, B., Kumari, S. S., Stenstrom, T. and Bux, F. 2016. Evaluation of phytotoxicity effect on selected crops using treated and untreated wastewater from different configurative domestic wastewater plants. *Environmental technology*, 37: 1782-1789.

Ray, S. S., Gusain, R. and Kumar, N. 2020. *Carbon nanomaterial-based adsorbents for water purification: Fundamentals and applications*. Elsevier.

Ren, H., Bi, Y., Liu, F., Zhang, C., Wei, N., Fan, L. and Zhou, R. 2022. Removal of ofloxacin from wastewater by chloride electrolyte electro-oxidation: Analysis of the role of active chlorine and operating costs. *Science of The Total Environment*, 850: 157963.

Ritchie, H. and Roser, M. 2018. Plastic pollution. *Our world in data*, Article ID.

Rochman, C. M., Tahir, A., Williams, S. L., Baxa, D. V., Lam, R., Miller, J. T., Teh, F.-C., Werorilangi, S. and Teh, S. J. 2015. Anthropogenic debris in seafood: Plastic debris and fibers from textiles in fish and bivalves sold for human consumption. *Scientific reports*, 5: 1-10.

Rosa, E. V., Fascineli, M. L., da Silva, I. C., Rodrigues, M. O., Chaker, J. A., Grisolia, C. K., Moya, S. E., Campos, A. F. and Sousa, M. H. 2021. Carbon nitride nanosheets magnetically decorated with Fe3O4 nanoparticles by homogeneous precipitation: adsorption-photocatalytic performance and acute toxicity assessment. *Environmental Nanotechnology, Monitoring & Management*, 16: 100549.

Rossatto, A., Arlindo, M. Z. F., de Morais, M. S., de Souza, T. D. and Ogrodowski, C. S. 2023. Microplastics in aquatic systems: A review of occurrence, monitoring and potential environmental risks. *Environmental Advances*, Article ID: 100396.

Sacco, N. A., Zoppas, F. M., Devard, A., González Muñoz, M. d. P., García, G. and Marchesini, F. A. 2023. Recent advances in microplastics removal from water with special attention given to photocatalytic degradation: Review of scientific research. *Microplastics*, 2: 278-303.

Sahoo, S. K., Padhiari, S., Biswal, S., Panda, B. and Hota, G. 2020. Fe3O4 nanoparticles functionalized GO/g-C3N4 nanocomposite: an efficient magnetic nanoadsorbent for adsorptive removal of organic pollutants. *Materials Chemistry and Physics*, 244: 122710.

Sahu, O., Gupta, V., Chaudhari, P. and Srivastava, V. C. 2015. Electrochemical treatment of actual sugar industry wastewater using aluminum electrode. *International journal of environmental science and technology*, 12: 3519-3530.

Saleh, T. A. and Gupta, V. K. 2014. Processing methods, characteristics and adsorption behavior of tire derived carbons: a review. *Advances in colloid and interface science*, 211: 93-101.

Santhosh, C., Daneshvar, E., Kollu, P., Peräniemi, S., Grace, A. N. and Bhatnagar, A. 2017. Magnetic SiO2@ CoFe2O4 nanoparticles decorated on graphene oxide as efficient adsorbents for the removal of anionic pollutants from water. *Chemical Engineering Journal*, 322: 472-487.

Sarcletti, M., Park, H., Wirth, J., Englisch, S., Eigen, A., Drobek, D., Vivod, D., Friedrich, B., Tietze, R. and Alexiou, C. 2021. The remediation of nano-/microplastics from water. *Materials Today*, 48: 38-46.

Sarkar, P., Neogi, S. and De, S. 2023. Accelerated radical generation from visible light driven peroxymonosulfate activation by Bi2MoO6/doped gCN S-scheme heterojunction towards Amoxicillin mineralization: Elucidation of the degradation mechanism. *Journal of Hazardous Materials*, 451: 131102.

Scheurer, M. and Bigalke, M. 2018. Microplastics in Swiss floodplain soils. *Environmental science & technology*, 52: 3591-3598.

Schreuders, C., Leparoux, M., Shin, J.-W., Miyazoe, H. and Siegmann, S. 2005. *Quenching design for plasma synthesis of nanoparticles*. na.

Scircle, A., Cizdziel, J. V., Tisinger, L., Anumol, T. and Robey, D. 2020. Occurrence of microplastic pollution at oyster reefs and other coastal sites in the Mississippi sound, USA: impacts of freshwater inflows from flooding. *Toxics*, 8: 35.

Şen, Ö., Emanet, M., Çulha, M. J. F. i. b. and biotechnology. 2018. One-step synthesis of hexagonal boron nitrides, their crystallinity and biodegradation. 6: 83.

Shah, A., Arjunan, A., Baroutaji, A. and Zakharova, J. 2023. A review of physicochemical and biological contaminants in drinking water and their impacts on human health. *Water Science and Engineering*, Article ID.

Shandilya, M., Rai, R. and Singh, J. 2016. Hydrothermal technology for smart materials. *Advances in Applied Ceramics*, 115: 354-376.

Sharma, S., Basu, S., Shetti, N. P., Nadagouda, M. N. and Aminabhavi, T. M. 2021. Microplastics in the environment: occurrence, perils, and eradication. *Chemical Engineering Journal*, 408: 127317.

Shi, W., Han, Y., Sun, S., Tang, Y., Zhou, W., Du, X. and Liu, G. 2020. Immunotoxicities of microplastics and sertraline, alone and in combination, to a bivalve species: size-dependent interaction and potential toxication mechanism. *Journal of hazardous materials*, 396: 122603.

Shi, W., Liu, Y., Sun, W., Hong, Y., Li, X., Lin, X., Guo, F. and Shi, J. 2022a. Improvement of synergistic effect photocatalytic/peroxymonosulfate activation for degradation of amoxicillin using carbon dots anchored on rod-like CoFe2O4. *Chinese Journal of Chemical Engineering*, 52: 136-145.

Shi, W., Wu, N., Zhang, Z., Liu, Y., Chen, J. and Li, J. 2023. A global review on the abundance and threats of microplastics in soils to terrestrial ecosystem and human health. *Science of The Total Environment*, Article ID: 169469.

Shi, X., Zhang, X., Gao, W., Zhang, Y. and He, D. 2022b. Removal of microplastics from water by magnetic nano-Fe3O4. *Science of The Total Environment*, 802: 149838.

Shirsath, D. and Shirivastava, V. 2015. Adsorptive removal of heavy metals by magnetic nanoadsorbent: an equilibrium and thermodynamic study. *Applied Nanoscience*, 5: 927-935.

Sillanpää, M. and Sainio, P. 2017. Release of polyester and cotton fibers from textiles in machine washings. *Environmental Science and Pollution Research*, 24: 19313-19321.

Simmons, J., Nichols, B., Baker, S., Marcus, M. S., Castellini, O., Lee, C.-S., Hamers, R. and Eriksson, M. 2006. Effect of ozone oxidation on single-walled carbon nanotubes. *The journal of physical chemistry B*, 110: 7113-7118.

Singh, A. and Chatterjee, K. 2017. Cloud security issues and challenges: A survey. *Journal of Network and Computer Applications*, 79: 88-115.

Singh, N., Bhagat, J., Tiwari, E., Khandelwal, N., Darbha, G. K. and Shyama, S. 2021a. Metal oxide nanoparticles and polycyclic aromatic hydrocarbons alter nanoplastic's stability and toxicity to zebrafish. *Journal of Hazardous Materials*, 407: 124382.

Singh, N., Khandelwal, N., Ganie, Z. A., Tiwari, E. and Darbha, G. K. 2021b. Eco-friendly magnetic biochar: An effective trap for nanoplastics of varying surface functionality and size in the aqueous environment. *Chemical Engineering Journal*, 418: 129405.

Singh, N., Khandelwal, N., Tiwari, E., Naskar, N., Lahiri, S., Lützenkirchen, J. and Darbha, G. K. 2021c. Interaction of metal oxide nanoparticles with microplastics: impact of weathering under riverine conditions. *Water Research*, 189: 116622.

Singh, P., Ladwani, K., Ladwani, K., Deshbhratar, P. and Ramteke, D. 2013. Impact of paper mill wastewater on soil properties and crop yield through lysimeter studies. *Environmental technology*, 34: 599-606.

Singh, S., Kalyanasundaram, M., Diwan, V. J. W. S. and Technology. 2021d. Removal of microplastics from wastewater: available techniques and way forward. 84: 3689-3704.

Singh, S. and Lo, S.-L. 2017. Catalytic performance of hierarchical metal oxides for per-oxidative degradation of pyridine in aqueous solution. *Chemical Engineering Journal*, 309: 753-765.

Singh, S. and Nalwa, H. S. 2007. Nanotechnology and health safety–toxicity and risk assessments of nanostructured materials on human health. *Journal of nanoscience and nanotechnology*, 7: 3048-3070.

Singh, Z. 2016. Applications and toxicity of graphene family nanomaterials and their composites. *Nanotechnology, science and applications*, Article ID: 15-28.

Sonwani, S., Madaan, S., Arora, J., Suryanarayan, S., Rangra, D., Mongia, N., Vats, T. and Saxena, P. 2021. Inhalation exposure to atmospheric nanoparticles and its associated impacts on human health: a review. *Frontiers in Sustainable Cities*, 3: 690444.

Strady, E., Dang, T. H., Dao, T. D., Dinh, H. N., Do, T. T. D., Duong, T. N., Duong, T. T., Hoang, D. A., Kieu-Le, T. C. and Le, T. P. Q. 2021. Baseline assessment of microplastic concentrations in marine and freshwater environments of a developing Southeast Asian country, Viet Nam. *Marine Pollution Bulletin*, 162: 111870.

Strungaru, S.-A., Jijie, R., Nicoara, M., Plavan, G. and Faggio, C. 2019. Micro-(nano) plastics in freshwater ecosystems: abundance, toxicological impact and quantification methodology. *TrAC trends in analytical chemistry*, 110: 116-128.

Su, L., Xue, Y., Li, L., Yang, D., Kolandhasamy, P., Li, D. and Shi, H. 2016. Microplastics in taihu lake, China. *Environmental Pollution*, 216: 711-719.

Subbaramaiah, V., Srivastava, V. C. and Mall, I. D. 2013. Catalytic wet peroxidation of pyridine bearing wastewater by cerium supported SBA-15. *Journal of Hazardous Materials*, 248: 355-363.

Sun, C., Wang, Z., Zheng, H., Chen, L. and Li, F. 2021. Biodegradable and re-usable sponge materials made from chitin for efficient removal of microplastics. *Journal of Hazardous Materials*, 420: 126599.

Sun, J., Dai, X., Wang, Q., Van Loosdrecht, M. C. and Ni, B.-J. 2019. Microplastics in wastewater treatment plants: Detection, occurrence and removal. *Water research*, 152: 21-37.

Sussarellu, R., Suquet, M., Thomas, Y., Lambert, C., Fabioux, C., Pernet, M. E. J., Le Goïc, N., Quillien, V., Mingant, C. and Epelboin, Y. 2016. Oyster reproduction is affected by

exposure to polystyrene microplastics. *Proceedings of the national academy of sciences*, 113: 2430-2435.

Sutton, R., Mason, S. A., Stanek, S. K., Willis-Norton, E., Wren, I. F. and Box, C. 2016. Microplastic contamination in the san francisco bay, California, USA. *Marine pollution bulletin*, 109: 230-235.

Szalewicz, K., Bukowski, R. and Jeziorski, B. 2003. Nature of Many-Body Forces in Water Clusters and Bulk. In: *Water in Confining Geometries*. Springer, 7-23.

Tabrizchi, H. and Kuchaki Rafsanjani, M. 2020. A survey on security challenges in cloud computing: issues, threats, and solutions. *The journal of supercomputing*, 76: 9493-9532.

Taghavi, S. M., Momenpour, M., Azarian, M., Ahmadian, M., Souri, F., Taghavi, S. A., Sadeghain, M. and Karchani, M. 2013. Effects of Nanoparticles on the Environment and Outdoor Workplaces. *Electronic physician*, 5.

Talvitie, J., Mikola, A., Koistinen, A. and Setälä, O. 2017. Solutions to microplastic pollution–Removal of microplastics from wastewater effluent with advanced wastewater treatment technologies. *Water research*, 123: 401-407.

Tanaka, K. and Takada, H. 2016. Microplastic fragments and microbeads in digestive tracts of planktivorous fish from urban coastal waters. *Scientific reports*, 6: 1-8.

Tang, Y., Zhang, S., Su, Y., Wu, D., Zhao, Y. and Xie, B. 2021. Removal of microplastics from aqueous solutions by magnetic carbon nanotubes. *Chemical Engineering Journal*, 406: 126804.

Tang, Z., Zhao, X., Zhao, T., Wang, H., Wang, P., Wu, F. and Giesy, J. P. 2016. Magnetic nanoparticles interaction with humic acid: in the presence of surfactants. *Environmental Science & Technology*, 50: 8640-8648.

Tani, T., Watanabe, N. and Takatori, K. 2003. Emulsion combustion and flame spray synthesis of zinc oxide/silica particles. *Journal of Nanoparticle Research*, 5: 39-46.

Tatarchuk, T., Soltys, L. and Macyk, W. 2023. Magnetic adsorbents for removal of pharmaceuticals: A review of adsorption properties. *Journal of Molecular Liquids*, Article ID: 122174.

Terai, T. and Kobayashi, T. 2000. Properties of carbon films produced from polyimide by high-energy ion irradiation. *Nuclear Instruments and Methods in Physics Research Section B: Beam Interactions with Materials and Atoms*, 166: 627-631.

Thiruvengadam, M., Chi, H. Y. and Kim, S.-H. 2024. Impact of nanopollution on plant growth, photosynthesis, toxicity, and metabolism in the agricultural sector: An updated review. *Plant Physiology and Biochemistry*, Article ID: 108370.

Thomas, R. T., Nair, V. and Sandhyarani, N. 2013. TiO2 nanoparticle assisted solid phase photocatalytic degradation of polythene film: A mechanistic investigation. *Colloids and Surfaces A: Physicochemical and Engineering Aspects*, 422: 1-9.

Tian, C., Zhao, H., Sun, H., Xiao, K. and Wong, P. K. 2020. Enhanced adsorption and photocatalytic activities of ultrathin graphitic carbon nitride nanosheets: Kinetics and mechanism. *Chemical engineering journal*, 381: 122760.

Touqeer, H., Zaman, S., Amin, R., Hussain, M., Al-Turjman, F. and Bilal, M. 2021. Smart home security: challenges, issues and solutions at different IoT layers. *The Journal of Supercomputing*, 77: 14053-14089.

Trefil, J. 2001. *The encyclopedia of science and technology*. Routledge.

Tu, C.-H., Wang, A.-Q., Zheng, M.-Y., Wang, X.-D. and Zhang, T. 2006. Factors influencing the catalytic activity of SBA-15-supported copper nanoparticles in CO oxidation. *Applied Catalysis A: General*, 297: 40-47.

Uddin, M. N., Shimoyama, I., Baba, Y., Sekiguchi, T. and Nagano, M. 2005. X-ray photoelectron spectroscopic observation on B–C–N hybrids synthesized by ion beam deposition of borazine. *Journal of Vacuum Science & Technology A*, 23: 497-502.

Ullah, M., Ali, M. E. and Abd Hamid, S. B. 2014. SURFACTANT-ASSISTED BALL MILLING: A NOVEL ROUTE TO NOVEL MATERIALS WITH CONTROLLED NANOSTRUCTURE-A REVIEW. *Reviews on Advanced Materials Science*, 37.

Van Do, M., Le, T. X. T., Vu, N. D. and Dang, T. T. 2022. Distribution and occurrence of microplastics in wastewater treatment plants. *Environmental Technology & Innovation*, 26: 102286.

Van Dongen, J. T., Ammerlaan, A. M., WOUTERLOOD, M., Van Aelst, A. C. and Borstlap, A. C. 2003. Structure of the developing pea seed coat and the post-phloem transport pathway of nutrients. *Annals of Botany*, 91: 729-737.

Vemury, S., Pratsinis, S. E. and Kibbey, L. 1997. Electrically controlled flame synthesis of nanophase TiO2, SiO2, and SnO2 powders. *journal of materials research*, 12: 1031-1042.

Veneral, C., Camargo, A. F., Klein, G. H., Veneral, J. and Treichel, H. 2023. From Macro to Micro: Plastic as an Environmental Problem. *Environmental Nanotechnology, Monitoring & Management*, Article ID: 100906.

Vivekanand, A. C., Mohapatra, S. and Tyagi, V. K. 2021. Microplastics in aquatic environment: Challenges and perspectives. *Chemosphere*, 282: 131151.

Walkinshaw, C., Lindeque, P. K., Thompson, R., Tolhurst, T. and Cole, M. 2020. Microplastics and seafood: lower trophic organisms at highest risk of contamination. *Ecotoxicology and environmental safety*, 190: 110066.

Wan, H., Wang, J., Sheng, X., Yan, J., Zhang, W. and Xu, Y. 2022. Removal of polystyrene microplastics from aqueous solution using the metal–organic framework material of ZIF-67. *Toxics*, 10: 70.

Wang, C., Fan, H., Ren, X., Fang, J., Ma, J. and Zhao, N. 2018. Porous graphitic carbon nitride nanosheets by pre-polymerization for enhanced photocatalysis. *Materials Characterization*, 139: 89-99.

Wang, F., Wu, H., Wu, W., Wang, L., Liu, J., An, L. and Xu, Q. 2021a. Microplastic characteristics in organisms of different trophic levels from Liaohe Estuary, China. *Science of The Total Environment*, 789: 148027.

Wang, H., Han, X., Chen, Y., Guo, W., Zheng, W., Cai, N., Guo, Q., Zhao, X. and Wu, F. 2021b. Effects of F−, Cl−, Br−, NO3−, and SO42− on the colloidal stability of Fe3O4 nanoparticles in the aqueous phase. *Science of the Total Environment*, 757: 143962.

Wang, H., Kou, X., Pei, Z., Xiao, J. Q., Shan, X. and Xing, B. 2011. Physiological effects of magnetite (Fe3O4) nanoparticles on perennial ryegrass (Lolium perenne L.) and pumpkin (Cucurbita mixta) plants. *Nanotoxicology*, 5: 30-42.

Wang, J., Guo, X. and Xue, J. 2021c. Biofilm-developed microplastics as vectors of pollutants in aquatic environments. *Environmental Science & Technology*, 55: 12780-12790.

Wang, J., Sun, C., Huang, Q.-X., Chi, Y. and Yan, J.-H. 2021d. Adsorption and thermal degradation of microplastics from aqueous solutions by Mg/Zn modified magnetic biochars. *Journal of hazardous materials*, 419: 126486.

Wang, J., Wang, M., Kang, J., Tang, Y., Liu, J., Li, S., Xu, Z. and Tang, P. 2022a. The promoted tetracycline visible-light-driven photocatalytic degradation efficiency of g-C3N4/FeWO4 Z-scheme heterojunction with peroxymonosulfate assisting and mechanism. *Separation and Purification Technology*, 296: 121440.

Wang, L., Liu, Y., Pang, D., Song, H. and Zhang, S. 2022b. Simultaneous electrochemical degradation of tetracycline and metronidazole through a high-efficiency and low-energy-consumption advanced oxidation process. *Chemosphere*, 292: 133469.

Wang, M., Cui, S., Yang, X. and Bi, W. 2015. Synthesis of g-C3N4/Fe3O4 nanocomposites and application as a new sorbent for solid phase extraction of polycyclic aromatic hydrocarbons in water samples. *Talanta*, 132: 922-928.

Wang, S., Chen, Z., Cai, Y., Wu, X.-L., Wang, S., Tang, Z., Hu, B., Li, Z. and Wang, X. 2023. Application of COFs in capture/conversion of CO2 and elimination of organic/inorganic pollutants. *Environmental Functional Materials*, 2: 76-92.

Wang, W., Lin, J., Xing, C., Chai, R., Abbas, S., Song, T., Tang, C. and Huang, Y. 2017a. Fe3O4 nanoparticle-coated boron nitride nanospheres: Synthesis, magnetic property and biocompatibility study. *Ceramics International*, 43: 6371-6376.

Wang, W., Ndungu, A. W., Li, Z. and Wang, J. 2017b. Microplastics pollution in inland freshwaters of China: A case study in urban surface waters of Wuhan, China. *Science of the Total Environment*, 575: 1369-1374.

Wang, X. L. and Yang, H. G. 2017. Facile fabrication of high-yield graphitic carbon nitride with a large surface area using bifunctional urea for enhanced photocatalytic performance. *Applied Catalysis B: Environmental*, 205: 624-630.

Wang, Y., Gu, X., Quan, J., Xing, G., Yang, L., Zhao, C., Wu, P., Zhao, F., Hu, B. and Hu, Y. 2021e. Application of magnetic fields to wastewater treatment and its mechanisms: A review. *Science of the Total Environment*, 773: 145476.

Wei, W., Hao, Q., Chen, Z., Bao, T. and Ni, B.-J. 2020. Polystyrene nanoplastics reshape the anaerobic granular sludge for recovering methane from wastewater. *Water research*, 182: 116041.

Wei, W., Huang, Q.-S., Sun, J., Dai, X. and Ni, B.-J. 2019. Revealing the mechanisms of polyethylene microplastics affecting anaerobic digestion of waste activated sludge. *Environmental science & technology*, 53: 9604-9613.

Wierzbicka, M. and Obidzińska, J. 1998. The effect of lead on seed imbibition and germination in different plant species. *Plant science*, 137: 155-171.

Wilhelm, M. J., Gh, M. S., Wu, T., Li, Y., Chang, C.-M., Ma, J. and Dai, H.-L. 2021. Determination of bacterial surface charge density via saturation of adsorbed ions. *Biophysical Journal*, 120: 2461-2470.

Worstell, J. 2014. *Adiabatic fixed-bed reactors: practical guides in chemical engineering*. Butterworth-Heinemann.

Wu, Y., Xie, Y., Liu, X., Li, Y., Wang, J., Chen, Z., Yang, H., Hu, B., Shen, C. and Tang, Z. 2023. Functional nanomaterials for selective uranium recovery from seawater: Material design, extraction properties and mechanisms. *Coordination Chemistry Reviews*, 483: 215097.

Xia, H.-b., Foo, P. and Yi, J. 2009. Water-dispersible spherically hollow clusters of magnetic nanoparticles. *Chemistry of Materials*, 21: 2442-2451.

Xiao, G., Wang, Y., Xu, S., Li, P., Yang, C., Jin, Y., Sun, Q. and Su, H. 2019. Superior adsorption performance of graphitic carbon nitride nanosheets for both cationic and anionic heavy metals from wastewater. *Chinese Journal of Chemical Engineering*, 27: 305-313.

Xing, C., Yu, G., Zhou, J., Liu, Q., Chen, T., Liu, H. and Li, X. 2022. Solar energy-driven upcycling of plastic waste on direct Z-scheme heterostructure of V-substituted phosphomolybdic acid/g-C3N4 nanosheets. *Applied Catalysis B: Environmental*, 315: 121496.

Xiong, C., Wang, W., Tan, F., Luo, F., Chen, J. and Qiao, X. 2015. Investigation on the efficiency and mechanism of Cd (II) and Pb (II) removal from aqueous solutions using MgO nanoparticles. *Journal of hazardous materials*, 299: 664-674.

Xu, B., Liu, F., Cryder, Z., Huang, D., Lu, Z., He, Y., Wang, H., Lu, Z., Brookes, P. C. and Tang, C. 2020. Microplastics in the soil environment: occurrence, risks, interactions and fate–a review. *Critical Reviews in Environmental Science and Technology*, 50: 2175-2222.

Xu, T., Tang, X., Qiu, M., Lv, X., Shi, Y., Zhou, Y., Xie, Y., Naushad, M., Lam, S. S. and Ng, H. S. 2023. Degradation of levofloxacin from antibiotic wastewater by pulse electrochemical oxidation with BDD electrode. *Journal of environmental management*, 344: 118718.

Yadav, B. and Srivastava, V. C. 2017. Catalytic peroxidation of recalcitrant quinoline by ceria impregnated granular activated carbon. *Clean Technologies and Environmental Policy*, 19: 1547-1555.

Yadav, S., Gupta, E., Patel, A., Srivastava, S., Mishra, V. K., Singh, P. C., Srivastava, P. K. and Barik, S. K. 2022. Unravelling the emerging threats of microplastics to agroecosystems. *Reviews in Environmental Science and Bio/Technology*, 21: 771-798.

Yadav, V. K., Ali, D., Khan, S. H., Gnanamoorthy, G., Choudhary, N., Yadav, K. K., Thai, V. N., Hussain, S. A. and Manhrdas, S. 2020. Synthesis and characterization of amorphous iron oxide nanoparticles by the sonochemical method and their application for the remediation of heavy metals from wastewater. *Nanomaterials*, 10: 1551.

Yamakov, V., Wolf, D., Phillpot, S., Mukherjee, A. and Gleiter, H. 2004. Deformation-mechanism map for nanocrystalline metals by molecular-dynamics simulation. *Nature materials*, 3: 43-47.

Yang, H., Chen, G. and Wang, J. J. T. 2021. Microplastics in the marine environment: sources, fates, impacts and microbial degradation. 9: 41.

Yang, J., Chen, H., Gao, J., Yan, T., Zhou, F., Cui, S. and Bi, W. 2016. Synthesis of Fe3O4/g-C3N4 nanocomposites and their application in the photodegradation of 2, 4, 6-trichlorophenol under visible light. *Materials Letters*, 164: 183-189.

Yano, K. A., Geronimo, F. K., Reyes, N. J. and Kim, L. H. 2021. Characterization and comparison of microplastic occurrence in point and non-point pollution sources. *Science of the Total Environment*, 797: 148939.

Yaqoob, A. A., Parveen, T., Umar, K. and Mohamad Ibrahim, M. N. 2020. Role of nanomaterials in the treatment of wastewater: A review. *Water*, 12: 495.

Yaranal, N. A., Subbiah, S. and Mohanty, K. 2021. Distribution and characterization of microplastics in beach sediments from Karnataka (India) coastal environments. *Marine Pollution Bulletin*, 169: 112550.

Yeganeh, M., Sobhi, H. R., Ghambarian, M. and Esrafili, A. 2024. Sono-assisted photocatalytic degradation of ciprofloxacin in aquatic media using g-C3N4/MOF-based nanocomposite under visible light irradiation. *Environmental Science and Pollution Research*, 31: 35811-35823.

Yousefi, M., Farzadkia, M., Mahvi, A. H., Kermani, M., Gholami, M. and Esrafili, A. 2024. Photocatalytic degradation of ciprofloxacin using a novel carbohydrate-based nanocomposite from aqueous solutions. *Chemosphere*, 349: 140972.

Yuan, F., Yue, L., Zhao, H. and Wu, H. 2020. Study on the adsorption of polystyrene microplastics by three-dimensional reduced graphene oxide. *Water Science & Technology*, 81: 2163-2175.

Zbyszewski, M. and Corcoran, P. L. 2011. Distribution and degradation of fresh water plastic particles along the beaches of Lake Huron, Canada. *Water, Air, & Soil Pollution*, 220: 365-372.

Zeng, W., Liang, H., Zhang, H., Luo, X., Lin, D. and Li, G. 2022. Efficient electrochemical oxidation of sulfamethoxazole by a novel reduced TiO2 nanotube arrays-based flow-through electrocatalytic membrane. *Separation and Purification Technology*, 289: 120720.

Zhang, G. and Liu, Y. 2018. The distribution of microplastics in soil aggregate fractions in southwestern China. *Science of the Total Environment*, 642: 12-20.

Zhang, L., Tian, S., Tang, Z., Wang, Y., Du, S. and Cang, D. 2024. Exploration of sulfamethoxazole removal triggered by copper slag-based geopolymer: Radical versus nonradical contributions. *Chemical Engineering Journal*, Article ID: 154310.

Zhang, S., Liu, Y., Lv, S. and Cheng, J. 2023. Surface modification of polymers by ion irradiation: Reactivity principle and application. *Nuclear Instruments and Methods in Physics Research Section B: Beam Interactions with Materials and Atoms*, 543: 165097.

Zhang, X., Lian, G., Zhang, S., Cui, D. and Wang, Q. J. C. 2012. Boron nitride nanocarpets: controllable synthesis and their adsorption performance to organic pollutants. 14: 4670-4676.

Zhang, Z. and Chen, Y. 2020. Effects of microplastics on wastewater and sewage sludge treatment and their removal: a review. *Chemical Engineering Journal*, 382: 122955.

Zhao, L.-X., Li, M.-H., Jiang, H.-L., Xie, M., Zhao, R.-S. and Lin, J.-M. 2022. Activation of peroxymonosulfate by a stable Co-Mg-Al LDO heterogeneous catalyst for the efficient degradation of ofloxacin. *Separation and Purification Technology*, 294: 121231.

Zhao, S., Zhu, L. and Li, D. 2015. Microplastic in three urban estuaries, China. *Environmental pollution*, 206: 597-604.

Zhao, T., Fang, M., Tang, Z., Zhao, X., Xie, F., Wu, F. and Giesy, J. P. 2019. Effects of fulvic acid on aggregation, sedimentation, and adsorption of Fe 3 O 4 magnetic nanoparticles. *Environmental Science and Pollution Research*, 26: 21463-21474.

Zhao, Z., Xia, Z., Liu, C., Huang, H. and Ye, W. 2017. Green synthesis of Pd/Fe3O4 composite based on polyDOPA functionalized reduced graphene oxide for electrochemical detection of nitrite in cured food. *Electrochimica Acta*, 256: 146-154.

Zheng, B., Li, B., Wan, H., Lin, X. and Cai, Y. 2022. Coral-inspired environmental durability aerogels for micron-size plastic particles removal in the aquatic environment. *Journal of Hazardous Materials*, 431: 128611.

Zhong, L., Xu, H., Yu, Z. and Yun, K. 2020. Bowl-shaped graphene oxide/Fe 3 O 4 composites on Au-PCB electrode for electrochemical detection of dopamine. *Ionics*, 26: 4171-4181.

Zhou, G., Huang, X., Xu, H., Wang, Q., Wang, M., Wang, Y., Li, Q., Zhang, Y., Ye, Q. and Zhang, J. 2022. Removal of polystyrene nanoplastics from water by CuNi carbon material: the role of adsorption. *Science of The Total Environment*, 820: 153190.

Zhou, X., Jin, B., Chen, R., Peng, F. and Fang, Y. 2013. Synthesis of porous Fe3O4/g-C3N4 nanospheres as highly efficient and recyclable photocatalysts. *Materials Research Bulletin*, 48: 1447-1452.

Zhu, B., Xia, P., Ho, W. and Yu, J. 2015. Isoelectric point and adsorption activity of porous g-C3N4. *Applied Surface Science*, 344: 188-195.

Zhu, H., Han, J., Xiao, J. Q. and Jin, Y. 2008. Uptake, translocation, and accumulation of manufactured iron oxide nanoparticles by pumpkin plants. *Journal of Environmental monitoring*, 10: 713-717.

Zhu, J., Xiao, P., Li, H. and Carabineiro, S. 2014. Graphitic carbon nitride: synthesis, properties, and applications in catalysis. *ACS applied materials & interfaces*, 6: 16449-16465.

Ziani, K., Ioniță-Mîndrican, C.-B., Mititelu, M., Neacșu, S. M., Negrei, C., Moroșan, E., Drăgănescu, D. and Preda, O.-T. 2023. Microplastics: a real global threat for environment and food safety: a state of the art review. *Nutrients*, 15: 617.

APPENDIX

Appendix 1

tsu00 | ACSJCA | JCA11.2.5208/W Library-x64 | manuscript.3f (R5.2.i3:5013 | 2.1) 2022/08/03 13:05:00 | PROD-WS-121 | rq_1052141 | 10/20/2023 10:54:36 | 14 | JCA-DEFAULT

ACS ES&T Water

pubs.acs.org/estwater

Review

Nanomaterials for Microplastic Removal from Wastewater: Current State of the Art Nanomaterials and Future Prospects

Riona Indhur, Isaac Amoah, Faizal Bux, and Sheena Kumari*

Cite This: https://doi.org/10.1021/acsestwater.3c00203

Read Online

ACCESS | Metrics & More | Article Recommendations

ABSTRACT: Microplastics (MPs) and nanoplastics (NPs) infiltrate aquatic environments at an alarming rate, posing a serious threat to aquatic ecosystems and human health. Wastewater treatment plants are significant sources of MPs/NPs contamination in the aquatic environment, since they are inadequate at removing these MPs/NPs. This calls for the development and application of new technologies for MPs/NPs removal. Recent studies have demonstrated that nanomaterials (NMs) are effective in the removal of MPs from wastewater. This review examines MPs/NPs removal from wastewater using NMs. Despite a specific synthesis of NMs adapted for MP removal from water bodies not being clearly defined, the review assesses the current state of knowledge in relation to MPs/NPs removal from wastewater using NMs and the effect of water characteristics on the removal mechanism. Additionally, various insights into NM development based on specific interactions are addressed and linked to their suitability for wastewater treatment. There is currently considerable interest in chemically synthesizing NMs for the removal of MPs from wastewater. However, further developments are needed in the areas of physical and green synthesis of NMs for the removal of MPs. This review provides a baseline for future research and development of NMs for removing MPs from wastewater.

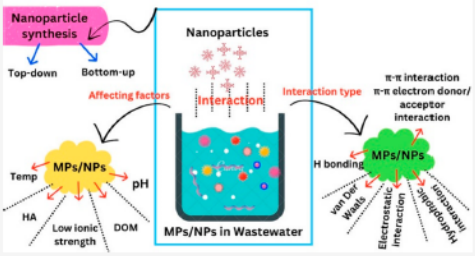

INTRODUCTION

Over the past few decades the global plastic pollution crisis has intensified[1] and continues to exhibit an exponential projected trajectory.[2] Approximately 8 million metric tons of plastic waste enter the aquatic ecosystem annually, and this amount is projected to rise 4-fold by 2050.[2] It has garnered a lot of concern from the scientific community, which has embarked on a quest to counter the catastrophic consequences of this situation.[1] The majority of plastic products are nondegradable, meaning they persist for around 100 years. This extended lifespan is highly disproportionate to the current rates of plastic disposal.[1] Among the concerning detriments of this plastic pollution is the emergence of microplastics and nanoplastics because these emerging contaminants pose an imminent threat to the environment,[3] marine life,[3] and human health.[4] Additionally, pollution of freshwater bodies contributes to the scarcity of freshwater, adding additional pressure to the available resources.

Wastewater treatment plants (WWTP) have demonstrated a relatively high efficiency in removing MPs, as they can remove a significant majority of these particles. During the WWTP process, MPs may be degraded to much smaller particles known as NPs, which are difficult to remove and detect. In addition, even a very modest amount of MPs released per liter of effluent can result in significant concentrations of MPs being released into the environment.[7] Gies and teammates

Appendix 2

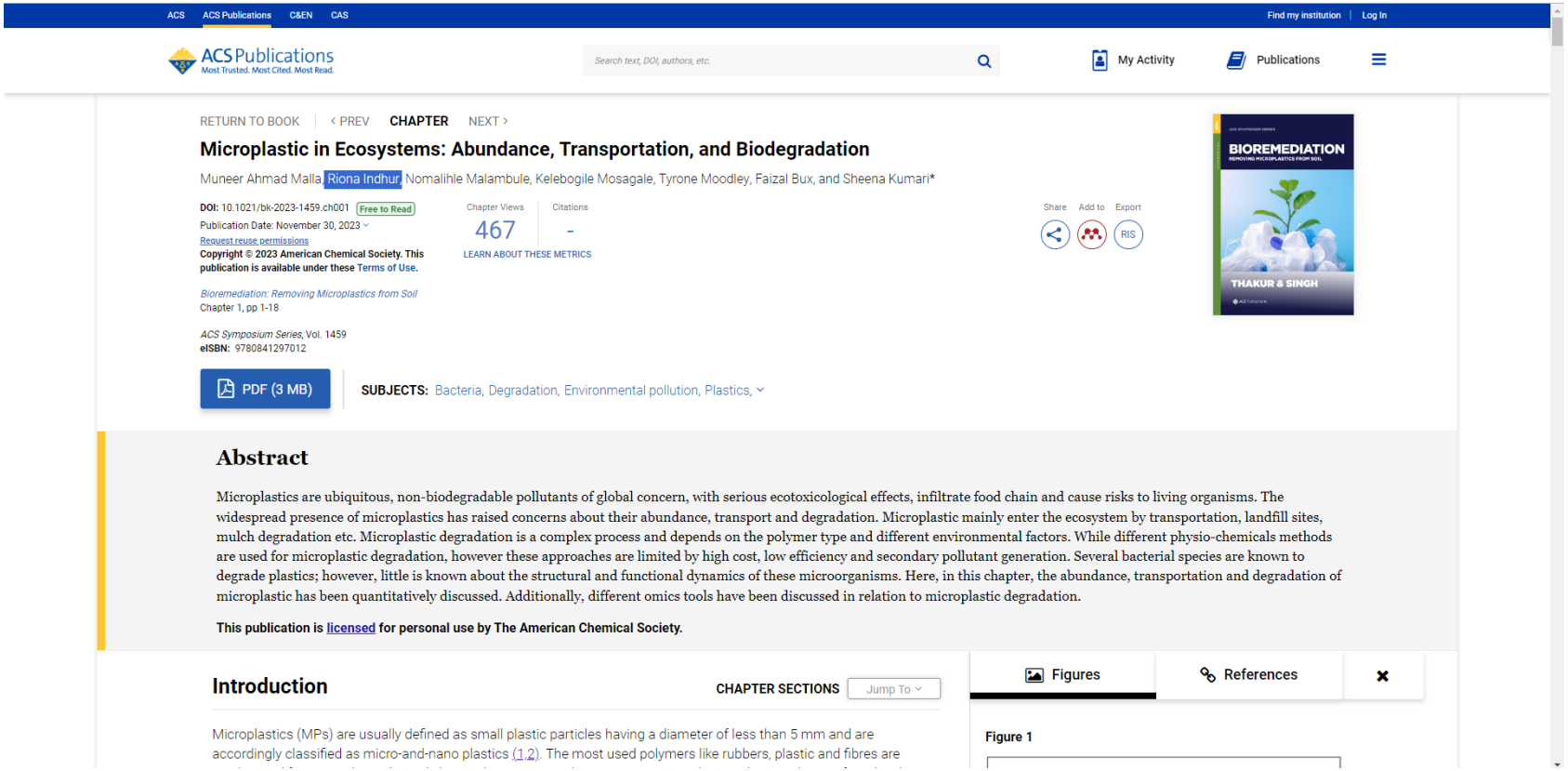
ACS
ACS Publications
C&EN
CAS
Find my institution | Log In
ACS Publications
Most Trusted. Most Cited. Most Read.
Search text, DOI, authors, etc.
My Activity
Publications
RETURN TO BOOK
< PREV
CHAPTER
NEXT >
Microplastic in Ecosystems: Abundance, Transportation, and Biodegradation
Muneer Ahmad Malla, Riona Indhur, Nomalihle Malambule, Kelebogile Mosagale, Tyrone Moodley, Faizal Bux, and Sheena Kumari*
DOI: 10.1021/bk-2023-1459.ch001
Free to Read
Publication Date: November 30, 2023
Request reuse permissions
Copyright © 2023 American Chemical Society. This publication is available under these Terms of Use.
Chapter Views
467
LEARN ABOUT THESE METRICS
Citations
-
Share
Add to
Export
RIS
Bioremediation: Removing Microplastics from Soil
Chapter 1, pp 1-18
ACS Symposium Series, Vol. 1459
eISBN: 9780841297012
BIOREMEDIATION
THAKUR & SINGH
PDF (3 MB)
SUBJECTS: Bacteria, Degradation, Environmental pollution, Plastics,
Abstract
Microplastics are ubiquitous, non-biodegradable pollutants of global concern, with serious ecotoxicological effects, infiltrate food chain and cause risks to living organisms. The widespread presence of microplastics has raised concerns about their abundance, transport and degradation. Microplastic mainly enter the ecosystem by transportation, landfill sites, mulch degradation etc. Microplastic degradation is a complex process and depends on the polymer type and different environmental factors. While different physio-chemicals methods are used for microplastic degradation, however these approaches are limited by high cost, low efficiency and secondary pollutant generation. Several bacterial species are known to degrade plastics; however, little is known about the structural and functional dynamics of these microorganisms. Here, in this chapter, the abundance, transportation and degradation of microplastic has been quantitatively discussed. Additionally, different omics tools have been discussed in relation to microplastic degradation.
This publication is licensed for personal use by The American Chemical Society.
Introduction
CHAPTER SECTIONS
Jump To
Figures
References
Figure 1
Microplastics (MPs) are usually defined as small plastic particles having a diameter of less than 5 mm and are accordingly classified as micro-and-nano plastics (1,2). The most used polymers like rubbers, plastic and fibres are

Appendix 3


tandfonline.com/doi/
Taylor & Francis Online
Environmental Technology Reviews ›
Volume 13, 2024 - Issue 1
Open access
0 Views
0 CrossRef citations to date
0 Altmetric
Listen
Review Article
A review on conventional and novel adsorbents to boost the sorption capacity of heavy metals: current status, challenges and future outlook
Arvind Kumar, Riona Indhur, Abdul Gaffar Sheik, Suresh Babu Naidu Krishna, Sheena Kumari & Faizal Bux
Pages 521-543 | Received 01 Feb 2024, Accepted 22 Jun 2024, Published online: 01 Aug 2024
Cite this article
Check for updates
Full Article
Showing
Figures & data

Appendix 4

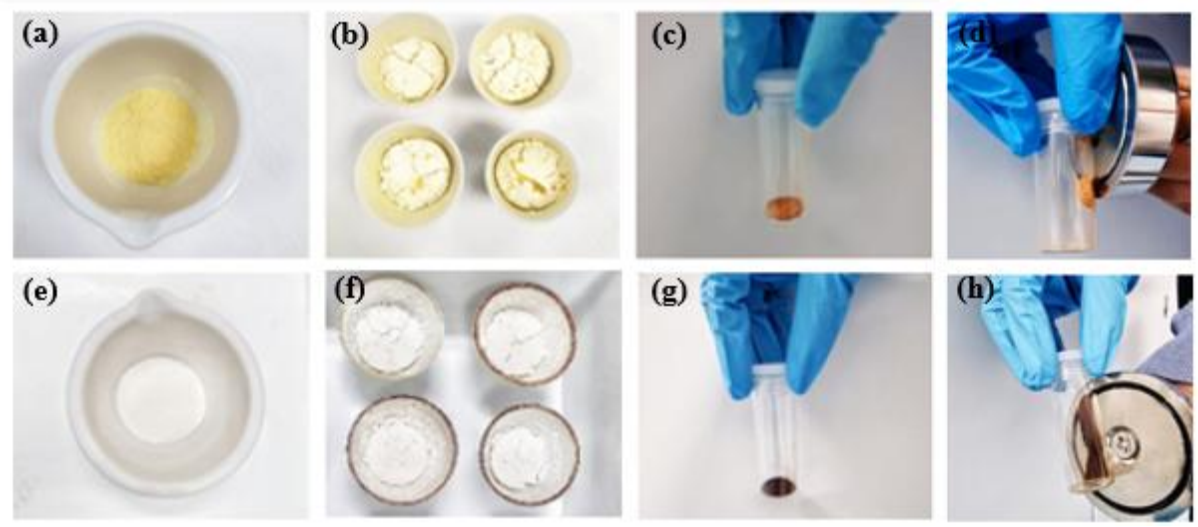

Figure 35: The nanomaterials at different stages of synthesis, (a) g-C_3N_4 before calcination, (b) g-C_3N_4 after calcination, (c) g-C_3N_4@Fe_3O_4 after synthesis, (d) g-C_3N_4@Fe_3O_4 with magnetic field applied, (e) BNNS before calcination, (f) BNNS after calcination, (g) BNNS@Fe_3O_4 after synthesis and (h) BNNS-Fe_3O_4 with magnetic field applied

Appendix 5

Application of optimised parameters on different sizes and types of MPS

Size	g-C_3N_4-Fe_3O_4	BNNS- Fe_3O_4
PE only (125 µM)		
PS only (180 µM)		
PE+PS (125 and 180 µM)		
PS only (500 µM)		

Figure 36: Flasks containing different MP types and sizes after adsorption experiments using optimum operating parameters

Appendix 6

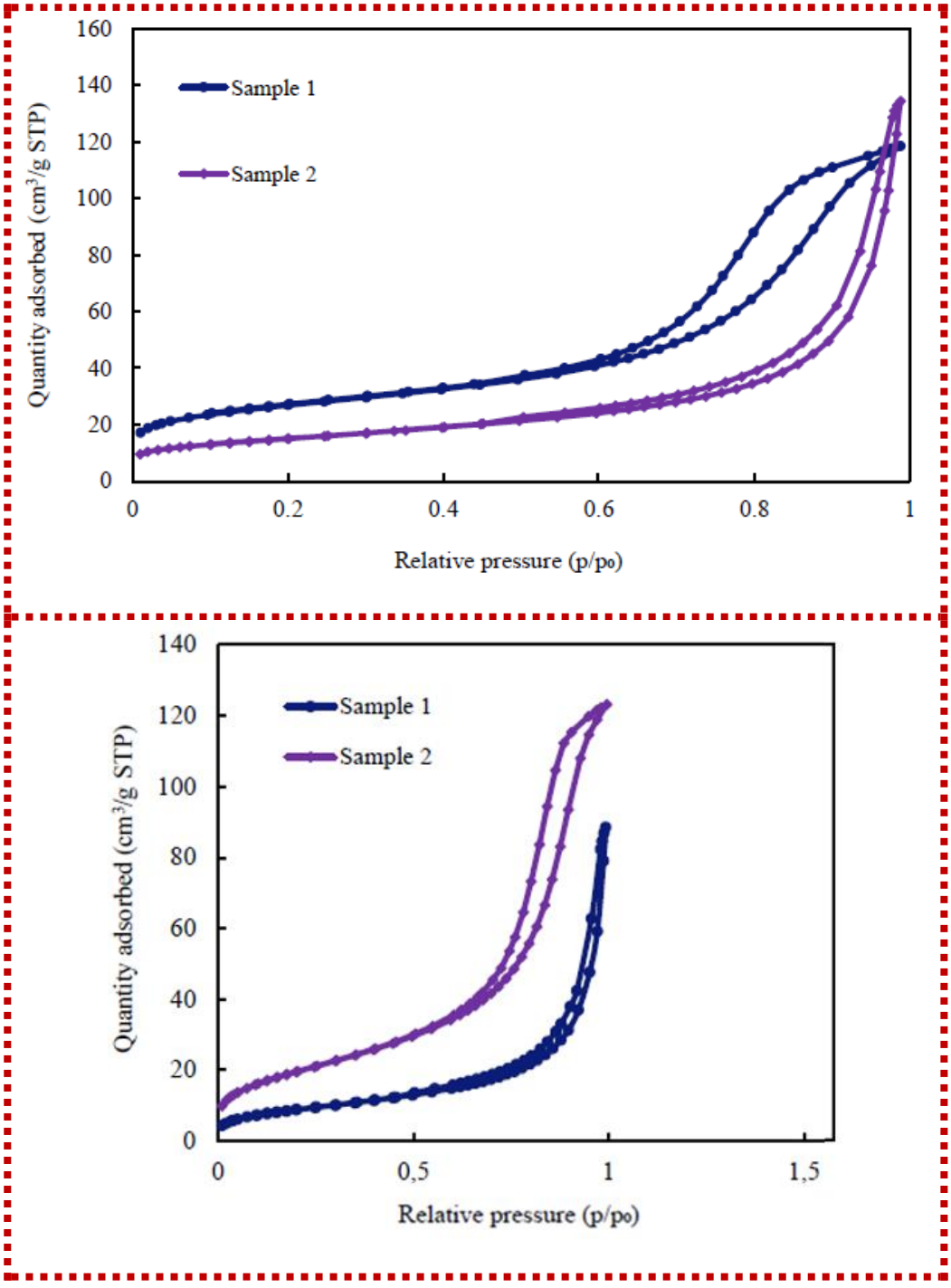

Figure 37: Plot of adsorption-desorption isotherm for (a) fresh g-C_3N_4@Fe_3O_4 (sample 1) and BNNS@Fe_3O_4 (sample 2), (b) used BNNS@Fe_3O_4 (sample 1) and g-C_3N_4@Fe_3O_4 (sample 2)

Appendix 7

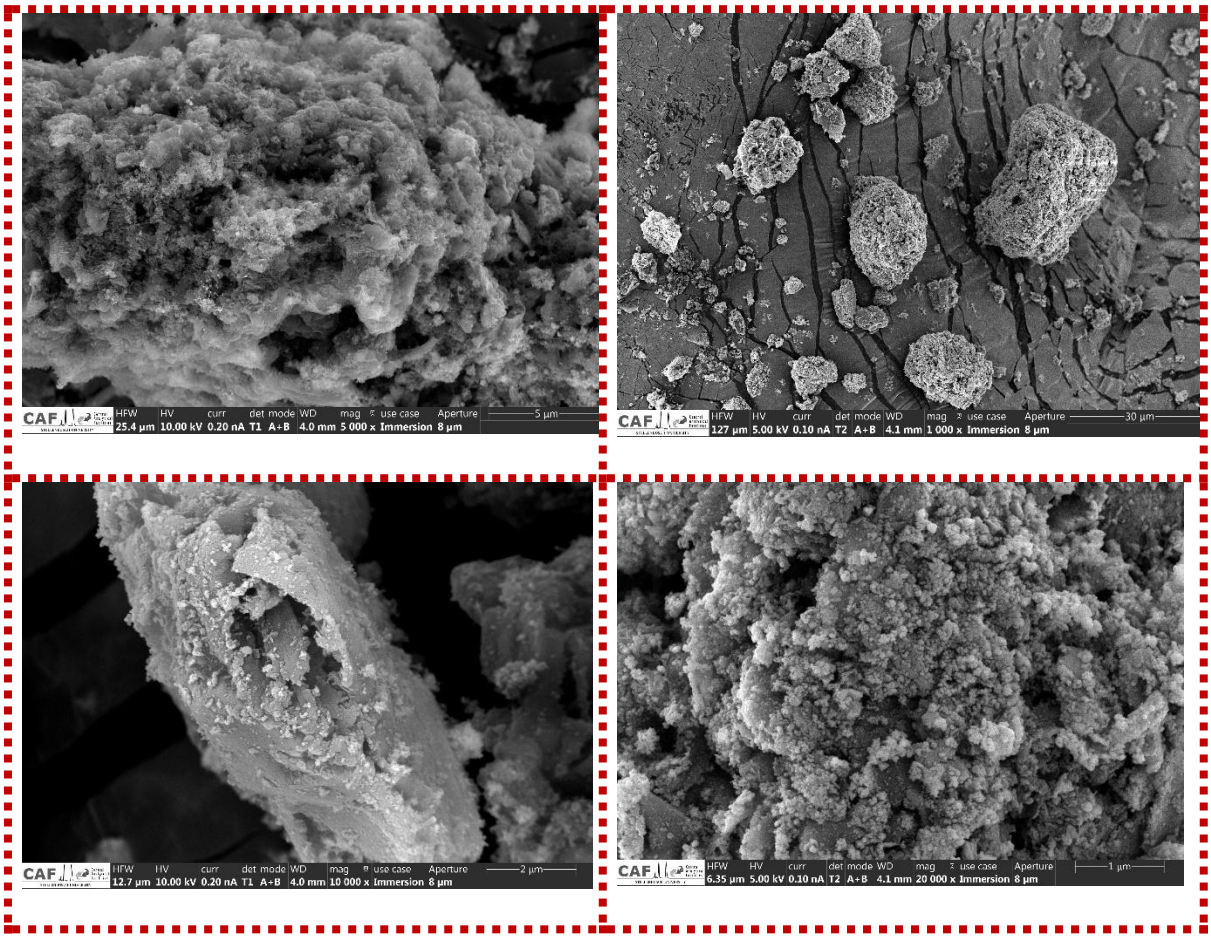

Figure 38: SEM micrograph of fresh g-C_3N_4@Fe_3O_4

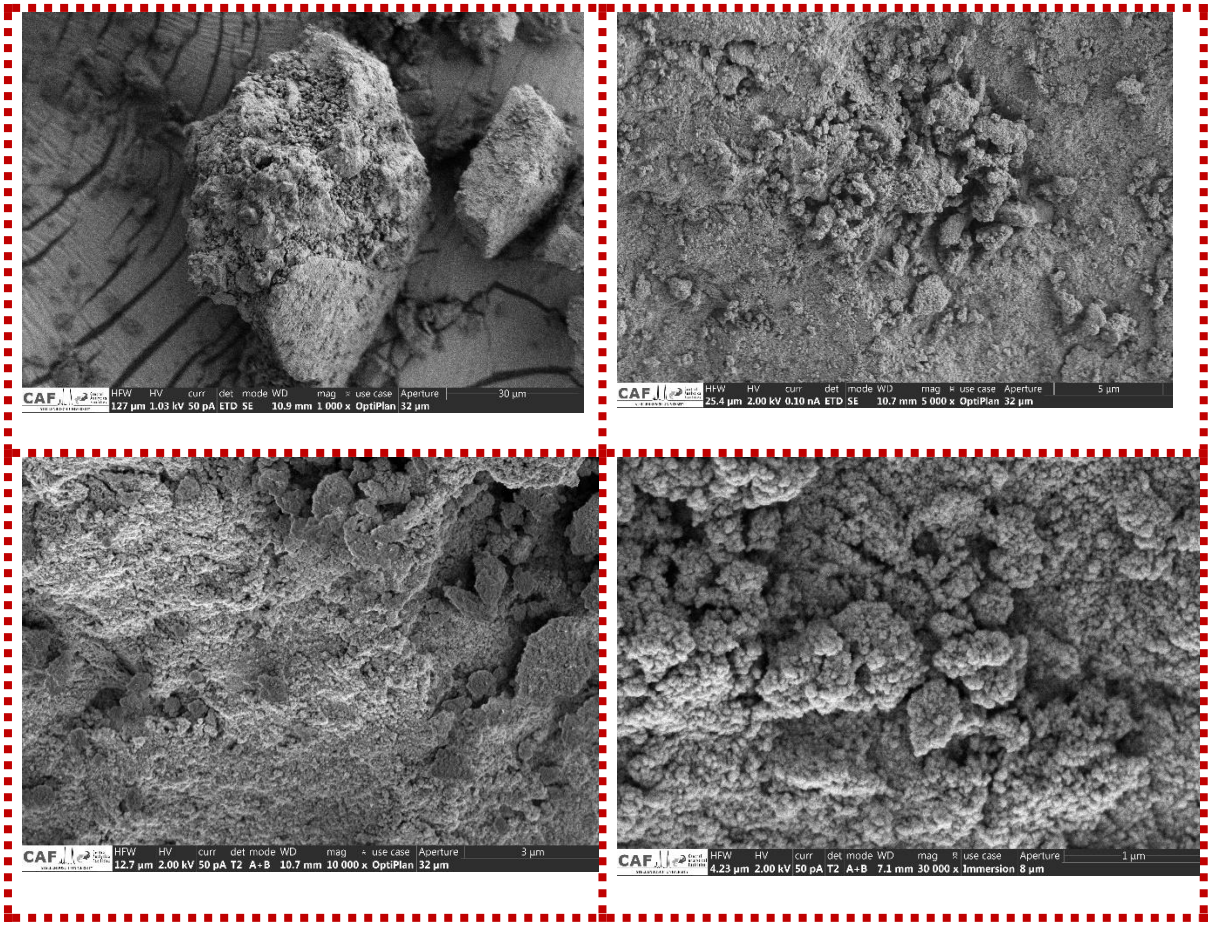

Figure 39: SEM micrograph of fresh BNNS@Fe_3O_4

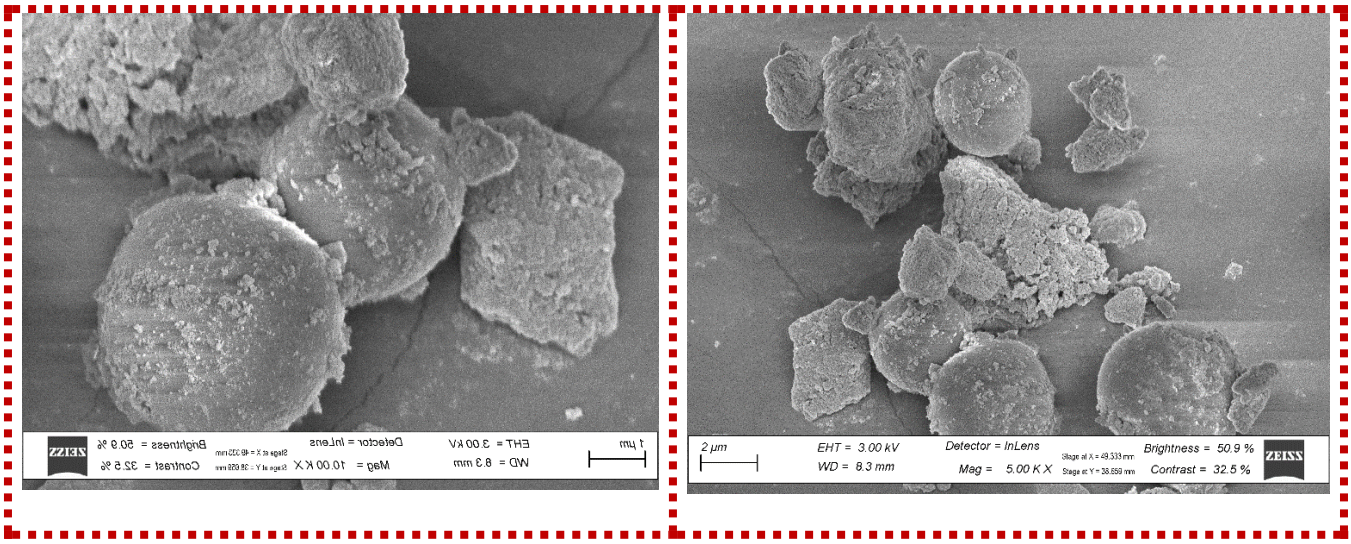

Figure 40: SEM micrograph of used (a) g-C_3N_4@Fe_3O_4, (b) BNNS@Fe_3O_4 showing MP adsorption

Appendix 8

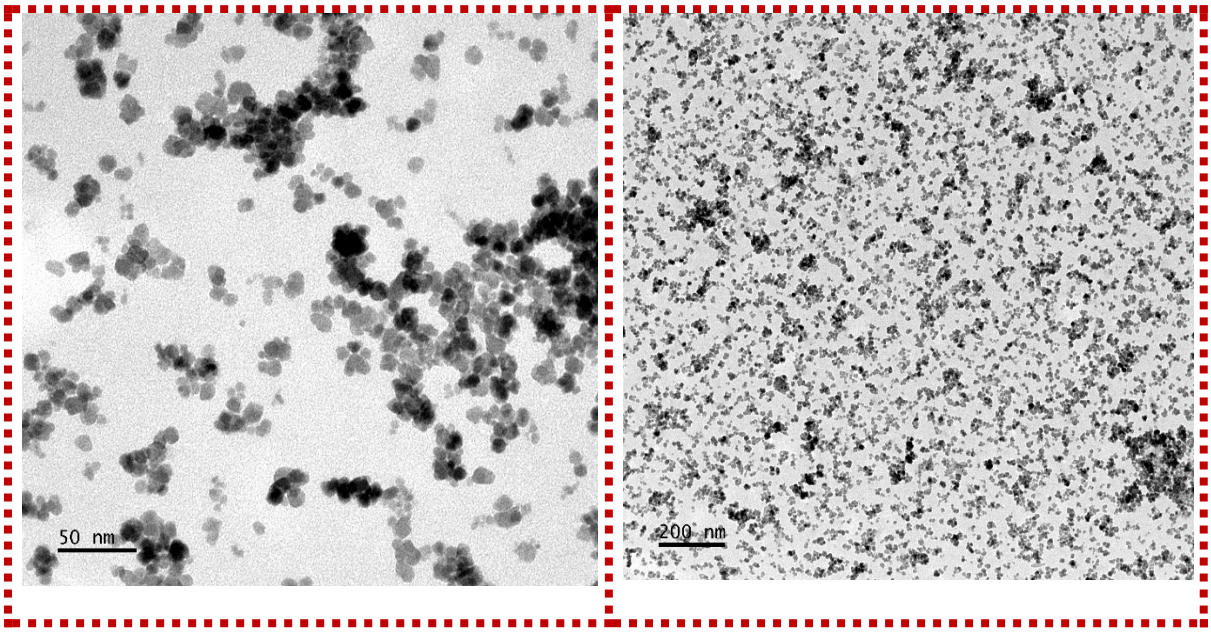

Figure 41: TEM micrograph of fresh BNNS@Fe_3O_4

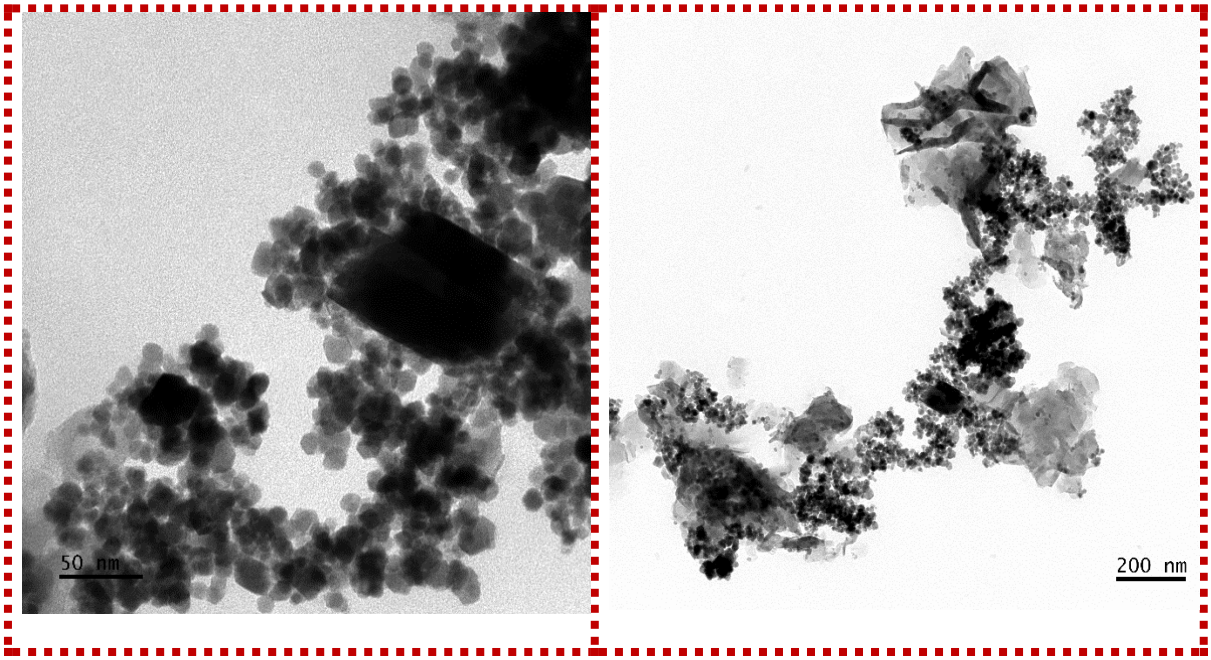

Figure 42: TEM micrograph of fresh g-C_3N_4@Fe_3O_4

Appendix 9

Figure 43: Images of used (a) g-C_3N_4@Fe_3O_4, (b) BNNS@Fe_3O_4 showing the adsorption of MPs onto the MNCs after treatment